Research and Perspectives in Neurosciences

Henry Kennedy
David C. Van Essen
Yves Christen *Editors*

Micro-, Meso- and Macro-Connectomics of the Brain

FONDATION IPSEN
POUR LA RECHERCHE THERAPEUTIQUE

OPEN

Springer

Research and Perspectives in Neurosciences

More information about this series at http://www.springer.com/series/2357

Henry Kennedy • David C. Van Essen •
Yves Christen
Editors

Micro-, Meso- and Macro-Connectomics of the Brain

Springer

OPEN

Editors
Henry Kennedy
Stem-Cell & Brain Res. Institute
Inserm U846
Bron, France

David C. Van Essen
Anatomy and Neurobiology Dept.
Washington Univ. School of Medicine
St. Louis, Missouri
USA

Yves Christen
Fondation Ipsen
Boulogne Billancourt, France

ISSN 0945-6082 ISSN 2196-3096 (electronic)
Research and Perspectives in Neurosciences
ISBN 978-3-319-27776-9 ISBN 978-3-319-27777-6 (eBook)
DOI 10.1007/978-3-319-27777-6

Library of Congress Control Number: 2016932376

Printed on acid-free paper

This Springer imprint is published by Springer Nature
The registered company is Springer International Publishing AG Switzerland

Acknowledgments

The editors wish to express their gratitude to Mrs. Mary Lynn Gage for her editorial assistance and Mrs. Astrid de Gérard for the organization of the meeting.

Contents

List of Contributors

Andreas Burkhalter Department of Neuroscience, Washington University School of Medicine, St. Louis, MO, USA

Edward M. Callaway The Salk Institute for Biological Studies, La Jolla, CA, USA

Karl Deisseroth Departments of Bioengineering and Psychiatry, Howard Hughes Medical Institute, Stanford University, Stanford, CA, USA

Donna L. Dierker Anatomy and Neurobiology Department, Washington University School of Medicine, St. Louis, MO, USA

Chad Donahue Anatomy and Neurobiology Department, Washington University School of Medicine, St. Louis, MO, USA

Mária Ercsey-Ravasz Faculty of Physics, Babeş-Bolyai University, Cluj-Napoca, Romania

Matthew F. Glasser Anatomy and Neurobiology Department, Washington University School of Medicine, St. Louis, MO, USA

Derrek P. Hibar Imaging Genetics Center, University of Southern California, Los Angeles, CA, USA

Neda Jahanshad Imaging Genetics Center, University of Southern California, Los Angeles, CA, USA

Henry Kennedy Stem Cell and Brain Research Institute, Bron, France

Université de Lyon, Lyon, France

Kenneth Knoblauch Stem Cell and Brain Research Institute, Bron, France

Université de Lyon, Lyon, France

Gautam Prasad Imaging Genetics Center, University of Southern California, Los Angeles, CA, USA

Terrence J. Sejnowski Howard Hughes Medical Institute, The Salk Institute for Biological Studies, La Jolla, CA, USA

Division of Biological Sciences, University of California at San Diego, La Jolla, CA, USA

Olaf Sporns Department of Psychological and Brain Sciences, Indiana University, Bloomington, IN, USA

Jason L. Stein Imaging Genetics Center, University of Southern California, Los Angeles, CA, USA

Paul M. Thompson Imaging Genetics Center, University of Southern California, Los Angeles, CA, USA

Zoltán Toroczkai Department of Physics and Interdisciplinary Center for Network Science and Applications, University of Notre Dame, Notre Dame, IN, USA

Nathalie Tzourio-Mazoyer Institut des Maladies Neurodégénératives (IMN), CEA CNRS Université de Bordeaux, UMR 5293, GIN Team 5, Bordeaux, France

Wim Vanduffel Department of Neurosciences, Laboratory for Neuro-and Psychophysiology, KU Leuven Medical School, Leuven, Belgium

Harvard Medical School, Boston, MA, USA

Martinos Center for Biomedical Imaging, Massachusetts General Hospital, Charlestown, MA, USA

David C. Van Essen Anatomy and Neurobiology Department, Washington University School of Medicine, St. Louis, MO, USA

Nanoconnectomics

Terrence J. Sejnowski

Abstract The neuropil is a complicated 3D tangle of neural and glial processes. Recent advances in microconnectomics has made it possible to reconstruct neural circuits from serial-section electron microscopy at the micron scale. Electron microscopy allows even higher resolution reconstructions on the nanometer scale. Nanoconnectomic reconstructions approaching molecular resolution allow us to explore the topology of extracellular space and the precision with which synapses are modified by patterns of neural activity.

The reconstruction of a neural circuit is an essential step in understanding how signals are processed in the circuit; without this 'wiring diagram,' it is difficult to interpret the signals recorded from elements in the circuit. Connectomics attempts to reconstruct complete circuits, which can be accomplished at many spatial scales, as illustrated in Fig. 1. At the microconnectomic level, recent studies have focused on the retina (Kim et al., Nature 509:331–336, 2014) and the visual cortex (Bock et al., Nature 471:177–182, 2011). At the macroconnectomic level, the long-range cortical connections can be trace with diffusion tensor imaging (Van Essen, Neuron 80:775–790, 2013). This chapter will focus on nanoconnectomics, whose goal is to produce an accurate reconstruction of the neuropil at the nanometer scale.

Nanoconnectomics

At the level of nanometers, the neuropil is a tangled mass of synapses, dendrites, axons and glial cells surrounded by extracellular space. Each of these compartments contains specialized molecular structures for specialized functions and, in particular, those related to the processing of neural signals over a wide range of time

T.J. Sejnowski (✉)
Howard Hughes Medical Institute, The Salk Institute for Biological Studies, La Jolla, CA 92037, USA

Division of Biological Sciences, University of California at San Diego, La Jolla, CA 92093, USA
e-mail: terry@salk.edu

H. Kennedy et al. (eds.), *Micro-, Meso- and Macro-Connectomics of the Brain*, Research and Perspectives in Neurosciences, DOI 10.1007/978-3-319-27777-6_1

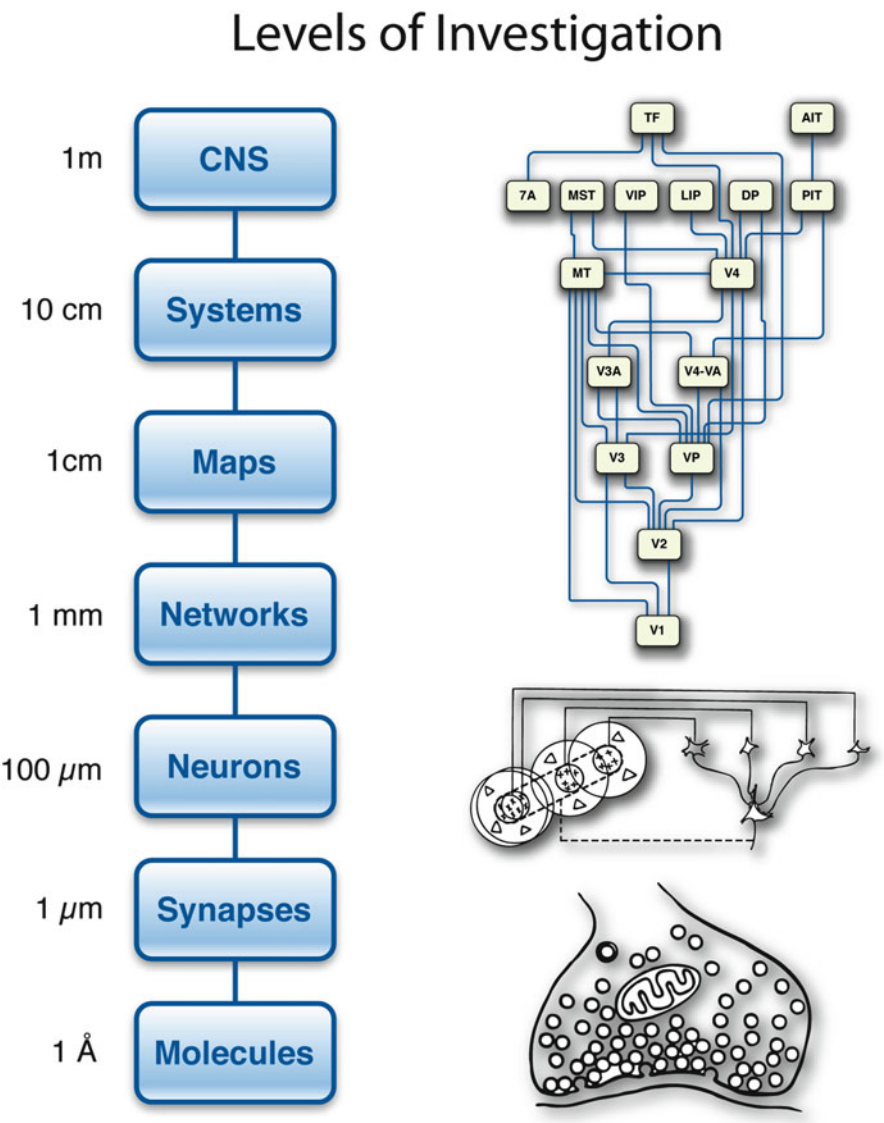

Fig. 1 Levels of investigation in the brain span 10 orders of spatial scale, from the molecular level to the entire central nervous system (CNS). Important structures and functions are found at each of these levels. Macroconnectomics provides the long-range connections between neurons in maps and systems, microconnectomics focuses on the network level, and nanoconnectomics extends down to synapses and molecules [adapted from Churchland and Sejnowski (1988)]

scales. We seek to reconstruct these compartments to understand the functions that are being implemented at the molecular level. Biochemistry is as important as electricity at these small spatial scales; at longer temporal scales beyond the second, biochemistry reigns supreme.

Biochemists typically carry out chemical reactions in test tubes, where the molecular reactants are well mixed and often in equilibrium. This approach makes spatial scales irrelevant, which is an advantage in measuring reaction rates and dissociation constants. In cells, however, strong concentration gradients exist on the nanoscale, and many important signaling pathways are not in equilibrium. Molecular signaling, such as the release of neurotransmitter at synapses or the entry of calcium into a dendritic spine, depends on changes in the concentration of the signaling molecules and is often transient, which may be on the microsecond time scale in nanovolumes and on much longer time scales in larger volumes.

Extracellular Space

To explore the consequences of transient neural signals in small volumes, a 3D $6 \times 6 \times 5\ \mu m^3$ reconstruction of hippocampal neuropil was created via serial section transmission electron microscopy of tissue obtained from the middle of stratum radiatum in CA1 of hippocampus in an adult male rat (Mishchenko et al. 2010; Kinney et al. 2013). Although this was a relatively small volume of neuropil, within it there were 446 axons, 449 synapses, 149 dendritic branches and a small part of a single astrocyte. In addition, we took special care to reconstruct the extracellular space, which is an important compartment that is often neglected in reconstructions. Our goals were accuracy and completeness in order to serve as a test-bed for Monte-Carlo simulations of molecular cell signaling. However, there is much to be learned by just looking at the anatomy.

Imagine that the extracellular space was itself a compartment with its own geometry. What would it look like? Despite its importance for brain function, the morphology of the extracellular space (ECS) on the submicron scale is largely unknown. The ECS is tens of nanometers in width based on electron microscopy (EM) images (Thorne and Nicholson 2006), below the resolution of light microscopy. However, in vivo measurements of the ECS are available for the extracellular volume fraction, which captures the fraction of total tissue volume that lies outside of cells and the total tortuosity that accounts for the observed reduction in rate of diffusion of small molecules through the ECS compared to free diffusion due to geometric inhomogeneities and interactions with the extracellular matrix (Sykova and Nicholson 2008). In early development, the extracellular volume fraction is 40 % and decreases with age (Fiala et al. 1998) and during periods of anoxia (Sykova and Nicholson 2008). The extracellular volume fraction in the adult rat hippocampus is 20 % and total tortuosity is 1.45, based on the diffusion of small probe molecules in the ECS (Nicholson and Phillips 1981).

The processing of tissue for EM involves dehydration that results in tissue shrinkage, which reduces the extracellular space. To compensate for a range of possible volume shrinkages and in vivo variations, we explored quantitatively the range of physiological geometries of the ECS by rescaling the reconstruction (along three orthogonal dimensions), and we varied its lacunarity or ratio of the largest to the smallest membrane separations (Kinney et al. 2013). The reconstruction

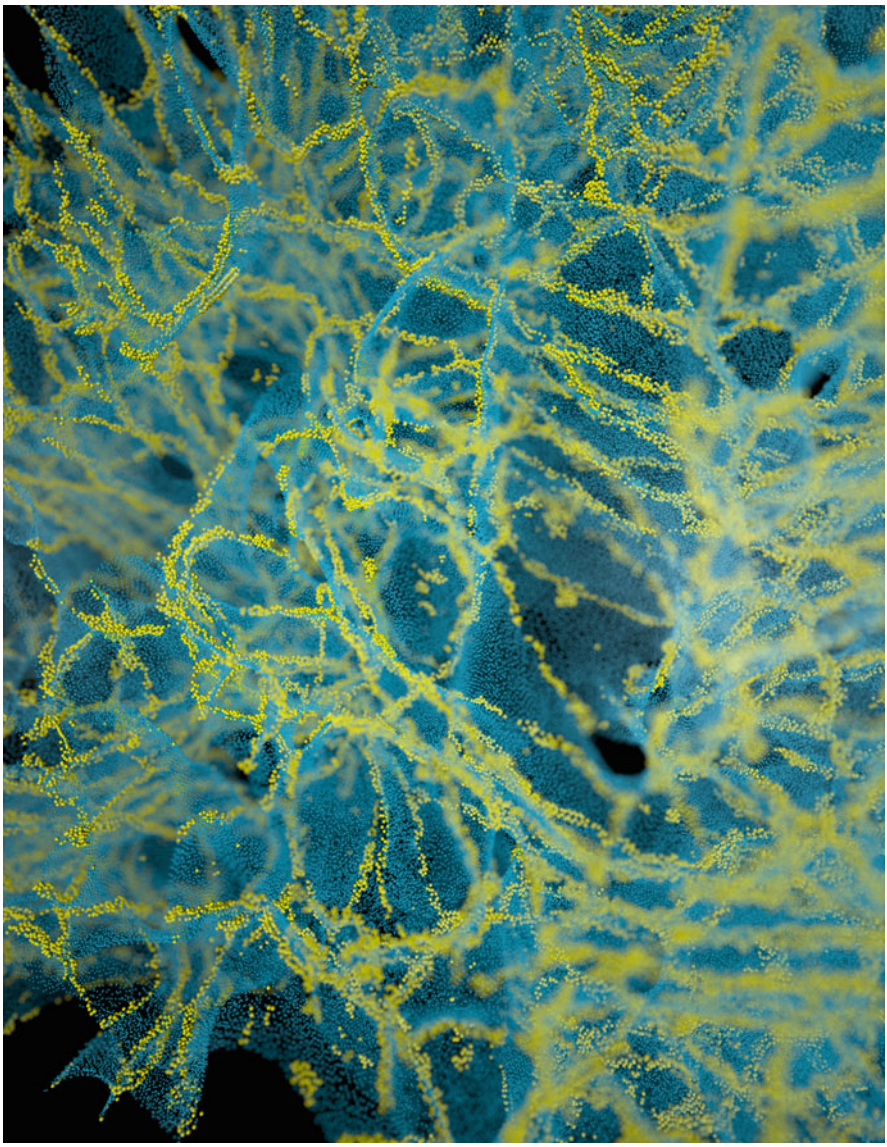

Fig. 2 Structure of the extracellular space between cells in the neuropil of the rat. In the reconstructed neuropil, 20–40-nm thick sheets (*blue dots*) separated pairs of cells and 40–80-nm tunnels occurred where three or more cells met (*yellow dots*). The topology of the extracellular space resembles that of soap bubbles [Justin Kinney]

revealed an interconnected network of 40–80-nm diameter tunnels, formed at the junction of three or more cellular processes and spanned by sheets between pairs of cell surfaces with 10–40 nm width. The tunnels tended to occur around synapses and axons, and the sheets were enriched around astrocytes. The intricate complexity of the ECS is shown in Fig. 2, which illustrates the geometry linking the sheets and

the tunnels. The non-uniformity found in the ECS may have specialized functions for signaling (sheets) and volume transmission (tunnels).

The ECS is a dynamic compartment and Fig. 2 should be considered a single snapshot. During sleep, for example, the extracellular volume increases by 60 %, allowing convective streaming to clear debris from the ECS (Xie et al. 2013).

Simulating Signaling in Small Spaces

Microdomains inside cells are small volumes, such as the femtoliter volumes of dendritic spines, in which concentrations of molecules can increase transiently and drive chemical reactions. We have simulated the transient release of neurotransmitters in the ECS and the entry of calcium into postsynaptic spines using MCell (mcell.org), a powerful and highly successful open source modeling tool for realistic simulation of cellular signaling in microdomains (Coggan et al. 2005; Nadkarni et al. 2012). At such small subcellular scales, macroscopic continuum assumptions do not apply and stochastic behavior dominates. MCell uses highly optimized Monte Carlo algorithms to track the stochastic behavior of discrete molecules in space and time as they diffuse and interact with other discrete effector molecules (e.g., ion channels, enzymes, transporters) heterogeneously distributed within the 3D geometry and on the 2D membrane surfaces of the subcellular environment. Monte Carlo methods are the best choice for reaction/diffusion simulation when the total number of interacting particles in a spatial domain is small, and/or when spatial particle gradients are steep. A further advantage of these methods is that, because individual particles are treated as reactive agents, reaction networks that exhibit combinatorial complexity can be described and simulated without simplification.

The postsynaptic density (PSD) in the active zone of a spine head contains hundreds of types of proteins in a large macromolecular complex. Because the PSD contains neurotransmitter receptors, the concentrations of ions in the PSD can transiently reach high concentrations briefly after receptor activation. For example, the volumes around voltage-dependent calcium channels are nanodomains, where calcium levels can reach concentrations that are several orders of magnitude higher than inside the spine (Tour et al. 2007). When calcium enters the spine head through NMDA receptors in the PSD, the calcium binds to calcium-binding proteins (Keller et al. 2008), which creates a strong gradient across the volume of the spine (Fig. 3). When calcium binds to calmodulin, one of the calcium-binding proteins, calmodulin can in turn bind to and activate calcium/calmodulin-dependent protein kinase II (CAMKII), which can lead to long-term potentiation of the synapse (Kennedy et al. 2005).

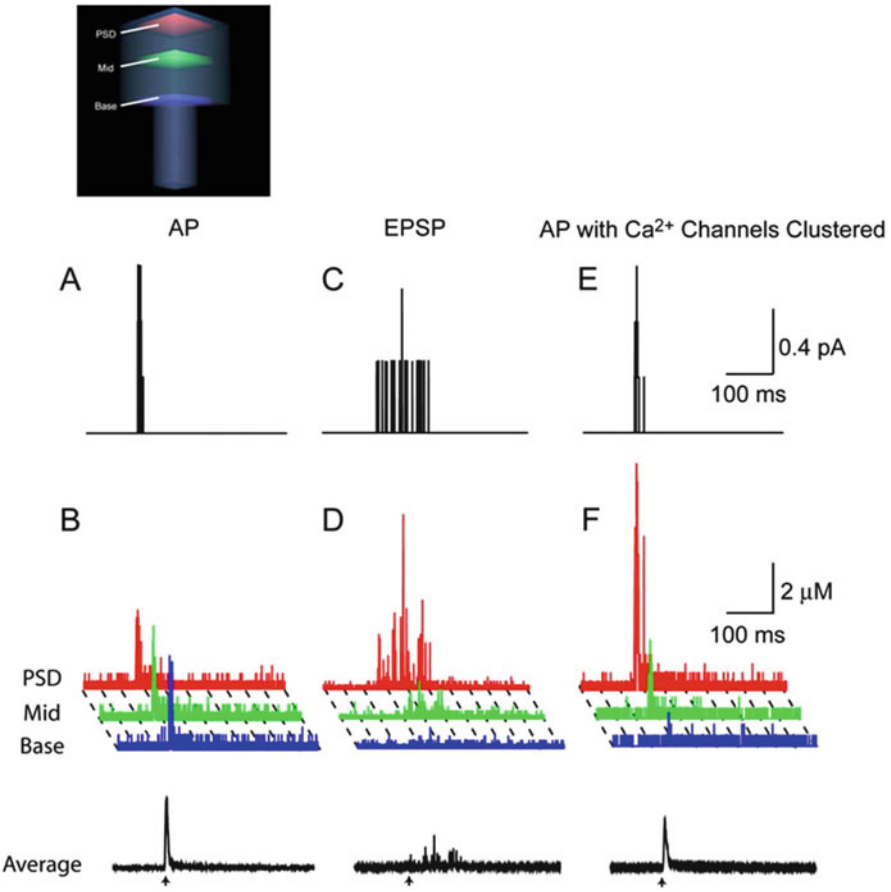

Fig. 3 Simulations of calcium entry into a spine and calcium gradients across the spine in the presence of 45 mM calbindin-D28k. Schematic (*upper left*) shows the spine subdivided into three distinct sampling regions: the postsynaptic density (PSD, *red*), the middle (MID, *green*), and the base (*blue*) of the spine. The volume averages are depicted below (*black*). (**a**) Instantaneous calcium current through voltage-dependent calcium channels in the spine during a back-propagating action potential (BAP). The time of somatic current injections is indicated by the *arrow*. (**b**) Calcium concentration in each of the three sampling regions is shown during the action potential. The colors of traces correspond to the three sampling regions shown in the schematic. Action potentials did not result in calcium gradients across the spine. The *black trace* at the *bottom* of the figure shows the volume-averaged $[Ca2+]_i$ in the entire spine. (**c**) Instantaneous calcium current through NMDARs during an excitatory postsynaptic potential. (**d**) Calcium concentration in each of the three subregions of the spine during an excitatory postsynaptic potential as well as the volume average. Excitatory postsynaptic potentials resulted in large calcium gradients across the spine. (**e**) Open voltage-dependent calcium channels during an action potential simulation in which voltage-dependent calcium channels were clustered at the postsynaptic density. (**f**) Input-dependent calcium gradients across the spine during the BAP when the calcium channels were clustered in the PSD [adapted from Keller et al. (2008)]

Precision of Synaptic Plasticity

Excitatory synapses on dendritic spines of hippocampal pyramidal neurons have a wide range of sizes that are highly correlated with their synapse strengths (Harris and Stevens 1989). Pairs of spines on the same dendrite that received input from the same axon were of the same size and had nearly identical head volumes (Fig. 4). When plotted against one another, the paired head volumes were highly correlated with slope 0.91 and, despite the small sample size, were significantly different from random pairings of spines. In contrast, the spine neck volumes of the pairs were not well correlated, suggesting a different function.

Spine heads ranged in size over a factor of 60 from smallest to largest, allowing approximately 24 different strengths to be reliably distinguished across this range,

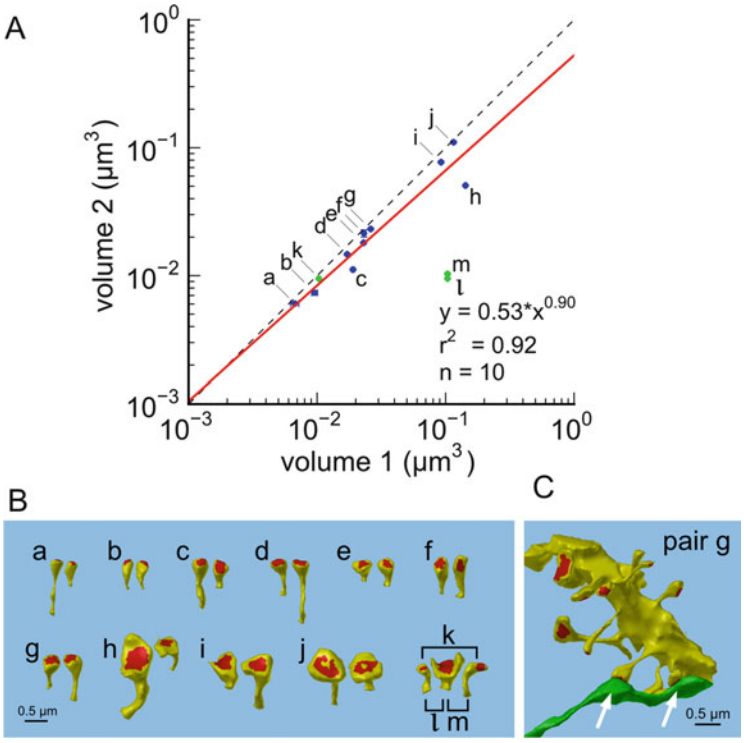

Fig. 4 Pairs of spines from the same axon on the same dendritic branch have highly correlated volumes. (**A**) Volumes of pairs of axonally coupled spines on the same dendritic branch plotted against one another (larger volumes on X axis, *blue* and *green* points, *error bars* show SEM). Labels a–m correspond to spine pairings in (**B**). Regression line of *blue points* is shown in *red*. *Green points* correspond to outlier pairings k, l, and m in (**b**). *Dashed diagonal line* represents line of perfect correlation. (**B**) Corresponding pairs of spines, isolated for visualization. (**C**) Example of a pair of axonally coupled spines on the same dendritic branch in situ. *White arrows* point to the spine heads [adapted from Bartol et al. (2015)]

assuming CV = 0.083 and a 75 % discrimination threshold. This corresponds to 4.6 bits of information that can be stored at each synapse (Bartol et al. 2015). The precision of the majority of smaller spines is as good as that of the minority larger spines (Fig. 4), suggesting that accurately maintaining the size of every synapse, regardless of size and strength, could be important for the function, flexibility and computational power of the hippocampus.

How can the high precision in spine head volume be achieved despite the many sources of stochastic variability observed in synaptic responses? Time-window averaging could smooth out fluctuations due to plasticity and other sources of variability. To set a lower bound on averaging time, we chose to examine neurotransmitter release probability as a single source of variability. Release can be analyzed using a binomial model in which n presynaptic action potentials, each with a probability p_r of releasing one or more vesicles, leads to a mean number of releases $m = n\ p_r$ having variance $\sigma^2 = n\ p_r\ (1-p_r)$. The coefficient of variation around the mean is $CV = sqrt(\sigma^2)/m = sqrt\ [(1-p_r)/(n\ p_r)]$ and can be compared with the measured values. Therefore, the number of spikes that are needed to reduce the variability to achieve a given CV is $n = (1-p_r)/(p_r\ CV^2)$. Table 1 gives averaging time windows for representative values of p_r and a range of spiking rates of the presynaptic axon, which extends to many minutes for the smaller synapses. Accounting for other known sources of variability at dendritic spines would require even longer time windows.

Phosphorylation of CaMKII, which is required for some forms of synaptic plasticity, integrates calcium signals over 10–20 min and is a critical step in enzyme cascades leading to structural changes induced by long-term potentiation (LTP) and long-term depression (LTD; Kennedy et al. 2005), including rearrangements of the cytoskeleton (Kramár et al. 2012). The time course over which CaMKII integrates calcium signals is within the range of time windows that we predict would be needed for averaging (Table 1). Similar time windows occur in synaptic tagging and capture: inputs that are too weak to trigger LTP or LTD can be "rescued" by a stronger input to neighboring synapses if it occurs within an hour (Frey and Morris 1997; O'Donnell and Sejnowski 2014), which also requires CaMKII (Redondo and Morris 2011; de Carvalho Myskiw et al. 2014).

The reconstruction that we have analyzed is a tiny part of the hippocampus, but if it is representative, then the precision with which the spatial organization of the brain is constructed is at the nanolevel. Thus, evolution has optimized many of the structures at synapses that are essential for the long-term storage of information.

Table 1 Lower bounds on time window for averaging binomially distributed synaptic input to achieve CV = 0.083

Release probability (p_r)	Presynaptic spikes (n)	Averaging time (Rate = 1 Hz)	Averaging time (Rate = 25 Hz)
0.1	1306	21.8 min	52.2 s
0.2	581	9.68 min	23.2 s
0.5	145	2.42 min	5.8 s

In conclusion, nanoconnectomics is revealing the extraordinary precision of synaptic plasticity and, together with Monte Carlo simulations of biochemical interaction and physiological responses, we can begin to see how the reactions between relatively small numbers of molecules in small volumes can accurately and efficiently create memories of past experiences.

Acknowledgments This research was supported by the Howard Hughes Medical Institute, the National Institutes of Health and the National Science Foundation. The neuropil reconstruction was a joint project with Kristen Harris, Chandra Bajaj and Justin Kinney and Thomas Bartol, Jr., who is the chief architect of MCell. Bartol, Mary Kennedy, Daniel Keller and Kevin Franks made important contributions to the simulations of calcium in spines heads.

References

Bartol TM, Bromer C, Kinney JP, Chirillo MA, Bourne JN, Harris KM, Sejnowski TJ (2015) Hippocampal spine head sizes are highly precise. BioRxiv. doi: http://dx.doi.org/10.1101/016329

Bock DD, Lee WC, Kerlin AM, Andermann ML, Hood G, Wetzel AW, Yurgenson S, Soucy ER, Kim HS, Reid RC (2011) Network anatomy and in vivo physiology of visual cortical neurons. Nature 471:177–182

Churchland PS, Sejnowski TJ (1988) Perspectives on cognitive neuroscience. Science 242:741–745

Coggan JS, Bartol TM, Esquenazi E, Stiles JR, Lamont S, Martone ME, Berg DK, Ellisman MH, Sejnowski TJ (2005) Evidence for ectopic neurotransmission at a neuronal synapse. Science 309:446–451

de Carvalho Myskiw J, Furini CRG, Benetti F, Izquierdo I (2014) Hippocampal molecular mechanisms involved in the enhancement of fear extinction caused by exposure to novelty. Proc Natl Acad Sci USA 111:4572–4577

Fiala JC, Feinberg M, Popov V, Harris KM (1998) Synaptogenesis via dendritic filopodia in developing hippocampal area CA1. J Neurosci 18:8900–8911

Frey U, Morris RGM (1997) Synaptic tagging and long-term potentiation. Nature 385:533–536

Harris KM, Stevens JK (1989) Dendritic spines of CA1 pyramidal cells in the rat hippocampus: serial electron microscopy with reference to their biophysical characteristics. J Neurosci 9:2982–2997

Keller DX, Franks KM, Bartol TM, Sejnowski TJ (2008) Calmodulin activation by calcium transients in the postsynaptic density of dendritic spines. PLoS ONE 3(4):e2045

Kennedy MB, Beale HC, Carlisle HJ, Washburn LR (2005) Integration of biochemical signalling in spines. Nat Rev Neurosci 6:423–434

Kim JS, Greene MJ, Zlateski A, Lee K, Richardson M, Turaga SC, Purcaro M, Balkam M, Robinson A, Behabadi BF, Campos M, Denk W, Seung HS, EyeWirers (2014) Space-time wiring specificity supports direction selectivity in the retina. Nature 509:331–336

Kinney JP, Spacek J, Bartol TM, Bajaj CL, Harris KM, Sejnowski TJ (2013) Extracellular sheets and tunnels modulate glutamate diffusion in hippocampal neuropil. J Comp Neurol 521:448–464

Kramár EA, Babayan AH, Gavin CF, Cox CD, Jafari M, Gall CM, Rumbaugh G, Lynch G (2012) Synaptic evidence for the efficacy of spaced learning. Proc Natl Acad Sci USA 109:5121–5126

Mishchenko Y, Hu T, Spacek J, Mendenhall J, Harris KM, Chklovskii DB (2010) Ultrastructural analysis of hippocampal neuropil from the connectomics perspective. Neuron 67:1009–1020

Nadkarni S, Bartol TM, Stevens CF, Sejnowski TJ, Levine H (2012) Short-term plasticity constrains spatial organization of a hippocampal presynaptic terminal. Proc Natl Acad Sci USA 109:14657–14662

Nicholson C, Phillips JM. (1981) Ion diffusion modified by tortuosity and volume fraction in the extracellular microenvironment of the rat cerebellum. J Physiol 321:225–257

O'Donnell C, Sejnowski TJ (2014) Selective memory generalization by spatial patterning of protein synthesis. Neuron 83:398–412

Redondo RL, Morris RGM (2011) Making memories last: the synaptic tagging and capture hypothesis. Nat Rev Neurosci 12(1):17–30

Sykova E, Nicholson C (2008) Diffusion in brain extracellular space. Physiol Rev 88:1277–1340

Thorne RG, Nicholson C (2006) In vivo diffusion analysis with quantum dots and dextrans predicts the width of brain extracellular space. Proc Natl Acad Sci USA 103:5567–5572

Tour O, Adams SR, Kerr RA, Meijer RM, Sejnowski TJ, Tsien RW (2007) Calcium-green-FlAsH: a genetically targeted small molecule calcium indicator. Nat Chem Biol 3:423–431

Van Essen DC (2013) Cartography and connectomes. Neuron 80:775–790

Xie L, Kang H, Xu Q, Chen MJ, Liao Y, Thiyagarajan M, O'Donnell J, Christensen DJ, Nicholson C, Iliff JJ, Takano T, Deane R, Nedergaard M (2013) Sleep drives metabolite clearance from the adult brain. Science 342:373–377

Inhibitory Cell Types, Circuits and Receptive Fields in Mouse Visual Cortex

Edward M. Callaway

Abstract The diversity and the specialized connectivity and function of inhibitory cortical neurons have been the focus of intense research for many decades (Fishell and Rudy, Ann Rev Neurosci 34:535–567, 2011). Until recently, technical limitations have restricted the power of experiments that could be conducted in vivo. Nevertheless, in vitro studies identified dozens of distinct cortical inhibitory neuron types, each with unique chemical properties, intrinsic firing properties and connection specificity. And at the same time, post-mortem studies from human patients have demonstrated defects of inhibitory circuit markers in diseases such as schizophrenia (Curley and Lewis, J Physiol 590:715–724, 2012; Stan and Lewis, Curr Pharm Biotech 13:1557–1562, 2012; Lewis, Curr Opin Neurobiol 26:22–26, 2014). Together, these observations have led to the hypothesis that distinct types of inhibitory neurons play distinct functional roles in the dynamic regulation of brain states and in the context-dependent extraction of sensory information, cognitive function, and behavioral output—functions thought to be disrupted in disorders such as schizophrenia and autism.

Despite the wealth of evidence in support of this hypothesis, tools have only recently emerged to allow detailed studies of neural circuit mechanisms underlying in vivo dynamics and to implicate specific inhibitory cell types and connections in specific functions (Luo et al., Neuron 57:634–660, 2008). Now, rather than broadly surveying inhibitory neuron properties and connections in vitro, studies have begun to focus more deeply on the in vivo contributions of those inhibitory cell types that are genetically accessible and can therefore be interrogated with modern genetic tools for manipulating and monitoring activity of specific cell types.

Mouse lines that express Cre-recombinase selectively in three major, non-overlapping groups of inhibitory cortical neurons—Parvalbumin-expressing (PV), somatostatin-expressing (SST), and vasoactive intestinal peptide-expressing (VIP; Lee et al., J Neurosci 30:16796–16808, 2010; Xu et al. J Comp Neurol 518:389–404, 2010; Rudy et al., J Comp Neurol 518:389–404, 2011; Taniguchi et al., J Comp Neurol 518:389–404, 2011)—have allowed detailed studies of the connectivity and in vivo functional roles of these cell groups. Such studies have

E.M. Callaway (✉)
The Salk Institute for Biological Studies, 10010 North Torrey Pines Road, La Jolla, CA 92037, USA
e-mail: callaway@salk.edu

H. Kennedy et al. (eds.), *Micro-, Meso- and Macro-Connectomics of the Brain*,
Research and Perspectives in Neurosciences, DOI 10.1007/978-3-319-27777-6_2

implicated PV inhibitory neurons in gain control (Atallah et al., Neuron 73:159–170, 2012; Lee et al., Nature 488:379–383, 2012; Nienborg et al., J Neurosci 33:11145–11154, 2013), SST interneurons in the suppression of lateral and feedback (top-down) interactions (Adesnik and Scanziani, Nature 464:1155–1160, 2010; Nienborg et al., J Neurosci 33:11145–11154, 2013), and VIP interneurons in the dynamic regulation of SST cells under the control of brain state-dependent neuromodulators (Kawaguchi, J Neurophysiol 78:1743–1747, 1997; Alitto and Dan, Front Syst Neurosci 6:79, 2012; Lee et al., Nat Neurosci 16:1662–1670, 2013; Pi et al., Nature 503:521–524, 2013; Polack et al., Nat Neurosci 16:1331–1339, 2013; Fu et al., Cell 156:1139–1152, 2014; Stryker, Cold Spring Harbor Symp Quant Biol 79:1–9, 2014; Zhang et al., Science 345:660–665, 2014).

Differences in Connectivity, Visual Responses and Functional Impact of PV Versus SST Interneurons

The in vivo functional role of any given neuron type is dictated by it sources of inputs, the way that it integrates those inputs, and the other neurons in the network to which it provides outputs. These differences result in measurable differences in visual receptive fields and differences in functional impact that can be assayed to understand how networks of neurons work together to generate perception and behavior.

Differential Outputs and Inputs Among the first differences observed between SST and PV interneurons were morphological differences related to the locations of their synaptic contacts onto excitatory pyramidal neurons. The great majority of PV neurons are basket cells, so named because their axon terminals have the appearance of baskets. Basket cells make multiple, large synapses on the proximal dendrites and cell bodies of pyramidal neurons (Jones and Hendry 1984) and, therefore, even the connections originating from a single neuron may profoundly influence the activity of a recipient pyramid (Tamas et al. 2000, 2004). The typical basket cell expresses PV and is fast-spiking (FS; Cauli et al. 1997; Gonchar and Burkhalter 1997; Kawaguchi and Kubota 1997). FS basket cells are the most common inhibitory cell type and comprise about half of all cortical inhibitory neurons. In contrast, SST interneurons are dendrite targeting and most are "Martinotti cells" (Kawaguchi and Kubota 1997; Wang et al. 2004; Xu and Callaway 2009). Martinotti cells are regular spiking and have axons that typically extend to layer 1, where they make connections onto the apical dendrites of pyramidal cells. This observation led to the suggestion that Martinotti cells selectively inhibit excitatory inputs that impinge on the apical tufts of pyramids. This hypothesis was first suggested with respect to Martinotti cells in the hippocampus (Somogyi et al. 1998) where they might selectively influence input from the perforant path versus the Schaeffer collaterals that selectively target the corresponding regions of CA1 pyramidal neurons. In the cortex, however, there is

a much more diverse population of excitatory neurons of both pyramidal and spiny stellate morphology, situated across multiple cortical layers. There are also diverse sources of excitatory input onto apical dendritic tufts. Nevertheless, prominent sources of input to the apical tufts of neocortical pyramidal neurons include feedback connections from other cortical areas as well as local lateral axonal arbors of other pyramidal neurons. These observations contributed to early hypotheses that SST-expressing Martinotti cells might preferentially regulate feedback and lateral influences, as tested in experiments described below. Taken together, even the earliest observations of differences in the outputs of PV versus SST interneurons suggested that PV-expressing basket cells have a global influence on pyramidal neurons whereas SST-expressing Martinotti cells have a more selective influence on inputs to apical dendrites.

PV and SST cells also differ in their sources of input. While PV cells in superficial cortical layers receive strong feedforward excitatory input from layer 4, as well as recurrent connections from within layer 2/3, excitatory inputs to SST neurons are dominated by layer 2/3 (Dantzker and Callaway 2000; Xu and Callaway 2009; Adesnik et al. 2012). Further exploration of the excitatory inputs to SST neurons shows that they collect local input over a longer lateral extent than pyramidal neurons, but PV neurons were not explored (Adesnik et al. 2012). Inhibitory inputs to PV neurons arise predominantly from layer 2/3 whereas SST cells receive more balanced inhibition from layers 2/3 and 4 as well as layer 5 (Xu and Callaway 2009).

Visual Responses Because PV neurons are FS cells, they can be identified during extracellular recordings in vivo. This ability has allowed their visual responses to be measured in diverse species, including ferrets, cats, and monkeys and mice. However, observations of the visual responses of SST neurons have only been described in mice, where they can be targeted genetically. In general, both PV and SST neurons appear to have visual responses that reflect the combined responses of their surrounding excitatory neurons. Thus, in species that have orientation columns, PV neurons have orientation-selective visual receptive fields. However, in mice, which lack orientation columns, PV and SST neurons are generally not orientation selective (Kerlin et al. 2010), apparently due to the indiscriminate collection of excitatory inputs from orientation-selective excitatory neurons that are tuned to a diversity of orientations. This connectional scheme fits with the functional role of PV neurons in providing gain control (see below). By monitoring the activity of its neighboring excitatory neurons, a PV neuron will increase its activity when the local network is most active and then provide feedback inhibition to keep activity levels under control. An important visual response feature that appears to be unique to SST cells, however, is that their visual responses increase in magnitude as the radius of a drifting grating stimulus increases (surround summation; Adesnik et al. 2012). More typical cells, including PV cells and excitatory neurons, instead display surround suppression (Adesnik et al. 2012). This feature of SST cells appears to be a consequence of the prominent lateral inputs that these neurons receive (see above) and has led to the hypothesis that they are the neurons

responsible for generating surround suppression in other cell types (see further details below; Adesnik et al. 2012).

Functional Impact The advent or Cre-driver mice combined with optogenetic tools has allowed direct tests of the functional impact of SST and PV neurons on visual responses. These experiments have demonstrated the importance of PV neurons in gain control and SST neurons in mediating surround influences. As expected, optogenetic activation of either inhibitory cell type results in decreased activity within the local cortical network, and such decreases are most prominent when PV cells are activated. For PV neurons, optogenetic activation decreases visual responses of excitatory neurons without altering their orientation tuning (Atallah et al. 2012; Lee et al. 2012). And when neurons are tested with visual stimuli of increasing radius, PV neuron activation mimics the effects of reducing the contrast of the visual stimulus; surround summation is observed rather than surround suppression (Nienborg et al. 2013). All of these effects indicate linear influences of PV cells and point to their role in controlling gain.

The functional influence of SST neurons, on the other hand, is non-linear. The classic feature of "end-stopping" in cortical neurons (Hubel and Wiesel 1968) is now better known as surround suppression. Here a visual stimulus presented in a zone that does not by itself generate any visual response in the subject neuron (outside the classical receptive field) can suppress the response to a stimulus within the classical receptive field. This interaction is clearly non-linear in that the response to the combined stimuli does not reflect the sum of the responses to the stimuli when they are presented separately. Optogenetic activation of SST neurons increases surround suppression in anesthetized animals where suppression is typically weak (Nienborg et al. 2013), and optogenetic inactivation of SST cells reduces surround suppression (Adesnik et al. 2012). Therefore, SST cells clearly contribute to the generation of surround suppression. It should be noted, however, that surround suppression is also present in the input to the cortex and this suppression is not prevented by cortical inactivation (Sceniak et al. 2006). Furthermore, inactivation of SST cells does not completely eliminate surround suppression of cortical neurons (Adesnik et al. 2012). Thus SST cells are likely responsible for cortical contributions to surround suppression but cannot be responsible for the suppression observed in the LGN input.

Calretinin (CR) and VIP-Expressing Interneurons Target SST Interneurons

Historically, the first study to implicate a specific type of cortical inhibitory neuron in local dis-inhibition was published by Meskenaite in 1997. This manuscript combined electron microscopy (EM) and antibody staining to show that CR-positive axon terminals in layer 2/3 of monkey V1 made 81 % of their contacts onto GABAergic neurons, but in layer 5 only 20 % of the contacts were onto

GABAergic neurons. The remaining 80 % of contacts in layer 5 were onto pyramidal neurons, where they formed strong basket-like synapses. Furthermore, these contacts appeared to be biased toward large layer 5 pyramids (that project sub-cortically and lack local projections to layer 2/3) rather than small pyramids (that make dense recurrent projections to layer 2/3 and lack extrinsic projections in primate V1; Callaway and Wiser 1996). Meskenaite suggested that "the CR-immunoreactive neurons appear to have a dual function of disinhibiting superficial layer neurons and inhibiting pyramidal output neurons in the deep layers." Meskenaite's findings were closely followed by analogous EM experiments in the rat visual cortex, showing a similar trend for CR+ axon terminals targeting inhibitory neurons in layer 2/3 and pyramids in layer 5 (Gonchar and Burkhalter 1999).

In view of this evidence, why is it that recent studies of disinhibition in layer 2/3 of mouse cortex have focused on VIP inhibitory neurons rather than CR neurons? Prior to the emergence of the mouse as the most prevalent rodent model, studies in rats had shown that PV, SST, and CR neurons make up three distinct and non-overlapping cell groups in that species (Kawaguchi and Kondo 2002). Similar antibody-labeling studies conducted in mice revealed that there was substantial overlap between CR and SST expression (Xu et al. 2006), but that there was no comparable overlap between VIP and SST (Xu et al. 2010). Thus, when Cre driver lines became available to separately target gene expression to PV, SST, VIP, or CR neurons (Taniguchi et al. 2011), VIP was favored over CR because of the ability to target a population that was separate from PV or SST neurons. Studies of VIP neurons have so far proceeded without concern for the known diversity of VIP cell types, and the grouping of these cells into a monolithic population has appeared to be justified by the striking differences in the connectivity and functional impact of these cells when compared to PV or SST cells (Lee et al. 2013; Pfeffer et al. 2013).

However, it was already predictable from the published literature (Xu et al. 2006; Caputi et al. 2009) that the CR-expressing subpopulation of VIP neurons preferentially targets SST cells in layer 2/3 of mouse. Caputi et al. (2009) produced and studied a mouse line in which GFP was expressed in CR neurons. They conducted extensive paired recordings to evaluate the rate of connectivity between numerous cell types, primarily focusing on the GFP-positive CR neurons. They noted that there were two types of CR/GFP neurons in their material, bipolar and multipolar. Remarkably, they found that the bipolar neurons had an astounding 76.4 % rate of connectivity (13/17 pairs) onto the multipolar neurons in layer 2/3 but made connections far less frequently onto layer 2/3 pyramids (11.6 %, 7 of 60). Connections from layer 2/3 to layer 5 were not assessed in this study. While Caputi et al. appeared not to appreciate it at the time, reporting the most salient observations only in a table, the published literature clearly showed that their multipolar GFP neurons are SST-expressing Martinotti cells, whereas their bipolar cells are CR positive and SST negative (Xu et al. 2006). Thus, it is apparent that mouse CR bipolar cells preferentially target SST neurons in layer 2/3. In this context, it is not entirely surprising that later studies systematically investigating the connectivity of PV, SST and VIP neurons found strong connections from VIP neurons onto SST neurons in layer 2/3 and not in layer 5 (Lee et al. 2013; Pfeffer et al. 2013). It remains unclear

whether this is a feature of all VIP interneurons or only of the CR-expressing subpopulation. Nevertheless, it would be surprising if there were not differences in the connectivity and function of CR-positive versus CR-negative VIP interneurons.

Functional Impact of VIP Interneurons

Based on the preferential connections of VIP neurons onto SST neurons, it is natural to predict that VIP neurons selectively regulate the impact of SST cells. For example, conditions that increase VIP neuron activity might be expected to inhibit SST cells, allowing greater influence from the lateral and feedback excitatory connections that target the apical tufts of pyramidal neurons. On the other hand, if the population of VIP neurons is diverse, the effects of manipulating these cells might be less predictable.

Recent studies have demonstrated that VIP neurons in mouse visual cortex are engaged during locomotion, apparently through a mechanism involving locomotion-induced increases in cholinergic input to the cortex (Fu et al. 2014; Reimer et al. 2014; Stryker 2014). However, rather than simply decreasing the activity of SST neurons, locomotion appears to have diverse effects (Polack et al. 2013; Reimer et al. 2014). These discrepancies might be related to the diversity of VIP neurons or could be attributable to other unknown differences in experimental methods. It is likely, however, that further dissection of the VIP neuron population using intersectional genetic methods will help to resolve these issues.

References

Adesnik H, Scanziani M (2010) Lateral competition for cortical space by layer-specific horizontal circuits. Nature 464:1155–1160

Adesnik H, Bruns W, Taniguchi H, Huang ZJ, Scanziani M (2012) A neural circuit for spatial summation in visual cortex. Nature 490:226–231

Alitto HJ, Dan Y (2012) Cell-type-specific modulation of neocortical activity by basal forebrain input. Front Syst Neurosci 6:79

Atallah BV, Bruns W, Carandini M, Scanziani M (2012) Parvalbumin-expressing interneurons linearly transform cortical responses to visual stimuli. Neuron 73:159–170

Callaway EM, Wiser AK (1996) Contributions of individual layer 2-5 spiny neurons to local circuits in macaque primary visual cortex. Vis Neurosci 13:907–922

Caputi A, Rozov A, Blatow M, Monyer H (2009) Two calretinin-positive GABAergic cell types in layer 2/3 of the mouse neocortex provide different forms of inhibition. Cereb Cortex 19: 1345–1359

Cauli B, Audinat E, Lambolez B, Angulo MC, Ropert N, Tsuzuki K, Hestrin S, Rossier J (1997) Molecular and physiological diversity of cortical nonpyramidal cells. J Neurosci 17: 3894–3906

Curley AA, Lewis DA (2012) Cortical basket cell dysfunction in schizophrenia. J Physiol 590: 715–724

Dantzker JL, Callaway EM (2000) Laminar sources of synaptic input to cortical inhibitory interneurons and pyramidal neurons. Nat Neurosci 3:701–707

Fishell G, Rudy B (2011) Mechanisms of inhibition within the telencephalon: "where the wild things are". Annu Rev Neurosci 34:535–567

Fu Y, Tucciarone JM, Espinosa JS, Sheng N, Darcy DP, Nicoll RA, Huang ZJ, Stryker MP (2014) A cortical circuit for gain control by behavioral state. Cell 156:1139–1152

Gonchar Y, Burkhalter A (1997) Three distinct families of GABAergic neurons in rat visual cortex. Cereb Cortex 7:347–358

Gonchar Y, Burkhalter A (1999) Connectivity of GABAergic calretinin-immunoreactive neurons in rat primary visual cortex. Cereb Cortex 9:683–696

Hubel DH, Wiesel TN (1968) Receptive fields and functional architecture of monkey striate cortex. J Physiol 195:215–243

Jones EG, Hendry SHC (1984) Basket cells. In: Peters A, Jones EG (eds) Cerebral cortex. Plenum, New York, pp 309–336

Kawaguchi Y (1997) Selective cholinergic modulation of cortical GABAergic cell subtypes. J Neurophysiol 78:1743–1747

Kawaguchi Y, Kondo S (2002) Parvalbumin, somatostatin and cholecystokinin as chemical markers for specific GABAergic interneuron types in the rat frontal cortex. J Neurocytol 31:277–287

Kawaguchi Y, Kubota Y (1997) GABAergic cell subtypes and their synaptic connections in rat frontal cortex. Cereb Cortex 7:476–486

Kerlin AM, Andermann ML, Berezovskii VK, Reid RC (2010) Broadly tuned response properties of diverse inhibitory neuron subtypes in mouse visual cortex. Neuron 67:858–871

Lee S, Hjerling-Leffler J, Zagha E, Fishell G, Rudy B (2010) The largest group of superficial neocortical GABAergic interneurons expresses ionotropic serotonin receptors. J Neurosci 30: 16796–16808

Lee SH, Kwan AC, Zhang S, Phoumthipphavong V, Flannery JG, Masmanidis SC, Taniguchi H, Huang ZJ, Zhang F, Boyden ES, Deisseroth K, Dan Y (2012) Activation of specific interneurons improves V1 feature selectivity and visual perception. Nature 488:379–383

Lee S, Kruglikov I, Huang ZJ, Fishell G, Rudy B (2013) A disinhibitory circuit mediates motor integration in the somatosensory cortex. Nat Neurosci 16:1662–1670

Lewis DA (2014) Inhibitory neurons in human cortical circuits: substrate for cognitive dysfunction in schizophrenia. Curr Opin Neurobiol 26:22–26

Luo L, Callaway EM, Svoboda K (2008) Genetic dissection of neural circuits. Neuron 57:634–660

Meskenaite V (1997) Calretinin-immunoreactive local circuit neurons in area 17 of the cynomolgus monkey, *Macaca fascicularis*. J Comp Neurol 379:113–132

Nienborg H, Hasenstaub A, Nauhaus I, Taniguchi H, Huang ZJ, Callaway EM (2013) Contrast dependence and differential contributions from somatostatin- and parvalbumin-expressing neurons to spatial integration in mouse V1. J Neurosci 33:11145–11154

Pfeffer CK, Xue M, He M, Huang ZJ, Scanziani M (2013) Inhibition of inhibition in visual cortex: the logic of connections between molecularly distinct interneurons. Nat Neurosci 16: 1068–1076

Pi HJ, Hangya B, Kvitsiani D, Sanders JI, Huang ZJ, Kepecs A (2013) Cortical interneurons that specialize in disinhibitory control. Nature 503:521–524

Polack PO, Friedman J, Golshani P (2013) Cellular mechanisms of brain state-dependent gain modulation in visual cortex. Nat Neurosci 16:1331–1339

Reimer J, Froudarakis E, Cadwell CR, Yatsenko D, Denfield GH, Tolias AS (2014) Pupil fluctuations track fast switching of cortical states during quiet wakefulness. Neuron 84: 355–362

Rudy B, Fishell G, Lee S, Hjerling-Leffler J (2011) Three groups of interneurons account for nearly 100 % of neocortical GABAergic neurons. Dev Neurobiol 71:45–61

Sceniak MP, Chatterjee S, Callaway EM (2006) Visual spatial summation in macaque geniculocortical afferents. J Neurophysiol 96:3474–3484

Somogyi P, Tamas G, Lujan R, Buhl EH (1998) Salient features of synaptic organisation in the cerebral cortex. Brain Res Brain Res Rev 26:113–135

Stan AD, Lewis DA (2012) Altered cortical GABA neurotransmission in schizophrenia: insights into novel therapeutic strategies. Curr Pharm Biotechnol 13:1557–1562

Stryker MP (2014) A neural circuit that controls cortical state, plasticity, and the gain of sensory responses in mouse. Cold Spring Harb Symp Quant Biol 79:1–9

Tamas G, Buhl EH, Lorincz A, Somogyi P (2000) Proximally targeted GABAergic synapses and gap junctions synchronize cortical interneurons. Nat Neurosci 3:366–371

Tamas G, Szabadics J, Lorincz A, Somogyi P (2004) Input and frequency-specific entrainment of postsynaptic firing by IPSPs of perisomatic or dendritic origin. Eur J Neurosci 20:2681–2690

Taniguchi H, He M, Wu P, Kim S, Paik R, Sugino K, Kvitsiani D, Fu Y, Lu J, Lin Y, Miyoshi G, Shima Y, Fishell G, Nelson SB, Huang ZJ (2011) A resource of Cre driver lines for genetic targeting of GABAergic neurons in cerebral cortex. Neuron 71:995–1013

Wang Y, Toledo-Rodriguez M, Gupta A, Wu C, Silberberg G, Luo J, Markram H (2004) Anatomical, physiological and molecular properties of Martinotti cells in the somatosensory cortex of the juvenile rat. J Physiol 561:65–90

Xu X, Callaway EM (2009) Laminar specificity of functional input to distinct types of inhibitory cortical neurons. J Neurosci 29:70–85

Xu X, Roby KD, Callaway EM (2006) Mouse cortical inhibitory neuron type that coexpresses somatostatin and calretinin. J Comp Neurol 499:144–160

Xu X, Roby KD, Callaway EM (2010) Immunochemical characterization of inhibitory mouse cortical neurons: three chemically distinct classes of inhibitory cells. J Comp Neurol 518: 389–404

Zhang S, Xu M, Kamigaki T, Hoang Do JP, Chang WC, Jenvay S, Miyamichi K, Luo L, Dan Y (2014) Selective attention. Long-range and local circuits for top-down modulation of visual cortex processing. Science 345:660–665

Form Meets Function in the Brain: Observing the Activity and Structure of Specific Neural Connections

Karl Deisseroth

Abstract Recent advances in neuroscience have enabled increasingly detailed insight into the activity and structure of brain circuitry. In previous work, we have developed and applied methods for precisely controlling the activity of specific cells and projections within neural systems during behavior (optogenetics). Here I review distinct complementary technological approaches for observing natural activity patterns in these cells and projections during behavior (fiber photometry) and for obtaining anatomical insights into the wiring and molecular phenotype of these circuit elements within the intact mammalian brain (CLARITY-optimized lightsheet microscopy). Together these approaches may help further advance understanding of the circuit dynamics and wiring patterns that underlie adaptive and maladaptive behavior.

Introduction

As we and others have noted (Tomer et al. 2014), a goal of modern neuroscience is to map neural circuits with wiring-level resolution, with brainwide perspective, and with knowledge of the natural and causal activity patterns occurring in these circuits in the context of behavior. Principles fundamental to the understanding of neural systems could result from such an integrative approach, but while progress has been made, many challenges and opportunities remain. Here I review our recent efforts to develop a recording technique sensitive enough to track the real-time dynamics of genetically and topologically specified subsets of neuronal projections in freely moving mice for direct in vivo measurement of a previously inaccessible variable: the coordinated activity of neuronal afferents projecting to a particular downstream target in the brain of a behaving animal (Gunaydin et al. 2014). Complementing this technology for the observation of natural behaviorally evoked

K. Deisseroth (✉)
Departments of Bioengineering and Psychiatry, Howard Hughes Medical Institute, Stanford University, 318 Campus Drive West, Clark Center W080, Stanford, CA 94305, USA
e-mail: deissero@stanford.edu

H. Kennedy et al. (eds.), *Micro-, Meso- and Macro-Connectomics of the Brain*, Research and Perspectives in Neurosciences, DOI 10.1007/978-3-319-27777-6_3

activity patterns, I review rapid light-sheet microscopy methods for the efficient collection of high-resolution anatomical information within mammalian brains that have been made transparent to light (and permeable to macromolecular labels) with the CLARITY technology (Tomer et al. 2014). These two technologies can be employed alongside optogenetic tools that, in turn, can define the causal roles of these same projections in modulating behavior.

CLARITY

As we have described (Tomer et al. 2014), circuit wiring questions have attracted attention from generations of scientists, beginning with Cajal's detailed representations of neurons visualized at high resolution with the Golgi staining technique while still embedded within semi-intact brain tissue. Over the last few decades, electron microscopy (EM) has emerged as a foundational method for deciphering details of neuronal circuit structure (Bock et al. 2011; Briggman et al. 2011). The key advantage of EM in this regard (relative to light microscopy) is identification of the presynaptic active zones containing neurotransmitter vesicles apposed to postsynaptic structures. In addition, EM facilitates visualization of some of the very finest branches of axons. However, EM tissue mapping requires relatively slow steps involving ultrathin sectioning/ablation and reconstruction; most importantly, the sample contrast preparation is largely incompatible with rich molecular phenotyping that could provide critical information on cell and synapse type. Ideally, datasets resulting from intact-brain mapping should be linkable to molecular information on the types of cells and synapses that are imaged structurally and even to dynamical information on natural activity pattern history (in these same circuits) known to be causally relevant to animal behavior. Suitable light-based imaging approaches, combined with specific genetic or histochemical molecular labeling methods, have emerged as important tools to visualize the structural, molecular and functional architecture of biological tissues, with a particularly vital role to play in emerging brainwide, high-resolution neuroanatomy.

Confocal methods revolutionized light microscopy by enabling optical sectioning in thick (tens of micrometers) fluorescently labeled samples, thereby allowing 3D reconstruction without the need for ultrathin physical sectioning (Conchello and Lichtman 2005). Two-photon microscopy further increased the accessible imaging depth (to hundreds of micrometers) even in living tissue samples (Helmchen and Denk 2005), and adaptive-optics approaches have improved imaging depth further (Tang et al. 2012). However, light microscopy remains limited for imaging throughout intact vertebrate nervous systems (for example, mouse brains span many millimeters even in the shortest spatial dimension and are opaque on this scale, due chiefly to light scattering). A common work-around to this limitation has been to slice brains into thin sections, in manual or automated fashion, followed by confocal or two-photon imaging (Micheva et al. 2010; Ragan et al. 2012); however, detailed labeling and reconstruction from thin sections have been (so far) limited to

small volumes of tissue. An ideal integrative approach would be to label and image entirely intact vertebrate brains at high resolution.

As a step in this direction, new methods have emerged to increase tissue transparency (Dodt et al. 2007; Hama et al. 2011; Ke et al. 2013) by chemically reducing the scattering of light travelling through the tissue sample. While intriguing and effective, these approaches are not generally suitable for detailed molecular phenotyping, since most tissues (such as the intact mature brain) remain largely impenetrable to macromolecular antibody or oligonucleotide labels (Kim et al. 2013). In cases where pieces of soft tissue such as mammary glands can be stained using hydrophobic clearing solutions that reduce lipid barriers to antibody labeling (Ertürk et al. 2012), fluorophores become highly unstable or quenched in the clearing process (a step that nevertheless must follow the antibody-staining phase, as transparency is otherwise lost; Ertürk et al. 2012). These limitations motivated the recent development of CLARITY (Chung et al. 2013; Kim et al. 2013), which involves removal of lipids in a stable hydrophilic chemical environment to achieve transparency of intact tissue, preservation of ultrastructure and fluorescence, and accessibility of native biomolecular content to antibody and nucleic acid probes. Subsequent screens for diverse hydrophilic lipid solubilization compounds have been productive and can be integrated with CLARITY (Susaki et al. 2014). The CLARITY technical platform enables multiple rounds of molecular, structural and activity-history interrogation throughout intact adult mammalian brains, which is relevant not only for neuroscience but also for research into any intact biological system.

Clarifying Large Tissue Volumes

CLARITY (Chung et al. 2013) builds upon chemical principles to grow hydrogel polymers from inside the tissue to provide a support framework for structural and biomolecular content (Fig. 1). This is achieved first by infusing a cold (4 °C) cocktail of hydrogel monomers (for example, acrylamide with bisacrylamide, but other types of monomers may also be used; Chung et al. 2013), formaldehyde, and thermally triggered initiators into the tissue, followed by polymerization of the hydrogel at 37 °C. Formaldehyde serves the dual purposes of cross-linking amine-containing tissue components to each other and covalently binding the hydrogel monomers to these native biomolecules, which include proteins, nucleic acids and other small molecules but not the vast majority of cellular membrane phospholipids. After the hydrogel polymerization is triggered, lipids (responsible for preventing access of both photons and molecular labels to deep structures) can then be readily removed without destroying or losing native tissue components using strong ionic detergent-based clearing solution (borate-buffered 4 % sodium-dodecyl-sulfate) at 37 °C, either passively with gentle recirculation or with active electrophoretic forcing (the latter greatly accelerates clearing but introduces some experimental complexity and risk). The resulting lipid-extracted and structurally

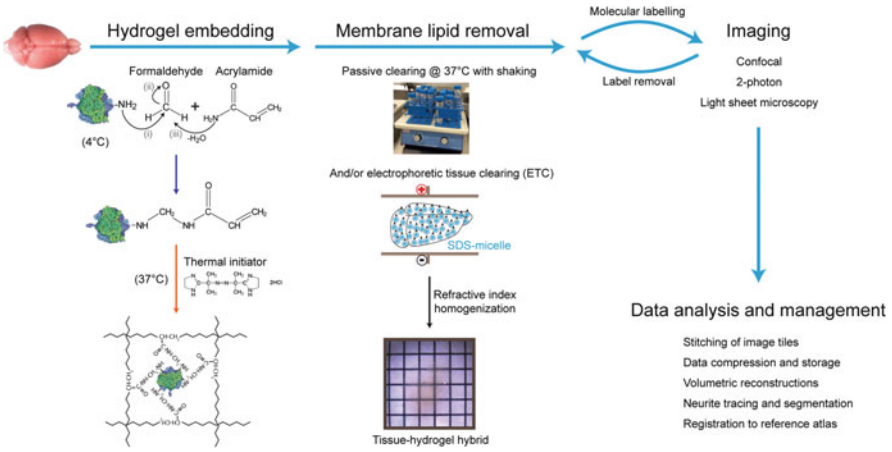

Fig. 1 CLARITY pipeline overview. The tissue sample, e.g. an intact mouse brain, is perfused with cold hydrogel monomer solution that contains a cocktail of acrylamide, bisacrylamide, formaldehyde and thermal initiator. Formaldehyde mediates crosslinking of biomolecules to acrylamide monomers via amine groups; the presumptive chemistry of this process is shown. Hydrogel polymerization is initiated by incubating the perfused tissue at 37 °C, resulting in a meshwork of fibers that preserves biomolecules and the structural integrity of the tissue. Lipid membranes are removed by passive thermal clearing in SBC solution at 37 °C or by electrophoretic tissue clearing (ETC). The resulting intact tissue-hydrogel hybrid can undergo multiple rounds of molecular and structural interrogation using immunohistochemistry and light microscopy. A dedicated computational infrastructure is needed to analyze and store the data. Figure and text adapted from Tomer et al. (2014)

stable tissue-hydrogel hybrid is immersed in a refractive index homogenization solution to render the intact brain transparent to light (Chung et al. 2013).

An additional feature of the stable hydrogel-tissue hybrid is that it can be subjected to multiple rounds of molecular interrogation (Chung et al. 2013). Typically, immunohistochemistry methods only allow investigation of two to three biomarkers at once in a tissue sample, but more simultaneous labels are required to define cells in terms of precise molecular/genetic identity, wiring, and activity history. This limitation is traditionally approached by combining information from multiple samples into a standard reference atlas. However, this strategy fails to fully phenotype individual cells, cannot capture the joint statistics among the different kinds of labels within a single preparation, and suffers from 3D alignment artefacts and variability among different individual tissue samples. By allowing multiple rounds of histochemical labeling and elution in the same tissue, CLARITY provides unusually rich access to molecular and structural information (Chung et al. 2013).

This extensive lipid removal intrinsic to CLARITY appears to be essential not only for transparency but also for achieving efficient antibody penetration throughout intact brains; this stringent de-lipidation would normally be a destructive process causing extensive loss of biological molecules (Chung et al. 2013), but it

is enabled by the hydrophilic hydrogel-tissue hybrid in a way that also preserves fine processes and ultrastructure even over multiple rounds of staining and elution (Chung et al. 2013). Many variations are possible and will continue to be explored; the "CUBIC" screen (Susaki et al. 2014) recently provided an intriguing diversity of additional hydrophilic lipid solubilization reagents, including aminoalcohols that can be used in CLARITY protocols (Susaki et al. 2014), though it was noted that the aminoalcohol incubation leaves behind significant lipid content in the tissue (Susaki et al. 2014), such that lipid-rich structures including white matter remain partially opaque. Also, the approach may not allow antibody penetration for molecular labeling and resolution of fine processes deeper than 0.5–0.8 mm into mature brain tissue (Susaki et al. 2014). The ETC process (though not essential even for whole-mouse-brain CLARITY, as in a typical 3-week passive-CLARITY approach that achieves full transparency and antibody access) still accelerates de-lipidation and might, therefore, help enhance an aminoalcohol approach to CLARITY, though this remains to be seen and will depend on the size and charge of the resulting lipid-containing particles.

CLARITY-Optimized Light Sheet Microscopy

Not only the speed of de-lipidation but also the speed of imaging is crucial for CLARITY. While confocal and two-photon microscopes have been the workhorse systems in volumetric imaging for the reasons described above, over the past two decades light sheet fluorescence microscopy has emerged as a powerful approach for high-speed volumetric imaging. Confocal and two-photon microscopies are point-scanning techniques, detecting optical signals point-by-point to construct an image. Confocal achieves optical sectioning by the use of a pinhole at the detection focal plane to reject out-of-focus light, whereas two-photon utilizes the fact that only simultaneous absorption of two photons results in fluorescence emission, an event much more likely to occur at the point of highest light intensity in the sample (the focal plane). Light sheet microscopy, in contrast, builds upon a 100-year-old idea to illuminate the sample from the side with a thin sheet of light and detect the emitted fluorescence signal with an in-focus orthogonally arranged objective (Siedentopf and Zsigmondy 1903; Huisken and Stainier 2009). The optical sectioning is achieved by the confinement of illumination to a selective plane, which allows use of fast CCD or sCMOS cameras to capture the whole image simultaneously, and results in an increase of 2–3 orders of magnitude in imaging speed compared to confocal and two-photon microscopy. Moreover, light sheet microscopy minimizes photo-bleaching by confining illumination to the plane of interest. Taken together, these properties of light sheet microscopy may be well suited for the imaging of large clarified samples, consistent with its previously demonstrated utility for minimizing unnecessary illumination.

For high-speed collection of imaging data from large clarified volumes, COLM is 100–1000 times faster than conventional scanning methods, leading to vastly

decreased photo-bleaching (Tomer et al. 2014). The properties of COLM are not only useful for mouse brains but also will be particularly relevant for maintaining this high cellular and subcellular resolution at practical speeds in brains from larger-brained organisms. The fast COLM approach described here for clarified intact mouse brains maintains high resolution even 5–6 mm deep in tissue using the 0.95 NA objective; ultimate resolution in any light microscope, of course, remains limited by the laws of diffraction ($\lambda/2NA = \sim 180$ nm), but the emergence of super-resolution (or "diffraction unlimited") imaging methods, such as STED/RESOLFT and PALM/STORM, could in the future allow a further four- to fivefold improvement in achievable resolution.

We assess the compatibility of clarified samples with light sheet, observing greater than two orders of magnitude faster imaging speed (Tomer et al. 2014) with minimal photo-bleaching results (Fig. 2). For example, it was possible to image an entire mouse brain in about 4 h using a 10× magnification objective and in about 1.5 days using a 25× objective, as opposed to many days and months, respectively, with a confocal microscope. COLM is especially well suited for interrogation of large tissue samples labeled with transgenic or histochemical

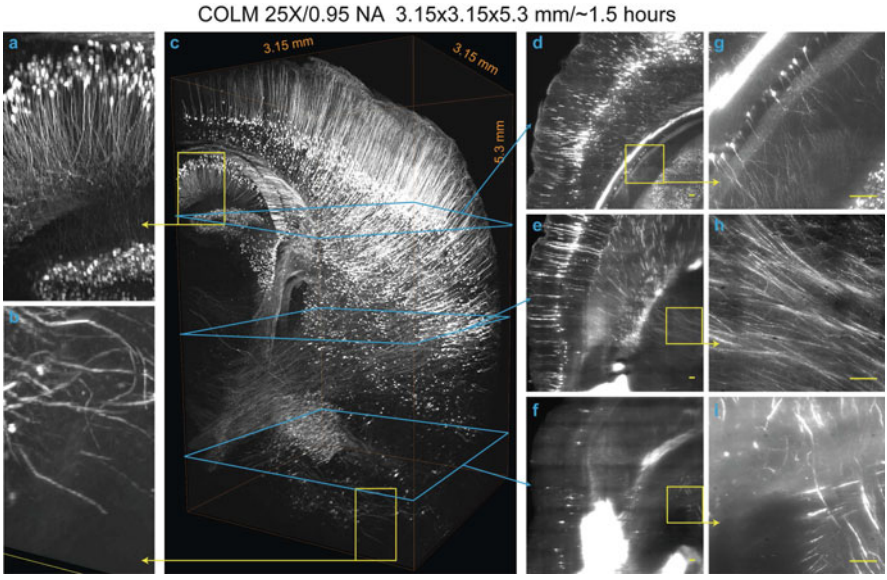

Fig. 2 Fast high-resolution imaging of clarified brain using COLM. A 3.15 mm × 3.15 mm × 5.3 mm volume acquired from an intact clarified Thy1-eYFP mouse brain using COLM with ×25 magnification; the brain had been perfused with 0.5 % acrylamide monomer solution. The complete image dataset was acquired in ~1.5 h; for optimal contrast, the LUT of zoomed-in images was linearly adjusted between panels (**a**) and (**b**), magnified views from the panel (**c**) region defined by *yellow squares* (**d–i**), maximum-intensity projections of over a 50 µm-thick volume, as shown by the progression of *cyan* and *yellow boxes* and *arrows*. A camera exposure time of 20 ms was used; refractive index liquid 1.454 was used as the immersion medium. All scale bars: 100 µm. Figure and text adapted from Tomer et al. (2014)

approaches. The increased speed of acquisition and higher quality of data generated via CLARITY using new microscopy methods, combined with high-speed CLARITY processing itself enabled by efficient tissue transformation protocols, define a versatile and efficient platform for structural and molecular interrogation of large and fully assembled tissues (Tomer et al. 2014).

As a final comment for future work, we note that very large datasets result from this new capability for high-speed imaging of large tissue volumes at high resolution, and extensive innovation will be needed in image analysis and data management (for example, if the intact 0.3 cm^3 mouse brain is represented by $0.5 \times 0.5 \times 0.5$ cubic-micron 16-bit voxels, at least 4.8 terabytes of raw data result). Fortunately, big-data and high-performance computing have led to advanced image-compression technologies such as JPEG 2000 3D, increased computational capacity with GPU parallel computation technology, and cloud infrastructures (such as Amazon S3) for data storage and sharing. We expect that the integration and application of these methods to CLARITY (Tomer et al. 2014) will allow increasingly complete access to, and understanding of, the molecular and structural organization of large intact tissues.

Tracking Activity in Deep Genetically Targeted Neurons of Behaving Animals

To observe not only the structure but also the real-time activity of specified neural cells and projections, we developed a method termed fiber photometry, with a simple design (only a single multimode optical fiber), suitable for recording from deep brain structures and sensitive enough to detect activity changes not only in cell bodies but also in axons during behavior, where signals are considerably smaller (Gunaydin et al. 2014). This fiber photometry (light measurement with a single-fiberoptic device sensitive enough to detect activity in axonal fibers) relies on a lock-in amplifier and a high-sensitivity photoreceiver along with custom software to record (through an implanted 400 μm optical fiber) the population activity of neural circuit elements expressing a genetically encoded Ca^{2+} indicator (Fig. 3). The single fiber allows chronic, stable, minimally disruptive access to deep brain regions and interfaces with a flexible patchcord on the skull surface (Gunaydin et al. 2014).

For cell type-specific recording of Ca^{2+} transients—a proxy for certain neural activity—we injected a Cre-dependent adeno-associated virus (AAV) carrying the GCaMP5g gene into VTA of transgenic TH::Cre mice and implanted an optical fiber in VTA for simultaneous delivery of 473 nm excitation light and collection of GCaMP5g fluorescence emission (Gunaydin et al. 2014). Activity-dependent fluorescence emitted by cells in the volume was collected simultaneously; after propagating back through the same patchcord used to deliver excitation light, this fluorescence was spectrally separated using a dichroic, passed through a single

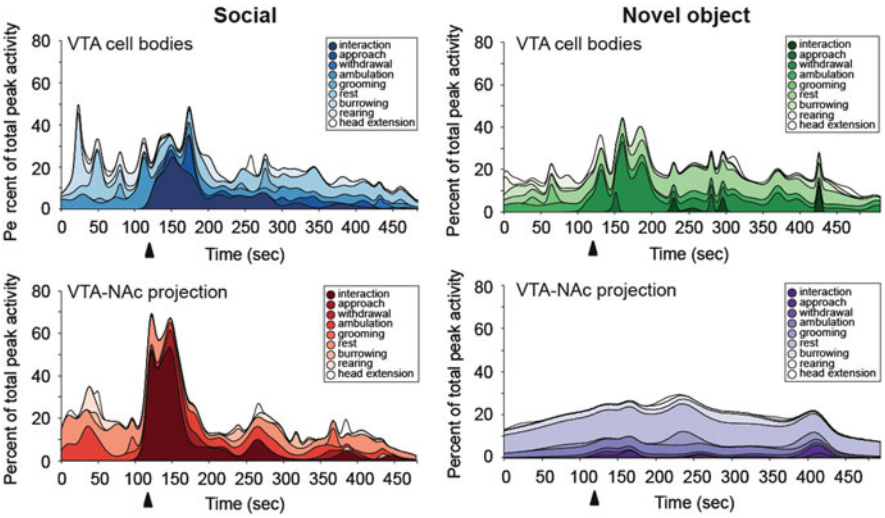

Fig. 3 VTA-NAc projection activity encodes social interaction. Area plots, smoothed behavioral score: %total Ca^{2+} peaks representing specific social target-related and novel-object behaviors during VTA cell body (*top*) and VTA-NAc projection (*bottom*) fiber photometry (5 min; n = 10 and n = 11 mice, respectively). *Arrows*: target introduction. Note encoding of social interaction by VTA cell body and VTA-NAc projection activity. Figure and text adapted from Gunaydin et al. (2014)

band filter, and focused onto a photodetector. To first test if this system would be capable of detecting VTA activity in a temporally precise manner, we recorded Ca^{2+} signals in VTA neurons of TH-GCaMP mice given access to sucrose solution, an established natural reward. Sucrose consumption was assessed using a contact "lickometer," which registered an event every time the mouse completed a circuit from a metal spout to a metal operant chamber floor, time-locked to the Ca^{2+} recording. This setup enabled readout of the VTA response with temporal precision on the order of milliseconds. VTA signals were tightly correlated in time with onset of licking bouts and habituated over recording epochs (Gunaydin et al. 2014).

Neural Activity that Encodes and Predicts Social Interaction

Next we applied fiber photometry during same-sex social interaction. We recorded from the VTA of female mice during home-cage social interaction, in which a novel social target mouse was introduced into the test mouse cage for a 5-min epoch, and video time-locked to the VTA GCaMP signal was collected (Gunaydin et al. 2014). Upon introduction of the social target, we observed a marked increase in activity of the targeted VTA neurons during interaction with this novel mouse. Such activity was absent in the eYFP control, indicating that observed transients were Ca^{2+}

signals and not motion artifacts (Gunaydin et al. 2014). In separate trials, we exposed test mice to a novel object placed in the home cage (counterbalanced with novel-mouse exposure). Nevertheless, VTA activity in response to the novel object resembled peak VTA activity during social interaction, with similar amplitude (mean peak dF/F during interaction: 16.4 % ± 2.1 % SEM for social, 13.7 % ± 1.4 % SEM for novel object, n = 10; Wilcoxon signed-rank test, p = 0.5).

While these data were consistent with hypothesized importance of the VTA-NAc projection in social behavior, direct observation of endogeneous activity in the projection during social behavior remained lacking. This would require measuring a previously inaccessible but fundamental neural circuit quantity: native activity in a specific projection during behavior. Fiber photometry was designed for this technical challenge, and we next tested real-time tracking of Ca^{2+} transients in genetically specified VTA inputs to NAc. Using TH-GCaMP mice, we implanted an optical fiber in medial NAc to detect activity specifically in axon fibers corresponding to the projection in question during home cage social interaction and novel object investigation (Gunaydin et al. 2014).

We observed robust GCaMP signals across many social interaction bouts, demonstrating that fiber photometry could be used to selectively record from neuronal projections during behavior (Gunaydin et al. 2014). We observed smaller projection activation to novel object (n = 11, Wilcoxon signed rank test, mean peak dF/F: 6.9 % ± 1.4 % for social, 3.5 % ± 0.7 % for novel object, p = 0.016). Stronger encoding of social than of object interactions by the VTA-NAc projection (not seen at the cell bodies) supports the hypothesis that there are distinctly wired relevant subpopulations of VTA neurons. We sought to capitalize on this ability to track projection activity during behavior by probing in greater detail the encoding of specific behaviors by the VTA projection to NAc (in comparison with activity in VTA cell bodies) using multifactorial high-resolution quantitative behavioral assessment. We first employed an automated peak-finding algorithm to detect all Ca^{2+} peaks throughout the 5-min testing period, blind to mouse behaviors, for social and novel object conditions during both VTA cell body and VTA-NAc projection recordings. Next we automatically segmented video clips centered (±1 s) around the time of each Ca^{2+} peak and scored video segments for interaction, approach, withdrawal, ambulation, grooming, rest, burrowing, rearing, and head extension (Gunaydin et al. 2014).

Area plots of all VTA-DA Ca^{2+} peak times subdivided by behavioral category (Fig. 3) allowed direct comparison of total peak activity over time attributable to each category, including as a percent of total overall Ca^{2+} peak activity (Gunaydin et al. 2014). In the social case, a larger proportion of total Ca^{2+} peak activity occurred during interaction for VTA-to-NAc projections than for cell bodies, supporting the conclusion that this projection more selectively encodes social interaction than does the cell body signal. For novel object behavior, both cell bodies and projections poorly encoded approach or interaction; interestingly, while the VTA cell bodies seemed to strongly encode withdrawal from the object, the VTA-NAc projection only weakly encoded this specific behavior (Fig. 3). Across the entire 5-min testing period, VTA-NAc projections showed a decreased proportion of Ca^{2+} peak activity (compared with VTA cell-body data) occurring during

target-relevant behavior (accounted for by withdrawal) in the case of novel object but not social behavior (Fig. 3). These data together support the conclusion that VTA-NAc projection activity represents a signal with specific importance to social behavior relative to object interactions (Gunaydin et al. 2014). Not only is this projection-specific activity parameter especially predictive in behavior (Fig. 3) but projection-specific activity is also in general particularly important for causal elicitation of complex behaviors (Deisseroth 2014). Therefore, this new ability to directly measure the activity of projections between brain regions provides a potentially relevant source of data on the behaviorally significant dynamics of information flow (Deisseroth 2014).

Outlook

We have developed and applied two new methods, fiber photometry and COLM, for direct measurement of the activity and structure of specified neuronal afferents projecting to a particular downstream target. Together, these results demonstrate the integrative value of complementary optical techniques in causally mapping specific projections and postsynaptic targets within neural circuitry. Projection-specific optogenetic manipulations complement the specificity of fiber photometry and COLM by enabling control of the corresponding projection dynamics. This approach may suggest circuit-based targets for further research into physiological or neuropsychiatric disease-related symptoms and may be generally applicable for investigation of specific circuit elements in mammalian behavior.

Acknowledgments We thank the entire Deisseroth lab for helpful discussions. K.D. is supported by the DARPA Neuro-FAST program, NIMH, NSF, NIDA, the Simons Foundation, and the Wiegers Family Fund. All tools and methods described are distributed and supported freely (optogenetics.org, clarityresourcecenter.org, http://wiki.claritytechniques.org) and discussed in an open forum (forum.claritytechniques.org). Text and figures were taken from our in-press papers (Gunaydin et al. 2014; Tomer et al. 2014), and I am grateful to my collaborators and co-authors on these papers: Lisa Gunaydin, Logan Grosenick, Joel Finkelstein, Isaac Kauvar, Lief Fenno, Avishek Adhikari, Stephan Lammel, Julie Mirzabekov, Raag Airan, Kay Tye, Polina Anikeeva, Rob Malenka, Raju Tomer, Li Ye, and Brian Hsueh.

References

Bock DD, Lee WC, Kerlin AM, Andermann ML, Hood G, Wetzel AW, Yurgenson S, Soucy ER, Kim HS, Reid RC (2011) Network anatomy and in vivo physiology of visual cortical neurons. Nature 471:177–182. doi:10.1038/nature09802

Briggman KL, Helmstaedter M, Denk W (2011) Wiring specificity in the direction-selectivity circuit of the retina. Nature 471:183–188. doi:10.1038/nature09818

Chung K, Wallace J, Kim SY, Kalyanasundaram S, Andalman AS, Davidson TJ, Mirzabekov JJ, Zalocusky KA, Mattis J, Denisin AK, Pak S, Bernstein H, Ramakrishnan C, Grosenick L, Gradinaru V, Deisseroth K (2013) Structural and molecular interrogation of intact biological systems. Nature 497:332–337. doi:10.1038/nature12107

Conchello JA, Lichtman JW (2005) Optical sectioning microscopy. Nat Methods 2:920–931. doi:10.1038/nmeth815

Deisseroth K (2014) Circuit dynamics of adaptive and maladaptive behaviour. Nature 505:309–317

Dodt HU, Leischner U, Schierloh A, Jährling N, Mauch CP, Deininger K, Deussing JM, Eder M, Zieglgänsberger W, Becker K (2007) Ultramicroscopy: three-dimensional visualization of neuronal networks in the whole mouse brain. Nat Methods 4:331–336. doi:10.1038/nmeth1036

Ertürk A, Becker K, Jährling N, Mauch CP, Hojer CD, Egen JG, Hellal F, Bradke F, Sheng M, Dodt HU (2012) Three-dimensional imaging of solvent-cleared organs using 3DISCO. Nat Protoc 7:1983–1995. doi:10.1038/nprot.2012.119

Gunaydin LA, Grosenick L, Finkelstein JC, Kauvar IV, Fenno LE, Adhikari A, Lammel S, Mirzabekov JJ, Airan RA, Tye KM, Anikeeva P, Malenka RC, Deisseroth K (2014) Natural neural projection dynamics underlying social behavior modulation. Cell 157:1535–1551

Hama H, Kurokawa H, Kawano H, Ando R, Shimogori T, Noda H, Fukami K, Sakaue-Sawano A, Miyawaki A (2011) Scale: a chemical approach for fluorescence imaging and reconstruction of transparent mouse brain. Nat Neurosci 14:1481–1488. doi:10.1038/nn.2928

Helmchen F, Denk W (2005) Deep tissue two-photon microscopy. Nat Methods 2:932–940. doi:10.1038/nmeth818

Huisken J, Stainier DY (2009) Selective plane illumination microscopy techniques in developmental biology. Development 136:1963–1975. doi:10.1242/dev.022426

Ke MT, Fujimoto S, Imai T (2013) SeeDB: a simple and morphology-preserving optical clearing agent for neuronal circuit reconstruction. Nat Neurosci 16:1154–1161. doi:10.1038/nn.3447

Kim SY, Chung K, Deisseroth K (2013) Light microscopy mapping of connections in the intact brain. Trends Cogn Sci 17:596–599. doi:10.1016/j.tics.2013.10.005

Micheva KD, Busse B, Weiler NC, O'Rourke N, Smith SJ (2010) Single-synapse analysis of a diverse synapse population: proteomic imaging methods and markers. Neuron 68:639–653. doi:10.1016/j.neuron.2010.09.024

Ragan T et al (2012) Serial two-photon tomography for automated ex vivo mouse brain imaging. Nat Methods 9:255–258. doi:10.1038/nmeth.1854

Siedentopf H, Zsigmondy R (1903) Uber Sichtbarmachung und Grössenbestimmung ultramikroskopischer Teilchen, mit besonderer Anwendung auf Goldrubingläser. Ann Phys 10:1–39

Susaki EA, Tainaka K, Perrin D, Kishino F, Tawara T, Watanabe TM, Yokoyama C, Onoe H, Eguchi M, Yamaguchi S, Abe T, Kiyonari H, Shimizu Y, Miyawaki A, Yokota H, Ueda HR (2014) Whole-brain imaging with single-cell resolution using chemical cocktails and computational analysis. Cell 157:726–739

Tang J, Germain RN, Cui M (2012) Superpenetration optical microscopy by iterative multiphoton adaptive compensation technique. Proc Natl Acad Sci USA 109:8434–8439. doi:10.1073/pnas.1119590109

Tomer R, Ye L, Hsueh B, Deisseroth K (2014) Advanced CLARITY methods for rapid and high-resolution imaging of large intact tissues. Nat Protoc 9:1682–1697

The Network for Intracortical Communication in Mouse Visual Cortex

Andreas Burkhalter

Abstract New techniques for identifying cell types, tracing their synaptic partners, imaging and manipulating their activity in behaving organisms have made mice a widely used model for linking brain circuits to behavior. Most behaviors are tied to vision: identifying objects, guiding movements of body parts, navigating through the environment, and even social interactions. Reason enough to focus on the mouse visual cortex. To find our way around in the occipital cortex, we needed a map. We took a classic approach and traced in the same animal the outputs from multiple retinotopic sites of primary visual cortex (V1) and compared the relative location of projections in the extrastriate cortex. We found nine extrastriate maps and showed by single unit recordings that each of the connectional maps contained visually responsive neurons whose receptive fields were mapped in orderly fashion and completely covered the visual field. Remarkably, a tiny region of one sixth of a dime contained a two- to three-times larger number of areas than the highly developed somatosensory and auditory cortices. By tracing the connections, we found that each of the ten visual areas projected to 25–35 cortical targets and interconnected virtually all of the areas reciprocally with one another. Although the binary graph density of the connection matrix was nearly complete, the connection strengths between areas within the ventral and dorsal cortex differed, indicating that the information from V1 flowed into distinct but interconnected streams. Unit recordings and calcium imaging studies showed that the ventral and dorsal streams processed different spatiotemporal information, which aligned with known properties of streams in primates. Analyses of the laminar patterns of interareal projections showed that areas were organized at multiple levels, suggesting that each stream represented a processing hierarchy.

A. Burkhalter (✉)
Department of Neuroscience, Washington University School of Medicine, St. Louis, MO 63110, USA
e-mail: burkhala@pcg.wustl.edu

H. Kennedy et al. (eds.), *Micro-, Meso- and Macro-Connectomics of the Brain*, Research and Perspectives in Neurosciences, DOI 10.1007/978-3-319-27777-6_4

Introduction

Over the past decades, neuroscience research has shown that sensory inputs are processed at multiple locations distributed across the brain. These regions do not encode specific mental faculties but are responsible for specific unitary operations (Kandel and Hudspeth 2013). Cognition arises in a network of serial and parallel pathways between functionally discrete units, each responsible for elements—but not all aspects—of a given function. Although the tenet of functional localization holds that neural processing is modular, the structure of the underlying network and the rules of interareal communication are not well understood. Thanks to the development of powerful new tools for recording, labeling and genetically manipulating brain circuits, the mouse visual system has emerged as a tractable system in which these questions can be addressed with unprecedented precision (Luo et al. 2008; Huberman and Niell 2011; Oh et al. 2014; Zingg et al. 2014).

Mice are most active at night and rely heavily on their whiskers for recognizing objects and their ears and noses for hearing and social communication (Holy and Guo 2005; Jadhav and Feldman 2010; Stowers et al. 2013). When starved for food, mice are diurnal and use dichromatic vision for guiding their actions in the field (Jacobs et al. 2004; Daan et al. 2011; Baden et al. 2013). Through their small eyes with afoveate retinas, the world looks blurred and lacks the rich detail experienced by humans, whose vision is 100 times sharper. At close range, however, the acuity of 0.5 cycles/deg is sufficient to resolve landmark features that can be used for referencing locomotion-dependent path integration signals during spatial navigation (Prusky et al. 2000; Prusky and Douglas 2005; Chen et al. 2013). In fact, experiments on visual object recognition have shown that rats, and presumably mice, can use invariant shape information to identify landmarks from a variety of different viewing angles (Alemi-Neissi et al. 2013). These studies demonstrate that mice process multiple complex visual cues and associate them with motor actions. Many of these computations are performed in interconnected cortical and subcortical networks, bringing up the questions of what the architecture of these networks is and how do functionally distinct areas communicate with each other.

Thalamocortical Projections to Mouse Visual Cortex

The visual cortex receives thalamic input from the lateral geniculate (LGN) and the lateral posterior (LP) nuclei. LGN inputs to V1 terminate most densely in layers 3 and 4, and more sparsely in layer 1 and at the layer 5/6 border (Dräger 1974; Antonini et al. 1999). In addition, sparse projections from the LGN terminate in the lateral extrastriate areas but avoid medial extrastriate cortex (Antonini et al. 1999). V1 also receives thalamocortical inputs from LP, which terminate in layers 1 and 5. LP inputs to surrounding extrastriate cortex terminate in layers 1, 3, 4 and 6 (Hughes 1977; Herkenham 1980). Although the extrastriate target areas of

these connections were not positively identified, the results show that thalamocortical inputs from thalamic relays are deployed to V1 as well as to surrounding extrastriate cortex (Sanderson et al. 1991). With this thalamocortical input in place, it is not surprising that expression of the activity-dependent immediate early gene, *Arc*, shows that much of the thalamorecipient cortex is driven by visual input (Burkhalter et al. 2013).

Cortical Cartography

Inspired by the emerging field of genetics of the mouse brain (Sidman et al. 1965), Caviness (1975) rang in the modern era of mouse cartography. Refining the surface-based maps of lissencepahlic mouse cortex constructed by the classic 'cytoarchitects' (Woolsey 1967), Caviness introduced the flatmap format that displayed the cortex in a single map that preserved the natural topology of parcels (Van Essen 2013). In this map, 26 neocortical parcels were identified and, for the first time, clearly showed the shape and extent of V1, including the surrounding extrastriate areas 18a and 18b. A more detailed surface-based map based on the Allen Reference Atlas identified 34 cytoarchitectonic parcels (Dong 2008; Ng et al. 2010), which is similar to the 37 parcels identified in a widely used slice-based atlas by Franklin and Paxinos (2007). Using a variety of histochemical and immunological markers in tangential sections of physically flattened cortex, we were able to identify only 23 parcels, but many with much greater confidence than possible with the classic Nissl stain (Wang et al. 2011, 2012). Notably, our parcellation scheme falls short in the auditory, posterior parietal and visual cortices, which are at the very locations in which we found multiple topographic maps (Wang and Burkhalter 2007). Thus, it appears that some of the areas annotated in the atlases are inspired by our area map, but in reality their borders are too subtle to be identified with confidence by cytoarchitectonic criteria.

Areal Organization of Visual Cortex

Early topographic mapping studies using microelectrodes showed that extrastriate cortex surrounding V1 contains multiple orderly maps of the visual field (Dräger 1975; Wagor et al. 1980). The conclusion from the layout of the visuotopic maps was that V1 is adjoined on the lateral side by area V2, which is flanked by V3. On the medial side, V1 is adjoined by two additional maps, a rostral area Vm-r and a caudal area Vm-c (Wagor et al. 1980). This primate-inspired areal layout was soon challenged by the discovery that V1 projection targets vastly outnumbered the reported visuotopic areas (Olavarria and Montero 1989). In the eyes of some investigators, the mismatch argued against an organization in which V1 was surrounded by a string of areas and favored a scheme in which the projection

patches represented inputs to distinct modules within a single area (Kaas et al. 1989). With rodents rapidly taking center stage in neuroscience, the time was ripe to revisit the issue. By labeling the connections of two to three distinct visuotopic locations of V1 with different tracers in the same animal, making side-by-side comparisons of projections in extrastriate cortex and mapping receptive fields, we produced maps of rat and mouse visual cortex (Coogan and Burkhalter 1993; Wang and Burkhalter 2007; Fig. 1). In both species we found maps that strongly argued against the primate-inspired scheme proposed by Wagor et al. (1980), in which a single large area surrounded lateral and rostral V1. Instead,

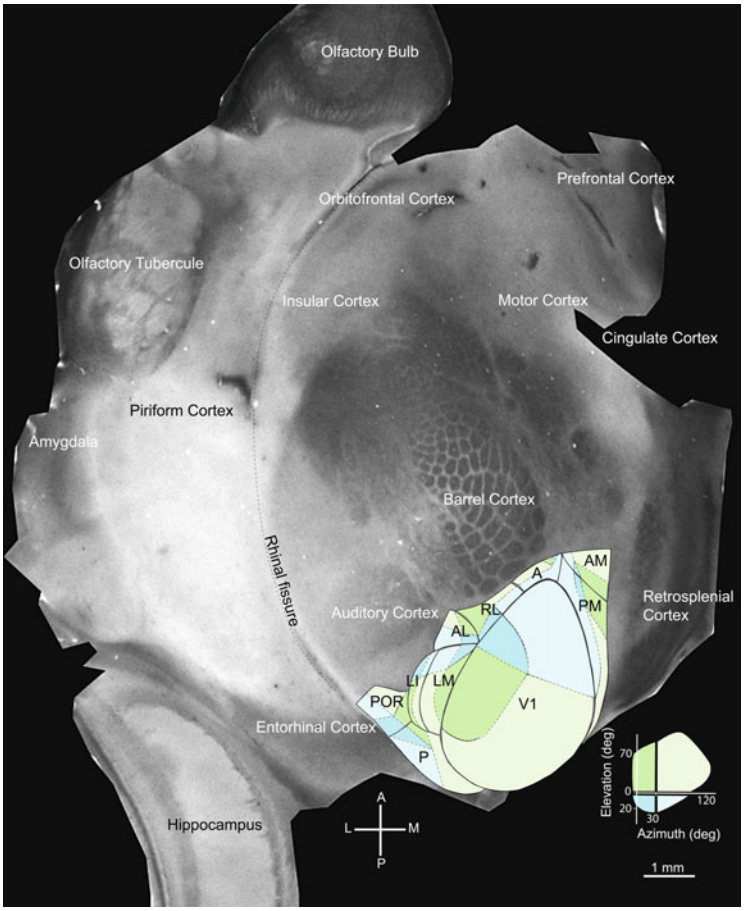

Fig. 1 Area map of mouse visual cortex. Tangential section through flatmounted left cortical hemisphere stained with an antibody against the muscarinic type 2 acetylcholine receptor. The different colors indicate different quadrants of the right visual field. Abbreviations: *A* anterior area, *AL* anterolateral area, *AM* anteromedial area, *LI* laterointermediate area, *LM* lateromedial area, *V1* primary visual cortex, *P* posterior area, *PM* posteromedial area, *POR* postrhinal area, *RL* rostrolateral area, *A* Anterior, *L* lateral, *M* medial, *P* posterior

the results showed an organization in which V1 was surrounded by a string of small areas that each contained a complete map of the visual field. This finding suggested that ancestral cortex had a complex organization and that select areas identified in primates might be homologous to primordial extrastriate areas in rodents (Rosa and Krubitzer 1999). One of these may be the lateromedial area (LM), which is the only area that shares the vertical meridian with V1 and, for that reason, resembles V2 in primates (Allman and Kaas 1971). But, unlike V2, which has a split horizontal meridian representation, the map in LM is topologically equivalent to the visual field. In fact, this is true for every visuotopic map we have identified, which all show that the margins of the visual field are mapped along the areal borders. To minimize the length of the connections between areas, matching topographic locations in different maps are aligned across shared borders. One of the lessons from these studies is that extrastriate cortex surrounding V1 contains a larger number of areas than annotated in widely used atlases (Franklin and Paxinos 2007; Dong 2008) and employed as references for the mesoscale connectome (Oh et al. 2014; Zingg et al. 2014). It is important to note that, except for the V1 border, which is readily detected in Nissl-stained sections, the cytoarchitecture of the surrounding extrastriate cortex is remarkably uniform. The single exception is the LM/anterolateral area (AL) border, which can be identified by Nissl staining but only when the eyes are keyed to the cytoarchitectonic transition, highlighted by the expression of the muscarinic type 2 acetylcholine receptor (Wang et al. 2011). However, perhaps the most surprising result is that the mouse visual cortex, which is one third the size of barrel cortex, contains at least ten areas, seven more than the somatosensory cortex. One interpretation of the unexpected multitude of visuotopic maps is that vision for perception and for guiding motor actions arises from a larger number of unitary operations than somatosensation and that these elementary processes are represented in different visual areas.

Interareal Connections

To study the interareal network of visual cortex, we injected the anterograde tracer biotinylated dextran amine (BDA) into ten areas, which we identified by their location relative to callosal landmarks (Wang et al. 2012). Projections to 40 targets were identified based on a combination of cytoarchitectonics and the expression of various molecular markers. The projection strength of each pathway was determined by the optical density of labeled axon branches and terminals in the target zone relative to the total output. Earlier studies have shown that optical density is tightly correlated with bouton density (Wang et al. 2011). The results of the 10×40 connectivity matrix show 307 of 390 possible linkages (79 %), which accounts for a 13 % higher graph density than in the macaque cortex (Markov et al. 2013). The connection density within the visual cortex proper is even higher, showing that virtually all of the ten visuotopically organized areas are interconnected reciprocally with one another (Wang et al. 2012). The connection strengths span at least

three orders of magnitude, showing a long-tailed distribution with small numbers of strong and a large numbers of weak connections. Although the connection strength in mouse cortex varies over a narrower range than in macaque (Markov et al. 2011), the lognormal distribution found in both species indicates that the fundamental principles of cortical connectivity are evolutionarily conserved.

In primates, visual information is processed in dorsal and ventral cortical streams specialized for 'where' an object is located or for guiding actions and 'what' an object is (Ungerleider and Mishkin 1982; Goodale and Milner 1992). If such streams exist in mice, how do they arise from a network with seemingly low binary specificity? One way this might be achieved is by routing the flow of information through pathways with different connection strengths. Consistent with this notion, we found that each source area of visual cortex had a unique profile of connection strengths. We assessed between-area similarities and found that the projection strengths among dorsal and ventral networks were distinct. The dorsal network consisted of areas AL, rostrolateral area (RL), anteromedial area (AM), posteromedial area (PM) and anterior area (A), whereas V1, LM, lateointermediate area (LI), postrhinal area (POR) and posterior area (P) were grouped in the ventral network (Wang et al. 2012). Although streams were revealed in the graph of cortex-wide connections, we wondered whether they were present in the 10×10 connectivity graph of visuotopically organized areas. The graph of projection strengths clearly grouped areas into dorsal (i.e., AL, RL, AM, PM, A) and ventral (i.e., V1, LM, LI, POR, P) communities in which connections within modules were twice as strong as those between modules. Within modules, the shortest pathways were always direct. By contrast, the shortest pathways between modules were often indirect, which means that the combined strength of the indirect path was stronger that the direct path. Thus, for communication between modules, the most effective path may be indirect. Interestingly, not a single short path linking the two modules travels through V1, indicating that, similar to cat and monkey (Sporns et al. 2007), V1 is not a network hub for interareal communication. Instead, judged by the number of connections, this role belongs to area LM. Although lower in the hierarchy than monkey V4, which has a similar status in the network, LM may play a critical role in integrative processing of visual information.

Cortical Hierarchy

The idea that hierarchical relationships between areas of mouse visual cortex can be derived from the laminar organization of connections goes back to analyses of primate cerebral cortex (Felleman and Van Essen 1991; Markov et al. 2014). In monkey, it was noticed that many reciprocal connections consisted of feedforward projections terminating in layer 4 and feedback projections terminating outside of layer 4. Such asymmetrical linkages are present between most reciprocally connected pairs of cortical areas. In rat and mouse, reciprocal interareal connections share many of the features found in primate (Coogan and Burkhalter 1990, 1993;

Dong et al. 2004a). However, unlike in primates, feedforward axonal projections from V1 are not restricted to layer 4. Instead, the projections terminate in a column across all layers. Importantly, however, feedforward connections always include layer 4. In contrast, feedback projections from surrounding extrastriate cortex to layer 4 of V1 are extremely sparse and preferentially terminate in layers 1, 2, 3, 5 and 6. Thus, the asymmetry in the innervation strength of layer 4 is the hallmark feature of reciprocal interareal connections. While these are striking similarities to feedforward and feedback connections in monkey, it is important to note that the columnar pattern of feedforward connections in rodents differs from that in monkey, which is restricted to layer 4. In fact, rodent feedforward connections resemble more closely the lateral connections in monkey (Felleman and Van Essen 1991). A likely reason for this difference is that feedforward connections in rodents originate from layers 2–6 (Coogan and Burkhalter 1988), whereas, in monkey, layers 2 and 3 are the main sources of these connections (Felleman and Van Essen 1991). From a developmental perspective, Dehay and Kennedy (2007) have argued that layers 2 and 3 in primates are different from layers 2 and 3 in mice, which lack the computational components of primate cortex. Abandoning input from deep layers in feedforward connections and increasingly relying on inputs from layers 2 and 3 may be a structural manifestation of the superior sophistication in interareal communication in primates.

In primates, different hierarchical levels are associated with different stages of visual processing (Felleman and Van Essen 1991). One way stimulus complexity is expressed is by the convergence of input reflected in the size of receptive fields. Recordings in mouse visual cortex show that receptive fields in V1 are small (10 deg) and increase across different extrastriate visual areas to reach a size that covers most of the visual field (Wang and Burkhalter 2007). Indirect support for an areal hierarchy also comes from the pattern of subcortical connections. For example, only areas V1 and LM receive input from the main afferent LGN nucleus (Oh et al. 2014). Thalamocortical inputs to all other visual areas originate from the LP nucleus (Oh et al. 2014). In addition, projections from V1 to the superior colliculus terminate in the most superficial sensory layers, whereas the outputs from higher areas are sent to deeper visuomotor layers (Coogan and Burkhalter 1993; Wang and Burkhalter 2013).

Synaptic Organization of Feedforward and Feedback Connections

Signatures for a cortical hierarchy are also observed in the distinct synaptic connectivity of feedforward and feedback connections. Both types of interareal connections are made by excitatory, glutamatergic pyramidal cells (Johnson and Burkhalter 1994; Domenici et al. 1995; Dong et al. 2004b), whereas long-range projections of GABAergic neurons are negligible (McDonald and Burkhalter 1993;

but see Caputi et al. 2013). In rat and mouse, feedforward and feedback connections to higher (i.e., LM) and lower visual areas (i.e., V1) provide monosynaptic input to pyramidal cells and GABAergic neurons (Dong et al. 2004b). Among the targets in layers 2 and 3, we found a handful of somatostatin- and calretinin-expressing interneurons but the vast majority of GABAergic cells expressed parvalbumin (Gonchar and Burkhalter 1999, 2003). Thus, in the target region, responses of pyramidal cells to excitatory feedforward and feedback inputs are influenced by disynaptic feedforward inhibition from parvalbumin neurons. Although the laminar projection pattern of feedforward and feedback circuits are distinct (Dong et al. 2004a), structurally the circuits for feedforward inhibition are similar in both pathways (Gonchar and Burkhalter 1999). Physiologically, however, the responses of pyramidal cells to feedforward inputs are opposed by stronger inhibition than the responses to feedback inputs (Shao and Burkhalter 1996; Dong et al. 2004b). The reasons for the pathway-specific excitatory/inhibitory balance are that feedforward inputs to parvalbumin-expressing neurons are relatively stronger than to pyramidal cells whereas feedback inputs to both types of cells are similar (Yang et al. 2013). The stronger excitation of parvalbumin neurons is probably due to signaling via calcium-permeable GluR2-lacking AMPA receptors that elicit large quantal amplitude responses with fast kinetics (Hull et al. 2009). By contrast, feedforward inputs to pyramidal cells are mediated by slow, small-amplitude AMPA receptors (Hull et al. 2009). The result of the fast/large amplitude AMPA-mediated currents at feedforward inputs onto parvalbumin-expressing neurons is that feedforward inhibition is initiated reliably and in a precisely timed manner. In contrast, small amplitude and slower AMPA-mediated currents at feedback synapses facilitate integration of convergent inputs onto pyramidal neurons. The motif of feedforward inhibition not only balances excitation but influences circuit gain and dynamics (Kepecs and Fishell 2014). We can only speculate what effects diverse feedforward inhibition might have on the processing of visual signals in feedforward and feedback circuits. In the static mode, feedforward circuits are good for selecting correlated inputs. Computational modelling has shown that this enhances stimulus detection and improves the accuracy of stimulus representation, whereas, in the default mode, the feedback circuit may improve response probability to sensory input (Kremkow et al. 2010). However, when top-down attention is focused on a stimulus, the excitatory/inhibitory balance may change and improve the accuracy of stimulus detection (Wang et al. 2013).

Dorsal and Ventral Processing Streams

Motivated by the perplexing number of visual areas and their striking connectivity within hierarchically organized dorsal and ventral streams, it was natural to search for analogies to the distributed processing within ‘where’ and ‘what/action’ streams of primates (Ungerleider and Mishkin 1982; Goodale and Milner 1992). The proposal that rat cortex contains distinct streams that are specialized for visual

guidance and object recognition was made almost 25 years ago (Kolb 1990). Since then, numerous studies have shown that deficits in pattern discrimination were associated with lesions in lateral extrastriate visual cortex, whereas damage to cortex anterior and medial to V1 affected polysensory integration and spatial navigation (Kolb and Walkey 1987; Wong and Brown 2006; Torrealba and Valdes 2008; Zhang et al. 2010). But the lesioning techniques used in these studies did not afford the spatial resolution for linking the behavioral deficit unequivocally to specific areas, a problem that will likely be overcome by optogenetic approaches (Lien and Scanziani 2013). Recently, significant progress was made by two-photon imaging of calcium transients in upper layer neurons of multiple areas in mouse visual cortex (Andermann et al. 2011; Marshel et al. 2011; Roth et al. 2012). These recordings showed that tuning to high spatial frequency was more common in LI than in AL, RL and AM, which are more selective for high temporal frequency and the direction of motion. Although these findings are broadly consistent with the concept that ventral stream areas are specialized for image detail and dorsal stream areas preferentially respond to transient inputs (Van Essen and Gallant 1994), the results show inconsistencies. For example, neurons of the ventral stream area, LM, have low spatial acuity and are tuned to high temporal frequencies. It is possible that, similar to V2 of primates (Nassi and Callaway 2009), LM consists of functionally distinct compartments and the true response properties were masked by averaging across modules. Further, counter to the prediction, neurons in the dorsal stream area, PM, have high spatial acuity and prefer longer-lasting, slow moving objects. One way to explain these inconsistencies is that high spatial acuity and sensitivity to slow visual motion recorded in PM provides landmark information, which is used to calibrate distance and direction signals from locomotion used for path integration (Harvey et al. 2012; Saleem et al. 2013).

Although distinct streams are observed in the cortex, functionally distinct channels emerge from the retina, are present in the LGN and can be traced throughout the afferent visual pathway to V1 (Piscopo et al. 2013; Cruz-Matin et al. 2014; Dhande and Huberman 2014). In V1, neural responses represent a weighted combination of inputs from parallel afferent geniculocortical pathways and feedback inputs from higher cortical areas with distinct spatiotemporal properties (Gao et al. 2010). From V1, impulses are sent to different areal streams. The question then is whether the functional differences arise in V1 or are generated in the dorsal or ventral areas to which V1 sends its output. To address this question, Glickfeld et al. (2013) labeled striate cortical inputs from V1 with the calcium indicator GCaMP3.3 and imaged calcium transients in axon terminals projecting to LM, AL and PM. The results show that the visual preferences of each projection are different and matched those of neurons in the target area, suggesting that each area inherits the response properties from functionally specialized neurons in V1. The important conclusion of this work is that different V1 neurons transmit information tailored to its projection target. This organization is consistent with our observation that individual V1 neurons largely lack collateral projections and project to single area of extrastriate cortex (Wang and Burkhalter 2005). More recently, similar results have been reported in the connectivity between V1, LM and AL, supporting

the idea that interareal transmission relies on dedicated neuronal connections (Berezovskii et al. 2011). The overall conclusion of these studies is that the binary specificity of the network of interareal connection might be much greater than indicated by pathway tracing of connections with tracers that lack cellular specificity.

Acknowledgments This work was supported by National Eye Institute Grants RO1EY-05935, RO1EY-016184, RO12EY20525 and RO1EY22090, the McDonnell Center for Systems Neuroscience and the Human Frontier Science Program. We thank Greg De Angelis, Yarimar Carrasquillo, Luciano Domenici, Hongwei Dong, Enquan Gao, Yuri Gonchar, Bryan Hooks, Weiqing Ji, Jeanne Nerbonne, Zhengwei Shao, Katia Valkova, Quanxin Wang, Akiko Yamashita and Weiguo Yang for their contributions.

References

Alemi-Neissi A, Roselli FB, Zoccolan D (2013) Multifeatural shape processing in rats engaged in invariant object recognition. J Neurosci 33:5939–5956

Allman JM, Kaas JH (1971) Representation of the visual field in striate and adjoining cortex of the owl monkey (*Aotus trivirgatus*). Brain Res 35:89–106

Andermann ML, Kerlin AM, Roumis DK, Glickfeld LL, Reid RC (2011) Functional specialization of mouse higher visual cortical areas. Neuron 72:1025–1039

Antonini A, Fagolini M, Stryker MP (1999) Anatomical correlates of functional plasticity in mouse visual cortex. J Neurosci 19:4388–4408

Baden T, Schibert T, Chang L, Wei T, Zaichuk M, Wissinger B, Euler T (2013) A tale of two domains: near—optimal sampling of achromatic contrasts in natural scenes through asymmetric photoreceptor distribution. Neuron 80:1206–2017

Berezovskii VK, Nassi JJ, Born RT (2011) Segregation of feedforward and feedback projections in mouse visual cortex. J Comp Neurol 519:3672–3683

Burkhalter A, Sporns O, Gao E, Wang Q (2013) Network of mouse visual cortex. In: Werner JS, Chalupa LM (eds) The new visual neurosciences. MIT Press, Cambridge, MA, pp 243–254

Caputi A, Melzer S, Michael M, Monyer H (2013) The long and short of GABAergic neurons. Curr Opin Neurobiol 23:1–8

Caviness VS (1975) Architectonic map of neocortex of the normal mouse. J Comp Neurol 164:247–263

Chen G, King JA, Burgess N, O'Keefe J (2013) How vision and movement combine in the hippocampal place code. Proc Natl Acad Sci USA 110:378–383

Coogan TA, Burkhalter A (1988) Sequential development of connections between striate and extrastriate visual cortical areas in the rat. J Comp Neurol 278:242–252

Coogan TA, Burkhalter A (1990) Conserved patterns of cortico-cortical connections define areal hierarchy in rat visual cortex. Exp Brain Res 80:49–53

Coogan TA, Burkhalter A (1993) Hierarchical organization of areas in rat visual cortex. J Neurosci 13:3749–3772
Cruz-Matin A, El-Danaf RN, Osakada F, Sriram B, Dhande OS, Ngyuen PL, Callaway EM, Gosh A, Huberman AD (2014) A dedicated circuit links direction-selective retinal ganglion cells to the primary visual cortex. Nature 507:358–361
Daan S, Spoelstra K, Albrecht U, Schmutz I, Daan M, Daan B, Rienks F, Poletaeva l, Dell'Omo G, Vyssotski A, Lipp HP (2011) Lab mice in the field: unorthodox daily activity and effects of dysfunctional circadian clock allele. J Biol Rhythms 26:118–129
Dehay C, Kennedy H (2007) Cell-cycle control and cortical development. Nat Rev Neurosci 8:438–450
Dhande OS, Huberman AD (2014) Retinal cell maps in the brain: implications for visual processing. Curr Opin Neurobiol 24:133–142
Domenici L, Harding GW, Burkhalter A (1995) Patterns of synaptic activity in forward and feedback pathways within rat visual cortex. J Neurophysiol 74:2649–2664
Dong HW (2008) Allen reference atlas. A digital color atlas of the C57BL/6 J male mouse. Wiley, Hoboken, NJ
Dong H, Wang Q, Valkova K, Gonchar Y, Burkhalter A (2004a) Experience-dependent development pf feedforward and feedback circuits between lower and higher areas of mouse visual cortex. Vis Res 44:3389–3400
Dong H, Shao Z, Nerbonne JM, Burkhalter A (2004b) Differential depression of inhibitory synaptic responses in feedforward and feedback circuits between different areas of muse visual cortex. J Comp Neurol 475:361–373
Dräger UC (1974) Autoradiography of tritiated proline and fucose transported transneuronally from the eye to the visual cortex in pigmented and albino mice. Brain Res 82:284–292
Dräger UC (1975) Receptive field of single cells and topography in mouse visual cortex. J Comp Neurol 160:269–287
Felleman DJ, Van Essen DC (1991) Distributed hierarchical processing in the primate cerebral cortex. Cereb Cortex 1:1–47
Franklin KBJ, Paxinos G (2007) The mouse brain in stereotaxic coordinates. Elsevier, Amsterdam
Gao E, De Angelis GC, Burkhalter A (2010) Parallel input channels to mouse primary visual cortex. J Neurosci 30:5812–5926
Glickfeld LL, Andermann ML, Bonin V, Reid RC (2013) Cortico-cortical projections in mouse visual cortex are functionally target specific. Nat Neurosci 16:219–226
Gonchar Y, Burkhalter A (1999) Differential subcellular localization of forward and feedback interareal inputs to parvalbumin expressing GABAergic neurons in rat visual cortex. J Comp Neurol 406:346–360
Gonchar Y, Burkhalter A (2003) Distinct GABAergic targets of feedforward and feedback connections between lower and higher areas of rat visual cortex. J Neurosci 23:10904–10912
Goodale MA, Milner AD (1992) Separate visual pathways for perception and action. Trends Neurosci 15:20–25
Harvey CD, Coen P, Tank DW (2012) Choice-specific sequences in parietal cortex during a virtual-navigation decision task. Nature 484:62–68
Herkenham M (1980) Laminar organization of thalamic projection to the rat neocortex. Science 207:532–535
Holy TE, Guo Z (2005) Ultrasonic songs of male mice. PLoS Biol 3(12):e386
Huberman AD, Niell CM (2011) What can mice tell us about how vision works? Trends Neurosci 34:464–473
Hughes HC (1977) Anatomical and neurobehavioral investigations concerning the thalamocortical organization of the rat's visual system. J Comp Neurol 175:311–335
Hull C, Isaacson JS, Scanziani M (2009) Postsynaptic mechanisms govern the differential excitation of cortical neurons by thalamic inputs. J Neurosci 29:9127–9136
Jacobs GH, Williams GA, Fenwick JA (2004) Influence of cone pigment coexpression on spectral sensitivity and color vision in the mouse. Vis Res 44:1615–1622
Jadhav SP, Feldman DE (2010) Texture coding in the whisker system. Curr Opin Neurobiol 20:313–318

Johnson R, Burkhalter A (1994) Evidence for excitatory amino acid neurotransmitters in forward and feedback corticocortical pathways within rat visual cortex. Eur J Neurosci 6:272–286
Kaas JH, Krubitzer LA, Johanson KL (1989) Cortical connections of areas 17 (V-I) and 18 (V-II) of squirrels. J Comp Neurol 428:337–354
Kandel ER, Hudspeth AJ (2013) The brain and behavior. In: Kandel ER, Schwartz JH, Jessel TM, Siegelbaum SA, Hudspeth AJ (eds) Principles of neural science, 5th edn. McGraw Hill, New York, NY, pp 5–18
Kepecs A, Fishell G (2014) Interneuron cell types are fit to function. Nature 505:318326
Kolb B (1990) Posterior parietal and temporal association cortex. In: Kolb B, Tees RC (eds) The cerebral cortex of the rat. MIT Press, Cambridge, MA, pp 459–471
Kolb B, Walkey J (1987) Behavioral and anatomical studies of the posterior parietal cortex in the rat. Behav Brain Res 23:127–145
Kremkow J, Perrinet LU, Masson GS, Aertsen A (2010) Functional consequences of correlated excitatory and inhibitory conductances in cortical networks. J Comput Neurosci 28:579–594
Lien AD, Scanziani M (2013) Tuned thalamic excitation is amplified by visual cortical circuits. Nat Neurosci 16:1315–1323
Luo L, Callaway EM, Svoboda K (2008) Genetic dissection of neural circuits. Neuron 57:634–660
Markov NT, Misery P, Falchier A, Lamy C, Vezli J, Quilodran R, Gariel MA, Giroud P, Ercsey-Ravaz M, Pilaz LJ, Huissoud C, Barone P, Dehay C, Toroczkai Z, Van Essen DC, Kennedy H (2011) Weight consistency specifies regularities of macaque cortical networks. Cereb Cortex 21:1254–1274
Markov NT, Ercsey-Ravasz M-M, Lamy C, Gomes ARR, Magrou L, Misery P, Giroud P, Barone P, Dehay C, Toroczkai Z, Knoblauch K, Van Essen DC, Kennedy H (2013) The role of long-range connections on the specificity of the macaque interareal cortical network. Proc Natl Acad Sci USA 110:5187–5192
Markov NT, Vezoli J, Chameau P, Falchier A, Quilodran R, Huissoud C, Lamy C, Misery P, Giroud P, Ullman S, Barone P, Dehay C, Knoblauch K, Kennedy H (2014) Anatomy of hierarchy: feedforward and feedback pathways in macaque visual cortex. J Comp Neurol 522:225–259
Marshel JH, Garret ME, Nauhaus I, Callaway EM (2011) Functional specialization of seven mouse visual cortical areas. Neuron 72:1042–1054
McDonald CT, Burkhalter A (1993) Organization of long-range inhibitory connections within rat visual cortex. J Neurosci 13:768–781
Nassi JJ, Callaway EM (2009) Parallel processing strategies of the primate visual system. Nat Rev Neurosci 10:360–372
Ng L, Lau C, Sunkin SM, Bernard A, Chakrvarty MM, Lein ES, Jones AR, Hawrylycz M (2010) Surface-based mapping of gene expression and probabilistic expression maps in the mouse cortex. Methods 50:55–62
Oh SW, Harris JA, Ng L, Winslow B, Cain N, Mihalas S, Wang Q, Lau C, Kuan L, Henry AM, Mortrud MT, Ouellette B, Nguyen TN, Sorensen SA, Slaughterbeck CR, Wakeman W, Li Y, Feng D, Ho A, Micholas E, Hirokawa KE, Bohn P, Joines KM, Peng H, Hawrylycz MJ, Phillips JW, Hohmann JG, Wohnoutka P, Gerfen CR, Koch C, Bernard A, Dang C, Jones AR, Zeng H (2014) A mesoscale connectome of the mouse brain. Nature 508:207–214
Olavarria J, Montero VM (1989) Organization of visual cortex in the mouse revealed by correlating callosal and striate-extrastriate connections. Vis Neurosci 3:59–69
Piscopo DM, El-Danaf RN, Huberman AD, Niell CM (2013) Diverse visual features encoded in mouse lateral geniculate nucleus. J Neurosci 33:4642–4656
Prusky GT, Douglas RM (2005) Vision. In: Wishaw IQ, Kolb B (eds) The behavior of the laboratory rat. University Press, Oxford, pp 49–59
Prusky GT, West WR, Douglas RM (2000) Behavioral assessment of visual acuity in mice and rats. Vis Res 40:2201–2209
Rosa MGP, Krubitzer LA (1999) The evolution of visual cortex: where is V2? Trends Neurosci 22:242–248
Roth MM, Helmchen F, Kama BM (2012) Distinct functional properties of primary and posteromedial visual area of mouse neocortex. J Neurosci 32:9716–9726

Saleem AB, Ayaz A, Jeffery KJ, Harris KD, Carandini M (2013) Integration of visual motion and locomotion in mouse visual cortex. Nat Neurosci 16:1864–1869

Sanderson KJ, Dreher B, Gayer N (1991) Prosencephalic connections of striate and extrastriate areas of rat visual cortex. Exp Brain Res 85:324–334

Shao Z, Burkhalter A (1996) Differential balance of excitation and inhibition in forward and feedback circuits of rat visual cortex. J Neurosci 16:7353–7365

Sidman RL, Appel SH, Fuller JF (1965) Neurological mutants of the mouse. Science 150:513–516

Sporns O, Honey CJ, Kötter R (2007) Identification and classification of hubs in brain networks. PLoS One 2:e104910

Stowers L, Cameron P, Keller JA (2013) Ominous odors: olfactory control of instinctive fear and aggression in mice. Curr Opin Neurobiol 23:339–345

Torrealba F, Valdes JL (2008) The parietal association cortex of the rat. Biol Res 41:369–377

Ungerleider LG, Mishkin M (1982) Two cortical systems. In: Ingle DJ, Goodale MA, Mansfield RJW (eds) Analysis of visual behavior. MIT Press, Cambridge, pp 549–586

Van Essen DC (2013) Cartography and connectomes. Neuron 80:775–790

Van Essen DC, Gallant JL (1994) Neural mechanisms of form and motion processing in the primate visual system. Neuron 13:1–10

Wagor E, Mangini NJ, Pearlman AL (1980) Retinotopic organization of striate and extrastriate visual cortex in the mouse. J Comp Neurol 193:187–202

Wang Q, Burkhalter A (2005) Separate output streams from V1 to higher areas of mouse visual cortex. Soc Neurosci Abstr 854:1

Wang Q, Burkhalter A (2007) Area map pf mouse visual cortex. J Comp Neurol 502:339–357

Wang Q, Burkhalter A (2013) Stream-related preferences of inputs to the superior colliculus from area of dorsal and ventral stream of mouse visual cortex. J Neurosci 33:1696–1705

Wang Q, Gao E, Burkhalter A (2011) Gateways of ventral and dorsal streams in mouse visual cortex. J Neurosci 31:1905–1918

Wang Q, Sporns O, Burkhalter A (2012) Network analysis of corticocortical connections reveals ventral and dorsal processing streams in mouse visual cortex. J Neurosci 32:4386–4399

Wang C-T, Lee C-T, Wang X-J, Lo C-C (2013) Top-down modulation on perceptual decision with balanced inhibition through feedforward and feedback inhibitory neurons. PLoS One 8:e62379

Wong AA, Brown RE (2006) Visual detection, pattern discrimination and visual acuity in 14 strains of mice. Genes Brain Behav 5:389–403

Woolsey TA (1967) Somatosensory, auditory and visual cortical areas of the mouse. Johns Hopkins Med J 121:91–112

Yang W, Carrasquillo Y, Hooks BM, Nerbonne JM, Burkhalter A (2013) Distinct balance of excitation and inhibition in an interareal feedforward and feedback circuit of mouse visual cortex. J Neurosci 33:17373–17384

Zhang G-R, Cao H, Kong L, O'Brien J, Baughs A, Jan M, Zhao H, Wang X, Lu X-G, Cook RG, Geller AI (2010) Identified circuit in rat postrhinal cortex encodes essential information for performing specific visual shape discrimination. Proc Natl Acad Sci USA 107:14478–14483

Zingg B, Hintiryan H, Gou L, Song MY, Bay M, Bienkowski MS, Foster NN, Yamashita S, Bowman I, Toga AW, Dong H-W (2014) Neural networks of the mouse neocortex. Cell 156:1096–1111

The Brain in Space

Kenneth Knoblauch, Mária Ercsey-Ravasz, Henry Kennedy, and Zoltán Toroczkai

Abstract Recent connectomic tract tracing reveals that, contrary to what was previously thought, the cortical inter-areal network has high density. This finding leads to a necessary revision of the relevance of some of the graph theoretical notions, such as the small-world property, hubs and rich-clubs that have been claimed to characterize the inter-areal cortical network. Weight and projection distance relationships of inter-areal connections inferred from consistent tract tracing data have recently led to the definition of a novel network model, the exponential distance rule (EDR) model, that predicts many observed local and global features of the cortex. The EDR model is a spatially embedded network whose properties are determined by the physical constraints on wiring and geometry, in sharp contrast with the purely topological graph models used heretofore in the description of the cortex. We speculate that, when diving down to finer levels of the embedded cortical network, similar, physically constrained descriptions of connectivity may prove to be equally important for understanding cortical function.

Introduction

There has been a recent upsurge of interest in the connectome, leading to three major tract-tracing studies of cortical connectivity in the mouse and macaque that have important implications for understanding the human brain (Markov et al. 2014b; Oh et al. 2014; Zingg et al. 2014). These studies are unique as they

K. Knoblauch (✉) • H. Kennedy
Stem Cell and Brain Research Institute, INSERM U1208, 18 Avenue Doyen Lepine, 69500 Bron, France

Université de Lyon, Université Lyon I, 69003 Lyon, France
e-mail: henry.kennedy@inserm.fr

M. Ercsey-Ravasz
Faculty of Physics, Babeş-Bolyai University, Cluj-Napoca 400084, Romania

Z. Toroczkai
Department of Physics and Interdisciplinary Center for Network Science and Applications, University of Notre Dame, Notre Dame, IN 46556, USA

H. Kennedy et al. (eds.), *Micro-, Meso- and Macro-Connectomics of the Brain*, Research and Perspectives in Neurosciences, DOI 10.1007/978-3-319-27777-6_5

provide weighted and directed matrices of the cortex. They differ from previous anatomical work in that they are specifically aimed at providing spatial and strength/weight characteristics of the connections between areas, as well as providing a complete picture of connectivity based on consistent data bases rather than the fragmented investigations of earlier studies (Kennedy et al. 2013). The novel approach of these studies leads to capturing many weaker but consistent, long-range connections, resulting in a larger number of inputs to a given area and consequently a much denser cortical graph (i.e., density in terms of connections expressed as a percentage of the maximum possible connections). Such high-density graphs have important implications for the models that can be considered representative of the cortex. These studies collectively reinforce an emerging viewpoint of cortical connectivity in which principles of organization are constrained by distance and weight and which deeply contrasts with prevailing models that are purely topological and binary (i.e., connections expressed as existing or not) in nature. The high-density graph suggests that the specificity of the connectivity of cortical areas will be found in differences in the weights of individual links, or within sparse subsets (subgraphs) of the network distinguished by specific properties such as projection lengths. Indeed, it has been recently shown that weight heterogeneity is a salient feature of cortical connectivity and that it ranges over five orders of magnitude in strength (Markov et al. 2011b, 2014b; Oh et al. 2014). Earlier studies suggested that the functionality of an area was defined by a characteristic connectivity profile or fingerprint (Felleman and Van Essen 1991). This intuition proved to be correct but, given that cortical areas project to or receive input from between 30 and 90 % of all areas (Markov et al. 2014b; Oh et al. 2014; Zingg et al. 2014), it turns out that the specificity of the connectivity profile largely depends on the differences in weight values (Markov et al. 2011b).

The Promise of Network Theory

Over the last 15 years, advances in our characterization of connectivity across the cerebral cortex have greatly benefitted from exploiting developments in network science, an application of the mathematical theory of graphs to complex real world, natural and man-made networks (Newman 2010), permitting us to consider cortical structure in the light of canonical network (graph) theoretical models.

Although graph theory can be dated back to the solution of the Königsberg Bridges puzzle by Leonhard Euler in 1736, its applications to real-world phenomena started to take off only about two decades ago, mainly due to advancements in digital data recording and computation. A graph is a mathematical representation of the relationships/interactions within a set of objects (of any nature) called “nodes” (drawn as points), with the relationship between two nodes symbolized by a line segment called an “edge” or “link” connecting the nodes. If two nodes are not in interaction, the edge between them is missing. Prior to the “big data” revolution in networks, graph theory evolved on purely mathematical grounds, focusing on either

small or regular graphs, or purely random graphs, such as binomial random graphs, often referred to as Erdős-Rényi (ER) random graphs. In an ER random graph, every pair of nodes is connected with a given constant probability p, independently of other connections, and thus it is a homogeneous random structure. In the late 1990s, scientists started looking at graph representations of real-world networks and found that, in general, these did not conform to the types of graphs studied earlier by mathematicians, which were primarily introduced for reasons of mathematical tractability rather than in an effort to describe real-world systems. It is important to mention, however, that the language of graph theory, its mathematical tools and methods are still applicable; only the models have to be changed to describe real-world networks. There have been thousands of real-world networks studied with graph theory methods, such as various social networks, communication networks, including networks of computers (Internet) and of linked web pages (www), and networks in biology, including gene transcription, cell signaling, metabolism, neuronal networks and networks of trophic interactions. These have led to two main and influential schools of observations regarding real-world networks and the subsequent surge of graph theoretical models conforming to those observations. One of them, originating from social networks, is the so-called small-world (SW) property, introduced by Watts and Strogatz (1998); the other, mainly originating from technological and biological networks, is the so-called scale-free (SF) property introduced by Barabasi and Albert (1999).

The SW Property A network or graph is said to have the SW property if it has high clustering and a small average path length. Path length between two nodes in the graph is measured as the smallest number of edges (number of hops) necessary to go from one node to the other, and the average shortest path length is simply an average of such shortest paths over all node pairs that can be reached from one another in the graph. It is a purely topological measure in a given graph; it is independent of physical characteristics (such as physical distances or actual spatial positioning). The word "small" in the SW property comes from the fact that the average shortest path length is scaling only logarithmically with the number of nodes, i.e., almost all pairs of nodes are separated by a very small number of hops along edges (inspiring the "six degrees of separation" phrase in popular parlance). This short-path length property also holds for ER random graphs. What is drastically different from the ER graph, however, is that the SW property implies high clustering (which is vanishingly small in large ER graphs). Clustering refers to the level of incidence of connectivity among the members of a node's network neighborhood (measured by the frequency of triangles). A typical network with the SW property is the social network, where paths are short and clustering is high, simply because the acquaintances of a person tend to also become acquainted over time. Note that the SW property is only a property; it does not define a graph or a model. Watts and Strogatz (1998) introduced a simple method to test whether a network has the SW property: given a real-world network, one randomly rewires its edges (i.e., the total number of edges is held constant, only the connectivity is randomized) and measures the average path length and the clustering coefficient in the

randomized network. If the average path length does not change significantly, but the clustering coefficient drops significantly in the randomized network (which is essentially an ER graph), the original network has the SW property.

The SW property provides a potentially attractive feature of how the brain may support high modularity for functionally specialized computations while maintaining efficient communication across the brain for global integration. Interest in the SW property has led to the search for other features in the cortical circuitry that could be present in other real-world network models, such as the SF property, the presence of hubs (areas with significantly many more incident connections than others) and, more recently, preferential connectivity among hubs, referred to as a rich-club.

The SF Property A network is said to have the SF property if the histogram of the number of connections (called degree) of its nodes is heavily skewed (has a heavy right tail), well approximated by a power law. Such networks are characterized by the existence of a small number of hubs, which are nodes that connect to a significant fraction of all the other nodes (they are high degree nodes). Networks with SF property have been found in communications (Internet, www), citation networks, sexual interactions, metabolism, electronic circuits, and subroutine calls in large software packages. Network hubs channel many pathways between the nodes and thus they have a heightened importance and control over the rest of the network. It then becomes an interesting question whether these hubs are preferentially interconnected (more than just by random chance), forming a so-called rich-club, or, on the contrary, whether hubs are separated by lower degree nodes.

It is important to note that the SW and the SF properties are independent. There are networks in which one is present but not the other, or both, or none. While networks with the SF property have short (or ultra-short) average path length, they may have very low clustering (even zero), thus not qualifying as SW, and networks with the SW property can have arbitrary degree distributions, thus not qualifying as SF. One common feature for all the networks in which these properties were studied is that they were all *sparse* networks. A network is sparse when its density is very low. The density of a graph is measured as the ratio ρ between the number of edges M found in the network and the maximum number of edges it could have, which in directed networks is $N(N-1)$, where N is the number of nodes. In a sparse but connected network, M is on the order of N and thus ρ is on the order of a very small number for large networks. For the whole social network, this is 10^{-7} or 10^{-5} % density! For dense networks, however, their graph theoretical properties are entirely different from those in sparse graphs and they need other approaches for their study, as discussed below.

Finally, while properties such as SW, SF, and the presence of hubs or a rich-club have functional implications for the networks, they do not constitute network models, i.e., they do not provide falsifiable predictions about other properties (as discussed just above, the SW character says nothing about the SF character, etc.). Moreover, these features are at the binary/topological level, but we should not forget that brain networks are physical networks embedded in space and obeying

physical and physiological constraints needed for functioning. While there is a natural temptation to believe that brains may follow the same design principles as other functional complex networks in nature, or man-made networks, such claims need to be firmly rooted in empirical evidence. Unfortunately, the existence or absence of binary properties, as those discussed above, does not uniquely select for such principles, as these properties may occur as a result of many different mechanisms. Further, we believe that network models based on first principles invoking physical and geometrical constraints have a better chance of describing cortical networks than a small set of inferred binary features based on apparent similarity to other complex networks.

Empirical Evidence for a Principled Model of Cortical Connectivity: The EDR Model

Initially, the principle data sets from which the binary features of SW, hubs and rich-clubs were derived came from tract tracing experiments collated from the literature, using a variety of biological markers, and in which connectivity is indicated by the presence/absence of connections, i.e., binary connectivity. Nevertheless, connection strengths vary enormously depending on the projection, and it would seem probable that bringing on board this characteristic would importantly inform our understanding of the cortical network. More recently, these data sets have been supplemented by results from cerebral imaging experiments, using diffusion tensor imaging techniques (dMRI) or functional association through correlation measures from resting state MRI (rMRI). Currently, however, such techniques provide no information on the directionality of connections and yield only probabilistic, and as yet unvalidated, evidence for connections.

Interestingly, two landmark studies that predate the formulation of the SW property of the cortex stressed two important features of cortical organization not inherent in that framework. First, Van Essen et al. (1990) and Felleman and Van Essen (1991) built an extensive network of the visual system based on known principles of cortical hierarchy. The hierarchical relationship of two areas was derived from the laminar distribution of the projections between cortical areas. The projection from area A to B defines a feedforward projection if it originates from the upper cortical layers (supragranular layers 1–3) and targets the granular layer 4; conversely, if the projection originates from the deeper, infragranular layers and avoids layer 4, it is termed feedback. This system defines a binary order relation on cortical projections that can be used to define a hierarchy among cortical areas (Markov et al. 2014a). Second, using multidimensional scaling, Young (1992) showed that the spatial layout of cortical areas was consistent with their binary connectivity. Importantly, this finding also implied that spatial relations between areas might play an important role in cortical connectivity. In fact, the high clustering that occurs in the cortical network is dependent on the spatial separation

between areas (Markov et al. 2013b), suggesting that physical separation distance and clustering are tightly interconnected features. This finding shows that, for the brain, its binary connectivity may be rooted in physical and geometrical properties. Network models that are based on purely topological connectivity rules, such as many simple SW graph models, do not necessarily take into account such empirical facts.

Our initial work focused on quantifying laminar relations between cortical areas in the macaque (Barone et al. 2000; Markov et al. 2014a) to address the claim that the Felleman and Van Essen hierarchy is indeterminate (Hilgetag et al. 1996). This led us to invest a considerable effort in creating a consistent and weighted database of inter-areal connectivity in the macaque cortex. To obtain these data, we injected retrograde tracers in cortical areas and counted the number of labeled cell bodies in each area (from a segmented atlas of 91 areas) projecting onto the injection site. We exploited two measures of connectivity: the fraction of labeled neurons (FLN) in an area with respect to the total labeled in the cortex and the proportion of supragranular labelled neurons (SLN) in an area with respect to the total number of neurons marked in the area. The FLN is taken as a measure of projection strength whereas the SLN characterizes the laminar order relations between two areas. Currently, our published database consists of the results from injections in 29 areas distributed across the macaque cortex (Markov et al. 2011b, 2014b). These data provide a weighted and directed graph, termed $G_{29 \times 91}$ to indicate the dimensions of the adjacency matrix, that is a subset of the full graph $G_{91 \times 91}$ that would be obtained if we had data from injections in all 91 areas of our atlas. In addition, from the $G_{29 \times 91}$ graph, we obtain the edge-complete subset, $G_{29 \times 29}$, in which the status of connectivity among all pairs of injection sites is known. As the 29 areas sampled are distributed across the whole cortex, it is to be expected that many of the properties of this edge-complete graph will generalize to the full cortical graph.

One of our first observations on this data set was its high density. Sixty-six percent of all the possible connections were present (at 100 % each area would be connected to all other areas), which is considerably higher than that of the collated data sets used in previous analyses (Fig. 1a). In our exhaustive enumeration of neurons across the cortex, we uncovered many (36 %) projections that had not been previously described. While some of these connections were weak, they nevertheless overlapped in terms of weight with many known connections and were found to be largely consistent across individuals (Markov et al. 2014b). It is this large number of newly found projections that leads to the very high density of the cortical matrix.

The density of the matrix has a powerful influence on the properties of the network, and its increase with respect to earlier reports has far-reaching consequences, as we shall later demonstrate when discussing the SW property and rich-clubs. To explore how our results compare to earlier claims, we have sequentially removed connections, starting with the weakest (Fig. 1a). This process predictably leads to an increase in the average (shortest) path length, which is shown as a 95 % confidence interval (gray shading). As shown, the data from earlier reports fall on or

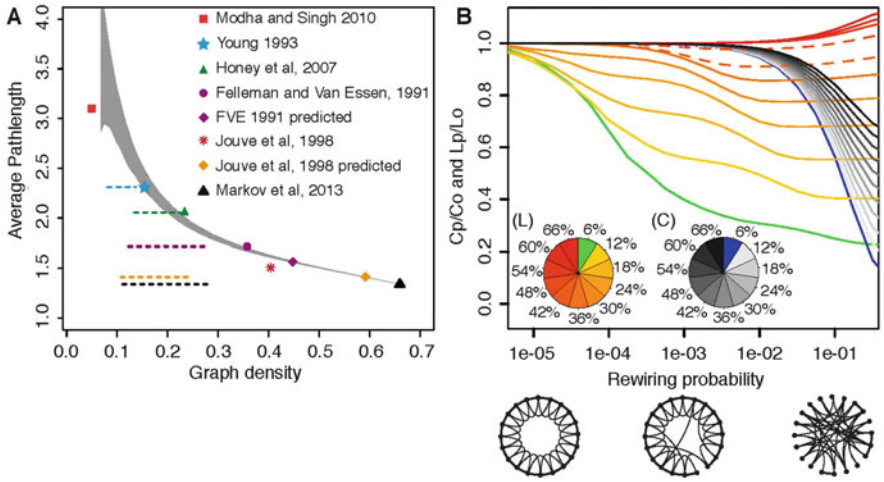

Fig. 1 Effects of density and network properties. (**a**) High density of the cortical graph. Comparison of the average shortest path length and density of the $\boldsymbol{G}_{29\times29}$ subgraph with the graphs of previous studies. Sequential removal of weak connections causes an increase in the characteristic path length. *Black triangle*: $\boldsymbol{G}_{29\times29}$; *gray area*: 95 % confidence interval following random removal of connections from $\boldsymbol{G}_{29\times29}$. *Dotted horizontal lines* indicate the 5–95 % interval with at least one unreachable node (following repeated and graded, random edge removal). Note that the three least dense graphs are near their 5 % unreachability levels. Data incompleteness meant that some of the initial networks have unreachable nodes; the latter are removed and not considered here, 14 unreachable nodes from Modha and Singh (2010), one unreachable node from Young (1993) and two unreachable nodes from Felleman and Van Essen (1991). Modha and Singh 2010: (Modha and Singh 2010); Young 1993: (Young 1993); Honey et al. 2007: (Honey et al. 2007); Felleman and Van Essen 1991: (Felleman and Van Essen 1991); Jouve et al. 1998: (Jouve et al. 1998); Markov et al. 2014b: (Markov et al. 2014b). "Jouve et al. (1998) predicted" indicates values of the graph inferred using the published algorithm (Jouve et al. 1998). (**b**) Effect of density on Watts and Strogatz's formalization of the SW. Clustering and average path-length variations generated by edge rewiring with probability range indicated on the "x" axis applied to regular lattices [of 1000 nodes in a 1D ring, as in Watts and Strogatz (1998)] of increasingly higher densities. The pie charts show graph density encoded via colors for path length (L) and clustering (C). On the y axis, we indicate the average path length ratio (Lp/Lo) and clustering ratio (Cp/Co) of the randomly rewired network, where Lo and Co are the path length (Lo) and clustering (Co) of the regular lattice, respectively. Lp and Cp are the same quantities measured for the network rewired with probability (p). Hence, for each density value indicated in the L and C pie charts, the corresponding Lp/Lo and Cp/Co curves can be identified. Three diagrams below the x axis indicate the lattice (*left*), sparsely rewired (*middle*) and randomized (*right*) networks. *Dashed lines* in (**b**) indicate 42 % and 48 % density levels

near the 95 % confidence interval but at much smaller densities, consistent with the fact that the earlier studies were missing the weak connections. The original database found its origin in the seminal work of Felleman and Van Essen (1991). These authors reported a density of 32 % but remarked that, if those connections that had not been tested were to be investigated, they would expect a density of 45 %. Subsequently, Jouve and colleagues (1998) updated the database with connections reported between 1991 and 1998, leading to a density of 37 %. This

study then used second order connections to infer the connectivity of untested connections, leading to a prediction of 58 % [in Fig. 1a, indicated as Jouve et al. (1998) predicted], which is not very different from the 66 % we reported (Markov et al. 2014b). All of the other studies appear in Fig. 1 to the left of the Felleman and Van Essen study, and they report densities significantly lower than that of these authors, ranging from 25 % (Honey et al. 2007), to 15 % (Young 1993) to 7 % (Modha and Singh 2010). These three modeling studies arrived at such low densities because they deemed that untested connections were absent and because they added additional areas to the original Felleman and Van Essen data set from the CoCoMac public source. Besides their artificially low density, these unreliable databases have two other consequences. Firstly, they contain variable unreachable nodes, as many as 14 in the case of Modha and Singh (2010). Secondly, repeated, graded and random removal of edges very rapidly leads to the break-up of these graphs into several components, as indicated by the 90 % confidence shown as dotted lines. In contrast, the graphs of Markov et al. (2014b) Jouve et al. (1998) and Felleman and Van Essen (1991) do not begin to break up until the removal of a large number of connections.

The high density raises difficulties for claiming that the inter-areal network at this level has the SW property. Recall that SW graphs are characterized by high clustering with low average path length between graph nodes, contrasting with the simplest model of random graphs, namely the ER random graphs, that, while having low average path length, have low clustering. High-density graphs, however, trivially, are highly clustered with low average path length (Humphries and Gurney 2008; Markov et al. 2013a). This is simply a consequence of the fact that, due to the large number of edges, there will be short paths between any two nodes, and triangles will occur frequently (high clustering). This is not an independent feature of the network (as it is in other, sparse real-world networks) but simply a consequence of density. As we show next, a simple calculation demonstrates that the cortical inter-areal network does not have the SW property. The procedure for determining whether the SW property is present was introduced by Watts and Strogatz (1998; Fig. 1b). First we determine the average path length and the clustering coefficient in the network of interest. Then we perform a rewiring of the edges so as to keep the average degree (thus the network density) constant. This produces an ER random graph as a null model, in which we measure again the average path length and the clustering coefficient. If the original network has the SW property, then rewiring causes the clustering coefficient to drop drastically, by as many as several orders of magnitude. Usually, the average path length changes as well, but only slightly. For example, in the Watts-Strogatz paper, for the network of film actors (a social network) the clustering coefficient drops from 0.79 to 0.00027, almost 3000-fold! For the power-grid the clustering coefficient drops 16-fold, whereas for the *C. elegans* neuronal network it drops 5.6-fold. In the $G_{29 \times 29}$ graph, there are 322 node pairs with connections (ignoring directionality) between them. The average degree of this undirected network is $\langle k \rangle = 2 \times \frac{322}{29} = 22.2$. In the corresponding ER random graph with the same number of nodes and edges (thus

average degree as well), the clustering coefficient is $C = \frac{\langle k \rangle}{N-1} = \frac{22.2}{28} = 0.79$ (Newman 2010). In the undirected form of the $G_{29 \times 29}$ we measured $C = 0.84$, a change of only 1.06-fold!

Figure 1b shows for the Watts-Strogatz model with the SW property (a ring lattice with partially rewired edges) a comparison of clustering coefficients and path lengths specified relative to those expected from a random graph plotted as a function of the percentage of randomly rewired lattice edges for increasing graph density (Markov et al. 2013a). By about 45 % density, there is very little wiggle room between the model graph and the rewired random graphs, which means that topological models like the Watts-Strogatz SW model (Watts and Strogatz 1998) cannot provide a good description of the inter-areal network.

Another regularity that we observed in our database is that the distribution of FLN values follows a log normal distribution (Markov et al. 2011b, 2014b). Similar behavior has since been reported in the mouse cortex as well (Wang et al. 2012; Oh et al. 2014), and a log normal distribution appears to be a characteristic at multiple physiological and anatomical levels in the brain (Buzsaki and Mizuseki 2014). Log normal distributions are positively (right) skewed and long-tailed, so that they contain many weak connections as well as a few very strong ones. It is important to note that, in evaluating a power law fit to cortical network data, in many instances the weakest connections are thresholded. In fact, if the weak connections were ignored, then our data might be attributed to a power law distribution. Ironically, extrapolation of such a truncated power law would imply an even larger number of weak connections than we actually observe. Note that these are weight distributions (fraction of node pairs connected by links with given weights), not degree distributions (number of neighbors). The few strong connections are always the nearest neighbors, implying a relation of distance to connectivity strength. In fact, we observe that the FLN is exponentially related to distance, as has also been recently confirmed in the mouse (Oh et al. 2014).

The observed weight-distance relations are described by an EDR that accounts for a surprising number of characteristics of the cortical network (Ercsey-Ravasz et al. 2013). First, given that the observed inter-areal distances are normally distributed, the EDR predicts that FLN will follow a log normal distribution. Second, random graphs of the same density as our edge-complete graph generated from the EDR model match our data in the numbers of bi-directional and uni-directional projections and in the distributions of triadic motifs of connectivity. This is not true for random graphs in which the probability of connection is constant as a function of distance (CDR graphs) and, in fact, the good agreement that we observe in the EDR-generated networks is sensitive to the value of the exponential space constant. This finding warrants defining both the generated graphs and the observed cortical graph as an EDR graph or network.

The above findings show that the EDR model captures local features of the cortical network. However, we found that this graph category also captures global properties. Firstly, the average distribution of eigenvalues of random EDR graphs (the graph spectrum) matches more closely the spectrum of our edge-complete

graph than does the CDR (note, graphs with the same eigenvalue spectra share many structural properties). Secondly, our cortical data show a large number (13 of them) of cliques of size 10 (complete subgraphs) that are highly inter-connected, forming a dense core (92 % connectivity). EDR graphs display this structure whereas CDR graphs do not. This behavior is reminiscent of the rich-club behavior observed in low-density networks but, in fact, on our dense graph, the rich-club index is barely significant (demonstrated below). Thirdly, EDR graphs display local and global communication efficiencies (measured as network conductances; see Ercsey-Ravasz et al. 2013) similar to those computed on our edge-complete graph $G_{29\times 29}$. We computed these efficiencies for our $G_{29\times 29}$ and evaluated their evolution as a function of the removal of weak and strong edges, respectively. The behavior observed was qualitatively similar to that obtained from EDR graphs but not CDR graphs. Fourthly, we found that the EDR model positions areas in a way that minimize total wire length whereas CDR graphs do not (Ercsey-Ravasz et al. 2013). Thus, the EDR and the spatial positioning of the areas appear to represent two fundamental constraints on cortical connectivity.

To emphasize that the EDR and binary graph models with SW property (such as the Watts-Strogatz model) are fundamentally different models of cortical organization, we summarize here some of the differences that we developed above. (1) Firstly, the node relations in the definition of the SW property are fundamentally topological, meaning that they are not spatially constrained. Secondly, these graphs are based on binary connectivity (connected/not connected), meaning that they are not weighted. Such networks are highly abstract and thus are far removed from real world networks (Boccaletti et al. 2006). In sharp contrast, the EDR graph is spatially embedded (i.e., laid out in space with distance values) and weighted, meaning that the connections have different strengths or weights. (2) In the SW property, clustering results because of the friend-of-my friend-is-my friend effect. In the modern world, friends are not confined to a specific location and can be scattered around the globe; thus clustering does not imply spatial proximity. Clustering is very high in the EDR model but is mediated by physical distance, so an analogous social network would correspond to a primitive tribal society where social groups are spatially located (Markov et al. 2011a). In the EDR graph, if a pair of areas are close in distance, then they are more likely to be connected and will have similar connectivity profiles (Markov et al. 2013b). Thus, clustering is inherently linked to space, as we have observed empirically. (3) The EDR has a heavy-tail log normal distribution, whereas binary SW models have constant weights on edges (of unity). (4) While many complex networks have the SF property with several orders for the range of variation for nodal degrees, the degree distributions in the $G_{29\times 29}$, or EDR vary less than threefold and do not conform to a power law. (5) Instead, the dense EDR graph exhibits a significant number of cliques, sets of areas that are completely inter-connected. Our edge-complete cortical graph contains 13 cliques of size 10, a remarkably improbable event if connectivity were independent of distance. (6) In several complex networks (and primarily those with the SF property), hubs are statistically more highly interconnected than expected, leading to a rich-club phenomenon. The EDR graph shows only weak evidence for

a rich-club organization in terms of the indices used to measure this tendency in SF networks. Instead, the cliques are highly connected, forming a dense core surrounded by a less dense periphery.

The EDR *is a network model*, not a property, and it is derived by the analysis of FLN values that characterize the strength of projection. Nevertheless, analysis of the distribution of SLN values reveals additional structure in the cortex, similar to a bowtie, based on the feedback/feedforward nature of the connections between the nodes in the periphery and the core. Below, we develop some of these ideas in more detail.

The Cortical Core-Periphery Structure

Complex networks that occur in nature as part of functional systems (natural or man-made) have been observed to have heterogeneous structure and behavior. Signatures of structural heterogeneity may appear as non-Poisson degree distributions, in deviations of motifs distributions from those in random graphs and in many cases in core-periphery structures. The latter observation, namely the existence of a denser interconnected core of nodes surrounded by a less dense periphery, is a hallmark of many information-processing networks (Csermely et al. 2013), and they have received considerable attention in the analysis of cortical networks as well. They were introduced for the first time by Zhou and Mondragon (2004) to test for the core-periphery properties of sparse SF networks such as the internet and the worldwide web. The existence of a rich-club has been defined informally as the tendency of hub nodes (nodes with the highest degrees) to form tightly interconnected communities. Its quantitative definition was later refined by Colizza et al. (2006) and applied to many real-world SF network datasets. For completeness, here we provide the standard definition by Colizza et al. (2006) and then discuss its applications by other authors to cortical inter-areal networks. We will then show that this definition is not suited for the detection of core-periphery structures in dense networks.

For now, let us consider undirected networks. We rank order the nodes by their degrees and consider the set of nodes with degrees larger than some given value k. Let us denote their number by $N_{>k}$ and by $M_{>k}$ the number of edges found between these $N_{>k}$ nodes only. The topological (based on binary connections only) rich-club coefficient for a degree value k is defined by the ratio:

$$\varphi(k) = \frac{2M_{>k}}{N_{>k}(N_{>k} - 1)} \tag{1}$$

This ratio expresses the fraction of existing edges between nodes of degree larger than a given minimum degree and the maximum number of edges that could exist among them, i.e., the density of the subgraph between all nodes with degree larger than k. However, there is also the effect that higher degree nodes will be more likely

to be connected to one another by chance only, because they have many more edges incident on them than an average node. To remove this degree-induced bias, $\varphi(k)$ is compared to a properly defined null model. Typically, the null model is generated from the studied network by random rewiring of its edges, preserving its degree sequence (which can be done by edge swaps). Let us denote the corresponding quantity (1) for this randomized null-model network by $\varphi_{rand}(k)$. Then the corresponding normalized rich-club measure of Colizza et al. is defined via:

$$\varphi_{norm}(k) = \frac{\varphi(k)}{\varphi_{rand}(k)} = \frac{M_{>k}}{M_{>k}^{rand}} \tag{2}$$

where $M_{>k}^{rand}$ is the number of edges found among all nodes with degree higher than k after randomizing. Accordingly, the set of nodes for which $\varphi_{norm}(k) > 1$ over some range of k values is called a rich-club, and it expresses the fact that these hub nodes have more connections between themselves than by pure chance. The extension of the above expressions is straightforward for directed networks, in which case we may also talk about an out-degree k_{out} based rich-club measure $\varphi^{out}(k)$ and an in-degree k_{in} based rich-club measure $\varphi^{in}(k)$ and their normalized versions.

The above rich-club detection method has been defined with sparse graphs and heterogeneous degree distributions in mind and, in particular, for SF networks. This measure, works well, indeed, for these types of networks. However, as we show next, it fails for dense networks, in spite of the fact that they may have a clear-cut core-periphery structure, as indeed is the case for our cortical network $G_{29\times29}$. Figure 2 shows the rich-club measures $\varphi(k)$ and $\varphi_{norm}(k)$ for the $G_{29\times29}$ graph. The first observation is that, although there is a range of degree values for which the normalized coefficient $\varphi_{norm}(k)$ is larger than unity, it is only slightly larger (less than 1.06), for the directed versions and less than 1.1 for the total degree based measure. In other words, the rich-club measure is not strongly selective for the core-periphery structure.

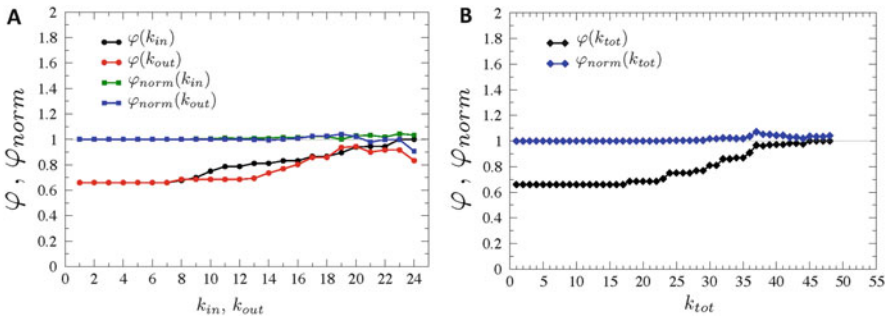

Fig. 2 Rich-club coefficients as function of degree. In (**a**), the *green symbols* show the normalized coefficient as function of in-degree, whereas *blue* shows the normalized coefficient as function of out-degree. In (**b**), we show the same as in (**a**), but for the total degree ($k_{tot} = k_{in} + k_{out}$). Neither of the curves climbs significantly above unity to indicate a rich-club structure

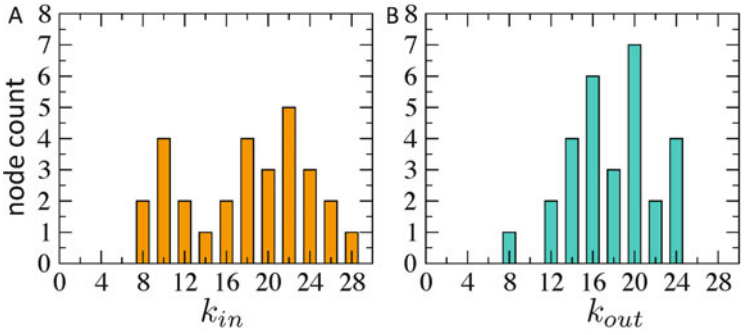

Fig. 3 Degree distributions. For the $G_{29\times29}$ cortical graph, expressed as the number of nodes with a given degree. (**a**), in-degree distribution and (**b**), out-degree distribution. In scale-free (SF) networks, this histogram would be a power law decay as function of degree

The $G_{29\times29}$ graph has a density of 66 % and it does not have a SF (power law) degree distribution, neither for the in- nor the out-degrees (see Fig. 3; a SF degree distribution falls as a power law as a function of the degree). Thus, for dense networks, alternative methods are needed to detect their core-periphery structure.

We introduced a novel method to detect core-periphery structures in dense graphs based on a clique distribution analysis (Ercsey-Ravasz et al. 2013). A clique is a subset of nodes that have all the possible connections between them. The largest clique in the $G_{29\times29}$ has ten nodes, and there are 13 such cliques of 10 in $G_{29\times29}$, all involving only 17 nodes, forming the core of $G_{29\times29}$ with a very high density of 92 %. The rest of the nodes form the periphery with a 49 % density of connections and a density of 54 % of connections between core and periphery nodes (Ercsey-Ravasz et al. 2013). This is a clear-cut core-periphery structure with a core of 92 % density surrounded by the rest of the graph having roughly 50 % density. The probability for seeing such a core-periphery structure in a random graph with the same number of nodes and edges is 10^{-17}, infinitesimally small. So why doesn't the rich-club measure (2) pick out this structure? The explanation lies with the second expression in Eq. (2), which shows that the normalized measure is simply the fraction of edges between the larger-than-k degree nodes and the same quantity for the randomly rewired network. Thus, this rich-club coefficient will be large only if the randomized network *has a significantly reduced density* between the same set of nodes. That can only happen in a sparse network and if the degree distribution is heterogeneous as well. In our network, due to its high density, even by random rewiring we cannot reduce significantly the density of connections between these particular nodes. Additionally, the network's degree distribution is not very heterogeneous; Table 1 and Figs. 3 and 4 show that most of the nodes are high-degree nodes. In particular, area 8l has an in-degree of 28, thus receiving connections from all the others within $G_{29\times29}$. There are 12 nodes with in-degree 20 or larger, meaning that 41.3 % of all nodes receive connections from at least $20/29 \cong 69$ %

Table 1 Degrees of nodes in the 17-node core of the edge-complete inter-areal network $G_{29\times 29}$

Areas of the core	In-degree	Out-degree	Total degree	Total degree inside the 17-core
	k_{in}	k_{out}	$k_{tot} = k_{in} + k_{out}$	
7A	24	25	49	28
8l	28	21	49	31
8m	26	22	48	32
STPc	23	25	48	30
9/46d	26	21	47	32
F5	24	22	46	29
STPr	21	24	45	30
46d	23	21	44	31
7m	25	17	42	28
9/46v	22	20	42	29
F7	22	20	42	32
24c	20	20	40	30
F2	19	20	39	27
8B	19	19	38	32
STPi	12	25	37	26
PBr	17	17	34	27
10	19	13	32	28

of all nodes. When randomizing such networks, it is impossible to disconnect high degree nodes from one another.

In an earlier publication, Harriger et al. (2012) presented a rich-club analysis of the macaque cortical network using data extracted by Modha and Singh (2010) from the CoCoMac data base, which is an online collation of tract tracing studies from various sources. This inter-cortical connectivity matrix included 242 regions (nodes) and 4090 directed links, providing a directed binary graph of 7 % density. As discussed above, unfortunately, this database does not report the status of all the connections between the nodes and it is, therefore, largely incomplete. The corresponding matrix contains links, non-links and entries that are simply unknown (i.e., it is not known if the connection is present or absent between the two nodes). The Harriger et al. study (and several others) treated the unknown connections as absent (non-existing), resulting in a sparse network. Unfortunately, this incompleteness strongly biases the graph theoretical conclusions drawn from such graphs, as seen previously in the case of the SW analysis. Harriger et al. (2012) reported on the existence of a rich-club structure, formed by several nested layers of node groups; however, no rich-club coefficient curves were shown (normalized or otherwise) to help assess the degree to which the rich-clubs emerged.

Failure of the Rich-Club One of the arguments one could bring into the rich-club study of $G_{29\times 29}$ is that the binary level analysis misses the fact that the cortical graph is weighted, showing strong heterogeneity in link-strength values spanning five orders of magnitude. However, once we have weights on links, the notion of the

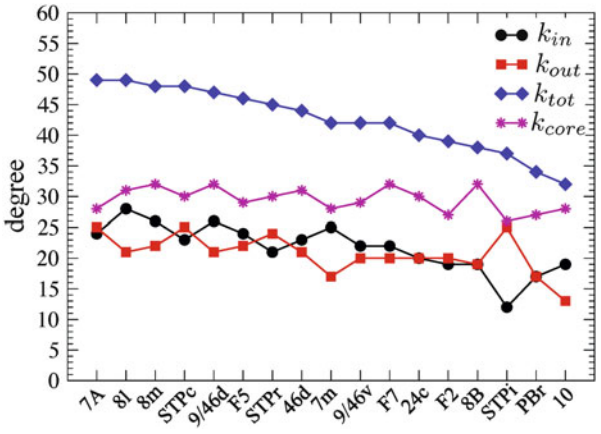

Fig. 4 Degree distribution of nodes in the 17-node core of $G_{29\times 29}$. k_{core} is the total (tot) degree (the in-degree plus the out-degree) *within* the core

rich-club becomes more elusive as it can be defined in many different ways, providing answers that sometimes are in stark contrast with one another, as we show below. Here we use the variants introduced by Opsahl et al. (2008), which were also adopted for cortical network analysis by van den Heuvel et al. (2012). In this definition, first we choose a quantity, the so-called "richness-parameter" r, by which we rank-order all the nodes. This parameter could be node degree, node in-degree, out-degree, total incoming weight of links to a node, average of incoming link weights, etc. We denote by $M_{>r}$ the number of edges found between all the nodes that have a richness parameter larger than r. Let $W_{>r}$ denote the sum of weights on these edges. For example, if this richness parameter is the in-degree of the nodes, we then sum the FLN weights of the edges that are incident on all the nodes with an in-degree larger than a given value (k_{in}). Next we rank-order all the links in the network *by their weight* (FLN) and then we sum the weights for the edges with the top weights, i.e., $\sum_{l=1}^{M_{>r}} w_l^{rank}$. We then form the weighted rich-club parameter $\varphi^w(r)$, via:

$$\varphi^w(r) = \frac{W_{>r}}{\sum_{l=1}^{M_{>r}} w_l^{rank}}. \tag{3}$$

To eliminate effects coming from heterogeneity of weights or the richness parameter, we normalize (3) by the corresponding quantity in a null-model network. This is typically taken as a randomized version of the original network. However, here too, there are several choices. One can randomly rewire the edges along with their weights or keep the edges where they are and shuffle around randomly only the weights associated with them, etc. Here we randomly reshuffle the edges along with their weights. In Fig. 5 we show the resulting weighted rich-club coefficients.

In Fig. 5a, the ranking is done by $r = k_{in}$ (blue) and $r = k_{out}$ (red). The weights in both cases are the FLN weights of the edges. In Fig. 5b, the ranking of the nodes is done by the sum of the FLN weights for the incoming edges to that node. Since

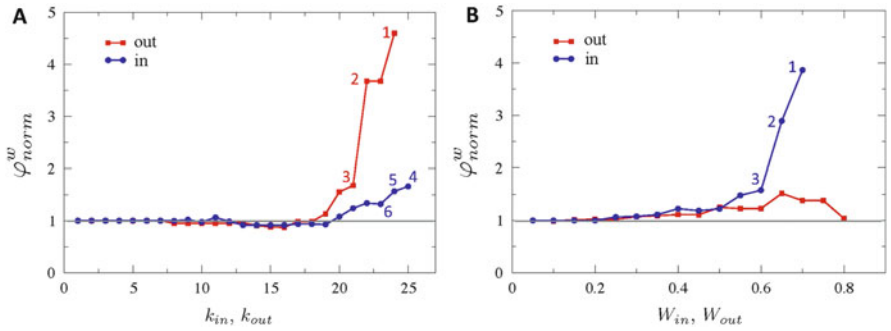

Fig. 5 Weighted rich-club measures. (**a**), Ranking is based on degrees. By out-degree, the weighted rich-club is formed by six nodes (group 3): 7A, STPc, STPi, STPr, 8m, F5. This can be decomposed into groups 2 and 1 of increasing rich-club measures. Group 2: 7A, STPc, STPi, STPr and Group 1: 7A, STPc, STPi. By in-degree, the weighted rich-club is formed by the six areas (group 3): 8l, 8m, 9/46d, 7m, 7A, F5. Group 2: 8l, 8m, 9/46d, 7m, and Group 1: 8l, 8m, 9/46d. (**b**), Ranking is based on FLN weights (within the 29×29 matrix). Based on total incoming weight (*blue*), the weighted rich-club in this case is formed by 11 areas (group 3): V1, V2, V4, 46d, DP, 9/46d, 5, F1, 8m, 8l, STPi. Within this are nested Group 2: V1, V2, V4, 46d, DP, 9/46d, 5, F1 and Group 1: V1, V2, V4, 46d, DP. By total outgoing weight (*red*), the weighted rich-club is formed by 9 areas: V2, V4, STPi, 8m, 9/46d, 7A, V1, F2, 46d (Group 2). Within this is nested Group 1: V2, V4, STPi, 8m, 9/46d, 7A, V1, F2

there is now a large heterogeneity between the link weights, $\varphi^w_{norm}(k)$ can take significantly larger values. Accordingly, all nodes with degrees (in- or out-) of 19 or larger are part of the corresponding (in- or out-) rich-club. For out-degrees based ranking, we obtain a nested structure with the largest out-degrees being the most interconnected among them. Based on in-degrees, it is a bit more difficult to make conclusive statements. When looking at ranking based on total incoming weight to a node (Fig. 5b), it shows a very different picture from what is presented in Fig. 5a. It shows rich-club ordering for the visual areas (which are mostly in the periphery, not core), because there is a lot of FLN concentrated among the neighboring visual areas, with strong connections between them.

Why the apparent arbitrariness in the identified rich-clubs using weighted measures? The weighted rich-club definition tries to detect correlations between a richness measure/parameter r and the weights on the links. The idea behind this is as follows. Weights on links usually represent strength of interaction/relationship. For example, in a social network, a large number of phone-calls going back-and-forth regularly between two people is a proxy for a strong social-tie, or interdependence. Given an empirical network, the strongest weights show the strongest interactions present in that network. Now let us assume we are interested in finding out if there is a correlation between tie strength and some other nodal property, such as personal wealth. We may look at the top 100 wealthiest people, find the connections between them, and sum the strengths of the connections running between them, representing the overall communication strength within this group. Is this communication strength as large as it could be, that is, would

this sum equal the sum of the 100 largest edge strength found in the network, irrespective of any other property? This ratio is the weighted, but non-normalized rich-club measure. The larger this ratio, the more there seems to be a connection between tie/link weight and the richness parameter *r*. However, such observations need to be interpreted carefully. In any finite, and relatively small, dataset, such apparent correlations might also be the result of variability and signal neither correlations nor causations. A large richness value *r* might be the result of an extraneous factor that is not contained in the analyzed data but happens to correlate with tie strength. For example, the incidence of hair loss/baldness among congressional members (the richness parameter *r*) might appear correlated by this method with the number of times two members have publicly supported one-another on some issue. This can certainly appear so, because hair loss has a tendency to increase with age, and more senior members have a tendency to share similar/perhaps more conservative views on issues. However, clearly the two variables (number of agreements and amount of hair) are not causally related in any significant way.

The Promise of the Bowtie Complex networks with directed edges may have a core-periphery organization that resembles a bowtie structure. In this case, the links between periphery nodes and nodes in the core can be divided into two classes forming the "wings" of a bowtie: a fan-in (left) wing and a fan-out (right) wing (Fig. 6). The nodes in the fan-in wing are sources of flow into the core, whereas the nodes in the fan-out wing, also called sinks, receive flow from the core. Bowtie topologies have been observed to occur both in man-made networks such as the

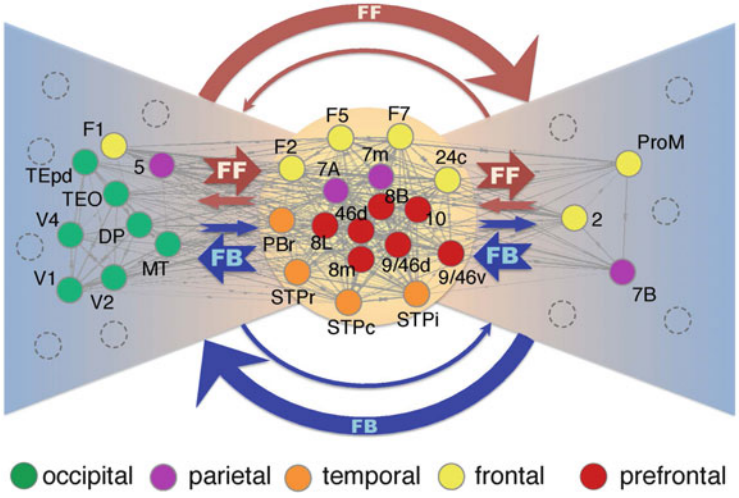

Fig. 6 Bowtie organization of the core-periphery. This organization is obtained from taking into account both the laminar asymmetry (SLN index) of the projections between the core and periphery nodes and their strength [FLN; see Markov et al. (2013a) for derivation details]. *FF* feedforward, *FB* feedback

worldwide web (Broder et al. 2000; Kleinberg and Lawrence 2001), the Internet (Tauro et al. 2001; Siganos et al. 2006), manufacturing processes (Csete and Doyle 2004) and biological systems (Csete and Doyle 2004; Kitano 2004), including metabolism (Ma and Zeng 2003; Ma et al. 2007), the immune system (Kitano and Oda 2006) and cell signaling (Natarajan et al. 2006; Supper et al. 2009). The reason for the widespread occurrence of this type of structural organization is possibly due to the fact that highly functional systems are also non-equilibrium systems (in a thermodynamic sense) and, as such, they have to maintain energy and matter flow through the system to optimize their functionality. In Markov et al. (2013a), we have shown that the cortical $G_{29\times 29}$ network exhibits a bowtie core-periphery organization. However, a naive interpretation of the links between the core and periphery will not lead to a bowtie organization, as almost all areas in the periphery have both incoming and outgoing pathways to the core. This organization emerges very clearly once we take into account the counter-stream hierarchical organization of the directed pathways between the core and periphery. Long-range inter-areal projections were observed to present a strong laminar asymmetry, which in turn can be used to define a hierarchical distance and reveal cortical hierarchies. As discussed in the introduction, pathways that originate mainly from supragranular layers and terminate in layer 4 qualify as feedforward (FF) pathways whereas pathways that originate mainly from infragranular layers and avoid layer 4 in lower areas qualify as feedback (FB) pathways. The corresponding SLN index provides a continuous measure that can be used to quantify hierarchical distances through the cortical network. In Markov et al. (2013a), we classified the links between the periphery and core into four classes corresponding to whether they fed into or from the core and were FF or FB. Using their SLN values and the FLN strengths of the connections, the periphery nodes clearly separate into a fan-in and fan-out wing surrounding the core of the bowtie (see Fig. 6). It is important to emphasize that this bowtie was not inferred from analogies with other networks. It was derived from empirical data.

Perhaps the most relevant finding to come out of the network analysis with respect to cortical function is the heterogeneity of the cortical graph. Here the bowtie topology (Markov et al. 2013a) is particularly interesting because it is based on cortical hierarchy and therefore is relevant to predictive coding theory (Clark 2013). Predictive coding, arguably a general computational theory of brain function, finds its roots in statistical physics and machine learning and proposes that hierarchical processing leads to ascending prediction errors and descending predictions in perception, motor control and learning networks. The integration of local and global processes involves interactions of the long-distance inter-areal pathways in to the local circuitry that makes up 80 % of the cortical machinery (Markov et al. 2011b; Bastos et al. 2012). This means that the bowtie structure implies definable functional roles in terms of predictive coding but also cognitive function. The distributed nature of the core of the bowtie, spanning prefrontal, frontal and parietal areas, corresponds to the requirements for the global neuronal work space, a cognitive architecture that, along with divergence convergence

zones, could play an important role in consciousness and multimodal convergence (Man et al. 2013; Dehaene et al. 2014).

Biology, Clustering and the Importance of Weak Links

In this short review of the cortical network, we have emphasized the distinction to be made between topological networks with the SW property and the spatially embedded EDR network. The first sums up the properties of a category of sparse complex graphs that are commonly found but which, we find, are not descriptive of the inter-areal network. While the SW property has been claimed by numerous studies, they have invariably employed data seemingly indicating a low density cortical network (see Bullmore and Sporns (2012)).

In contrast to the topological SW network, the EDR graph is anchored in the high *spatial clustering and geometrical positioning* of the nodes of the inter-areal network. Because the EDR predicts so many of the observed properties of the cortical network, we believe that it is likely to be a characteristic feature of the cortical networks found throughout all mammals. A strong argument in support of this position is the importance of spatial clustering of functionally related cortical areas. The layout of primary cortical areas across placental mammals is highly conserved, as shown in Fig. 7. In this figure the primary visual (dark blue), auditory (yellow), and somatosensory areas (red) exhibit stereotypic locations in all mammals. Surrounding the primary areas are the higher order association areas, which integrate information from the primary areas and generate complex behavior. In this figure, the association cortex is mostly shown in white, with the exception of two high-order visual areas (area V2 light blue; area MT green). Figure 7 shows that, during phylogenesis, there is an expansion of the cortical mantle and the association cortex so that, in the highly evolved primate brains, the association cortex is the major component, in contrast to the more primitive brains where the primary areas dominate. Van Essen and colleagues identified homologous areas in macaque and human, enabling them to quantify differential regional expansion in the two species (Van Essen and Dierker 2007; Hill et al. 2010). This shows an expansion of the association cortex located in temporal, parietal and frontal lobes. Comparison between human and chimp shows that the near threefold increase in size of the human brain is almost entirely due to a disproportional increase in human association cortex (Preuss 2011; Sherwood et al. 2012). The expansion of the association cortex during phylogenesis is speculated to be genetically driven by duplication of cortical areas, leading, for example, in the visual cortex to topographically defined areas sharing common borders defined with respect to the visual field (Allman and Kaas 1971). This is partially illustrated in Fig. 7, where the primary visual area, area V1 is bordered by area V2, indicated in light blue. This duplication leads to areas V1 and V2 sharing a common border that represents the vertical meridian. Rosa and Tweedale (2005) speculated that this duplication process led to the observed mosaic of extrastriate visual areas sharing well-defined

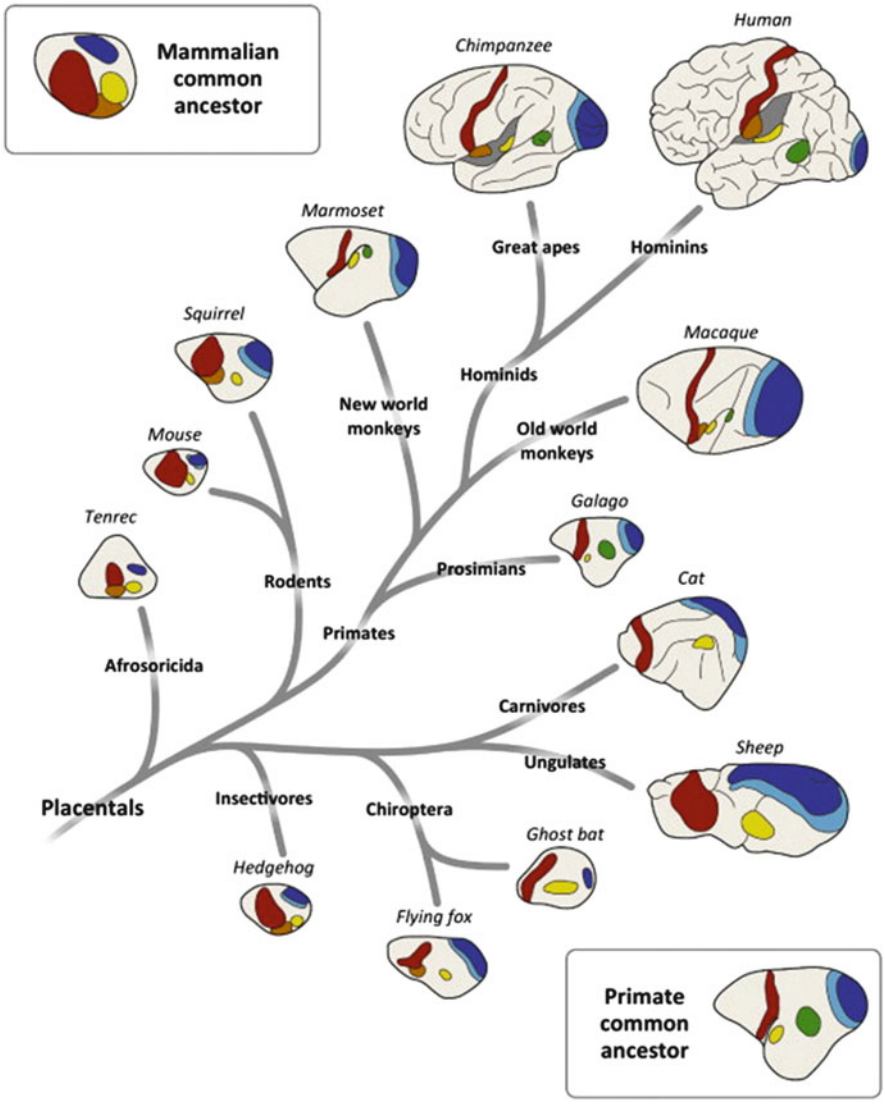

Fig. 7 Phylogeny of the neocortical sheet. Schema showing the layout of cortical areas in different classes of mammals. This figure shows that, during phylogenesis, the positions and dimensions of conserved primary areas (*colored*) are conserved, which contrasts with the progressive increase of the surrounding association cortex, indicated in white. The expansion of the association cortex is thought to accommodate the increase in the number of areas, possibly via a process of genetically driven duplication of areas. This can be seen for area V2 (*light blue*), a second-order visual area that surrounds the primary visual area, area V1 (*dark blue*). Note the highly consistent location in primates of MT (*green*), a higher-order visual area, with respect to areas V1 and V2. Throughout the phylogenetic tree, there is a remarkable consistency between the positions of the visual areas and the primary auditory area (*yellow*), somatosensory area (*red*) and secondary somatosensory cortex (*orange*). *Top left*, representation of common mammalian ancestor; *lower right*, common primate ancestor (Buckner and Krienen 2013)

maps of the visual field, where the primary visual area V1 and the higher order area MT act as anchors, a concept that has been generalized recently to a tethering hypothesis where conserved, regionally localized patterning centers ensure the observed stereotypic localization of primary areas during the massive cortical expansion that accompanies phylogenesis (Buckner and Krienen 2013). The tethering hypothesis speculates that the primary cortical areas would be integrated into the cortical network in a very different fashion from the association cortex, the latter being characterized by a greater abundance of long-distance connections. Our results do not support this speculation, but they do suggest a major difference. Whereas the primary cortical areas are located in the fans of the bowtie, the association cortex is part of the high-density cortical core and is part of the knot of the bowtie (Ercsey-Ravasz et al. 2013).

The above considerations go some way in explaining the developmental and phylogenetic basis of the high functional clustering of areas, thereby forming distinct constellations of areas centered on visual, auditory, somatosensory, motor and cognitive functions. The recent tract tracing data in both macaque and mouse and the network analysis of inter-areal connectivity begin to provide a coherent picture of the high-density cortical network. The anatomy tells us that there are many more connections than previously suspected, including numerous low-weight long-distance connections that can only be detected by connectomic approaches (Markov et al. 2014b; Oh et al. 2014; Zingg et al. 2014). It would be wise to resist the temptation to ignore such connections. The variables of functional and structural parameters, including synaptic weights and transmission probability, EPSPs, spine sizes, firing rates, correlations of population synchrony and axon diameters, show skewed log normal distributions (Buzsaki and Mizuseki 2014). Hence, at multiple levels, assemblies of many weak and few strong elements seem to be a characteristic feature of what makes brains work. With regards to the weak inter-areal connections, while their band-width will exclude dense information transfer, there is ample possibility for them to play a role in contraction dynamics of oscillatory coherence (Wang and Slotine 2005) and hence in shaping communication across the cortex (Fries 2005). The potential importance of the long-distance weak connection in the cortex, at least superficially, echoes that of the strength of weak ties in social networks, reputed to be important in integrating the individual into the social fabric (Granovetter 1973).

Conclusion and Perspectives

Structural heterogeneity in a network is thought to be a necessary condition for high functionality. In the inter-areal cortical network there are two propositions concerning heterogeneity: one is the linking of high-degree nodes or hubs to form a rich-club topology (van den Heuvel et al. 2012) and the other is the existence of maximally interconnected subgraphs or cliques (Ercsey-Ravasz et al. 2013).

The rich-club is solidly based on the concepts of hubs forming a means of efficient routing of information through the cortex. But to what extent is the notion of a hub allowing dynamic switching and relaying messages relevant to present-day understanding of brain function? While there are instances where neurons have been thought to play the role of a relay, careful scrutiny of such claims show that this is rarely or never the case. A case in point is the so-called relay neurons of the lateral geniculate nucleus (LGN), which receive input from the retinal ganglion cells and project to layer 4 of the primary visual cortex, area V1. It was the similarity of the receptive field of the LGN neuron and the retinal ganglion cell that partially fueled the notion of a relay function. However, even in this system it turns out that the LGN relay neurons receive large number of inputs from the thalamic reticular formation as well as feedback projections from the cortex, such feedback connectivity being characteristic of the visual pathway (Gilbert and Li 2013). Recent evidence shows that the layer 6 cortico-thalamic neurons of area V1 and extrastriate cortex projections to LGN relay neurons and via their interactions with the thalamic reticular nucleus ensure a complex spatial and cross-modal attentional modulation of LGN neurons (McAlonan et al. 2006, 2008; Jones et al. 2013) requiring a sophisticated alignment of the receptive fields of the cortical and thalamic neurons (Wang et al. 2006). The point we want to make here is that neurons do not passively relay messages and the cortical network should not be viewed as an elaborate system of switches. Instead, signals undergo an extensive integration, and this is particularly true in the cortex, where single neurons receive the inputs from hundreds of afferent neurons.

In the present review, we have argued that the topological SW property is not relevant to the inter-areal network. This contrasts with the EDR network, which is embedded in space and therefore considerably less abstract. Whereas the SW is only a property, the EDR model is a full-blown network model with the power to predict many features of network organization. While the predictability of the EDR graph speaks strongly in its favor, would a much lower density change our outlook? What would the cortical graph look like at a much finer granularity, such as the level of voxels? This indeed would cause a drop in density, so that the SW property might hold for the cortical network. But, more importantly, would the EDR network still be valid after the drop in density? Would it continue to predict global and local properties? We are at present addressing this issue by creating a fine-grained 2D surface map of inter-areal connection density. However, this will not address the question at the single neuron level. In the EDR network, connection weight is a proxy for probability, so that at a single neuron level this would amount to looking at the decrease in probability of interconnections between pairs of neurons at increasing distances. The probability of finding a connected pair is so low, even at short distances (Braitenberg and Schüz 1998), that existing electrophysiological techniques would seem to be inappropriate for searching for interconnected pairs at larger distances. One possibility is the recently proposed BOINC barcoding of individual neuron connectivity (Zador et al. 2012). Going down these avenues may be worth the effort in order to understand the brain in space at multiple scales.

Box 1—Glossary

Bowtie	a core-periphery organization of nodes and edges in a directed graph, as defined in the main text.
Clique	a subgraph (subset of nodes) of a graph for which all possible edges between the nodes are present.
Clustering	an index representing the fraction of edges present among the neighbors of a node and the maximum number of edges that could exist between these nodes.
Degree	the number of edges to which a node is connected. In a directed graph, the in-degree refers to the number of incoming edges and the out-degree to the number of outgoing edges.
Edge	a connected pair of points or nodes. The edge denotes a connection between the nodes. For example, a projection between two cortical areas constitutes an edge between the two areas, each considered as a node.
Edge-complete subgraph	a subgraph that has exactly the same connections between its nodes as the connections between the same nodes in the larger graph that this subgraph is part of (in mathematics this is called a vertex-induced subgraph).
EDR network	a category of random graphs constrained by the observed exponential decrease in weight, which represents probability of connection with physical distance. Because the graphs generated in this manner capture numerous features of the cortical network, the EDR graph is also representative of the cortical network.
Graph	mathematical structure consisting of two sets, a set of objects/entities represented as points that are termed nodes and a set of pairs of points that constitute the edges of the graph. If the points of an edge are ordered, i.e., the edge (a, b) between points a and b is considered to be different from the edge (b, a), the graph is termed *directed*. If a third set of values taken as weights are associated with the edges, then the graph is termed *weighted*.
Graph theory	the mathematical treatment of graphs as abstract objects, i.e., the sets of nodes and edges.
Hub	nodes of the highest degrees that are connected to a significant fraction of other nodes.
Log normal law	here used as a probability law for which the frequency of an event is distributed normally as a function of the log of its size. In the cortex, the log normal distribution describes the distribution of strengths of connections of areas projecting onto a given area. The plots below (Fig. 8) display examples of log normal (solid) and power law (dashed) distributions

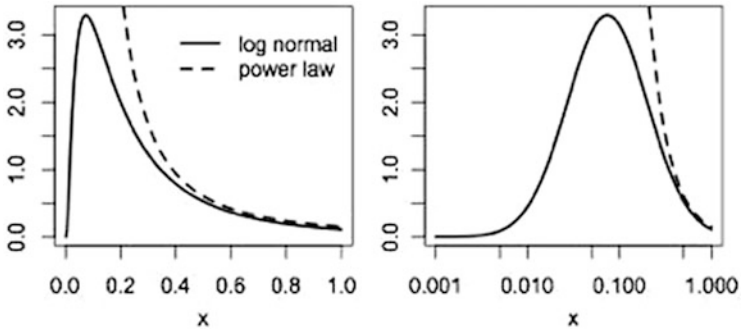

Fig. 8 Log normal and power laws

	as a function of a linear variable (left) and the same variable scaled logarithmically (right).
Neighborhood	the set of nodes to which a node is connected by an edge.
Node	a point used to identify an object/entity in a graph. For example, we could consider individual areas of the brain as nodes. On a finer scale, we could consider individual neurons as nodes.
Path length	the number of connected edges that must be traversed to travel between two nodes in a graph.
Power law	used here as a probability law for which the frequency of an event declines as a power of its size. In graph theory, a power law may be used to define the degree distribution of a graph in which the frequency of nodes with a given degree falls off as a power function of the degree. This results in many nodes with a small degree and a few nodes with a very large degree (hubs).
Rich-club	a higher-than-expected incidence of edges between hubs than between other nodes.
Small world graph	a topological graph with high clustering and low average path length.
Spatially embedded graph	a graph in which the spatial positions of the nodes (and, thus, the distances between them) are defined.
Topological or binary graph	a graph defined solely in terms of the relations implied by its nodes and edges but with no additional attributes, such as a metric distance or spatial position, weights or any other measures. It can be represented by a simple connectivity matrix, with 0's and 1's for its entries, indicating non-connections or connections, respectively.

Box 2—Network Structure: Topological Versus Spatial Clustering

We distinguish between network properties that are purely topological, i.e., expressed only in terms of whether and what nodes are connected and perhaps their strength of connection, and those that depend also on other attributes, such as physical distance. To make the distinction clear, in the simple four node graph in Fig. 9, node b is equidistant topologically from nodes a and c since it is connected to each through a single edge. It is spatially closer to nodes c and d, however, even though d is further topologically from b (two edges distant). It is important to distinguish whether the connections between nodes in a graph depend only on topological considerations or whether spatial factors come into play, as well. Whether or not spatial or simply topological distance is related to the probability of a connection between nodes in a graph is an interesting question, because the answer can be informative as to the processes that generated the connections and thereby created the graph or variants with similar properties.

Spatial clustering is a notion expressing the fact that objects tend to bunch together in a limited region of space (and are perhaps also connected to one another), whereas network (or topological clustering) refers to the density of triangles in a network, without any reference to spatial embedding or positioning. In the definition of the SW, clustering is meant exclusively as network clustering, that is, as the density of the triangles, and has no relation to spatial clustering. Next we illustrate using simple examples that the two notions are entirely disconnected, i.e., high spatial clustering does not imply high network clustering and vice-versa. In Fig. 10a, we show a regular network embedded in space, which in this case is a simple ring. Every node is connected to the two closest nodes to their right and to their left. This is a network that is clearly clustered spatially (nodes connecting to their four closest neighbors). It has a network clustering coefficient $C = 0.5$. In Fig. 10b, we show exactly the same network (the same connectivity matrix), but the connected nodes are physically far apart in distance along the ring. Because the connectivity matrix has not changed, the network-clustering coefficient stays the same; however, the connected nodes are no longer clustered spatially. Thus, just because in a SW network we have large clustering, it does not imply that the nodes connected into triangles have to also be physically close to one another. The SW definition is simply topological; it does not imply any spatial embedding.

Another, more realistic example comes from comparing the roadway network with the airline network. While both networks are embedded in space, they are drastically different. In the roadway network (formed by intersections of highways as nodes and edges as highway segments between intersections), there is strong *spatial* clustering (see Fig. 10c). Since there are no shortcuts in the roadway network, all network triangles are formed by nodes that are also physically close to one another, connected by road segments. By contrast, in the airline network (nodes are airports, edges are flights, Fig. 10d), which has a large *network* clustering coefficient ($C = 0.34$), the triangles are formed between physically distant nodes. There are typically no direct flights between physically close airports; instead we have to fly through network hubs to reach them.

Fig. 9 A four-node graph in which nodes a and c are topologically equidistant from node b but nodes c and d are physically closer to node b

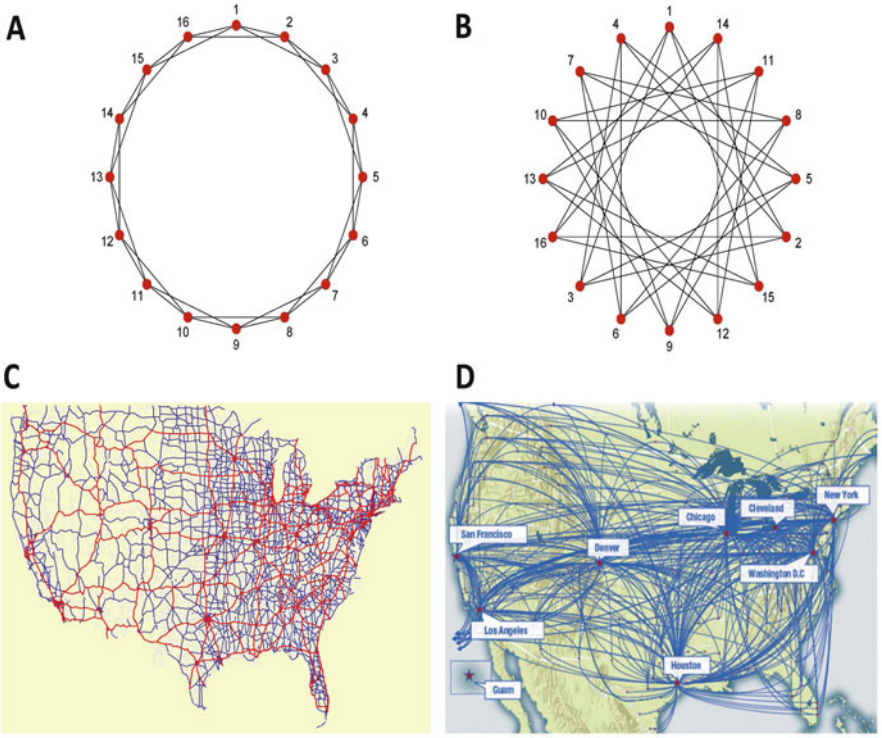

Fig. 10 Network clustering does not imply spatial clustering. A simple, regular network of 16 nodes embedded on a ring. In (**a**) the nodes are connected to their (spatially closest) four neighbors, whereas (**b**) shows the same network, therefore with identical network clustering, but without spatial clustering (the four neighbors of a node are at large distances from the node). (**c**) shows the US roadway (highway) network, in which nodes are spatially clustered (especially in densely populated areas), whereas (**d**) shows the United/Continental airline network, which has large network clustering but all triangles are between far-apart nodes. The SW property definition does not discriminate between (**a**) and (**b**) or (**c**) and (**d**)

The brain has some of both aspects: there is strong spatial and local network clustering between neighboring areas in the network, but there are also long-range links contributing to global clustering. Thus *network* clustering in this case is

composed of both types of clustering: on one hand there are many triangles between closely spaced areas and, on the other, there are also many triangles in which at least two sides of the triangles are made of long-range connections.

Acknowledgments This work was supported by FP6-2005 IST-1583 (HK); FP7-2007 ICT-216593 (HK); ANR-11-BSV4-501 (HK); LABEX CORTEX (ANR-11-LABX-0042) of Université de Lyon, within the program "Investissements d'Avenir" (ANR-11-IDEX-0007) operated by the French National Research Agency (ANR) (HK); PN-II-RU-TE-2011-3-0121, FP7-PEOPLE-2011-IIF-299915 (MER); in part, by grant FA9550-12-1-0405 from the U.S. Air Force Office of Scientific Research and Defense Advanced Research Projects Agency (ZT).

References

Allman JM, Kaas JH (1971) Representation of the visual field in striate and adjoining cortex of the owl monkey (Aotus trivirgatus). Brain Res 35:89–106

Barabasi AL, Albert R (1999) Emergence of scaling in random networks. Science 286:509–512

Barone P, Batardiere A, Knoblauch K, Kennedy H (2000) Laminar distribution of neurons in extrastriate areas projecting to visual areas V1 and V4 correlates with the hierarchical rank and indicates the operation of a distance rule. J Neurosci 20:3263–3281

Bastos AM, Usrey WM, Adams RA, Mangun GR, Fries P, Friston KJ (2012) Canonical microcircuits for predictive coding. Neuron 76:695–711

Boccaletti S, Latora V, Moreno Y, Chavez M, Hwang DU (2006) Complex networks: structure and dynamics. Phys Rep 424:175–308

Braitenberg V, Schüz A (1998) Cortex: statistics and geometry of neuronal connectivity, 2nd edn. Springer, Berlin

Broder A, Kumar R, Maghoul F, Raghavan P, Rajagopalan S, Stata R, Tomkins A, Wiener J (2000) Graph structure in the web. Comput Netw 33:309–320

Buckner RL, Krienen FM (2013) The evolution of distributed association networks in the human brain. Trends Cogn Sci 17:648–665

Bullmore E, Sporns O (2012) The economy of brain network organization. Nat Rev Neurosci 13:336–349

Buzsaki G, Mizuseki K (2014) The log-dynamic brain: how skewed distributions affect network operations. Nat Rev Neurosci 15:264–278

Clark A (2013) Whatever next? Predictive brains, situated agents, and the future of cognitive science. Behav Brain Sci 36:181–204

Colizza V, Flammini A, Serrano MA, Vespignani A (2006) Detecting rich-club ordering in complex networks. Nat Phys 2:110–115

Csermely P, London A, Wu L-Y, Uzzi B (2013) Structure and dynamics of core/periphery networks. J Complex Netw 1:93–123

Csete M, Doyle J (2004) Bow ties, metabolism and disease. Trends Biotechnol 22:446–450

Dehaene S, Charles L, King JR, Marti S (2014) Toward a computational theory of conscious processing. Curr Opin Neurobiol 25C:76–84

Ercsey-Ravasz M, Markov NT, Lamy C, Van Essen DC, Knoblauch K, Toroczkai Z, Kennedy H (2013) A predictive network model of cerebral cortical connectivity based on a distance rule. Neuron 80:184–197

Felleman DJ, Van Essen DC (1991) Distributed hierarchical processing in the primate cerebral cortex. Cereb Cortex 1:1–47

Fries P (2005) A mechanism for cognitive dynamics: neuronal communication through neuronal coherence. Trends Cogn Sci 9:474–480

Gilbert CD, Li W (2013) Top-down influences on visual processing. Nat Rev Neurosci 14:350–363

Granovetter MS (1973) The strength of weak ties. Am J Sociol 78:1360–1380

Harriger L, van den Heuvel MP, Sporns O (2012) Rich club organization of macaque cerebral cortex and its role in network communication. PLoS One 7:e46497

Hilgetag CC, O'Neill MA, Young MP (1996) Indeterminate organization of the visual system. Science 271:776–777

Hill J, Inder T, Neil J, Dierker D, Harwell J, Van Essen D (2010) Similar patterns of cortical expansion during human development and evolution. Proc Natl Acad Sci USA 107:13135–13140

Honey CJ, Kotter R, Breakspear M, Sporns O (2007) Network structure of cerebral cortex shapes functional connectivity on multiple time scales. Proc Natl Acad Sci USA 104:10240–10245

Humphries MD, Gurney K (2008) Network 'small-world-ness': a quantitative method for determining canonical network equivalence. PLoS One 3:e0002051

Jones HE, Andolina IM, Grieve KL, Wang W, Salt TE, Cudeiro J, Sillito AM (2013) Responses of primate LGN cells to moving stimuli involve a constant background modulation by feedback from area MT. Neuroscience 246:254–264

Jouve B, Rosenstiehl P, Imbert M (1998) A mathematical approach to the connectivity between the cortical visual areas of the macaque monkey. Cereb Cortex 8:28–39

Kennedy H, Knoblauch K, Toroczkai Z (2013) Why data coherence and quality is critical for understanding interareal cortical networks. Neuroimage 80:37–45

Kitano H (2004) Biological robustness. Nat Rev Genet 5:826–837

Kitano H, Oda K (2006) Robustness trade-offs and host-microbial symbiosis in the immune system. Mol Syst Biol 2:2006 0022

Kleinberg J, Lawrence S (2001) Network analysis. The structure of the web. Science 294:1849–1850

Ma H, Zeng AP (2003) Reconstruction of metabolic networks from genome data and analysis of their global structure for various organisms. Bioinformatics 19:270–277

Ma H, Sorokin A, Mazein A, Selkov A, Selkov E, Demin O, Goryanin I (2007) The Edinburgh human metabolic network reconstruction and its functional analysis. Mol Syst Biol 3:135

Man K, Kaplan J, Damasio H, Damasio A (2013) Neural convergence and divergence in the mammalian cerebral cortex: from experimental neuroanatomy to functional neuroimaging. J Comp Neurol 521:4097–4111

Markov NT, Ercsey-Ravasz MM, Gariel MA, Dehay C, Knoblauch A, Toroczkai Z, Kennedy H (2011a) The tribal networks of the cerebral cortex. In: Chalupa LM, Berardi N, Caleo M, Galli-Resta L, Pizzorusso T (eds) Cerebral plasticity. MIT Press, Cambridge, MA, pp 275–290

Markov NT, Misery P, Falchier A, Lamy C, Vezoli J, Quilodran R, Gariel MA, Giroud P, Ercsey-Ravasz M, Pilaz LJ, Huissoud C, Barone P, Dehay C, Toroczkai Z, Van Essen DC, Kennedy H, Knoblauch K (2011b) Weight consistency specifies regularities of macaque cortical networks. Cereb Cortex 21:1254–1272

Markov NT, Ercsey-Ravasz M, Van Essen DC, Knoblauch K, Toroczkai Z, Kennedy H (2013a) Cortical high-density counter-stream architectures. Science 342:1238406

Markov NT, Ercsey-Ravasz MM, Lamy C, Ribeiro Gomes AR, Magrou L, Misery P, Giroud P, Barone P, Dehay C, Toroczkai Z, Knoblauch K, Van Essen DC, Kennedy H (2013b) The role of long-range connections on the specificity of the macaque interareal cortical network. Proc Nat Acad Sci USA 110:5187–5192

Markov NT, Vezoli J, Chameau P, Falchier A, Quilodran R, Huissoud C, Lamy C, Misery P, Giroud P, Barone P, Dehay C, Ullman S, Knoblauch K, Kennedy H (2014a) The anatomy of hierarchy: feedforward and feedback pathways in macaque visual cortex. J Comp Neurol 522:225–259

Markov NT, Ercsey-Ravasz MM, Ribeiro Gomes AR, Lamy C, Magrou L, Vezoli J, Misery P, Falchier A, Quilodran R, Gariel MA, Sallet J, Gamanut R, Huissoud C, Clavagnier S, Giroud P, Sappey-Marinier D, Barone P, Dehay C, Toroczkai Z, Knoblauch K, Van Essen DC, Kennedy H (2014b) A weighted and directed interareal connectivity matrix for macaque cerebral cortex. Cereb Cortex 24:17–36

McAlonan K, Cavanaugh J, Wurtz RH (2006) Attentional modulation of thalamic reticular neurons. J Neurosci 26:4444–4450

McAlonan K, Cavanaugh J, Wurtz RH (2008) Guarding the gateway to cortex with attention in visual thalamus. Nature 456:391–394

Modha DS, Singh R (2010) Network architecture of the long-distance pathways in the macaque brain. Proc Natl Acad Sci USA 107:13485–13490

Natarajan M, Lin KM, Hsueh RC, Sternweis PC, Ranganathan R (2006) A global analysis of cross-talk in a mammalian cellular signalling network. Nat Cell Biol 8:571–580

Newman MEJ (2010) Networks: an introduction. Oxford University Press, Oxford

Oh SW, Harris JA, Ng L, Winslow B, Cain N, Mihalas S, Wang Q, Lau C, Kuan L, Henry AM, Mortrud MT, Ouellette B, Nguyen TN, Sorensen SA, Slaughterbeck CR, Wakeman W, Li Y, Feng D, Ho A, Nicholas E, Hirokawa KE, Bohn P, Joines KM, Peng H, Hawrylycz MJ, Phillips JW, Hohmann JG, Wohnoutka P, Gerfen CR, Koch C, Bernard A, Dang C, Jones AR, Zeng H (2014) A mesoscale connectome of the mouse brain. Nature 508:207–214

Opsahl T, Colizza V, Panzarasa P, Ramasco JJ (2008) Prominence and control: the weighted rich-club effect. Phys Rev Lett 101:168702

Preuss TM (2011) The human brain: rewired and running hot. Ann N Y Acad Sci 1225(Suppl 1): E182–E191

Rosa MG, Tweedale R (2005) Brain maps, great and small: lessons from comparative studies of primate visual cortical organization. Philos Trans R Soc Lond B Biol Sci 360:665–691

Sherwood CC, Bauernfeind AL, Bianchi S, Raghanti MA, Hof PR (2012) Human brain evolution writ large and small. Prog Brain Res 195:237–254

Siganos G, Tauro SL, Faloutsos M (2006) Jellyfish: a conceptual model for the as internet topology. J Commun Netw 8:339–350

Supper J, Spangenberg L, Planatscher H, Drager A, Schroder A, Zell A (2009) BowTieBuilder: modeling signal transduction pathways. BMC Syst Biol 3:67

Tauro SL, Palmer C, Siganos G, Faloutsos M (2001) A simple conceptual model for the Internet topology. In: Global Telecommunications Conference, 2001. GLOBECOM'01. IEEE, pp 1667–1671

van den Heuvel MP, Kahn RS, Goni J, Sporns O (2012) High-cost, high-capacity backbone for global brain communication. Proc Natl Acad Sci USA 109:11372–11377

Van Essen DC, Dierker DL (2007) Surface-based and probabilistic atlases of primate cerebral cortex. Neuron 56:209–225

Van Essen DC, Felleman DJ, DeYoe EA, Olavarria J, Knierim J (1990) Modular and hierarchical organization of extrastriate visual cortex in the macaque monkey. Cold Spring Harb Symp Quant Biol 55:679–696

Wang W, Slotine JJ (2005) On partial contraction analysis for coupled nonlinear oscillators. Biol Cybern 92:38–53

Wang W, Jones HE, Andolina IM, Salt TE, Sillito AM (2006) Functional alignment of feedback effects from visual cortex to thalamus. Nat Neurosci 9:1330–1336

Wang Q, Sporns O, Burkhalter A (2012) Network analysis of corticocortical connections reveals ventral and dorsal processing streams in mouse visual cortex. J Neurosci 32:4386–4399

Watts DJ, Strogatz SH (1998) Collective dynamics of 'small-world' networks. Nature 393:440–442

Young MP (1992) Objective analysis of the topological organization of the primate cortical visual system. Nature 358:152–155
Young MP (1993) The organization of neural systems in the primate cerebral cortex. Proc R Soc Lond B Biol Sci 252:13–18
Zador AM, Dubnau J, Oyibo HK, Zhan H, Cao G, Peikon ID (2012) Sequencing the connectome. PLoS Biol 10:e1001411
Zhou S, Mondragon RJ (2004) The rich-club phenomenon in the internet topology. IEEE Commun Lett 8:180–182
Zingg B, Hintiryan H, Gou L, Song MY, Bay M, Bienkowski MS, Foster NN, Yamashita S, Bowman I, Toga AW, Dong HW (2014) Neural networks of the mouse neocortex. Cell 156:1096–1111

In-Vivo Connectivity in Monkeys

Wim Vanduffel

Abstract Major efforts are underway to provide highly detailed descriptions of static anatomical brain connectivity in rodents, even down to the level of individual synapses. To fully understand brain functioning and to bridge the gap between rodents and humans, however, I argue in this chapter that effective connectivity studies in nonhuman primates are equally critical. The primate community should embrace the novel, high-precision genetic-based toolkits developed in invertebrates and rodents to study how activity in one brain region influences that in connected brain regions. These methods will allow us to measure true functional weights of anatomical connections during highly varying cognitive and perceptual demands in primates. Why monkeys, and why effective connectivity in addition to anatomical connectivity? First, the nonhuman primate is critically important to understand the functioning of the human brain since important brain regions, such as the granular prefrontal cortex carrying higher cognitive functions, are lacking in rodents as opposed to primates. Second, a pure anatomical description of connections at different scales may be useful to *constrain* models of brain functioning, however, it has little value to *explain* perception and behavior emerging from dynamic neuronal activity in distributed brain networks. Hence, tools that allow us to measure these dynamics at large scale and to causally interfere with the system at high temporal and spatial resolution are required to increase our understanding of changes in information processing at different stages within a functional network. In this chapter I will review past and emerging methods to study effective connectivity (mainly) in nonhuman primates, in other words how activity within a given brain area influences processing in anatomically connected brain regions. I will also argue that high-resolution whole brain imaging in monkeys may be invaluable to guide reversible perturbations and massive neurophysiological recordings simultaneously within multiple nodes of functional networks.

W. Vanduffel (✉)
Department of Neurosciences, Laboratory for Neuro-and Psychophysiology, KU Leuven Medical School, 3000 Leuven, Belgium

Harvard Medical School, Boston, MA 02115, USA

Martinos Center for Biomedical Imaging, Massachusetts General Hospital, Charlestown, MA 02129, USA
e-mail: wim@nmr.mgh.harvard.edu

H. Kennedy et al. (eds.), *Micro-, Meso- and Macro-Connectomics of the Brain*, Research and Perspectives in Neurosciences, DOI 10.1007/978-3-319-27777-6_6

Anatomical, Functional and Effective Connectivity in Animal Models

Perception and behavior emerges from the concerted activity of millions of neurons constituting a distributed but connected network of brain regions. To understand brain function, it will not suffice to define the detailed characteristics of single neurons or of a handful of "representative" neurons in one or a few areas simultaneously. A critical piece of information required for building biologically-plausible models of brain function is the manner in which these neurons are connected anatomically. Following decreasing interest in connectivity studies over several decades, this field has regained considerable impetus in recent years, mainly thanks to the appearance of new technologies allowing high throughput of connectivity data, which has been fueled by high-profile funding schemes such as the Connectome (Van Essen et al. 2012) and BRAIN (Devor et al. 2013) initiatives in the USA, the Human Brain Project (Markram 2012) in Europe and the BRAIN/MINDS (Okano et al. 2015) project in Japan. Also privately-sponsored institutes such as the Alan Institute and Janelia farms have launched projects aimed at collecting large-scale connectomics data, mainly in rodents. The resulting static descriptions of anatomical connections will be of great benefit for constraining models of cortical functioning at the micro-, meso- and macroscale.

However, critically important information, that cannot be gleaned from static descriptions of anatomical connectivity, concerns the variations in the functional strength of these connections across the highly-dynamic, constantly-varying states of the subject. Although intuitively one might expect that a strong anatomical connection exerts more weight on a target area than a weaker one, it actually depends on a variety of factors including the subject's behavioral state, the specific perceptual or task demands, the type of connection (i.e. feedforward or feedback), the excitation/inhibition balance, and the neurotransmitter systems involved. Therefore, the extent to which a set of neurons can influence processing in another set of neurons under various mental states and behavioral conditions constitutes crucial information required to fully understand brain function. In general, this is referred to as *effective* connectivity as opposed to *functional* connectivity (Friston 2011). Measures of functional connectivity are typically based on correlations of neuronal or hemodynamic activity across brain sites. Effective connectivity, on the other hand, relates to the mechanisms driving such correlated activity. This can be caused by common inputs, or by regions that actively influence activities in connected areas. Effective connectivity can be inferred statistically by, for example, using Granger causality, which relies on the fact that the history of activity in a source region is more predictive of activity in a target region than the history of the latter region itself. However, the only direct method to assess whether a particular region has a causal effect on processing in other regions is the use of focal perturbation methods in combination with a read-out tool such as electrophysiology, or any kind

of functional imaging. In this chapter I will briefly discuss several methods that are being used to investigate effective connectivity in awake animal models, thereby focusing on the past and current work of my group and speculating about future approaches.

Towards Causality: Effective Connectivity with Focal Perturbation Tools

The oldest perturbation tool is a simple lesion. The major disadvantage here is the irreversible nature of lesions, rendering test-retest experiments impossible. Moreover, the permanent nature of a lesion can trigger compensatory brain mechanisms whereby lost functionality at the site of the lesion may be partially assumed by other regions, although the temporal dynamics by which compensatory mechanisms are engaged remain unknown. Reversible perturbation methods are obviously advantageous compared to lesions.

Traditional focal, reversible perturbation tools used in animals include chemical, thermal, and electrical methods. Less focal, though non-invasive, inactivation protocols include transcranial magnetic stimulation (Gerits et al. 2011), and transcranial pulsed ultrasound methods (Tufail et al. 2010). Frequently-used chemical inactivation methods rely on the injection of local anesthetics or GABA-agonists such as muscimol (Hikosaka and Wurtz 1985). These chemicals have a relatively long half-life when injected, rendering them less than optimal for fast test-retest protocols and leaving them vulnerable to possible rapid functional reorganizations of the brain. Focal cooling of the brain is quite appealing, since the activity of neurons under the cooling probe can be blocked when the temperature falls below 20 °C without affecting transmission in traversing fibers (Lomber et al. 1994; Vanduffel et al. 1997; Lomber et al. 1999). Although several cycles of cooling can be performed within an experimental session, a major issue is that cooling is applicable mainly to easily accessible structures at the cortical surface. Cooling subcortical structures, or within a sulcus, without damaging tissue is technically demanding and affects neighboring tissue (such as both banks of a sulcus). Almost two decades ago, we cooled extrastriate cortex in awake cats in combination with deoxyglucose measurements, through which metabolic activity can be assessed throughout the entire brain (Vanduffel et al. 1997). As predicted by the excitatory nature of most cortico-cortical connections, we observed reduced metabolic activity in areas connected with the cooled region. Intriguingly, we observed that the effect on feedforward connections was stronger than predicted based on the anatomical strength of these connections alone, and that the converse was true for feedback connections. To the best of my knowledge, this was the first experimental evidence that the strength of an anatomical connection does not predict its functional weight (see Fig. 1).

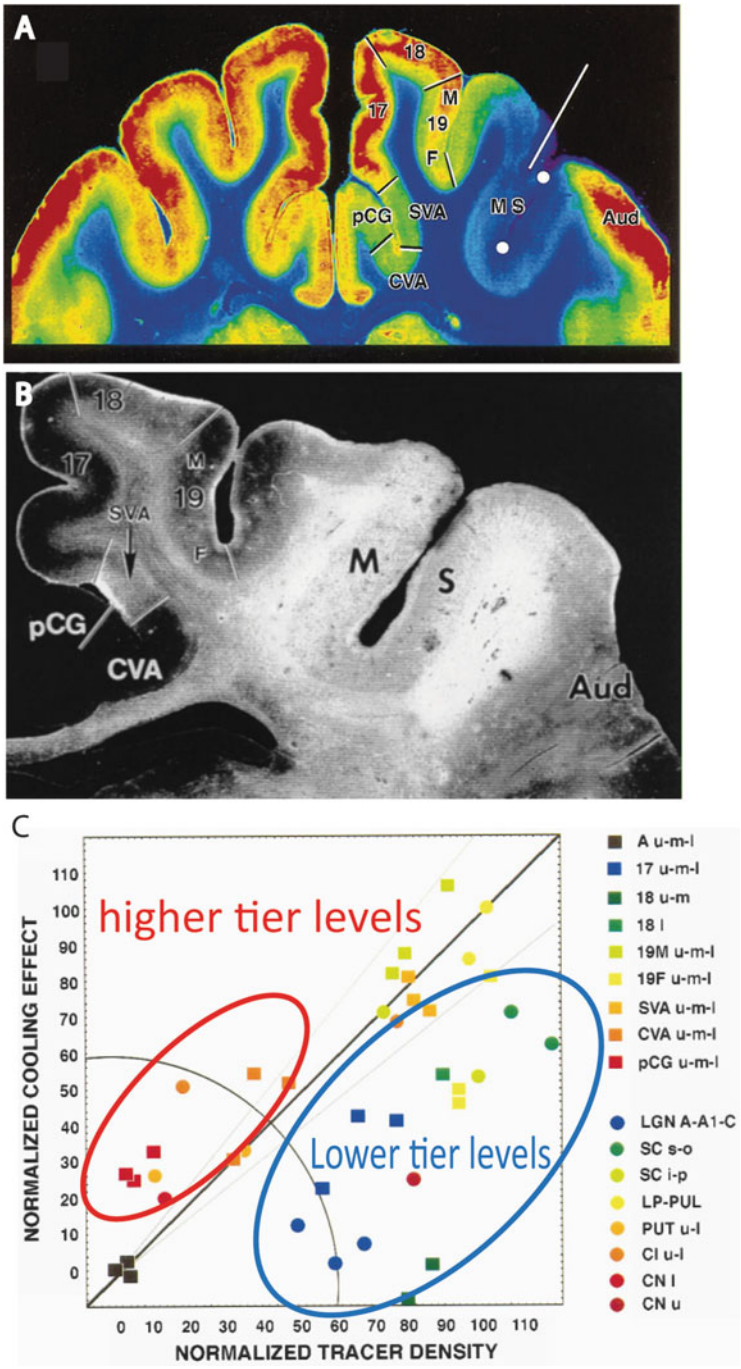

Fig. 1 (**a**) Color-coded image of 2-Deoxyglucose (2DG) concentrations in a coronal section of the cerebral cortex of the cat during cooling-induced deactivation of the middle suprasylvian sulcus (MS). *White circles* in MS sulcus represent position of the cooling probe. *Color scale* indicates

Electrical microstimulation is a focal perturbation tool used to map sensory cortex in humans (Rasmussen and Penfield 1947). Despite its high temporal resolution, microstimulation of local neuronal activity can be facilitatory or inhibitory, depending on parameters such as the amplitude, frequency, and duration of the stimulation trains (Tehovnik and Lee 1993). Another drawback relates to the microstimulation currents that can produce electrical artifacts during and immediately after the pulses when the procedure is combined with electrophysiology (Premereur et al. 2012, 2014; Moore and Armstrong 2003). Also, as nicely illustrated by Clay Reid's group, it is not always obvious which neuronal elements are affected at the electrode tip (Histed et al. 2009).

More recently, genetically-based perturbation tools with superior temporal and spatial resolution have emerged, the most established of these being optogenetics (Yizhar et al. 2011). This method enables one to manipulate activity of neurons on a millisecond time-scale. Optogenetics relies on light-sensitive proteins (opsins) incorporated into neuronal membranes using viral vectors or genetically engineered organisms [for details see Karl Deisseroth's (2015b)]. The activities of cells expressing the opsins can be manipulated by illumination with specific wavelengths. Depending on the opsin type, neurons and other cells can be depolarized (activated) or hyperpolarized (deactivated) when illuminated. The appeal of optogenetics is its millisecond temporal resolution and its superior spatial resolution relative to other techniques (Deisseroth 2015a). Although optogenetics allows modulation of activity in specific cell types, the results of cell-type specific optogenetics should be interpreted with some caution, because information arising from transduced cells is immediately transmitted to downstream neurons within the targeted micro-and macro circuitry. Therefore, any readout method (including behavior) with a temporal resolution lower than tens of milliseconds will encounter difficulties in differentiating between effects induced by the modulated cells and those (in)directly connected. Immediate downstream effects have been nicely demonstrated in monkeys by Bob Desimone's group, who observed, exactly as expected, enhanced neuronal activity, consequent to transduction with a depolarizing opsin, near the targeted site (Han et al. 2009). However, they also measured consistent suppressed neuronal activity in the site injected with the viral

Fig. 1 (continued) 2DG concentrations. *White scale bar*, 5 mm. *SVA* splenial visual area, *Aud* auditory cortex, *LGN* lateral geniculate nucleus, *Pul* pulvinar nucleus, *LP* lateral posterior nucleus; 17, 18 areas 17 and 18; 19M, 19F area 19 medial or fundal parts. (**b**) Distribution of [3H] proline and [3H] leucine transported after injections in the middle suprasylvian suclus. *Darkfield* illumination indicating strength of connections from MS sulcus. (**c**) Normalized tracer density versus normalized cooling effect on 2DG concentration for a variety of cortical and subcortical structures. *Solid line* represents slope of unity where tracer density and effects on 2DG uptake are equal. *Gray lines* represent 20 % deviation from these values. *Squares* indicate cortical structures, *circles* subcortical structures. The *color-coded labels* for the various structures reflect levels of visual processing: *blue*, early; *green yellow*, intermediate; and *red*, late. *Points* below the diagonal show a weaker 2DG effect than anticipated from the anatomy, whereas *points* above the diagonal show a stronger 2DG effect than anticipated. Figure adapted from Vanduffel et al. (1997)

vector construct. The latter effect appeared at longer latencies, thus in neurons that are at least one synapse away from the transduced neurons.

Other very promising genetically-based methods include DREADDs (designer receptors exclusively activated by designer drug), whereby an artificial receptor is expressed in the cell membranes which can be activated by an artificial ligand (Dong et al. 2010). Hence, this method is much less invasive than optogenetics since no optical fiber is required, only the administration of a drug that activates the receptor. These DREADD-type approaches are very promising, especially for applications where the temporal resolution of the perturbation is less important.

Ultimately, to completely understand the neuronal processes underlying perception and behavior, one will need to acquire electrophysiological signals at the single-cell level simultaneously from *all* brain sites involved in these processes. Furthermore, to clarify whether all such neuronal populations are critically involved, their activity needs to be up-or down regulated while the effect on perception or behavior is being assessed. Despite recent technological advances for recording from several dozens of single neurons simultaneously, even in multiple areas, and despite the astounding innovations in genetically-based methods to reversibly perturb activity in brain cells, this ambitious goal cannot be achieved as of yet, especially in primates. To make this daunting task somewhat tractable and to vastly reduce the needle-in-a-haystack aspect, I propose that targeting of these multiple recording sites should be guided by high-resolution whole-brain imaging (Vanduffel et al. 2014). We recently developed implanted phased-array coils in monkeys to obtain sub-millimeter whole-brain functional data with standard clinical MR scanners, which might serve this purpose (Janssens et al. 2012) (see Fig. 2).

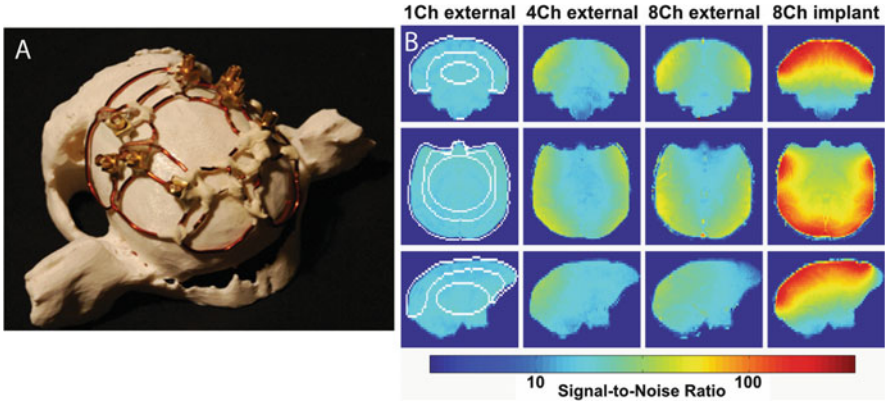

Fig. 2 (**a**) Photo of phased-array MR coil embedded in the headset of the monkeys (**b**) Increase in signal-to-noise ratio of implanted phased-array coil relative to other external phased-array coils. This coil allows sub-millimeter fMRI in monkeys at 3 T. Figure adapted from Janssens et al. (2012)

Effective Connectivity: Combined Electrical Microstimulation and Whole-Brain fMRI

In the past, we have employed whole-brain imaging during microstimulation of the FEF (FEF-EM), a region that can be behaviorally-defined, based on its involvement in saccade generation. When this region is electrically stimulated with low currents, monkeys make eye movements whose direction and amplitude depend on the exact location of the electrodes within the topographically-organized FEF. The endpoints of these saccade vectors correspond to the movement fields of the neurons surrounding the electrode tip. Mounting evidence suggests that, in addition to its functional role in generating eye movements, the FEF is an area sending selective top-down signals to occipital regions in order to modulate incoming sensory activity in an attention-dependent manner. FEF is well-positioned for the task, since it receives connections from several higher-order neighboring areas involved in cognitive control (Schall et al. 1995). Moreover, it comprises a topographic map representing the visual field in a relatively well-organized manner (Janssens et al. 2014), hence FEF has the capacity to send spatially-specific signals back to upstream areas (Schall 1997).

Electrophysiology has shown that when FEF is stimulated at current levels insufficient to generate a saccade, activity in single V4 (Moore and Armstrong 2003) and LIP (Premereur et al. 2014) neurons can be enhanced for stimuli placed in the stimulated movement fields—as opposed to stimuli shown outside these movement fields. Furthermore, the modulation of the V4 firing rates is more pronounced when competing stimuli are shown, mimicking distractors surrounding a target during a spatial attention experiment. These sorts of changes in neuronal firing rates resemble the selective spatial attention effects previously observed in V4 (McAdams and Maunsell 1999).

In a follow-up experiment, Tirin Moore's group also showed that this subthreshold electrical stimulation in FEF resulted in improved detection thresholds for low-contrast stimuli flashed in the FEF movement fields (Moore and Fallah 2004). Albeit indirect, the combination of the behavioral and electrophysiological results obtained in V4 provided strong evidence that FEF can influence neuronal activity in visual cortex, in a manner very similar to that observed during selective spatial attention. Indeed, selective attention to a specific location in the visual field will enhance the neuronal processing of stimuli presented at that location, and these effects are particularly pronounced for less salient stimuli and when distractor stimuli are present. A direct link between microstimulation results and selective attention remains unverified, however, since the behavioral and electrophysiology experiments were not performed concurrently. Hence, the existence of a direct link between enhanced V4 activity and improved perception cannot yet be confirmed.

To complement these two groups of experiments, we attempted to visualize how increased FEF activity modulates activity throughout the visual cortex, rather than at the single-neuron level, by combining FEF-EM with functional magnetic resonance imaging (fMRI) in monkeys (Ekstrom et al. 2008). We chose FEF as the

(first) target in a series of combined EM-fMRI experiments, since the behavioral read-out, i.e. EM-triggered saccades, is straightforward. This is especially beneficial during fMRI experiments, since currents induced in the electrodes, by the switching gradient fields of the MR scanner, would have been immediately apparent in the animal's eye-movements. In fact, simulations prior to the experiments, taking into account the MRI sequences, properties of the gradient coils, as well as tissue and electrode properties, indicated that we barely induced currents in the electrodes. When FEF was stimulated with currents well below those necessary to evoke saccades, exactly as in Tirin Moore's experiments (Moore and Armstrong 2003), we could visualize the network of areas that are anatomically linked with the FEF using concurrent fMRI. The EM-evoked activity patterns over the entire brain matched surprisingly well those patterns of connectivity obtained using traditional tract-tracing methods for which animals need to be sacrificed (see Fig. 3). Hence the combination of electrical microstimulation with whole-brain fMRI is an excellent tool for revealing, at least as a proxy, in-vivo anatomical connectivity information (with some caveats, see below).

More interestingly, when a visual stimulus was placed in the stimulated FEF movement fields, we observed modulation of fMRI activity in those parts of the visual cortex that are driven by the visual stimulus. This modulation was

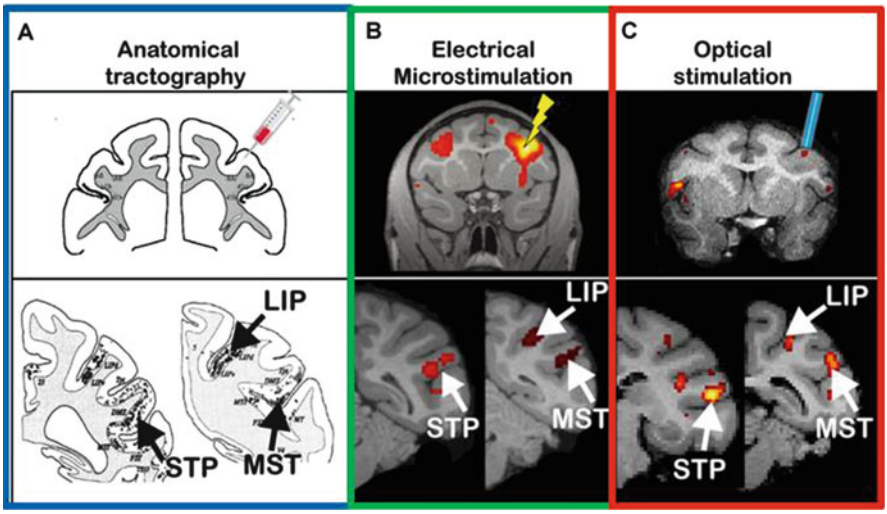

Fig. 3 Comparison between (**a**) anatomical tractography, (**b**) electrical microstimulation (EM), and (**c**) optical stimulation. Injections of tracer in the frontal eye fields (FEF) of macaque monkey produced labeled cells in the lateral intraparietal area (LIP), the medial superior temporal area (MST), and the superior temporal polysensory area (STP) (Schall et al. 1995). fMRI combined with EM of the FEF resulted in fMRI activations in LIP, MST, and STP [67] (Ekstrom et al. 2008). Monkey optogenetic-fMRI with channel-rhodopsin-transduced neurons in FEF also showed an increase in fMRI signal in LIP, MST, and STP (Gerits et al. 2012). Note the striking correspondence between the in-vivo microstimulation and optogenetic induced fMRI activations and the ex-vivo tractography data. Figure adapted from Gerits and Vanduffel (2013)

topographically-specific to the representations of the stimuli placed within the FEF movement fields and included regions with both increased and decreased fMRI activity.

Thus, as in Tirin Moore's experiments, we found modulation of fMRI activity in visual cortex for stimuli presented in the stimulated FEF movement fields. A surprising discrepancy between the results of this EM-fMRI experiment and single-unit data from V4, however, is that we generally observed decreased activity in the same voxels of visual cortex that are optimally driven by visual stimuli in the absence of FEF microstimulation. In contrast, voxels that were only weakly driven by the visual stimulus showed enhanced fMRI activity when the corresponding FEF movement fields were electrically stimulated. This counterintuitive result can be explained, however, by the nature of the stimuli and the experimental design. In our first series of experiments, we used high-contrast, colored gratings presented one at a time. If electrical stimulation of specific FEF-movement fields would mimic 'covert attention' to that location, one could argue that the evoked modulatory effects in visual cortex would be small for a highly salient (high-contrast) stimulus, since no additional 'attentional boost' is required. The same holds true for stimuli presented in isolation without competing distractors, as attention effects are typically stronger for targets embedded in a field of distractors compared to targets in isolation.

In two follow-up experiments, we addressed whether FEF-EM would induce stronger modulatory effects in visual cortex for low- versus high-salient stimuli by manipulating either the luminance contrast or by adding 'distractor' stimuli (Ekstrom et al. 2009; Ekstrom et al. 2008). These experiments confirmed that FEF-EM had a much stronger effect on the low-contrast luminance-defined stimuli (see Fig. 4). Activity in visual cortex was upregulated for low-contrast gratings and unaffected, or even suppressed for high-contrast stimuli, thus confirming the results of the first experiment with the high-contrast colored gratings. In essence, we observed a contrast-gain as opposed to an activity-gain effect, whereby the contrast-response curves were shifted to the left. In the second control experiment, concurrent FEF-EM demonstrated that the representation of a grating embedded in a scene including several competing gratings showed much larger modulatory effects compared to a grating presented in isolation, keeping all other experimental parameters identical.

These control experiments showed that FEF is capable of modulating representations in visual cortex in a manner that closely resembles attention-dependent effects. Although the experiments were performed in the absence of explicit attentional requirements, the effects observed are surprisingly similar to those obtained during selective spatial attention (Reynolds and Heeger 2009). This indicates that the necessary hardware, i.e. wiring, neurotransmitter systems, and axonal properties, exist that allow the FEF to alter sensory-driven activity in visual cortex based on non-retinal signals such as selective attention. As we have stated, conclusive evidence for this hypothesis needs to be provided by studies in which the FEF is stimulated while behavioral and neuronal effects are recording simultaneously.

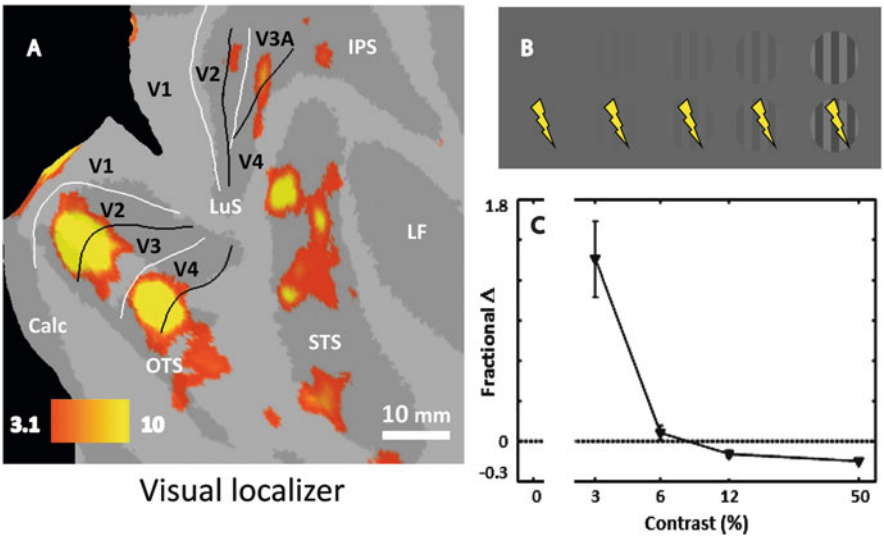

Fig. 4 Electrical microstimulation of monkey FEF boosts activity in visual cortex for low- but not high-contrast gratings. (**a**) Visually-driven activations by the stimuli on a flattened representation of occipital cortex. These voxels, obtained from the localizer experiment, were used to perform the analyses in panel (**c**). (**b**) Stimuli (contrast-varying gratings) used in the fMRI experiment. These were paired with and without concurrent electrical stimulation of the corresponding FEF movement fields. (**c**) Fractional differences in MR signal change in area V1, indicating the effective change in fMRI activity caused by FEF-EM relative to the visual-only activation level. In all panels, *error bars* indicate 1 SEM across epochs; some error bars are smaller than the symbol used. Note the large positive effect for low contrast and even a negative effect for high contrast stimuli. Figure adapted from Ekstrom et al. (2009)

Novel Genetically-Based Perturbation Methods?

A possible caveat in using electrical microstimulation pertains to the inherent difficulties in distinguishing between the ortho- and anti-dromic effects of EM. In other words, the EM effects observed in V4 neurons (Tirin Moore's studies) and in visual and parietal cortex in general (our studies) might be either the result of activation of the axon terminals of neurons with cell bodies in the visual cortex or, alternatively, of neurons located in the FEF that project to visual cortex. In lieu of FEF's proposed role as a source area sending higher-order cognitive signals to sensory cortex, the latter interpretation is the more favorable, yet conclusive evidence is largely lacking.

A possible solution to this conundrum is the use of focal pharmacological receptor (anta)gonists that specifically alter the output of the targeted area (Noudoost and Moore 2011). Alternatively, one could rely on optogenetics whereby, with the right combination of serotype and promoter in the viral vector construct, only projection cells are targeted, and no cells are retrogradely

transduced. Even more appealing approaches include the use of viral vectors with highly-efficient retrograde transduction capacities. These can be injected in the projection sites of FEF after which the retrogradely-labeled cell bodies in the FEF can be targeted with optogenetics (Yizhar et al. 2011). Although such retrograde, or other conditional gene expression, approaches have been highly successful in rodents (Packer et al. 2013), there are no studies to date where retrogradely-driven optogenetics has been used in the cerebrum of nonhuman primates. A very elegant study using a highly efficient retrograde transduction system in nonhuman primates, resulting in exclusive expression of neurotoxin-producing enzymes in projection cells, has shown its efficacy in the spinal cord of monkeys (Kinoshita et al. 2012). Conceivably, similar pathway-specific, genetically-based perturbation methods will soon become applicable in the cerebrum of macaques. The enormous advantage of such techniques is that, instead of a specific region, the functional role of a specific pathway between two regions can be investigated.

A few years ago, we optogenetically targeted specific regions in frontal cortex of monkeys performing a saccade task, guided by prior fMRI maps (Gerits et al. 2012). Although optogenetically-induced neuronal effects in monkeys had been described previously (Han et al. 2009; Diester et al. 2011), our fMRI-guidance strategy allowed us to observe, for the first time, an optogenetically-induced behavioral effect in monkeys—i.e. faster saccades during an eye-movement task. When combined with concurrent fMRI, we also observed increased activity in connected regions, strongly resembling the anatomically-connected areas, and hence mimicking the electrical microstimulation effects described above (see Fig. 3). Meanwhile, several groups replicated optogenetically-induced behavioral effects in monkeys with different tasks and targeting different regions but without fMRI-guidance (Cavanaugh et al. 2012; Dai et al. 2014; Ohayon et al. 2013; Jazayeri et al. 2012). fMRI-based guidance, however, will greatly facilitate experiments aimed at simultaneously targeting multiple sites in the same subjects. With optogenetics, one can then temporarily activate or inactivate one or several of these nodes, even within specific subcomponents of a behavioral task.

In conclusion, I would argue that the genetically-based tools, which have recently instigated a revolution in rodent-based neuroscience, will ultimately find their way into nonhuman primate research. Although achieving cell-specificity will be challenging in monkeys due to the lack of Cre-lines, this animal model is crucial for elucidating the underpinnings of high-level perceptual and cognitive processes absent in rodents. To study multiple nodes within a functional network, high-resolution functional imaging will greatly advance the precision of the targeting, be it with high-throughput electrodes, viral vector injections, or pharmacological agents.

Acknowledgements This work was supported by Inter-University Attraction Pole 7/11, the Research Foundation Flanders; KU Leuven (Programme Financing PFV/10/008), Hercules, and the Human Brain Project.

References

Cavanaugh J, Monosov IE, McAlonan K, Berman R, Smith MK, Cao V, Wang KH, Boyden ES, Wurtz RH (2012) Optogenetic inactivation modifies monkey visuomotor behavior. Neuron 76:901–907

Dai J, Brooks DI, Sheinberg DL (2014) Optogenetic and electrical microstimulation systematically bias visuospatial choice in primates. Curr Biol 24:63–69

Deisseroth K (2015a) Optogenetics: 10 years of microbial opsins in neuroscience. Nat Neurosci 18:1213–1225

Deisseroth K (2015b) Form meets function in the brain: observing the activity and structure of specific neural connections. In: Kennedy H, van Essen DC, Christen Y (eds) Micro-, meso- and macro- connectomics of the brain. Springer, Heidelberg

Devor A et al (2013) The challenge of connecting the dots in the B.R.A.I.N. Neuron 80:270–274

Diester I, Kaufman MT, Mogri M, Pashaie R, Goo W, Yizhar O, Ramakrishnan C, Deisseroth K, Shenoy KV (2011) An optogenetic toolbox designed for primates. Nat Neurosci 14:387–397

Dong S, Rogan SC, Roth BL (2010) Directed molecular evolution of DREADDs: a generic approach to creating next-generation RASSLs. Nat Protoc 5:561–573

Ekstrom LB, Roelfsema PR, Arsenault JT, Bonmassar G, Vanduffel W (2008) Bottom-up dependent gating of frontal signals in early visual cortex. Science 321:414–417

Ekstrom LB, Roelfsema PR, Arsenault JT, Kolster H, Vanduffel W (2009) Modulation of the contrast response function by electrical microstimulation of the macaque frontal eye field. J Neurosci 29:10683–10694

Friston K (2011) Functional and effective connectivity: a review. Brain Connect 1:13–36

Gerits A, Vanduffel W (2013) Optogenetics in primates: a shining future? Trends Genet 29:403–411

Gerits A, Ruff CC, Guipponi O, Wenderoth N, Driver J, Vanduffel W (2011) Transcranial magnetic stimulation of macaque frontal eye fields decreases saccadic reaction time. Exp Brain Res 212:143–152

Gerits A, Farivar R, Rosen BR, Wald LL, Boyden ES, Vanduffel W (2012) Optogenetically induced behavioral and functional network changes in primates. Curr Biol 22:1722–1726

Han X, Qian X, Bernstein JG, Zhou HH, Franzesi GT, Stern P, Bronson RT, Graybiel AM, Desimone R, Boyden ES (2009) Millisecond-timescale optical control of neural dynamics in the nonhuman primate brain. Neuron 62:191–198

Hikosaka O, Wurtz RH (1985) Modification of saccadic eye movements by GABA-related substances. I. Effect of muscimol and bicuculline in monkey superior colliculus. J Neurophysiol 53:266–291

Histed MH, Bonin V, Reid RC (2009) Direct activation of sparse, distributed populations of cortical neurons by electrical microstimulation. Neuron 63:508–522

Janssens T, Keil B, Farivar R, McNab JA, Polimeni JR, Gerits A, Arsenault JT, Wald LL, Vanduffel W (2012) An implanted 8-channel array coil for high-resolution macaque MRI at 3T. Neuroimage 62:1529–1536

Janssens T, Zhu Q, Popivanov ID, Vanduffel W (2014) Probabilistic and single-subject retinotopic maps reveal the topographic organization of face patches in the macaque cortex. J Neurosci 34:10156–10167

Jazayeri M, Lindbloom-Brown Z, Horwitz GD (2012) Saccadic eye movements evoked by optogenetic activation of primate V1. Nat Neurosci 15:1368–1370

Kinoshita M, Matsui R, Kato S, Hasegawa T, Kasahara H, Isa K, Watakabe A, Yamamori T, Nishimura Y, Alstermark B, Watanabe D, Kobayashi K, Isa T (2012) Genetic dissection of the circuit for hand dexterity in primates. Nature 487:235–238

Lomber SG, Cornwell P, Sun J-S, MacNeil MA, Payne BR (1994) Reversible inactivation of visual processing operations in middle suprasylvian cortex of the behaving cat. Proc Natl Acad Sci USA 91:2999–3003

Lomber SG, Payne BR, Horel JA (1999) The cryoloop: an adaptable reversible cooling deactivation method for behavioral or electrophysiological assessment of neural function. J Neurosci Methods 86:179–194

Markram H (2012) The human brain project. Sci Am 306:50–55

McAdams CJ, Maunsell JR (1999) Effects of attention on orientation-tuning functions of single neurons in macaque cortical area V4. J Neurosci 19:431–441

Moore T, Armstrong KM (2003) Selective gating of visual signals by microstimulation of frontal cortex. Nature 421:370–373

Moore T, Fallah M (2004) Microstimulation of the frontal eye field and its effects on covert spatial attention. J Neurophysiol 91:152–162

Noudoost B, Moore T (2011) Control of visual cortical signals by prefrontal dopamine. Nature 474:372–375

Ohayon S, Grimaldi P, Schweers N, Tsao DY (2013) Saccade modulation by optical and electrical stimulation in the macaque frontal eye field. J Neurosci 33:16684–16697

Okano H, Miyawaki A, Kasai K (2015) Brain/MINDS: brain-mapping project in Japan. Philos Trans R Soc Lond B Biol Sci 370

Packer AM, Roska B, Hausser M (2013) Targeting neurons and photons for optogenetics. Nat Neurosci 16:805–815

Premereur E, Vanduffel W, Roelfsema PR, Janssen P (2012) Frontal eye field microstimulation induces task-dependent gamma oscillations in the lateral intraparietal area. J Neurophysiol 108:1392–1402

Premereur E, Vanduffel W, Janssen P (2014) The effect of FEF microstimulation on the responses of neurons in the lateral intraparietal area. J Cogn Neurosci 26(8):1672–1684

Rasmussen T, Penfield W (1947) The human sensorimotor cortex as studied by electrical stimulation. Fed Proc 6:184

Reynolds JH, Heeger DJ (2009) The normalization model of attention. Neuron 61:168–185

Schall JD (1997) Visuomotor areas of the frontal lobe. In: Rockland K (ed) Cerebral Cortex. Plenum Press, New York, pp 527–638

Schall JD, Morel A, King DJ, Bullier J (1995) Topography of visual cortex connections with frontal eye field in macaque: convergence and segregation of processing streams. J Neurosci 15:4464–4487

Tehovnik EJ, Lee K (1993) The dorsomedial frontal cortex of the rhesus monkey: topographic representation of saccades evoked by electrical stimulation. Exp Brain Res 96:430–442

Tufail Y, Matyushov A, Baldwin N, Tauchmann ML, Georges J, Yoshihiro A, Tillery SI, Tyler WJ (2010) Transcranial pulsed ultrasound stimulates intact brain circuits. Neuron 66:681–694

Van Essen DC et al (2012) The Human Connectome Project: a data acquisition perspective. Neuroimage 62:2222–2231

Vanduffel W, Payne BR, Lomber SG, Orban GA (1997) Functional impact of cerebral connections. Proc Natl Acad Sci USA 94:7617–7620

Vanduffel W, Zhu Q, Orban GA (2014) Monkey cortex through fMRI glasses. Neuron 83:533–550

Yizhar O, Fenno LE, Prigge M, Schneider F, Davidson TJ, O'Shea DJ, Sohal VS, Goshen I, Finkelstein J, Paz JT, Stehfest K, Fudim R, Ramakrishnan C, Huguenard JR, Hegemann P, Deisseroth K (2011) Neocortical excitation/inhibition balance in information processing and social dysfunction. Nature 477:171–178

Parcellations and Connectivity Patterns in Human and Macaque Cerebral Cortex

David C. Van Essen, Chad Donahue, Donna L. Dierker, and Matthew F. Glasser

Abstract To decipher brain function, it is vital to know how the brain is wired. This entails elucidation of brain circuits at multiple scales, including microscopic, mesoscopic, and macroscopic levels. Here, we review recent progress in mapping the macroscopic brain circuits and functional organization of the cerebral cortex in primates—humans and macaque monkeys, in particular. There are many similarities across species in terms of overall patterns of cortical gray matter myelination as well as functional areas that are presumed to be homologous. However, there are also many important species differences, including cortical convolutions that are much more complex and more variable in humans than in monkeys. Our ability to analyze structure and function has benefited from improved methods for inter-subject registration that cope with this individual variability. To characterize long-distance connectivity, powerful but indirect methods are now available, including resting-state functional connectivity and diffusion imaging coupled with probabilistic tractography. We illustrate how connectivity inferred from diffusion imaging and tractography can be evaluated in relation to 'ground truth' based on anatomical tracers in the macaque. Interspecies registration between human and macaque cortex based on presumed interspecies homologies demonstrates an impressive degree of areal expansion in regions associated with higher cognitive function.

Introduction

The past decade has seen an explosion of interest and information about mammalian brain connectivity over a wide range of spatial scales, including the macroscopic, microscopic, and mesoscopic levels discussed in the present volume. For the human brain, there has been exciting progress in examining brain connectivity and function using increasingly powerful methods of noninvasive imaging. These

D.C. Van Essen (✉) • C. Donahue • D.L. Dierker • M.F. Glasser
Anatomy and Neurobiology Department, Washington University School of Medicine, St. Louis, MO 63110, USA
e-mail: vanessen@brainvis.wustl.edu

H. Kennedy et al. (eds.), *Micro-, Meso- and Macro-Connectomics of the Brain*, Research and Perspectives in Neurosciences, DOI 10.1007/978-3-319-27777-6_7

methods include the systematic acquisition, analysis and sharing of large amounts of high-quality data through efforts such as the Human Connectome Project (HCP; Van Essen et al. 2012a, 2013). However, the indirect nature of in vivo imaging methods makes it critical to interpret results carefully and to seek better ways to compare and validate against 'ground truth' information available in animal models, particularly nonhuman primates such as the intensively studied macaque monkey. This chapter focuses on the functional organization and connectivity of human and macaque cerebral cortex. We consider (1) cortical organization, individual variability, and parcellation in both species; (2) connectivity in the macaque as revealed by tracers and by tractography; (3) connectivity of human cortex as revealed by noninvasive imaging methods; and (4) interspecies registration as a way to facilitate evolutionary comparisons and for cross-species connectivity validation.

Cortical Cartography and Parcellation

Useful Cortical Numbers It is informative to review a few basic anatomical facts about cortical organization, starting with some numbers related to the neocortex as a whole in macaques and humans. The cerebral neocortex is a sheet-like structure that in the macaque contains ~1.4 billion neurons/hemisphere deployed over a surface area of ~105 cm^2 per hemisphere—equivalent to a pair of ~12 cm diameter cookies (Collins et al. 2010; Van Essen et al. 2012b). Human cortex has about fourfold more neurons (~8 billion/hemisphere) and ninefold greater surface area ($\sim 973 \pm 88$ cm^2/hemisphere), equivalent to a pair of 35 cm pizzas (Azevedo et al. 2009; Van Essen et al. 2012c). The average number of neurons underneath each mm^2 of the cortical surface is lower in humans (8×10^3) than in the macaque (1.4×10^4). Neuronal density is even lower in humans because the neocortex is on average slightly thicker in humans (2.44 mm, from Van Essen et al. 2012c; 2.68 ± 0.40 mm for 196 HCP subjects—Glasser et al. 2013b) than in macaques (1.86 ± 0.40 mm from 19 macaques—Glasser et al. 2013b).

Convolutions and Folding Variability In lissencephalic species (e.g., mice and marmosets), the cerebral neocortex wraps smoothly around most of the underlying white matter and subcortical gray matter structures, with no excess surface area. In contrast, gyrencephalic species have a disproportionately large number of neocortical relative to subcortical neurons, owing to differential neuronal proliferation (Finlay and Darlington 1995). Convolutions arise because the resultant expansion of neocortical surface area exceeds that of the subcortical nuclei and white matter (Van Essen 2006); they keep the brain physically compact, allowing a large cortical surface area to fit inside a cranial vault of modest volume. The specific pattern of cortical convolutions is distinct for each species, as is the degree of individual variability. Macaque cerebral cortex contains a dozen major sulci, with little variability across individuals in the pattern of folding or in the relationship of

cortical areas to these folds. In contrast, the ninefold larger human cortical sheet is far more convoluted, with many primary, secondary and tertiary folds. It is also far more variable in the pattern of convolutions and in the relation of areal boundaries to cortical folds (Amunts et al. 2007; Fischl et al. 2008; Van Essen et al. 2012c).

Figure 1 illustrates the variability of human cortical folding in six exemplar right hemispheres, shown on the left as 3D 'midthickness' surfaces and on the right as FreeSurfer 'sulc' (depth) maps on inflated surfaces. This figure makes two important additional points, arising because the six individuals represent three pairs of monozygotic (MZ) twins taken from the HCP dataset. By visual inspection, MZ twins differ markedly in their folding patterns; qualitatively, the within-pair differences (between columns) are comparable to those between unrelated individuals (between rows). For example, the inferior frontal sulcus (IFS, red arrows) and posterior inferior temporal sulcus (pITS, yellow arrows) differ between MZ twins in the extent, depth, and relationship to nearby sulci. Quantitatively, however, the correlation of folding patterns in MZ twins is actually greater than that for unrelated individuals, as shown by K. Botteron, D. Dierker, D. Van Essen, R. Todd (2008 OHBM abstract and unpublished observations) and confirmed in the HCP dataset (Van Essen et al. 2014b). Moreover, the correlations are greater for MZ twins compared to dizygotic (DZ) twins, implying that there is significant heritability of folding patterns, though it is modest in magnitude (Van Essen et al. 2014b).

Developmental Considerations Given the complexity and variability of cortical convolutions, it is useful to briefly consider the underlying developmental events that provide useful mechanistic insights. Cortical folding takes place mainly in late prenatal development (the third trimester in humans) and has been suggested to be driven by mechanical tension along long-distance axons within the white matter

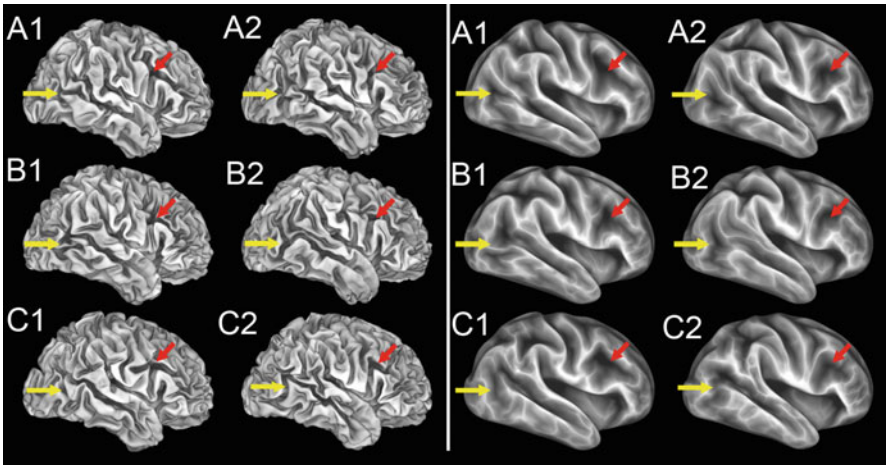

Fig. 1 Folding variability in human cortex is pronounced, even in identical twins. *Left panels*: three pairs of identical (MZ) twin pairs (A1–2, B1–2, C1–2), shown on midthickness surfaces. *Right panels*: corresponding inflated surfaces displaying FreeSurfer 'sulc' maps

(Van Essen 1997). If the hypothesis of tension-based folding is correct, folding variability should largely reflect individual differences in connectivity, which in turn should reflect differences in the size as well as the connectivity profile of each cortical area. Consistent folding (e.g., the central sulcus) may arise from regions dominated by large areas and major pathways, whereas variable folding may reflect competition among smaller areas with greater connectional diversity. This hypothesis raises the intriguing puzzle of why cortical folding patterns differ so much in MZ twins. One possibility is that areal sizes and connectivity profiles are indeed markedly different in MZ twin pairs, owing to epigenetic and intrauterine environmental factors that impact cortical differentiation and wiring (in ways that are currently not understood). Alternatively, very different patterns of cortical folding in MZ twins may arise from subtle mechanical influences that 'buckle' or 'crumple' the cortex in ways that reflect stochastic fluctuations (e.g., external pressure on the cranium that affects overall brain shape) despite similar areal sizes and connectivity profiles. Careful analysis of the MZ and DZ twins in the HCP datasets may yield further insights that help address these issues.

Intersubject Alignment Irrespective of its developmental origins, folding variability poses important practical challenges whenever one aims to compare neuroimaging results obtained in different individuals. A widely used general strategy is to register individuals to a common spatial framework, i.e., an atlas. Intensive efforts have gone into improving brain atlases and the associated registration methods. For cerebral cortex, surface-based registration (SBR) and surface-based atlases have inherent advantages over conventional, volume-based registration because they respect the topology of the cortical sheet (Anticevic et al. 2008; Fischl et al. 1999; 2008; Frost and Goebel 2012; Tucholka et al. 2012; Van Essen et al. 2012c). Until recently, the available methods for SBR have used shape cues related to the folding pattern to constrain the registration from individuals to the atlas. This approach is inherently problematic for dealing with regions of high folding variability, especially since the location of the cortical areas and functionally specialized regions vary in relation to gyral and sulcal landmarks. Fortunately, new registration methods have recently emerged that capitalize on functionally relevant features (e.g., myelin maps, fMRI data) in conjunction with shape-based information (Sabuncu et al. 2010; Robinson et al. 2013). In the examples illustrated below, we capitalize on the Multimodal Surface Matching (MSM) method as applied to HCP and macaque datasets (Robinson et al. 2013, 2014; Glasser et al. 2014).

Regional Patterns Primate neocortex has a common overall architecture, but some features that vary systematically across the cortical sheet provide valuable guides to its functional organization. We first consider regional differences in myelin content, neuronal density, and dendritic arbor size, which collectively reflect important overall patterns that are independent of any particular parcellation scheme. Myelin content within the cortical ribbon can be estimated by taking the ratio between T1-weighted and T2-weighted structural MRI scans at each voxel and mapping this ratio onto the cortical surface (Glasser and Van Essen 2011). Figure 2 illustrates population-average maps of myelin content, displayed on inflated atlas surfaces of

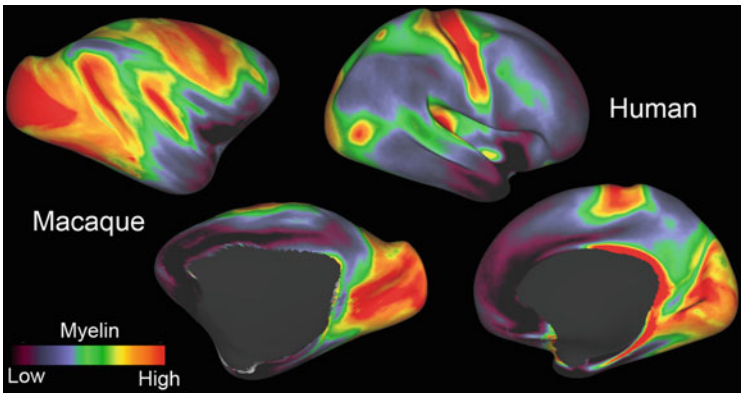

Fig. 2 Group-average myelin maps for macaque (n = 19, Yerkes19) and human (n = 196, HCP), adapted from Glasser et al. (2013a, 2014). Myelin maps were generated by computing the T1w/T2w ratio for each cortical gray matter voxel, mapping it to individual cortical surfaces, and registering the individuals to a species-specific atlas surface (Glasser and Van Essen 2011) using the MSM registration method (Robinson et al. 2013, 2014)

the macaque and human right hemispheres (Glasser et al. 2013b). Several important commonalities in the overall pattern for the two species are readily discernible. Most notably, early sensory and motor areas are heavily myelinated (red, yellow), whereas lightly myelinated regions (blue, indigo) occur mainly in regions of lateral temporal, parietal, and prefrontal cortex that are generally associated with higher cognitive functions. The most striking species difference is that the proportion of lightly myelinated cortex in humans far exceeds that in the macaque. This finding provides important clues about evolutionary expansion that are considered in a later section.

In the macaque, a fivefold range of neuronal cell density (neurons per gram of cortex) has been demonstrated using quantitative methods of cell fractionation applied to small patches of cortical gray matter (Collins et al. 2010). These cell density differences are correlated with the pattern of myelination, insofar as high neuronal density occurs in heavily myelinated early sensory and low density in the lightly myelinated 'higher' cortical areas (though the correlation is imperfect as heavily myelinated motor cortex has low neuronal density). Another important correlation is with dendritic arbor sizes (basal dendritic area) and spine numbers, determined by labeling individual neurons in lightly fixed tissue sampled from different cortical regions. Average dendritic arbor area and number of spines per neuron are low in areas V1 and V2 and are several-fold greater in temporal and prefrontal cortex (Elston 2000, 2002; Elston and Rosa 1997; Elston et al. 1999, 2001, 2006). In humans, comparable regional differences in dendritic arbor size and even larger differences in spine number have been demonstrated (Elston et al. 2001, 2006). There are also interesting correlations with patterns of cortical development. Human cortical surface area expands threefold after birth, but this postnatal expansion is nonuniform. The largest expansion (~4-fold) occurs mainly in the lightly

myelinated higher cognitive regions, whereas the least expansion (~2-fold) occurs in early sensory areas (Hill et al. 2010). A likely cellular-level correlate is that, in the macaque, dendritic arbors sizes and synapse number increase between birth and adulthood in inferotemporal cortex, whereas there is a net decrease in both measures for early visual areas (Elston et al. 2010). Thus, in both species regional differences in neuronal density, average dendritic arbor size, and myelin content conform to a general pattern that provides important insights for understanding brain function, evolution, and development.

Cortical Parcellation Over the past century, a growing arsenal of methods has been used to parcellate cerebral cortex—that is, to identify distinct cortical areas based on differences across one or more four broad domains: architecture (cyto-, myelo- chemo-, and immunocyto-architectonics), connectivity (tracers and/or imaging-based), topography (e.g., retinotopy, somatotopy), and function (based on neurophysiology, lesions, and neuroimaging). Arguably the most accurate parcellation of mammalian cortex to date is in the lissencephalic mouse, where there is strong evidence for about 40 cortical areas based on a multi-modal analysis of architectonics, topography, and connectivity (Wang et al. 2012; see Burkhalter 2015). For macaque and human cortex, a consensus parcellation has yet to be attained in either species despite intensive efforts, because the differences between adjacent cortical areas are often subtle, are not always in concordance across different measures, and are susceptible to a variety of neurobiological confounds (e.g., differences in areal size across individuals, and in areal location relative to cortical folds) and other methodological confounds. Figure 3 illustrates composite parcellation schemes for macaque and human cortex based on studies that mapped

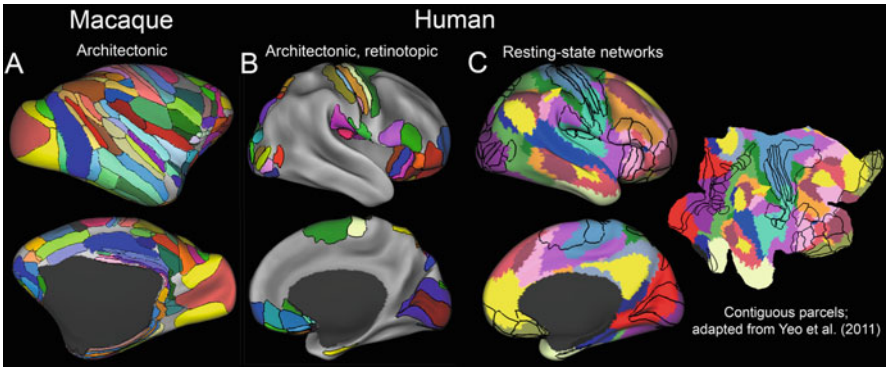

Fig. 3 Parcellations of macaque and human cortex. (**a**) A composite parcellation of macaque cortex into 129 areas based on published architectonic maps [adapted, with permission, from Van Essen et al. (2012b)]. (**b**) A 52-area parcellation of human cortex that is a composite of five published parcellations [adapted, with permission, from Van Essen et al. (2012c)]. (**c**) Resting-state network (RSN) parcels, from splitting Yeo et al.'s 17 networks into spatially contiguous subregions at least 50 mm^2 in surface area. Areal boundaries from panel (**b**) are superimposed for comparison on inflated and flatmap surfaces

parcels to the cortical surface accurately in individual subjects and then from individuals to an atlas surface using surface-based registration.

The macaque parcellation (Fig. 3a), based on a composite drawn from three architectonic analyses, includes 129 areas covering 93 % of neocortex (Van Essen et al. 2012b). The size (surface area) of different areas spans a 100-fold range, and across individuals the size of any given area varies twofold or more. Comparisons across 15 published parcellation schemes registered to the atlas surface reveal a consensus for only a minority of these areas. For example, retinotopic mapping studies reveal a finer-grained parcellation of extrastriate visual cortex than in the above architectonic scheme (Kolster et al. 2009), but a consensus among parcellations based on different modalities has yet to be attained in the macaque for visual cortex beyond V1–V4 and MT (Van Essen et al. 2012b). Moreover, there is strong evidence for 'patch-like' functional specializations within some higher cortical regions. For example, lateral occipital and temporal cortex contains patches associated with processing of faces (Tsao et al. 2008) and color (Lafer-Sousa and Conway 2013), with each color patch just ventral to one of the face patches. An important but unresolved question is whether face and color patches should each be considered a distinct cortical 'area.' A plausible alternative is to consider them modular components of larger areas that are heterogeneous in function and connectivity, analogous to the modularity identified in areas V1, V2, and V4 (Deyoe et al. 1990). Reconciliation of the many discrepancies among extant macaque cortical parcellations will require additional data from multiple modalities that are acquired and analyzed with careful attention to spatial fidelity at every stage, including accurate intersubject registration to a surface-based atlas.

For human cortex, analyses based on accurate surface maps of architectonic and retinotopic areas have enabled identification of 52 areas, encompassing about one-third of the cortical sheet, to be mapped to a surface-based atlas (Fig. 3b; Van Essen et al. 2012c). If the intervening regions contain areas that are similar or slightly smaller in average surface area, as suggested by architectonic analyses yet to be accurately surface-mapped (Amunts et al. 2007), human cortex may contain 150–200 distinct areas in each hemisphere.

A valuable noninvasive approach to parcellating the entire cerebral cortex makes use of resting-state functional connectivity. 'Resting-state networks' (RSNs) represent regions that have similar fMRI (BOLD) time courses, as revealed using independent components analysis (ICA) or other ways of analyzing fMRI timeseries data. Importantly, many RSN components ('nodes') include spatially noncontiguous domains that can be widely dispersed (e.g., in different cortical lobes), reflecting a spatially distributed arrangement of regions that share similar fMRI time courses and are presumed to be involved in similar functions. To facilitate comparisons with spatially contiguous cortical areas derived using other methods (e.g., the architectonic and retinotopic areas in Fig. 3a, b), it is useful to subdivide each RSN into parcels that include only contiguous subregions. For example, Fig. 3c shows the 17 RSNs identified by Yeo et al. (2011) after splitting into a total of about 50 contiguous RSN parcels per hemisphere, displayed on a flatmap as well as inflated surfaces. Comparison of these RSN parcels with the

overlaid boundaries of architectonic/retinotopic areas (from Fig. 3b) reveals numerous mismatches, because RSN parcel boundaries generally do not align with cortical areas defined by architectonic and topographic criteria. For example, the complex of early somatomotor areas (architectonic areas 1, 3a, 3b, and 4) includes two large RSN parcels that are split on the basis of somatotopy rather than areal boundaries. The cyan RSN parcel includes the face representation of somatomotor cortex but also extends into much of auditory cortex. The blue RSN parcel covers the body and limb representations but, except for the posterior boundary of area 2 (yellow arrow), the architectonic and RSN boundaries are not co-aligned. The separation into face vs. body RSN components is consistent with tracer studies in the macaque indicating differential anatomical connectivity patterns relating to somatotopy (Johnson et al. 1996; Matelli et al. 1998; Tanne-Gariepy et al. 2002; Luppino et al. 2003). The visual cortex includes three RSN components. One (in red) represents central vision of V1 and V2, plus many third-tier and fourth-tier retinotopic areas and additional portions of ventral occipito-temporal cortex. A second (purple) represents peripheral V1 and V2 and other medial regions that emphasize peripheral vision. The third (light green) includes the 'IPS complex' of parietal visual areas but extends as a narrow strip laterally and ventrally.

Both neurobiological and methodological factors contribute to the mismatches between RSN-based and architectonic/retinotopic-based parcellation boundaries. Genuinely heterogeneous connectivity patterns within well-defined cortical areas are likely to be a major contributor, for reasons already noted above. Methodological factors include (1) inaccurate mapping to the cortical surface arising from cross-sulcal bleeding and mapping of signals from draining veins rather than cortical gray matter, both of which are exacerbated by larger voxel sizes (e.g., 3-mm isotropic voxels in Yeo et al. 2011); (2) noisy data arising from short-duration fMRI scans and imperfect denoising; and (3) inaccurate intersubject alignment when generating a population-average parcellation.

Prospects for improved human cortical parcellations are excellent, particularly in view of the high-quality data made available by the HCP (Van Essen et al. 2013; Smith et al. 2013). Of particular relevance are (1) more accurate cortical segmentation and surface reconstructions (higher resolution, improved algorithms; Glasser et al. 2013a); (2) higher quality rfMRI scans (1-h duration, multiband acquisition enabling 2 mm spatial and 0.7 s temporal resolution); (3) improved intersubject alignment using the aforementioned MSM algorithm (Robinson et al. 2014); plus additional methods refinements (Glasser et al. 2014). Even with these advances, there are significant challenges to improving the fidelity of cortical parcellation. For example, independent component analysis (ICA) can be used to generate 'soft' parcellations (each gray ordinate can have a weighted contribution to several network components), which can yield many ICA components that are substantially finer-grained than those illustrated in Fig. 3 (Van Essen et al. 2013; Smith et al. 2013). However, for reasons already mentioned, it is challenging to identify cortical areas by relying on RSNs alone. An attractive alternative in general is to use multiple MRI modalities (rfMRI, tfMRI, myelin, and cortical thickness being the most informative) and to combine across modalities in ways that maximize the

prospect of identifying neurobiologically well-defined areas and sub-areas. Given the growing body of freely available HCP data, combined with ongoing methods refinements (especially in multimodal registration), high quality group-average human cortical parcellations are anticipated in the near future.

Distributed Cortical Connectivity

Our understanding of general principles of cortico-cortical connectivity has evolved dramatically in recent decades. Early studies suggested that each cortical area received only a few inputs and outputs (Van Essen 1979). Subsequent analyses using more sensitive tracers revealed evidence for hundreds of pathways among dozens of visual areas (Felleman and Van Essen 1991). There was also a growing realization that different pathways ranged widely in strength. Accurate quantitation of connection strengths and mapping to a surface-based parcellation is feasible (Lewis and Van Essen 2000a, b; Van Essen et al. 2001) but is tedious and technically demanding. Major progress on this front has come from a recent systematic effort from the laboratory of Henry Kennedy, revealing that connectivity profiles are more highly distributed and that connection strengths span a much wider range than previously realized (Knoblauch et al. 2015). Using a 91-area cortical parcellation and retrograde tracers injected into 29 cortical areas, Markov et al. (2012) determined that each cortical area receives on average inputs from 55 other areas out of a (minimum) 26 and (maximum) 87; when expressed as the fraction of retrogradely labeled neurons, these pathways vary over five orders of magnitude in connection strength (Markov et al. 2011, 2012; Knoblauch et al. 2015). This translates to 1615 inter-areal pathways out of 2610 possible in a 29×91 connectivity matrix. Most pathways are reciprocal and comparable in strength for the forward and feedback components, though the incidence of uni-directional pathways is greater than previously suspected (Markov et al. 2012).

These findings demonstrate that cortical connectivity is far from sparse, or 'small world,' when expressed as area-to-area connectivity. On the other hand, connections are much sparser when evaluated at finer-grained levels such as those of individual neurons or small patches of cortex. For example, each cortical neuron receives and makes about 10^4 synapses on average; given 10^9 neurons in the macaque, the upper bound of direct contacts is about ~1 neuron in 10^5 (and even lower for human cortex). At an intermediate level of granularity, it is of interest to estimate the spatial extent of cortex that provides some degree of direct input to any given patch of cortex. Each mm^2 patch of macaque cortex contains ~10^5 neurons and may contain ~10^9 synapses (but with significant regional variability, as noted above). An estimated 80 % of inputs come from local (intra-areal) circuits, within a radius of several mm of a given patch (Markov et al. 2011). The remaining 20 % of long-distance within-hemisphere inputs are distributed across the 10,000-mm^2 surface area of each hemisphere. Inspection of the long-distance retrogradely labeled neurons seen in histological sections (Markov et al. 2012, supplemental

material) suggests that perhaps 10–20 % of these patches contain at least one labeled neuron (but often many) and thus provide direct input to any given tracer injection site (Van Essen 2013). It would be possible to estimate this more accurately by mapping retrogradely labeled neurons directly from individual sections onto surface reconstructions (of individual hemispheres or directly to a surface-based atlas). In any event, the density or sparseness of cortico-cortical connectivity depends greatly on the scale of analysis.

Similar principles of connectivity have recently been demonstrated in the mouse, based on an inter-areal parcellated connectome using anterograde tracers in ten areas of visual cortex (Wang et al. 2012; Burkhalter 2015) and on a meso-connectome regional analysis involving nearly 300 bidirectionally analyzed pathways (Oh et al. 2014). As in the macaque, connection patterns in the mouse are highly distributed, and connection strengths vary over many orders of magnitude, suggesting that these principles may reflect a common mammalian plan.

Tracers vs. Tractography in the Macaque The aforementioned quantitative tracer studies in the macaque provide the closest currently available to ground truth connectivity data and are invaluable for assessing the performance of more indirect methods for estimating connectivity. For example, we have used this approach to evaluate diffusion imaging (dMRI) and probabilistic tractography analyzed in a postmortem macaque brain. This is especially important because tractography shows a strong 'gyral bias,' in which streamlines tend to terminate on gyral crowns, both in human and macaque cortex. This bias has been suggested to reflect actual anatomical connectivity (Nie et al. 2012). However, we contend that it conflicts with ground-truth neuroanatomy and instead reflects the tendency for the dominant fiber orientation in white matter 'blades' to be oriented along the axis pointing towards the gyral crown (Van Essen et al. 2014a). In myelin-stained sections, fibers 'peel off' to provide axons to and from the sulcal banks, but their radius of curvature is typically smaller than the dMRI voxel size (Van Essen et al. 2014a).

Figure 4b shows that area 7a receives inputs from 60 of the 90 other areas shown in the Fig. 4a parcellation, and that connection strengths vary over >5 orders of magnitude, indicated by the logarithmic scale. Figure 4c shows the average connection strength (averaged across the two directions) for the subset of 29 areas that were also injection sites. For the tractography-based 'structural connectivity' and the same subset of areas (Fig. 4d), the strength of connectivity shows many similarities but also many differences, e.g., the pathway between area PBr is stronger for tractography than for tracers (arrows). A scatterplot of the pathway strength by the two methods for all connection pairs in the 29 × 29 matrix (Fig. 4e) shows a correlation that is significant for only the top ~20 % of tracer pathways (right of the vertical blue line).

Functional Connectivity Validation in the Macaque It is widely appreciated that functional connectivity is an inherently indirect surrogate for direct anatomical connectivity, because correlated activity can arise from common inputs and/or indirect anatomical pathways as well as direct connections (Smith et al. 2013). Hence, an important empirical question is the degree to which estimates of functional

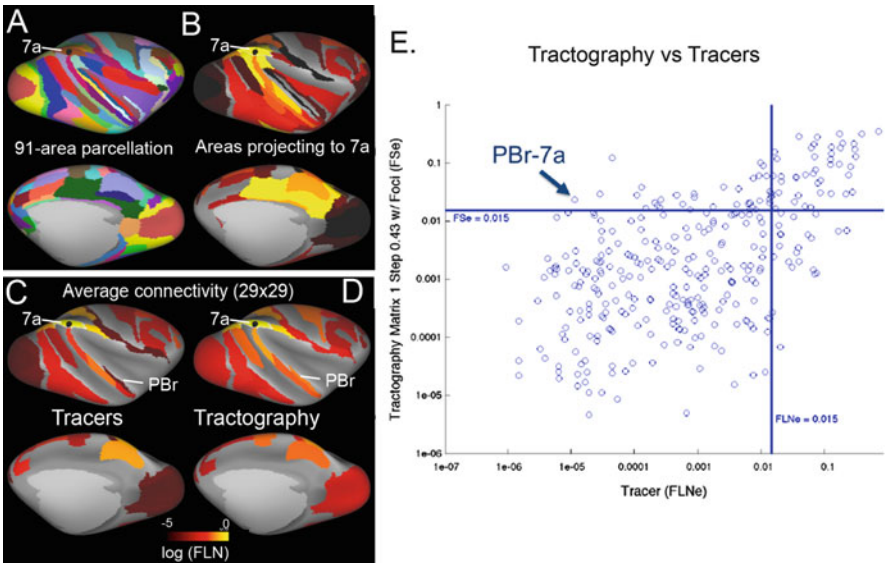

Fig. 4 (**a**) 91-area parcellation of macaque cortex on the inflated atlas surface. (**b**) Anatomical connectivity of area 7a based on a retrograde tracer injection into area 7a and quantitative mapping of its connection strength with all other areas (Markov et al. 2012). Connection strengths are on a log10 scale and span five orders of magnitude [same scale as for panels (**c**, **d**)]. (**c**) Average bidirectional tracer-based connectivity of area 7a based on the 29 × 29 'edge-complete' bidirectional connectivity matrix. (**d**) Tractography-based connectivity, also for area 7a but from a different macaque (cf., Van Essen et al. 2014a). *Arrows* in (**c**, **d**) point to area PBr, whose estimated connectivity based on tractography exceeds that determined using tracers. (**e**) Scatterplot of tracers-vs.-tractography connection strengths

connectivity correlate with anatomical connectivity in the macaque. Vincent et al. (2007) showed qualitatively that functional connectivity in the anesthetized macaque correlated well with anatomical connectivity when testing a seed region in the vicinity of area LIPv, whereas a seed region centered in area V1 revealed evidence of a combination of direct connections (e.g., with area MT) and indirect connections (e.g., with the horizontal meridian of contralateral area V1, which has no direct interhemispheric connections). A recent study showed a modest ($r = 0.35$) but highly significant correlation between functional connectivity in the anesthetized macaque and the Markov et al. (2012) quantitative parcellated connectivity matrix (Miranda-Dominguez et al. 2014). Importantly, the analysis revealed many false negatives (negative functional connectivity, or anti-correlation between areas that are strongly connected anatomically). Thus, as with tractography, it is important to remain mindful of the indirect nature of functional connectivity analyses and the limited capability for estimating actual connection strengths in nonhuman primates when using standard data acquisition and analysis methods.

Human Cortical Connectivity Structural connectivity (based on dMRI and tractography) and functional connectivity (based on resting-state fMRI) have

already been discussed in relation to the macaque and also in relation to cortical parcellation in humans. However, much of the interest in these approaches derives from the prospect of charting the actual 'wiring diagram' of the human brain, how it varies across individuals, and how it relates to and contributes to individual differences in behavior. Indeed, this is the central focus of the HCP, as discussed extensively elsewhere (Van Essen et al. 2013; Smith et al. 2013). Here, we focus on several key observations and issues about the opportunities and challenges associated with this endeavor.

We focus on data and initial results from the HCP, as this represents the state-of-the-art in acquiring and analyzing dMRI and rfMRI data in humans. Figure 5 shows a direct comparison between structural and functional connectivity in an individual HCP subject, using a seed location in the middle temporal gyrus (MTG, large green sphere). Structural connectivity based on probabilistic tractography (Fig. 5a) provides evidence of connectivity between the MTG and many regions, both nearby, at intermediate distances (two large patches in and near the angular gyrus, smaller green dots), and at long distances (e.g., on the inferior frontal gyrus). For the same seed location on the MTG (Fig. 5b), the map of functional connectivity shows many similarities but also many differences. The similarities indicate cross-modal consistency, suggesting that both patterns include many neurobiologically valid connections. For reasons already stated, differences may reflect neurobiological factors but also methodological biases or artifacts. For example, regions with strong functional connectivity but weak structural connectivity might in theory (white arrow in prefrontal cortex) reflect a pathway with only weak direct connections but strong indirect (polysynaptic) connections. Alternatively, a robust direct pathway may exist but fail to be captured by tractography owing to methodological limitations (e.g., inaccurate charting of the complex trajectories of fibers in white matter). Regions that suggest structural connectivity but not functional connectivity (e.g., red arrow in insular cortex) might reflect false positives in the tractography analysis

Despite these caveats and limitations, it is important to appreciate that the HCP structural and functional connectivity data represent major advances in our ability to acquire and analyze information about human brain circuitry. Examining

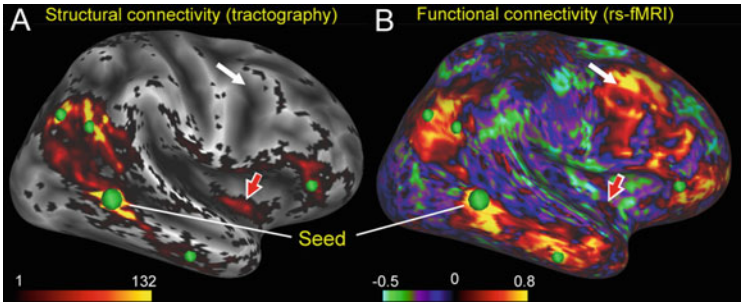

Fig. 5 Comparing structural connectivity (**a**) and functional connectivity (**b**) in an individual HCP subject for a seed vertex on the middle temporal gyrus [reproduced, with permission, from Van Essen et al. (2014a)]

seed-based connectivity in individual subjects reveals that MRI-based data are inherently noisy and subject to bias. To gain meaningful insights, it is necessary to integrate across space (i.e., to use parcel-based analyses) and/or across the population (i.e., to capitalize on the large and growing number of HCP subjects). The need for parcel-based analysis that is based on functionally distinct brain subdivisions is a strong driver for the ongoing effort to improve human cortical parcellation using multimodal analysis, as discussed in an earlier section. The need for group-based analyses is a strong driver for the ongoing effort to improve intersubject alignment. Progress on both of these fronts will enhance the utility and interpretability of the HCP datasets and also other datasets that capitalize on these methodological improvements.

Interspecies Registration

Figures 2 and 3 provided evidence of many similarities in the functional organization of macaque and human cortex but also for major species differences in the relative sizes of different areas and regions presumed to be homologous. Interspecies surface-based registration offers a useful approach to comparing across species in ways that are systematic, quantitative, and objective; it will enable the use of tracer-based connectivity data in the macaque to inform and validate structural and functional connectivity findings in humans.

We have previously used landmark-constrained registration using about two dozen landmark contours that represent areal boundaries or other functional transitions presumed to reflect evolutionary homologies (Denys et al. 2004; Van Essen 2005). This approach provides evidence of hotspots of human evolution in lateral temporal, parietal, and prefrontal cortex that have expanded dramatically in the human lineage relative to that in the macaque; the pattern is remarkably similar to human postnatal cortical expansion, between birth and adulthood (Van Essen and Dierker 2007; Hill et al. 2010). To better understand this pattern of evolutionary divergence, it is desirable to have a larger set of known or presumed homologies between specie, and also to have improved methods of interspecies registration that handle the highly nonuniform spatial patterns of expansion. Here, we illustrate a brief progress report in this direction. It includes a more extensive set of landmark contours (38 in all), including orbitofrontal, lateral temporal, and parietal regions suspected to reflect homologies (Fig. 6a). Another advance involves an improved landmark-based registration method (the 'LVD' algorithm; Van Essen et al. 2012b) relative to an earlier method. The resultant map of interspecies cortical expansion (Fig. 6b) suggests that cortical expansion in these hotspots exceeds 30-fold, compared to the twofold to fourfold expansion over most of early visual cortex. Refinements to this general picture can be anticipated by invoking additional features to constrain interspecies registration, along with improved registration algorithms such as the multimodal surface matching method (Robinson et al. 2014) that can use continuously varying features (e.g., the myelin maps

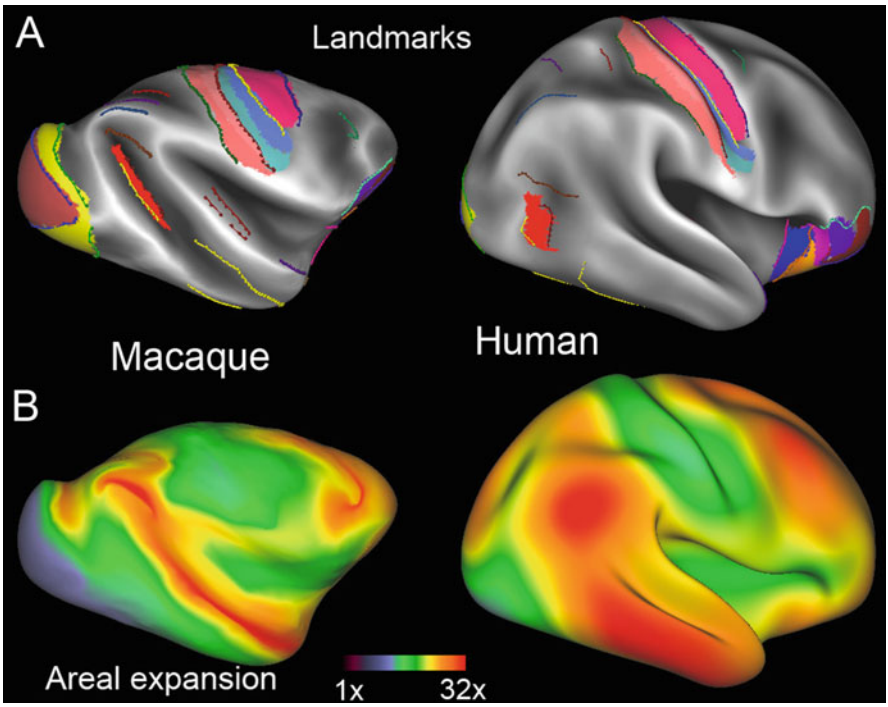

Fig. 6 (**a**) Landmarks used to register macaque to human cortex. (**b**) Areal expansion maps between human and macaque cortex, revealing hotspots of cortical expansion in lateral temporal, parietal, and frontal cortex. The expansion map was smoothed after initial computation of the interspecies area ratio to reduce neurobiologically implausible local irregularities

shown in Fig. 2) as well as discrete areal delimitations, rather than the purely landmark-constrained approach used to date. This will also be aided by incorporating chimpanzee cortex (Glasser et al. 2013b) as an important intermediary for examining evolutionary relationships.

It is now feasible to use interspecies registration as a test bed for evaluating human connectivity. Indeed, such an analysis was recently reported by Miranda-Dominguez et al. (2014), who used an earlier interspecies registration to compare human functional connectivity with the macaque tracer-based connectivity after registration to human cortex. They found a slightly higher correlation between human functional connectivity and interspecies-registered macaque connectivity ($r = 0.42$) than for the aforementioned macaque functional-vs.-tracer correlation ($r = 0.35$), raising the possibility that the quality of the functional connectivity data might be better for their human vs. their (anesthetized) macaque. Future analyses along these lines can be applied to tractography, different functional connectivity datasets (including HCP) and different ways of analyzing the structural and functional connectivity (e.g., with vs. without regression of mean-gray-timecourse;

partial vs. full correlation), and other possible measures as well as improved interspecies registrations.

Concluding Comments

Two decades ago, hardly anything was known about long-distance pathways in the human brain, other than the general distribution of major fiber tracts discernible from classical blunt dissection studies (e.g., Gluhbegovic and Williams 1980). This problem was famously articulated by Crick and Jones (1993) just when fMRI was beginning to emerge and before diffusion imaging began. The explosion of methodological advances has been dramatic but so have the many challenges of carefully analyzing and interpreting these highly complex datasets.

References

Amunts K, Armstrong E, Malikovic A, Homke L, Mohlberg H, Schleicher A, Zilles K (2007) Gender-specific left-right asymmetries in human visual cortex. J Neurosci 27:1356–1364

Anticevic A, Dierker DL, Gillespie SK, Repovs G, Csernansky JG, Van Essen DC, Barch DM (2008) Comparing surface-based and volume-based analyses of functional neuroimaging data in patients with schizophrenia. Neuroimage 41:835–848

Azevedo FA, Carvalho LR, Grinberg LT, Farfel JM, Ferretti RE, Leite RE, Jacob Filho W, Lent R, Herculano-Houzel S (2009) Equal numbers of neuronal and nonneuronal cells make the human brain an isometrically scaled-up primate brain. J Comp Neurol 513:532–541

Burkhalter A (2015) The network for intracortical communication in mouse visual cortex. In: Kennedy H, Van Essen DC, Christen Y (eds) Micro-, meso- and macro-connectomics of the brain. Springer, Heidelberg

Collins CE, Airey DC, Young NA, Leitch DB, Kaas JH (2010) Neuron densities vary across and within cortical areas in primates. Proc Natl Acad Sci USA 107:15927–15932

Crick F, Jones E (1993) Backwardness of human neuroanatomy. Nature 361:109–110

Denys K, Vanduffel W, Fize D, Nelissen K, Sawamura H, Georgieva S, Vogels R, Van Essen D, Orban GA (2004) Visual activation in prefrontal cortex is stronger in monkeys than in humans. J Cogn Neurosci 16:1505–1516

Deyoe EA, Hockfield S, Garren H, Van Essen DC (1990) Antibody labeling of functional subdivisions in visual cortex: cat-301 immunoreactivity in striate and extrastriate cortex of the macaque monkey. Vis Neurosci 5:67–81

Elston GN (2000) Pyramidal cells of the frontal lobe: all the more spinous to think with. J Neurosci 20:RC95

Elston GN (2002) Cortical heterogeneity: implications for visual processing and polysensory integration. J Neurocytol 31:317–335

Elston GN, Rosa MG (1997) The occipitoparietal pathway of the macaque monkey: comparison of pyramidal cell morphology in layer III of functionally related cortical visual areas. Cereb Cortex 7:432–452

Elston GN, Tweedale R, Rosa MG (1999) Cortical integration in the visual system of the macaque monkey: large-scale morphological differences in the pyramidal neurons in the occipital, parietal and temporal lobes. Proc Biol Sci 266:1367–1374

Elston GN, Benavides-Piccione R, DeFelipe J (2001) The pyramidal cell in cognition: a comparative study in human and monkey. J Neurosci 21:163

Elston GN, Benavides-Piccione R, Elston A, Zietsch B, Defelipe J, Manger P, Casagrande V, Kaas JH (2006) Specializations of the granular prefrontal cortex of primates: implications for cognitive processing. Anat Rec A Discov Mol Cell Evol Biol 288:26–35

Elston GN, Oga T, Okamoto T, Fujita I (2010) Spinogenesis and pruning from early visual onset to adulthood: an intracellular injection study of layer III pyramidal cells in the ventral visual cortical pathway of the macaque monkey. Cereb Cortex 20:1398–1408

Felleman DJ, Van Essen DC (1991) Distributed hierarchical processing in the primate cerebral cortex. Cereb Cortex 1:1–47

Finlay BL, Darlington RB (1995) Linked regularities in the development and evolution of mammalian brains. Science 268:1578–1584

Fischl B, Sereno MI, Tootell RB, Dale AM (1999) High-resolution intersubject averaging and a coordinate system for the cortical surface. Hum Brain Mapp 8:272–284

Fischl B, Rajendran N, Busa E, Augustinack J, Hinds O, Yeo B, Mohlberg H, Amunts K, Zilles K (2008) Cortical folding patterns and predicting cytoarchitecture. Cereb Cortex 18:1973

Frost MA, Goebel R (2012) Measuring structural-functional correspondence: spatial variability of specialised brain regions after macro-anatomical alignment. Neuroimage 59:1369–1381

Glasser M, Van Essen DC (2011) Mapping human cortical areas in vivo based on myelin content as revealed by T1 and T2-weighted MRI. J Neurosci 31:11597–11616

Glasser MF, Sotiropoulos SN, Wilson JA, Coalson T, Fischl B, Andersson J, Xu J, Jbabdi S, Webster M, Polimeni J, Van Essen DC, Jenkinson M (2013a) The minimal preprocessing pipelines for the Human Connectome Projects. Neuroimage 80:105–124 (Special issue on mapping the Connectome)

Glasser MF, Goyal MS, Press TM, Raichle ME, Van Essen DC (2013b) Trends and properties of human cerebral cortex: correlations with cortical myelin content. Neuroimage 93 Pt 2: 165–175, (Special issue on In Vivo Brodmann Mapping). doi: 10.1016/n.neuroimage.2013.03.060

Glasser MF, Goyal MS, Press TM, Raichle ME, Van Essen DC (2013c) Trends and properties of human cerebral cortex: correlations with cortical myelin content. Neuroimage 93 Pt 2: 165–175, (Special issue on In Vivo Brodmann Mapping). doi: 10.1016/n.neuroimage.2013.03.060

Gluhbegovic N, Williams TH (1980) The human brain: a photographic guide. HarperCollins, New York, p 176

Hill J, Inder T, Neil J, Dierker D, Harwell J, Van Essen D (2010) Similar patterns of cortical expansion during human development and evolution. Proc Natl Acad Sci USA 107: 13135–13140

Johnson PB, Ferraina S, Bianchi L, Caminiti R (1996) Cortical networks for visual reaching: physiological and anatomical organization of frontal and parietal lobe arm regions. Cereb Cortex 6:102–119

Knoblauch K, Ercsey-Ravasz M, Kennedy H, Toroczkai Z et al (2015) The brain in space. In: Kennedy H, Van Essen DC, Christen Y (eds) Micro-, meso- and macro-connectomics of the brain. Springer, Heidelberg

Kolster H, Mandeville JB, Arsenault JT, Ekstrom LB, Wald LL, Vanduffel W (2009) Visual field map clusters in macaque extrastriate visual cortex. J Neurosci 29:7031–7039

Lafer-Sousa R, Conway BR (2013) Parallel, multi-stage processing of colors, faces and shapes in macaque inferior temporal cortex. Nat Neurosci 16:1870–1878

Lewis J, Van Essen D (2000a) Corticocortical connections of visual, sensorimotor, and multimodal processing areas in the parietal lobe of the macaque monkey. J Comp Neurol 428: 112–137

Lewis JW, Van Essen DC (2000b) Mapping of architectonic subdivisions in the macaque monkey, with emphasis on parieto-occipital cortex. J Comp Neurol 428:79–111

Luppino G, Rozzi S, Calzavara R, Matelli M (2003) Prefrontal and agranular cingulate projections to the dorsal premotor areas F2 and F7 in the macaque monkey. Eur J Neurosci 17:559–578

Markov NT, Misery P, Falchier A, Lamy C, Vezoli J, Quilodran R, Gariel MA, Giroud P, Ercsey-Ravasz M, Pilaz LJ, Huissoud C, Barone P, Dehay C, Toroczkai Z, Van Essen DC, Kennedy H, Knoblauch K (2011) Weight consistency specifies regularities of macaque cortical networks. Cereb Cortex 21:1254–1272

Markov NT, Ercsey-Ravasz MM, Ribeiro Gomes AR, Lamy C, Magrou L, Vezoli J, Misery P, Falchier A, Quilodran R, Gariel MA, Sallet J, Gamanut R, Huissoud C, Clavagnier S, Giroud P, Sappey-Marinier D, Barone P, Dehay C, Toroczkai Z, Knoblauch K, Van Essen DC, Kennedy H (2012) A weighted and directed interareal connectivity matrix for macaque cerebral cortex. Cereb Cortex 24(1):17–36, Epub 2012/09/27

Matelli M, Govoni P, Galletti C, Kutz DF, Luppino G (1998) Superior area 6 afferents from the superior parietal lobule in the macaque monkey. J Comp Neurol 402:327–352

Miranda-Dominguez O, Mills BD, Grayson D, Woodall A, Grant KA, Kroenke CD, Fair DA (2014) Bridging the gap between the human and macaque connectome: a quantitative comparison of global interspecies structure-function relationships and network topology. J Neurosci 34: 5552–5563

Nie J, Guo L, Li K, Wang Y, Chen G, Li L, Chen H, Deng F, Jiang X, Zhang T, Huang L, Faraco C, Zhang D, Guo C, Yap PT, Hu X, Li G, Lv J, Yuan Y, Zhu D, Han J, Sabatinelli D, Zhao Q, Miller LS, Xu B, Shen P, Platt S, Shen D, Hu X, Liu T (2012) Axonal fiber terminations concentrate on gyri. Cereb Cortex 22:2831–2839

Oh SW, Harris JA, Ng L, Winslow B, Cain N, Mihalas S, Wang Q, Lau C, Kuan L, Henry AM, Mortrud MT, Ouellette B, Nguyen TN, Sorensen SA, Slaughterbeck CR, Wakeman W, Li Y, Feng D, Ho A, Nicholas E, Hirokawa KE, Bohn P, Joines KM, Peng H, Hawrylycz MJ, Phillips JW, Hohmann JG, Wohnoutka P, Gerfen CR, Koch C, Bernard A, Dang C, Jones AR, Zeng H (2014) A mesoscale connectome of the mouse brain. Nature 2014(508):207–214

Robinson E, Jbabdi S, Andersson J, Smith S, Glasser M, Van Essen D, Burgess G, Harms M, Barch D, Jenkinson M (2013) Multimodal surface matching: fast and generalisable cortical registration using discrete optimisation. Information processing in medical imaging. Springer, New York, pp 475–476

Robinson EC, Jbabdi S, Glasser MF, Andersson J, Burgess GC, Harms MP, Smith SM, Van Essen DC, Jenkinson M (2014) MSM: a new flexible framework for multimodal surface matching. Neuroimage 100:414–426

Sabuncu MR, Singer BD, Conroy B, Bryan RE, Ramadge PJ, Haxby JV (2010) Function-based intersubject alignment of human cortical anatomy. Cereb Cortex 20:130–140

Smith SM, Vidaurre D, Beckmann CF, Glasser MF, Jenkinson M, Miller KL, Nichols TE, Robinson EC, Salimi-Khorshidi G, Woolrich MW, Barch DM, Ugurbil K, Van Essen DC (2013) Functional connectomics from resting-state fMRI. Trends Cogn Sci 17:666–682

Tanne-Gariepy J, Rouiller EM, Boussaoud D (2002) Parietal inputs to dorsal versus ventral premotor areas in the macaque monkey: evidence for largely segregated visuomotor pathways. Exper Hirnforsch 145:91–103

Tsao DY, Moeller S, Freiwald WA (2008) Comparing face patch systems in macaques and humans. Proc Natl Acad Sci USA 105:19514–19519

Tucholka A, Fritsch V, Poline JB, Thirion B (2012) An empirical comparison of surface-based and volume-based group studies in neuroimaging. Neuroimage 63:1443–1453

Van Essen DC (1979) Visual areas of the mammalian cerebral cortex. Annu Rev Neurosci 2: 227–263

Van Essen DC (1997) A tension-based theory of morphogenesis and compact wiring in the central nervous system. Nature 385:313–318

Van Essen DC (2005) A population-average, landmark- and surface-based (PALS) atlas of human cerebral cortex. Neuroimage 28:635–662

Van Essen DC (2006) Cerebral cortical folding patterns in primates: why they vary and what they signify. In: Kaas J (ed) Evolution of the nervous system. Academic, Oxford

Van Essen DC (2013) Cartography and connectomes. Neuron 80:775–790

Van Essen DC, Dierker DL (2007) Surface-based and probabilistic atlases of primate cerebral cortex. Neuron 56:209–225

Van Essen DC, Drury HA, Dickson J, Harwell J, Hanlon D, Anderson CH (2001) An integrated software suite for surface-based analyses of cerebral cortex. J Am Med Inform Assoc 8: 443–459

Van Essen DC, Ugurbil K, Auerbach E, Barch D, Behrens TE, Bucholz R, Chang A, Chen L, Corbetta M, Curtiss SW, Della Penna S, Feinberg D, Glasser MF, Harel N, Heath AC, Larson-Prior L, Marcus D, Michalareas G, Moeller S, Oostenveld R, Petersen SE, Prior F, Schlaggar BL, Smith SM, Snyder AZ, Xu J, Yacoub E (2012a) The human connectome project: a data acquisition perspective. Neuroimage 62:2222–2231

Van Essen DC, Glasser MF, Dierker D, Harwell J (2012b) Cortical parcellations of the macaque monkey analyzed on surface-based atlases. Cereb Cortex 22:2227–2240. doi:10.1093/cercor/bhr2290

Van Essen DC, Glasser MF, Dierker D, Harwell J, Coalson T (2012c) Parcellations and hemispheric asymmetries of human cerebral cortex analyzed on surface-based atlases. Cereb Cortex 22:2241–2262. doi:10.1093/cercor/bhr2291

Van Essen DC, Smith S, Barch D, Behrens TEJ, Yacoub E, Ugurbil K (2013) The WU-Minn human connectome project: an overview. Neuroimage 62:1299–1310, Jan 10 [Epub ahead of print]

Van Essen DC, Jbabdi S, Sotiropoulos SN, Chen C, Dikranian K, Coalson T, Harwell J, Behrens TEJ, Glasser MF (2014a) Mapping connections in humans and nonhuman primates: aspirations and challenges for diffusion imaging. In: Johansen-Berg H, Behrens T (eds) Diffusion MRI, 2nd edn. Academic, San Diego, pp 337–358

Van Essen D, Glasser MF, Robinson E, Xu C, Jenkinson M, Dierker D, Nichols T, Smith S (2014b) Heritability of brain structure, function, and connectivity in human connectome project data. In: Annual meeting of the organization for human brain mapping, Hamburg, Germany, 8–12 June 2014

Vincent JL, Patel GH, Fox MD, Snyder AZ, Baker JT, Van Essen DC, Zempel JM, Snyder LH, Corbetta M, Raichle ME (2007) Intrinsic functional architecture in the anaesthetized monkey brain. Nature 447:83–86

Wang Q, Sporns O, Burkhalter A (2012) Network analysis of corticocortical connections reveals ventral and dorsal processing streams in mouse visual cortex. J Neurosci 32:4386–4399

Yeo BT, Krienen FM, Sepulcre J, Sabuncu MR, Lashkari D, Hollinshead M, Roffman JL, Smoller JW, Zollei L, Polimeni JR, Fischl B, Liu H, Buckner RL (2011) The organization of the human cerebral cortex estimated by intrinsic functional connectivity. J Neurophysiol 106:1125–1165

Connectome Networks: From Cells to Systems

Olaf Sporns

Abstract Nervous systems are networks of neurons and brain regions that are structurally interconnected and dynamically linked in complex patterns. As mapping and recording techniques become increasingly capable of capturing neural structure and activity across widely distributed circuits and systems, there is a growing need for new analysis tools and modeling approaches to make sense of these rich "big data" sets. Modern network science offers a way forward. Both structural and functional brain data sets can be rendered in the form of complex networks and thus become amenable for network modeling and analysis, which can be carried out across scales, from the micro-scale of individual neurons to the macro-scale of whole-brain recordings. In this article, I sketch an overview of structural and functional brain network studies ranging from cells to systems. My emphasis will be on common themes in mapping network attributes across scales. In addition to highlighting important advances, I will outline some major challenges that need to be overcome to achieve a more complete understanding of connectome networks.

Defining the Connectome

Understanding the role of connectivity in brain function is a long-standing goal of both cellular and systems neuroscience (Sporns 2011; Schmahmann and Pandya 2007). Neuronal circuits have been at the center of anatomical and physiological investigation since the groundbreaking studies of Camillo Golgi and Santiago Ramón y Cajal in the late nineteenth century. Connectional anatomy was a core theme in early accounts of human brain function by Carl Wernicke, Theodor Meynert and Siegmund Exner that made reference to the layout and interconnectivity of brain regions and pathways. Anatomical studies that employed ever more sensitive histological staining and tracing tools and new insights into the

O. Sporns (✉)
Department of Psychological and Brain Sciences, Indiana University, Bloomington, IN 47405, USA
e-mail: osporns@indiana.edu

H. Kennedy et al. (eds.), *Micro-, Meso- and Macro-Connectomics of the Brain*, Research and Perspectives in Neurosciences, DOI 10.1007/978-3-319-27777-6_8

functioning of neurons and circuits led to theoretical notions of "neural networks." Such network models first gained momentum in the work of pioneers like Warren McCulloch and Frank Rosenblatt and ultimately transformed into "connectionism," which placed a strong emphasis on distributed processing and learning as key ingredients of neural computation.

A core theme in these historical developments is the foundational role of connectivity for brain function, an idea that has motivated the compilation of a complete connection map of the nervous system of *Caenorhabditis elegans* (White et al. 1986) as well as several landmark attempts to compile maps of interregional projections in the mammalian cerebral cortex (Zeki and Shipp 1988; Felleman and van Essen 1991; Young 1993). These early network maps triggered a string of theoretical and computational studies aimed at using connectivity data to define functional specialization (Passingham et al. 2002), spatial layout and wiring minimization (Chklovskii et al. 2002) as well as clusters and small-world attributes (Hilgetag et al. 2000). The importance of connectivity maps gave rise to the concept of the "connectome," first defined as "a comprehensive structural description of the network of elements and connections" of a given nervous system (Sporns et al. 2005). Several challenges were recognized right from the outset. First, brain networks span multiple spatial scales, from synaptic circuits among individual neurons all the way to whole-brain systems; integrating connectome maps across these multiple scales poses numerous conceptual and technological hurdles. Second, the connectome is changing across time as a result of neuroplasticity and development across the life span; mapping these changes requires comparative analysis of connectomes in relation to individual experience and across age. Third, connectome networks exhibit considerable variability across individuals; this structural variability may reflect individual differences in behavioral and cognitive performance. Finally, connectomics comprises a combination of structural mapping efforts and functional brain recordings, thus addressing the fundamental question of how observed brain dynamics emerge from the anatomical patterns of neural circuits.

This brief review article provides a selective overview of connectome studies that address a subset of these challenges. First, the article surveys structural mapping studies across multiple spatial scales, from connections among neurons to systems-level networks. Next, the article examines the relation of structural connectivity to dynamic brain function, including both spontaneous activity and stimulus-driven neuronal responses. The article closes with a brief summary of current efforts to use connectivity maps as key ingredients for computational models of brain function and a reflection on the status of connectomics as a foundational tool for understanding brain organization.

Brain Networks and Graph Theory

Brain networks are collections of nodes (neuronal elements) and edges (their interconnections; Fig. 1). Empirically, brain networks are constructed from measurements of structural or functional relationships between pairs of neurons or brain regions. These pairwise relations are summarized in the form of a connection matrix that describes the relations between nodes and edges, i.e., the network's topology. Empirical methods for extracting brain network data from structural or functional measurements are continually evolving and represent an area of rapid neurotechnological innovation. Current approaches include the reconstruction of single-cell neuronal morphology and connectivity using electron or light microscopy (e.g., Helmstaedter et al. 2013), novel labeling and tract tracing approaches (e.g., Oh et al. 2014), large-scale optical recordings (e.g., Ahrens et al. 2013), and refinements of noninvasive imaging techniques (e.g., Van Essen et al. 2012).

An important distinction concerns the difference between structural and functional brain networks. Structural networks are derived from anatomical data sets and represent physical synaptic connections between neural elements, whereas functional networks are derived from neural recordings and represent their statistical relationships, e.g., covariance or cross-correlation. Structural networks are often sparse (most possible structural connections do not exist) and relatively stable across time. In contrast, functional networks undergo rapid changes in the course of both spontaneous and task-evoked neural activity and can be configured from a large number of time series analysis measures. Importantly, statements about "connectivity" in functional networks only refer to the similarity or coherence of neural time courses that may be dependent on but do not directly correspond to structural connections.

Once brain network data have been rendered in matrix form, they are amenable to an extremely wide range of statistical and modeling tools coming from network science, especially the mathematical framework of graph theory (Bullmore and Sporns 2009). A comprehensive overview of the application and interpretation of graph-theoretical approaches to brain networks is beyond the scope of this chapter [for reviews, see Rubinov and Sporns (2010), Stam (2010), and Lohmann et al. (2013)]. Briefly, descriptive measures of brain network connectivity fall into at least three different categories, reporting on different aspects of network organization. Broadly, these aspects refer to segregation, integration, and influence. Segregation and integration are best considered jointly, as they represent somewhat opposite trends towards greater functional specialization and greater functional coherence, respectively (Sporns 2013a). Graph measures of segregation (or specialization) capture the extent to which nodes aggregate into separate clusters or communities, which can be expressed by computing the network's clustering coefficient or by its tendency to form distinct modules. In contrast, measures of integration are generally aimed at quantifying the ease with which communication may occur along network paths, presumably an important aspect of how nodes can exchange information; key measures of integration relate to

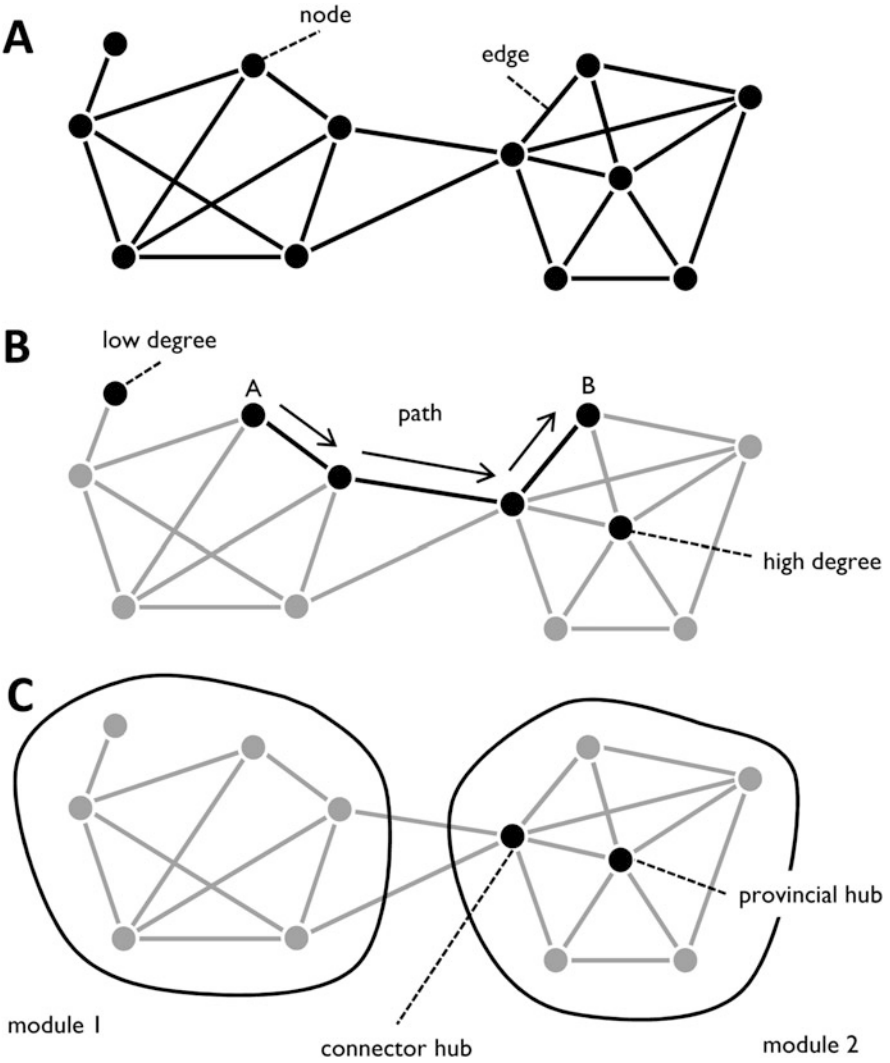

Fig. 1 Schematic illustration of a simple graph and several basic graph measures. (**a**) The graph represented here is binary and undirected, and it consists of a set of nodes and edges. (**b**) Based on the number of edges per node, some nodes can be described as low-degree and others as high-degree. Paths (sequences of edges) connect nodes to each other. In the example shown here, the shortest path linking nodes A and B consists of three edges—hence, the topological distance between A and B is three steps. (**c**) The network can be partitioned into two modules. Given the module partition, high-degree nodes can be classified as either connector hubs or provincial hubs. Connector hubs maintain many connections that link different modules, whereas provincial hubs mainly connect within one module only

communication efficiency and path length. The combination of high clustering (segregation) and short path length (integration) generally indicates the presence of "small world" organization, a mode of connectivity that has been found in numerous other social, technological and biological networks (Watts and Strogatz 1998).

Measures of influence aim at quantifying the importance of network elements (nodes or edges) for the global functionality of the network, for example, by expressing their centrality in communication or their vulnerability to structural damage. Influence or centrality measures are important for detecting network "hubs." While there is no precise definition for hubs in the network literature, hubs are most often identified on the basis of their node degree (the number of distinct connections they maintain across the network) or, alternatively, through a combination of multiple nodal metrics related to connectedness and communication (Sporns et al. 2007; van den Heuvel and Sporns 2013). Hubs represent nodes of special interest in many network studies since their central embedding in the network topology makes them attractive candidates for information integration while also rendering them vulnerable to attack. In some networks (including brains), hubs can be found to be highly interconnected to form a so-called "rich club" (van den Heuvel and Sporns 2011). The concept of hubs is strongly related to modularity and network communities; hubs that predominantly link nodes within one community are also referred to as "provincial hubs," whereas hubs that interconnect multiple communities are called "connector hubs" (Fig. 1). Increasingly, cross-cutting characterizations of brain network organization that simultaneously capture segregation, integration and influence rely on decomposing networks into modules or communities that are linked by bridge connections and hub nodes. Such modular accounts of brain networks are particularly appealing since they can be applied to both structural and functional networks, and since the resulting modules have been shown to have behavioral and cognitive relevance.

Network analysis based on graph theory is prone to a number of potential limitations and pitfalls (Sporns 2014). Like all quantitative analysis, its reliability, sensitivity and reproducibility are crucially dependent on the integrity of connectivity data. This issue becomes especially important in the area of node definition, i.e., the parcellation of neural tissue into coherent areas by applying some criteria of structural or functional homogeneity. The parcellation problem (and hence node definition) continues to present pressing challenges at the meso- and macro-scales of whole-brain connectomics. In parallel, the definition of edges, particularly the estimation of structural connections using sensitive microscopic, histological or imaging techniques, continues to be problematic. Both the detection of the presence or absence of connections or pathways and the estimation of their strength or weight (based on synaptic contact area, labeling density, or tractography measures) are subject to noise, statistical biases and observational error. Significant efforts to improve neural tracing and recording techniques are currently underway, and these efforts will continue to deliver ever more accurate and more highly resolved brain network data sets.

Topology of Structural Brain Networks

This section summarizes some recent studies reporting on the topology of structural brain networks at micro-, meso- and macro-scales. The focus is on studies that have yielded significant insights into characteristic patterns and motifs of network connectivity.

Microscale

Microscale studies of structural connectivity depend on the development of techniques for automated histology (electron microscopy or light microscopy) and reconstruction that combine sensitivity with scalability (Kleinfeld et al. 2011; Helmstaedter et al. 2011; Helmstaedter 2013). While these techniques have not yet delivered any whole-brain wiring diagrams for complex organisms, they have been successfully deployed to map specific circuits in both invertebrate and vertebrate nervous systems.

Recent studies in three model organisms (*C. elegans*, *Drosophila*, mouse) have yielded significant microscale connectivity data that have added to our knowledge of connectome architecture at the cellular level. Building on the ground-breaking work of White et al. (1986), recent studies have reported on the wiring diagram of the posterior nervous system of the *C. elegans* adult male, reconstructed from serial electron micrograph sections (Jarrell et al. 2012). Analysis of the resulting wiring pattern showed a network that was characterized by a number of features, including the presence of multiple parallel pathways that linked sensory neurons to effector neurons, some degree of recurrence within sensory systems, and the presence of structural modules. These connectional features could be related to specific aspects of sensorimotor processing and behavior. Other studies have provided additional insights for how circuit connectivity in *C. elegans* constrains function and behavior. Bumbarger et al. (2013) compared the synaptic connectivity of the pharyngeal nervous system of two different nematode species that exhibit very different feeding behavior. Employing graph-theoretic analyses, these behavioral differences could be traced to differences in synaptic rewiring that determined different roles of several neurons involved in regulating predatory feeding.

Studies of microscale wiring patterns in *Drosophila* have demonstrated that the topology of specific subcircuits can be explained on the basis of wiring length minimization and volume exclusion, both mechanisms directed at the economical conservation of space (Rivera-Alba et al. 2011). In a more recent electron microscopic study, Takemura et al. (2013) reconstructed a microscale circuit comprising 379 neurons and 8637 synapses within the optic medulla, a structure involved in visual motion detection. The circuit reconstruction revealed specific patterns of inter-neuronal connectivity that were consistent with the roles of individual neurons in generating direction selectivity.

Detection of directed visual motion was also studied in circuits of the mouse retina, reconstructed from data obtained with serial block-face electron microscopy (Briggman et al. 2011). Analysis showed anatomically specific patterns of connectivity between amacrine and ganglion cells that were in register with physiologically measured direction selectivity of individual neurons. In subsequent work, dense reconstruction of a significant portion of the mouse retina was carried out by Helmstaedter et al. (2013). The use of a combination of manual annotation and machine learning resulted in a synaptic "contact matrix" between 950 neurons in the inner plexiform layer. Microscale connection motifs in this matrix revealed circuit mechanisms underlying motion detection and other aspects of visual function.

Direct applications of graph theory or network science methods to microscale connectivity data are still scarce, in part due to the lack of data sets comprising more than just a few neurons. Quantitative network analysis has only just begun to contribute to microscale connectome studies. Important open questions in this area concern the specificity of connections between individual neurons, the prevalence of specific network motifs that might be specialized to carry out local computations, or the presence of small world organization. As more microscale connectome data accrue, network analysis will become increasingly important for characterizing circuit models of neural computation (Denk et al. 2012).

Mesoscale

Mesoscale efforts to assemble connectivity maps for large portions or even complete nervous systems are under way in a number of organisms, with some of the most important insights coming from *Drosophila* and mouse.

Chiang et al. (2011) collected high-resolution 3D images of approximately 16,000 single neurons in the *Drosophila* brain that were then used to assemble a whole-brain connectivity matrix. Aggregation of single-neuron images into functional subdivisions, so-called "local processing units," resulted in a mesoscale connectome comprising 41 nodes and their weighted interconnections. Cluster analysis revealed distinct network communities or modules whose members were functionally specialized to carry out visual, olfactory, auditory and motor processing. Ongoing work has begun to reveal additional network attributes, including additional submodules and small-world organization (Shih et al. 2013; 2015).

Mesoscale mouse connectome projects (as well as parallel efforts in the rat cerebral cortex; Bota et al. 2015) have produced similar insights. Wang et al. (2012) performed a detailed quantitative analysis of the anatomical connections of ten areas of mouse visual cortex, including both their mutual connectivity and their external projection targets. Modularity analysis demonstrated a division of mouse cortex into two processing streams, with some anatomical and physiological data suggesting a close correspondence to the dorsal/ventral streams found in primate visual cortex. Zingg et al. (2014) generated a connectivity matrix for mouse neocortex by combining data

from hundreds of tracer injections into a single network representation. The resulting directed connectivity network was shown to contain several modules corresponding to subdivisions or "subnetworks" involved in various sensory, motor and integrative functions. A parallel effort (Oh et al. 2014), involving high-resolution optical imaging and tracing of projections across the entire mouse brain, has resulted in another mouse connectome map that charts the directed and weighted anatomical links among 295 gray-matter regions. Initial network analysis of this map indicates the presence of high clustering as well as a number of highly connected network hubs.

Common themes in mesoscale connectomics across species are a prevalence of high clustering due to the existence of network modules, a strong association of these modules with distinct functional or behavioral domains, and the use of connection profiles of individual areas to build an understanding of their potential functional contributions. Network architectures involving modules interconnected by hubs appear to be shared among several species (invertebrate, mammalian, as well as the avian brain; see Shanahan et al. 2013).

Macroscale

The distinction between meso- and macro-scales is at present somewhat indistinct. Mesoscale maps result in connectivity data that report on areas and their inter-areal projections, as do most macroscale efforts that leverage tract tracing methods in non-human primates or noninvasive imaging in human brain. The macroscale studies summarized in this section all focus on inter-areal or large-scale projections in primate cerebral cortex.

Tract tracing has an important role to play for the study of anatomical connections in animal models, particularly in non-human primates. An extensive set of studies carried out by Henry Kennedy and colleagues (Markov et al. 2011, 2013a, b, 2014) have revealed the connectional anatomy of the macaque cerebral cortex in new detail. Injections of retrograde tracers in 29 cortical areas followed by rigorous quantification of label density across the entire cortex demonstrated a previously unknown degree of connectedness among areas. Numerous new (and mostly relatively weak) projections were uncovered, and the overall connectivity profile for each area was best approximated by a lognormal distribution (Markov et al. 2011), with a few strong projections and a large admixture of medium or weak pathways. Graph analysis provided evidence for a relatively high proportion of unidirectional links (Markov et al. 2014), a strong contribution of long-distance projections towards areal specificity (Markov et al. 2013a), significant distance-dependence of connection densities (Ercsey-Ravasz et al. 2013), and hierarchical arrangement of areas into "counter-streams" (Markov et al. 2013b). Several of these characteristic topological features are also found in other mammalian species, e.g., the cat or rodent brain. While the sensitivity and quantifiability of tract tracing data offer new opportunities for mapping connectome networks, the invasiveness of the method and the current inability to conduct whole-brain tracing across the entire network of

pathways simultaneously impose some limitations, especially in estimating individual variability and in relating connectivity patterns to behavior.

Human brain connectomics currently relies primarily on imaging and reconstructing structural connections on the basis of diffusion MRI and tractography. This approach uses signals that record the diffusion anisotropy of water or other small molecules within biological tissue. Based on these signals, reconstruction methods then deliver inferential and statistical models of fiber anatomy. Methods for data acquisition and fiber reconstruction are under continual development, with significant recent refinements involving increased spatial resolution (Uğurbil et al. 2013), more robust probabilistic methods for tractography (Sotiropoulos et al. 2013) and additional measures of white matter microstructure such as axonal diameters (Alexander et al. 2010). A unique feature of noninvasive imaging methods is that they allow the acquisition of data from large numbers of individuals, thus opening opportunities for measuring individual variability and relation of connectional features to behavioral and cognitive performance, taking steps towards "population neuroscience" (Falk et al. 2013).

A large number of studies have generated network maps of the human connectome (Hagmann et al. 2008; Gong et al. 2009; Bassett et al. 2010; van den Heuvel and Sporns 2011). Network studies of human structural connectivity patterns have consistently reported broad degree distributions, with a "heavy tail" of well-connected nodes, including some that maintain very high numbers of connections. The precise shape of the degree distribution remains somewhat uncertain, due to resolution limits and issues related to node parcellation, with most studies suggesting exponential or exponentially truncated power-law distributions for node degree. An intriguing question for future work is how these distributions might compare to the log-normal profiles of connection density and weight obtained from other species (see above). Another common feature encountered across most, if not all, network studies of the human connectome is "small-worldness," i.e., the presence of high clustering and short path length (Bassett and Bullmore 2006). This is significant as the presence of small-world organization is consistent with a balance between anatomical and functional segregation on the one side (as captured by high clustering) and a simultaneous capacity for global integration on the other side (as captured by short communication paths).

High clustering in the human brain (as well as in the nervous systems of other species) is mainly driven by the presence of modules, or network communities of densely interconnected neural elements. From a network perspective, structural modules offer a connectional substrate for rapid and efficient sharing of information among restricted sets of brain regions (often found to contribute to a common set of tasks) while also promoting the functional specialization of these regions by creating boundaries that limit the spread of information across the entire network. A complementary concept is that of network hubs. As discussed earlier, hubs are regions that are less central to specific modules but instead interconnect multiple modules to each other; such hubs are generally characterized by their high degree, high centrality, and diverse connection profiles. In the human cerebral cortex, hubs have been identified in portions of the medial and superior parietal cortex as well as

selected regions in orbitofrontal, superior frontal and lateral prefrontal cortex (Hagmann et al. 2008; Gong et al. 2009; van den Heuvel and Sporns 2013), with many of them previously described as multi- or transmodal association areas (e.g., Mesulam 1998).

Recently, several human connectivity studies have suggested a tendency for hubs to be densely interconnected in a structural core (Hagmann et al. 2008) or a "rich club" (van den Heuvel and Sporns 2011), again paralleling findings in other species (e.g., Zamora-López et al. 2010; Harriger et al. 2012). Across these different studies, a common prediction is that rich club nodes and their interconnections may have particularly important roles to play in brain communication (van den Heuvel et al. 2012). Computational studies of the human connectome have shown that a very high percentage of all short communication paths among non-rich club regions across the network must pass through the rich club. Furthermore, damage to connections that link rich club regions is predicted to have a larger disruptive effect on network communication than an equal amount of damage to connections among non-rich club regions.

Numerous common themes have emerged across different studies of primate cortex. The emerging picture is one of a modular small-world network, with clustered network communities that are interlinked by a coherent core or subnetwork (the rich club) of hub regions. The placement of the rich club within the overall network is strongly suggestive of a central role in global information flow and integration. The implications of such a structural core or rich club for cognition and behavior remain largely unexplored. One important conceptual link is that between rich-club organization and theories of "global workspace" in relation to cognition and consciousness (Dehaene and Changeux 2011). Workspace theories postulate mechanisms for integration across sensory, motor and cognitive domains that may require a dense subnetwork of distributed hub regions, i.e., the presence of a cortical rich club.

Comparison Across Scales and Challenges

How do connectome mapping efforts across different scales relate to each other? For the purpose of mapping whole nervous systems that are small and compact (such as those of many invertebrates) as well as for elucidating connectivity of local circuits in more complex brains, microscale approaches to structural connectomics are clearly of major importance. However, it seems unlikely that the application of microscale connectomics technology, even if successful across the whole brain, will ever entirely remove the need for measuring connectivity at coarser spatial scales. For descriptions of brain connectivity in large brains (e.g., in mammalian species), mesoscale and macroscale maps will remain essential as they allow establishing relations between connectivity and behavior. In addition, meso- and macroscale in vivo mapping strategies such as noninvasive neuroimaging, despite limits on resolution and various methodological biases, make an important

contribution by drawing links between individual variations in connectivity and individual differences in cognitive and behavioral performance. It is difficult to imagine at present how microscale approaches alone can address these important research goals of connectomics in the foreseeable future.

Several challenges for structural connectomics remain. As the field matures, there will be a growing need for annotation of connectome maps with additional physiological parameters, for example, data on connectional microstructure, neurotransmitter receptors, plasticity and neuromodulatory effects, all aspects that are crucial for interpreting the functional role of connectional topology. The goal of using connectome data for explaining and predicting the operation of neuronal circuits and populations requires the inclusion of these physiological features of connections that are known to have important impacts on how neurons interact and how circuits compute (Bargmann 2012). Another challenge is to map features of connectome topology across scales, from cells to whole-brain systems. Data on nervous systems across a range of species have demonstrated a surprising degree to which global network organization is preserved; virtually all brain network data sets examined so far share some degree of high clustering, short path length, modules and hubs, and even rich-club organization. It is unknown at present if similarities exist also across different scales within the same nervous system, for example, long-range pathways between brain areas as well as local cortical circuits.

Relations Between Structure and Function

Structure-function relationships are crucial for achieving a deeper understanding of biological processes. In line with this view, the relation of structural to functional connectivity offers a key motivation for mapping connectome networks. A number of studies across micro, meso and macro scale have suggested that patterns of structural connections are indeed instrumental in shaping the dynamics of neural activity.

Microscale

The relations between circuit topology, neural computation and behavior are still relatively unexplored. Significant inroads have been made in the network anatomy of specific subregions of the *C. elegans* nervous system and its relation to specific behaviors (see above). Another area where detailed reconstructions of cell morphology and circuit anatomy have helped understand circuit function is motion detection (Borst and Euler 2011), specifically motion detection circuits of *Drosophila* and the mouse retina (see above).

Important insights have been gained from microscale studies that are built on a combined structure-function approach. An example is an analysis of anatomy and

physiology of a subset of neurons in primary visual cortex of the mouse carried out by Bock et al. (2011). First, the authors characterized functional properties of neurons, such as their preferred stimulus orientation, using optical imaging. Then, they performed serial sectioning electron microscopy of the same tissue volume to map and reconstruct synaptic interconnections, eventually resulting in a network graph. Detailed analysis of the final connection diagram revealed some specific connectional features such as convergence of inputs from multiple pyramidal cells with diverse orientation preference onto inhibitory neurons. This pattern of convergence, while unrelated to the physiological specializations of the presynaptic cells, was partially predicted by axonal geometry, specifically the pair-wise spatial overlap of their synaptic boutons. Together with the study of Briggman et al. (2011) on direction selectivity in mouse retina (see above), this work represents an example of how the combined analysis of anatomy and physiology can inform neural accounts of computations that relate to behavior.

Large-scale recording methods applied to organisms such as the zebrafish larva can yield whole-brain recordings of highly resolved neural population activity (Ahrens et al. 2013). This dynamic circuit activity can be analyzed with time series methods, and there is evidence of functionally coherent circuits forming clusters or modules (Portugues et al. 2014). A near-term goal will be to relate the timing of correlated neural events to underlying anatomical connections that modulate whole-brain functional connectivity. Furthermore, modern molecular tools open the possibility to not only monitor but also manipulate circuit activity, for example, through the use of optogenetics (Portugues et al. 2013). This might eventually allow for uncovering causal (directed or effective) relationships between circuit elements, an aspect of connectome studies that is currently difficult to attain at the meso- and macroscales.

Mesoscale

Mesoscale studies of structural and functional connectivity have so far largely been carried out in the non-human primate. However, the increasing availability of mesoscale connectome data (e.g., Oh et al. 2014) as well as high-resolution functional MRI recordings (Mechling et al. 2014) may soon offer an opportunity to explore the issue in the mouse brain. Some important work in this area has been carried out in the macaque monkey.

Wang et al. (2013) studied the relationship between structural and functional connectivity at high spatial resolution within the monkey somatosensory cortex. Their focus of study was on connectivity within two specialized areas of the squirrel monkey somatosensory cortex (areas 3b and 1), both containing representations of the monkey's body surface, specifically the tips of the digits of the monkey's hand. Resting-state functional connectivity was recorded using high-field strength functional magnetic resonance imaging (fMRI) and revealed topographically precise coupling between corresponding digits across both areas, as well as within area 3b.

This pattern matched anatomical connectivity patterns observed after injections of anatomical tracers into specific digit representations. Overall, connectivity within the squirrel monkey somatosensory cortex appears to be organized anatomically and functionally in highly similar patterns, with two main "axes of information flow." One axis predominantly links representations of matched digits in area 3b to area 1, whereas the other axis links representations of different digits within area 3b.

At the whole-brain level, a study of functional connectivity driven by spontaneous neural activity in the macaque monkey cortex by Vincent et al. (2007) found that patterns of coherent spontaneous blood oxygenation level dependent (BOLD) fluctuations were similar to patterns of anatomical connectivity derived from tract tracing studies. Adachi et al. (2012) performed a similar analysis, comparing structural and functional connectivity across 39 regions of macaque cortex and demonstrating a significant statistical relationship. More detailed analysis of functional connectivity patterns demonstrated that strong coupling among brain regions could be observed even if no direct anatomical connection was present. These indirect functional relationships were found to be due to the flow of signals along indirect structural paths and other, more complex network-wide coupling effects. Both direct and indirect couplings could be successfully captured in computational models. Taken together, these findings further support a mechanistic role of structural connections in generating organized patterns of neural dynamics.

Macroscale

At the macroscale, comparisons of structural and functional connectivity have largely centered on spontaneous or endogenously driven neural activity. In human imaging, much of the emphasis over the past several years has been on fluctuations in BOLD activity in the human brain acquired during a "task-free" or resting state. Despite its unconstrained nature, numerous studies have shown that spatial and temporal patterns of resting brain activity can be richly informative about the brain's functional organization (Raichle 2011; Buckner et al. 2013). Resting-state functional connectivity is generally expressed as the cross-correlation of time series of BOLD signals recorded with fMRI across the whole brain.

Direct comparison of resting-state functional connectivity and structural connectivity (connectome) networks has revealed robust and reproducible statistical relationships, giving rise to the idea that structural connections shape functional connectivity. A systematic analysis of structural and functional connectivity in a small cohort of human participants used a parcellation of the cortex into approximately 1000 equal-sized regions of interest (Hagmann et al. 2008). The study reported robust correlations between the strengths of structural and functional connectivity across the entire cortical surface. A more detailed analysis of the same data set (Honey et al. 2009) demonstrated that this correlation persisted even after potential confounds such as spatial proximity between regions were

taken into account. The analysis also showed that indirect structural connections could account for a significant proportion of the functional connectivity observed between node pairs lacking direct linkage. This finding strongly suggested that functional connectivity may be partly due to the passing on of indirect influence along multi-step paths in the connectome (see Adachi et al. 2012). A parallel analysis (Skudlarski et al. 2008) also reported robust structural connectivity-functional connectivity correlations based on a voxel-by-voxel structural connectivity-functional connectivity comparison across the cerebral cortex.

Following these early analyses, numerous independent studies have confirmed the existence of robust and significant statistical relationships between structural and (resting state) functional connectivity in the human brain (e.g., Hermundstad et al. 2013). Several studies have focused on the role of spatial embedding (i.e., the distance dependence apparent in both structural and functional connections) for shaping the topology of structural and functional connections (e.g., Vértes et al. 2012; Samu et al. 2014). Other studies have compared structure-function relations across species (Miranda-Dominguez et al. 2014). The notion that structural connections shape and/or constrain functional connections is not only supported through comparisons of anatomical and functional connectivity but is also reinforced by interventional studies that have reported changes in functional connectivity resulting from manipulations of the anatomical substrate (Johnston et al. 2008; O'Reilly et al. 2013). Extending this notion to brain and mental disorders, a large number of studies have attempted to link dysregulation of functional connectivity patterns to underlying disturbances of structural connectivity, e.g., in disrupted hub or rich club connections [reviewed in van den Heuvel and Sporns (2013)].

Comparison Across Scales and Challenges

In summary, there is converging evidence suggesting that the connectional anatomy of neurons and brain regions is shaping or constraining the statistical dependencies that emerge as neurons and brain regions become functionally activated. Many studies have relied on simple measures of dependency (such as cross-correlation or covariance) to demonstrate this relationship. A future challenge is to develop and deploy more complex and specific measures, for example, measures that are based on partial correlations or directed influence, to better distinguish statistical dependencies due to transitive (correlative) couplings from others that are mediated by direct structural connections (and hence more causal in nature). Another challenge is to observe brain dynamics at both circuit and whole-brain levels, which is currently impossible with most standard recording techniques that either suffer from a limited "field of view" (recording only very few neurons in great detail) or limited spatial and temporal resolution (e.g., noninvasive imaging). Combining whole-brain coverage with fine spatial and temporal detail would allow capturing dynamic activity unfolding within a brain's structural connectome, perhaps even in

relation to behavior. Promising steps in this direction have been made, with the development of new activity-dependent probes and of whole-brain recordings in *C. elegans* and zebrafish (see above).

Future Perspectives

As the many contributions to this volume document, research in micro-, meso- and macroconnectomics is rapidly expanding and is offering a fresh perspective on brain function as emerging from the structure and dynamics of complex networks (Sporns 2011). The future of the field is difficult to predict. Extrapolating from the past, it seems likely that connectomics will be strongly influenced by new methodological and analytic developments in both data acquisition and analysis. In this final section of the article, I attempt to forecast some of the areas where the field of connectomics may make important contributions in the near future.

Computational models will play an increasingly important role, for example, in attempts to use connectome data to inform computational models of brain function and dynamics (Fig. 2). A series of such models have been used to investigate the structural basis of spontaneous or resting-brain functional connectivity as recorded with fMRI [reviewed in Deco et al. (2011)]. Model design generally combines sets of biophysical equations that specify the dynamics of neurons or neuronal populations with sets of coupling terms (for example, structural couplings specified by a connectome map). Model analysis proceeds by using some of the same time series measures (e.g., cross-correlations between neural activity patterns) that are also employed in empirical studies. Key findings coming from this modeling work include robust relations between empirical and simulated functional networks (Honey et al. 2007, 2009; Adachi et al. 2012), as well as an important role for conduction delays and noise in generating realistic resting-brain dynamics (Deco et al. 2009). This connectome-based modeling framework can be extended to include anatomically detailed models of dynamic effects induced by focal brain lesions (Alstott et al. 2009) or degeneration of brain connectivity (de Haan et al. 2012). While biophysically based models can generate simulations of rich brain dynamics, simpler models that are based on structural graph measures (Goñi et al. 2014) and/or models of diffusive processes (Abdelnour et al. 2014) and routing (Mišić et al. 2014) are gaining in importance due to their computational simplicity and analytic transparence.

Another challenge concerns the realization that brain networks are not static in time; instead, they exhibit dynamic changes on multiple time scales. Tracking such network dynamics across time presents major methodological and analytic hurdles. Networks change on slow time scales, for example, across development and the human life span, and a growing number of imaging studies are directed at characterizing the processes that guide network growth and maturation, as well as the changing distributions of hubs and network communities (e.g., Power et al. 2010). In addition to these slow changes across time, networks change on much faster time

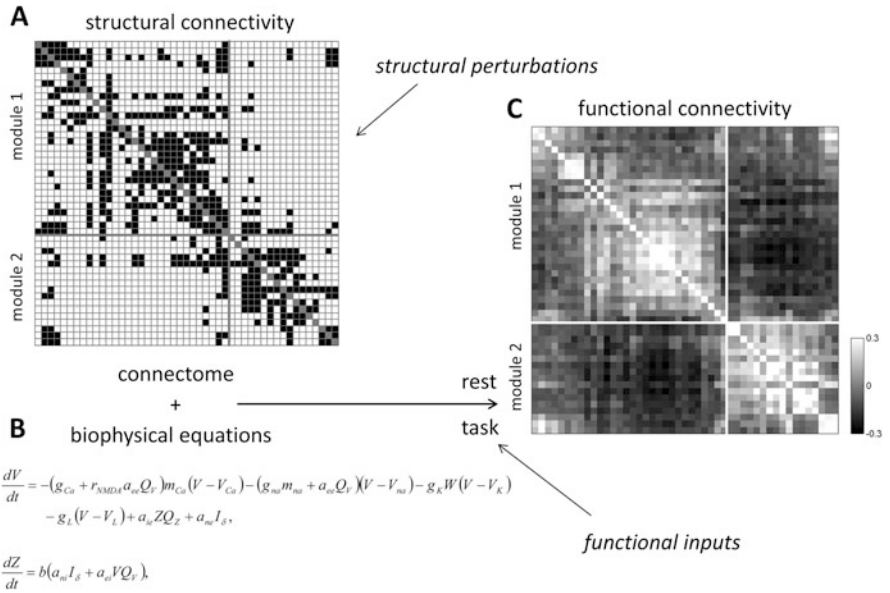

Fig. 2 An example of modeling the structure/function relationship in brain networks. (**a**) A structural connectivity matrix comprising 47 regions of the macaque cortex and their anatomical relationships, based on a collation of tract-tracing data [for more detail, see Honey et al. (2007)]. The matrix is binary and directed, with *black squares* indicating the presence of a connection from one area (*matrix row*) to another (*matrix column*). (**b**) Biophysical equations that describe nodal dynamics in a so-called neural mass model (Honey et al. 2007). (**c**) Combination of the structural connectivity matrix and the biophysical equations yields a time series for neuronal dynamics that can be rendered as functional connectivity. Structural perturbations (e.g., deletion of nodes or edges in the connectome) or functional inputs (e.g., simulating task performance) can be used to explore differences in functional connectivity. Both structural and functional connectivity are presented with identical arrangements of brain regions, and two functional modules are indicated (modules 1 and 2)

scales (seconds and milliseconds), both during "resting state" (more appropriately conceptualized as the "restless brain"; Raichle 2011) and in transitions between tasks. Informed by new approaches to network dynamics coming from network science (e.g., Mucha et al. 2010), recent studies have attempted to measure fast changes in network topology in brain recordings (Bassett et al. 2013).

In conclusion, as small data give way to "big data" in neuroscience (much of it coming from the domains of structural and functional connectivity), connectomics is likely to expand significantly in coming years. Several large-scale national and international projects and consortia directed at brain science are underway, including the Human Connectome Project and the BRAIN initiative in the U.S. as well as the Human Brain Project in the E.U. As these projects progress, there will be an increasing need for a theoretical framework that can underpin and help make sense of "big brain data" (Sporns 2013b). One promising candidate for such a framework

is the science of networks, with its many applications in the brain across different scales and systems.

Acknowledgment The author's work was supported by the J.S. McDonnell Foundation

References

Abdelnour F, Voss HU, Raj A (2014) Network diffusion accurately models the relationship between structural and functional brain connectivity networks. Neuroimage 90:335–347

Adachi Y, Osada T, Sporns O, Watanabe T, Matsui T, Miyamoto K, Miyashita Y (2012) Functional connectivity between anatomically unconnected areas is shaped by collective network-level effects in the macaque cortex. Cereb Cortex 22:1586–1592

Ahrens MB, Orger MB, Robson DN, Li JM, Keller PJ (2013) Whole-brain functional imaging at cellular resolution using light-sheet microscopy. Nat Methods 10:413–420

Alexander DC, Hubbard PL, Hall MG, Moore EA, Ptito M, Parker GJ, Dyrby TB (2010) Orientationally invariant indices of axon diameter and density from diffusion MRI. Neuroimage 52:1374–1389

Alstott J, Breakspear M, Hagmann P, Cammoun L, Sporns O (2009) Modeling the impact of lesions in the human brain. PLoS Comput Biol 5:e1000408

Bargmann CI (2012) Beyond the connectome: how neuromodulators shape neural circuits. Bioessays 34:458–465

Bassett DS, Bullmore ET (2006) Small world brain networks. Neuroscientist 12:512–523

Bassett DS, Brown JA, Deshpande V, Carlson JM, Grafton ST (2010) Conserved and variable architecture of human white matter connectivity. Neuroimage 54:1262–1279

Bassett DS, Porter MA, Wymbs NF, Grafton ST, Carlson JM, Mucha PJ (2013) Robust detection of dynamic community structure in networks. Chaos 23:013142

Bock DD, Lee WCA, Kerlin AM, Andermann ML, Hood G, Wetzel AW, Yurgenson S, Soucy ER, Kim HS, Reid RC (2011) Network anatomy and in vivo physiology of visual cortical neurons. Nature 471:177–182

Borst A, Euler T (2011) Seeing things in motion: models, circuits, and mechanisms. Neuron 71: 974–994

Bota M, Sporns O, Swanson LW (2015) Architecture of the cerebral cortical association connectome underlying cognition. Proc Natl Acad Sci USA 112:E2093–E2101

Briggman KL, Helmstaedter M, Denk W (2011) Wiring specificity in the direction-selectivity circuit of the retina. Nature 471:183–188

Buckner RL, Krienen FM, Yeo BT (2013) Opportunities and limitations of intrinsic functional connectivity MRI. Nat Neurosci 16:832–837

Bullmore E, Sporns O (2009) Complex brain networks: graph theoretical analysis of structural and functional systems. Nat Rev Neurosci 10:186–198

Bumbarger DJ, Riebesell M, Rödelsperger C, Sommer RJ (2013) System-wide rewiring underlies behavioral differences in predatory and bacterial-feeding nematodes. Cell 152:109–119

Chiang AS, Lin CY, Chuang CC, Chang HM, Hsieh CH, Yeh CW, Shih CT, Wu JJ, Wang GT, Chen YC, Wu CC, Chen GY, Ching YT, Lee PC, Lin CY, Lin HH, Wu CC, Hsu HW, Huang YA, Chen JY, Chiang HJ, Lu CF, Ni RF, Yeh CY, Hwang JK (2011) Three-dimensional reconstruction of brain-wide wiring networks in *Drosophila* at single-cell resolution. Curr Biol 21:1–11

Chklovskii DB, Schikorski T, Stevens CF (2002) Wiring optimization in cortical circuits. Neuron 34:341–347

de Haan W, Mott K, van Straaten EC, Scheltens P, Stam CJ (2012) Activity dependent degeneration explains hub vulnerability in Alzheimer's disease. PLoS Comput Biol 8:e1002582

Deco G, Jirsa V, McIntosh AR, Sporns O, Kötter R (2009) Key role of coupling, delay, and noise in resting brain fluctuations. Proc Natl Acad Sci USA 106:10302–10307

Deco G, Jirsa VK, McIntosh AR (2011) Emerging concepts for the dynamical organization of resting-state activity in the brain. Nat Rev Neurosci 12:43–56

Dehaene S, Changeux JP (2011) Experimental and theoretical approaches to conscious processing. Neuron 70:200–227

Denk W, Briggman KL, Helmstaedter M (2012) Structural neurobiology: missing link to a mechanistic understanding of neural computation. Nat Rev Neurosci 13:351–358

Ercsey-Ravasz M, Markov NT, Lamy C, Van Essen DC, Knoblauch K, Toroczkai Z, Kennedy H (2013) A predictive network model of cerebral cortical connectivity based on a distance rule. Neuron 80:184–197

Falk EB, Hyde LW, Mitchell C, Faul J, Gonzalez R, Heitzeg MM, Keating DP, Langa KM, Martz ME, Maslowsky J, Morrison FJ, Noll DC, Patrick ME, Pfeffer FT, Reuter-Lorenz PA, Thomason ME, Davis-Kearn P, Monk CS, Schulenberg J (2013) What is a representative brain? Neuroscience meets population science. Proc Natl Acad Sci USA 110:17615–17622

Felleman DJ, van Essen DC (1991) Distributed hierarchical processing in the primate cerebral cortex. Cereb Cortex 1:1–47

Gong G, He Y, Concha L, Lebel C, Gross DW, Evans AC, Beaulieu C (2009) Mapping anatomical connectivity patterns of human cerebral cortex using in vivo diffusion tensor imaging tractography. Cereb Cortex 19:524–536

Goñi J, van den Heuvel MP, Avena-Koenigsberger A, de Mendizabal NV, Betzel RF, Griffa A, Hagmann P, Corominas-Murtra B, Thiran JP, Sporns O (2014) Resting-brain functional connectivity predicted by analytic measures of network communication. Proc Natl Acad Sci USA 111:833–838

Hagmann P, Cammoun L, Gigandet X, Meuli R, Honey CJ, Wedeen V, Sporns O (2008) Mapping the structural core of human cerebral cortex. PLoS Biol 6:e159

Harriger L, van den Heuvel MP, Sporns O (2012) Rich club organization of macaque cerebral cortex and its role in network communication. PLoS One 7:e46497

Helmstaedter M (2013) Cellular-resolution connectomics: challenges of dense neural circuit reconstruction. Nat Methods 10:501–507

Helmstaedter M, Briggman KL, Denk W (2011) High-accuracy neurite reconstruction for high-throughput neuroanatomy. Nat Neurosci 14:1081–1088

Helmstaedter M, Briggman KL, Turaga SC, Jain V, Seung HS, Denk W (2013) Connectomic reconstruction of the inner plexiform layer in the mouse retina. Nature 500:168–174

Hermundstad AM, Bassett DS, Brown KS, Aminoff EM, Clewett D, Freeman S, Frithsen A, Johnson A, Tipper CM, Miller MB, Grafton ST, Carlson JM (2013) Structural foundations of resting-state and task-based functional connectivity in the human brain. Proc Natl Acad Sci USA 110:6169–6174

Hilgetag CC, Burns GA, O'Neill MA, Scannell JW, Young MP (2000) Anatomical connectivity defines the organization of clusters of cortical areas in the macaque monkey and the cat. Philos Trans R Soc Lond B 355:91–110

Honey CJ, Kötter R, Breakspear M, Sporns O (2007) Network structure of cerebral cortex shapes functional connectivity on multiple time scales. Proc Natl Acad Sci USA 104:10240–10245

Honey CJ, Sporns O, Cammoun L, Gigandet X, Thiran JP, Meuli R, Hagmann P (2009) Predicting human resting-state functional connectivity from structural connectivity. Proc Natl Acad Sci USA 106:2035–2040

Jarrell TA, Wang Y, Bloniarz AE, Brittin CA, Xu M, Thomson JN, Albertson DG, Hall DH, Emmons SW (2012) The connectome of a decision-making neural network. Science 337: 437–444

Johnston JM, Vaishnavi SN, Smyth MD, Zhang D, He BJ, Zempel JM, Shimony JS, Snyder AZ, Raichle ME (2008) Loss of resting interhemispheric functional connectivity after complete section of the corpus callosum. J Neurosci 28:6453–6458

Kleinfeld D, Bharioke A, Blinder P, Bock DD, Briggman KL, Chklovskii DB, Denk W, Helmstaedter M, Kaufhold JP, Lee WCA, Meyer HS, Micheva KD, Oberlaender M, Prohaska S, Reid RC, Smith SJ, Takemura S, Tsai PS, Sakmann B (2011) Large-scale automated histology in the pursuit of connectomes. J Neurosci 31:16125–16138

Lohmann G, Stelzer J, Neumann J, Ay N, Turner R (2013) "More is different" in functional magnetic resonance imaging: a review of recent data analysis techniques. Brain Connect 3: 223–239

Markov NT, Misery P, Falchier A, Lamy C, Vezoli J, Quilodran R, Gariel MA, Giroud P, Ercsey-Ravasz M, Pilaz LJ, Huissoud C, Barone P, Dehay C, Toroczkai Z, Van Essen DC, Kennedy H, Knoblauch K (2011) Weight consistency specifies regularities of macaque cortical networks. Cereb Cortex 21:1254–1272

Markov NT, Ercsey-Ravasz M, Lamy C, Gomes ARR, Magrou L, Misery P, Giroud P, Barone P, Dehay C, Toroczkai Z, Knoblauch K, Van Essen DC, Kennedy H (2013a) The role of long-range connections on the specificity of the macaque interareal cortical network. Proc Natl Acad Sci USA 110:5187–5192

Markov NT, Ercsey-Ravasz M, Van Essen DC, Knoblauch K, Toroczkai Z, Kennedy H (2013b) Cortical high-density counterstream architectures. Science 342:1238406

Markov NT, Ercsey-Ravasz MM, Gomes ARR, Lamy C, Magrou L, Vezoli J, Misery P, Falchier A, Quilodran R, Gariel MA, Sallet J, Gamanut R, Huissoud C, Clavagnier S, Giroud P, Sappey-Marinier D, Barone P, Dehay C, Toroczkai Z, Knoblauch K, Van Essen DC, Kennedy H (2014) A weighted and directed interareal connectivity matrix for macaque cerebral cortex. Cereb Cortex 24:17–36

Mechling A, Hübner N, Lee HL, Hennig J, von Elverfeldt D, Harsan LA (2014) Fine-grained mapping of mouse brain functional connectivity with resting-state fMRI. Neuroimage 96: 203–215, http://dx.doi.org/10.1016/j.neuroimage.2014.03.078

Mesulam MM (1998) From sensation to cognition. Brain 121:1013–1052

Miranda-Dominguez O, Mills BD, Grayson D, Woodall A, Grant KA, Kroenke CD, Fair DA (2014) Bridging the gap between the human and macaque connectome: a quantitative comparison of global interspecies structure-function relationships and network topology. J Neurosci 34:5552–5563

Mišić B, Sporns O, McIntosh AR (2014) Communication efficiency and congestion of signal traffic in large-scale brain networks. PLoS Comput Biol 10:e1003427

Mucha PJ, Richardson T, Macon K, Porter MA, Onnela JP (2010) Community structure in time-dependent, multiscale, and multiplex networks. Science 328:876–878

O'Reilly JX, Croxson PL, Jbabdi S, Sallet J, Noonan MP, Mars RB, Browning PGF, Wilson CRE, Mitchell AS, Miller KL, Rushworth MFS, Baxter MG (2013) Causal effect of disconnection lesions on interhemispheric functional connectivity in rhesus monkeys. Proc Natl Acad Sci USA 110:13982–13987

Oh SW, Harris JA, Ng L, Winslow B, Cain N, Mihalas S, Wang Q, Lau C, Kuan L, Henry AM, Mortrud MT, Quellette B, Nguyen TN, Sorensen SA, Slaughterbeck CR, Wakeman W, Li Y, Feng D, Ho A, Nicholas E, Hirokawa KE, Bohn P, Joines KM, Peng H, Hawrylycz MJ, Phillips JW, Hohmann JG, Wohnoutka P, Gerfen CR, Koch C, Bernard A, Dang C, Jones AR, Zeng H (2014) A mesoscale connectome of the mouse brain. Nature 508:207–214

Passingham RE, Stephan KE, Kötter R (2002) The anatomical basis of functional localization in the cortex. Nat Rev Neurosci 3:606–616

Portugues R, Severi KE, Wyart C, Ahrens MB (2013) Optogenetics in a transparent animal: circuit function in the larval zebrafish. Curr Opin Neurobiol 23:119–126

Portugues R, Feierstein CE, Engert F, Orger MB (2014) Whole-brain activity maps reveal stereotyped, distributed networks for visuomotor behavior. Neuron 81:1328–1343

Power JD, Fair DA, Schlaggar BL, Petersen SE (2010) The development of human functional brain networks. Neuron 67:735–748

Raichle ME (2011) The restless brain. Brain Connect 1:3–12

Rivera-Alba M, Vitaladevuni SN, Mishchenko Y, Lu Z, Takemura SY, Scheffer L, Meinertzhagen IA, Chklovskii DB, de Polavieja GG (2011) Wiring economy and volume exclusion determine neuronal placement in the *Drosophila* brain. Curr Biol 21:2000–2005

Rubinov M, Sporns O (2010) Complex network measures of brain connectivity: uses and interpretations. Neuroimage 52:1059–1069

Samu D, Seth AK, Nowotny T (2014) Influence of wiring cost on the large-scale architecture of human cortical connectivity. PLoS Comput Biol 10:e1003557

Schmahmann JD, Pandya DN (2007) Cerebral white matter—historical evolution of facts and notions concerning the organization of the fiber pathways of the brain. J Hist Neurosci 16: 237–267

Shanahan M, Bingman VP, Shimizu T, Wild M, Güntürkün O (2013) Large-scale network organization in the avian forebrain: a connectivity matrix and theoretical analysis. Front Comput Neurosci 7:89

Shih CT, Sporns O, Chiang AS (2013) Toward the Drosophila connectome: structural analysis of the brain network. BMC Neurosci 14(Suppl 1):P63

Shih CT, Sporns O, Yuan SL, Su TS, Lin YJ, Chuang CC, Wang TY, Lo CC, Greenspan RJ, Chiang AS (2015) Connectomics-based analysis of information flow in the Drosophila brain. Current Biol 25:1249–1258

Skudlarski P, Jagannathan K, Calhoun VD et al (2008) Measuring brain connectivity: diffusion tensor imaging validates resting state temporal correlations. Neuroimage 43:554–561

Sotiropoulos SN, Jbabdi S, Xu J, Andersson JL, Moeller S, Auerbach EJ, Glasser MF, Hernandez M, Sapiro G, Jenkinson M, Feinberg DA, Yacoub E, Lenglet C, Van Essen DC, Ugurbil K, Behrens TE (2013) Advances in diffusion MRI acquisition and processing in the human connectome project. Neuroimage 80:125–143

Sporns O (2011) Networks of the brain. MIT Press, Cambridge

Sporns O (2013a) Network attributes for segregation and integration in the human brain. Curr Opin Neurobiol 23:162–171

Sporns O (2013b) Making sense of brain network data. Nat Methods 10:491–493

Sporns O (2014) Contributions and challenges for network models in cognitive neuroscience. Nat Neurosci 17:652–660

Sporns O, Tononi G, Kötter R (2005) The human connectome: a structural description of the human brain. PLoS Comput Biol 1:245–251

Sporns O, Honey CJ, Kötter R (2007) Identification and classification of hubs in brain networks. PLoS One 2:e1049

Stam CJ (2010) Characterization of anatomical and functional connectivity in the brain: a complex networks perspective. Int J Psychophysiol 77:186–194

Takemura SY, Bharioke A, Lu Z, Nern A, Vitaladevuni S, Rivlin PK, Katz WT, Olbris DJ, Plaza SM, Winston P, Zhao T, Horne JA, Fetter RD, Takemura S, Blazek K, Chang LA, Ogundeyi O, Saunders MA, Shapiro V, Sigmund C, Rubin GM, Scheffer LK, Meinertzhagen IA, Chklovskii DB (2013) A visual motion detection circuit suggested by Drosophila connectomics. Nature 500:175–181

Uğurbil K, Xu J, Auerbach EJ, Moeller S, Vu AT, Duarte-Carvajalino JM, Lenglet C, Wu X, Schmitter S, Van de Moortele PF, Strupp J, Sapiro G, De Martino F, Wang D, Harel N, Garwood M, Chen L, Feinberg DA, Smith SM, Miller KL, Sotiropoulos SN, Jbabdi S, Andersson JLR, Behrens TEJ, Glasser MF, Van Essen DC, Yacoub E (2013) Pushing spatial and temporal resolution for functional and diffusion MRI in the Human Connectome Project. Neuroimage 80:80–104

van den Heuvel MP, Sporns O (2011) Rich-club organization of the human connectome. J Neurosci 31:15775–15786

van den Heuvel MP, Sporns O (2013) Network hubs in the human brain. Trends Cogn Sci 17: 683–696

van den Heuvel MP, Kahn RS, Goñi J, Sporns O (2012) A high-cost, high-capacity backbone for global brain communication. Proc Natl Acad Sci USA 109:11372–11377

Van Essen DC, Ugurbil K, Auerbach E, Barch D, Behrens TEJ, Bucholz R, Chang A, Chen L, Corbetta M, Curtiss SW, Della Penna S, Feinberg D, Glasser MF, Harel N, Heath AC, Larsen-Prior L, Marcus D, Michalareas G, Moeller S, Oostenveld R, Petersen SE, Prior F, Schlaggar BL, Smith SM, Snyder AZ, Xu J, Yacoub E (2012) The human connectome project: a data acquisition perspective. Neuroimage 62:2222–2231

Vértes PE, Alexander-Bloch AF, Gogtay N, Giedd JN, Rapoport JL, Bullmore ET (2012) Simple models of human brain functional networks. Proc Natl Acad Sci USA 109:5868–5873

Vincent JL, Patel GH, Fox MD, Snyder AZ, Baker JT, Van Essen DC, Zempel JM, Snyder LH, Corbetta M, Raichle ME (2007) Intrinsic functional architecture in the anaesthetized monkey brain. Nature 447:83–86

Wang Q, Sporns O, Burkhalter A (2012) Network analysis of corticocortical connections reveals ventral and dorsal processing streams in mouse visual cortex. J Neurosci 32:4386–4399

Wang Z, Chen LM, Négyessy L, Friedman RM, Mishra A, Gore JC, Roe AW (2013) The relationship of anatomical and functional connectivity to resting-state connectivity in primate somatosensory cortex. Neuron 78:1116–1126

Watts DJ, Strogatz SH (1998) Collective dynamics of "small-world" networks. Nature 393: 440–442

White JG, Southgate E, Thomson JN, Brenner S (1986) The structure of the nervous system of the nematode *Caenorhabditis elegans*. Philos Trans R Soc Lond B 314:1–340

Young MP (1993) The organization of neural systems in the primate cerebral cortex. Proc R Soc Lond B 252:13–18

Zamora-López G, Zhou C, Kurths J (2010) Cortical hubs form a module for multisensory integration on top of the hierarchy of cortical networks. Front Neuroinform 4:1

Zeki S, Shipp S (1988) The functional logic of cortical connections. Nature 335:311–317

Zingg B, Hintiryan H, Gou L, Song MY, Bay M, Bienkowski MS, Foster NN, Yamashita S, Bowman I, Toga AW, Dong HW (2014) Neural networks of the mouse neocortex. Cell 156:1096–1111

Intra- and Inter-hemispheric Connectivity Supporting Hemispheric Specialization

Nathalie Tzourio-Mazoyer

Abstract Hemispheric specialization (HS), or hemispheric dominance, is a nineteenth century concept that relates to the fact that a given hemisphere is the pilot of a given function such as, for example, the left hemisphere is dominant for language and for right-handedness. HS is grounded in both intra-hemispheric white matter connections, supported by associative bundles, and inter-hemispheric connections between cortical areas located in mirrored positions (homotopic), through the corpus callosum (CC) fiber tracts. Imaging investigations have measured anatomical and/or functional asymmetry, assessing HS at the voxelwise, regional, or hemispheric level. Comparison of these simple measures obtained with functional imaging during language tasks with results from the Wada test has validated that asymmetries do size up HS and pave the way for the investigation of HS in healthy humans. Anatomical asymmetries explain only a fraction of functional variability in lateralization, likely because structural and functional asymmetries develop at different periods of life. Anatomical asymmetries appear as early as the 26th week of gestation; at birth they are identical to those of adults. In contrast, functional neuroimaging investigations have revealed that inter-hemispheric connectivity appears at birth and is leftward asymmetrical in auditory areas, whereas in high-order language areas, this inter-hemispheric connectivity slowly shifts during development to a predominant intra-hemispheric connectivity in the adult. The precise timing and neural basis of this shift are still unknown, but it has been nevertheless shown that the connectivity is not yet in place at the age of seven and that it parallels an increase in leftward asymmetry during language tasks. Abnormal development of this asymmetry is observed in severe mental illnesses that exhibit language symptoms, such as schizophrenia and autism. In addition, after a dominant hemisphere lesion, good language capacities are associated with the recovery of a leftward asymmetry during language tasks. However, neuroimaging studies have shown that HS variability for language, up to rightward dominance, exists in healthy individuals and is partly explained by both behavioral (handedness) and anatomical (i.e., brain volume, size of the left planum temporale) factors, with these factors possibly interacting with one another. Knowledge of the setting up of

N. Tzourio-Mazoyer (✉)
Institut des Maladies Neurodégénératives (IMN), CEA CNRS Université de Bordeaux, UMR 5293, GIN Team 5, Bordeaux, France
e-mail: nathalie.tzourio-mazoyer@u-bordeaux.fr

H. Kennedy et al. (eds.), *Micro-, Meso- and Macro-Connectomics of the Brain*, Research and Perspectives in Neurosciences, DOI 10.1007/978-3-319-27777-6_9

language HS is still fractional and very little is known about right hemisphere dominance and complementary specialization of the two hemispheres. Considering the complexity of the question, progress will come from the acquisition and analysis of databases developed to answer those questions, such as the BIL&GIN, which includes a sample of 450 healthy volunteers balanced for handedness and gender. Each participant has been characterized for cognitive abilities, anatomy, resting state connectivity and activated networks during motor, language and visuospatial tasks.

Introduction

Human Dualism: Two Hands, Two Brains

Hemispheric specialization (HS) relates to the symmetry and asymmetry of the human body and behavior, which have imprinted human thinking. Since the birth of the first cosmological religions, the most prominent behavioral asymmetry of humans, namely handedness, has embodied dualism (in the sense of opposition) and Manichaeism. In these primitive religions, when facing the morning sun, humans had darkness and cold on their left side, warmth and light on their right side, which also faced the entire course of the sun in the sky. The association of right with south and left with north is seen in various languages, such as Celtic, old French, Irish, Sanskrit, and Hebrew (Bertrand 2001). In a still lively religion such as Catholicism, one may observe that the left is the side of evil and Inferno and the right is the side of God and Heaven. Although not explicitly stated, and although left-handers are no longer constrained or persecuted in Europe or USA, these ideas are still alive. One example can be found in Charles Laughton's 1955 movie, "The Night of the Hunter," in which the devilish reverend Harry Powell asks the children he is chasing, "Would you like me to tell you the little story of right-hand/left-hand. The story of good and evil?" At this stage, the movie star Robert Mitchum has the word "LOVE" tattooed on his right hand fingers and "HATE" on his left ones. Such an embodiment of dualism is present not only at the cultural level but also at the individual level. A recent psychological investigation demonstrated that right-handers place "good" things (namely animals in the referenced experiment) on their right, whereas left-handers do the opposite (Casasanto and Henetz 2012).

At level of the brain, handedness, one of the most lateralized behavior in humans, is related to the fact that one hemisphere—the left in right-handers—is dominant for hand control, a feature characteristic of HS. Although Max Dax and his son first conceptualized HS (Manning and Thomas-Antérion 2011), early on Broca associated the occurrence of aphasia after a left hemispheric lesion with the high prevalence of right-handedness in humans. The left hemisphere—hosting both right-handedness and language control—was declared "dominant" or "major," as opposed to the right hemisphere, which was considered as "minor." Later neuro-psychological studies confirmed that, in most humans, a lesion of the left

hemisphere leads to aphasia and apraxia whereas a lesion on the right leads to spatial neglect, attesting right hemisphere dominance for attention and visuospatial processes.

Major input to the role of each hemisphere came from split-brain investigations that have revealed the existence of hemisphere-dedicated functions, which have been demonstrated when the two hemispheres are disconnected. This approach has demonstrated the crucial role of inter-hemispheric connectivity in the setting up of HS [review in Gazzaniga (2000)]. A Manichaeism view of the hemispheres' role and function emerged in the 1980's, with a "cold" left brain hosting language and logic versus an "emotional" and creative right brain, a view that is still present in current thinking, as evidenced, for example, by recent advertising staging pictures of hemispheres with strongly contrasting characteristics.

Asymmetries Measured with Brain Imaging

The advent of functional neuroimaging has permitted the investigation of HS in healthy subjects; the first step has been to compare functional imaging results with those of Wada testing. Because the Wada procedure consists of testing language functions after anesthesia in one hemisphere, the first imaging approach designed for classifying individuals in terms of their language-dominant hemisphere has been to compute left *minus* right differences of activations during various language tasks, and then to categorize individuals according to an asymmetry index (positive corresponding to left-hemisphere dominance, negative to atypical individuals). Whatever the language tasks used or the technology (fCTD, fMRI) or the methodology (hemispheric, regional) applied to the computation of this asymmetry index, very consistent results have been obtained when comparing such an index with Wada testing in the same patients (Dym et al. 2011). Such validation paves the way for the use of functional imaging to investigate, through the study of inter-individual variability, the factors at stake in the setting up of HS.

It is remarkable that the search for the underpinnings of hemispheric specificity, in terms of anatomical as well as functional investigations, has mainly relied on a very simple model: the calculation of a left *minus* right value. The implicit model underlying such a computation is that of an elementary network composed of pairs of areas, most generally located in mirrored locations, and thus principally grounded on callosal connections. As we will see, tackling differences in intra-hemispheric organization has occurred more recently and was first addressed with anatomical imaging using a connectomics approach after virtually removing the corpus callosum connections (Iturria-Medina et al. 2011).

In this chapter, we will first present the current knowledge and hypotheses regarding the anatomical and functional support of HS. Second, we will discuss the consequences of recent literature describing the developmental time course of anatomical and functional inter-hemispheric organization. Third, we will present results and hypotheses regarding the relationships between HS, cognitive abilities

and developmental/psychiatric illness. Lastly, we will comment on a tool we have designed to study HS in healthy humans, the BIL&GIN database, with the aim of investigating the lateralization of motor, verbal, and visuospatial functions.

Anatomo-Functional Support of HS

Gray Matter Macroscopic Asymmetries and HS

The search for relationships between anatomical asymmetries in the brain and HS for language was revolutionized in 1968 when Geschwind and Levitsky (1968) reported on a leftward asymmetry of a temporal cortex area involved in speech sound processing, namely, the planum temporale (PT). This seminal finding, which was obtained through measurements of the PT surface area in post-mortem brains, was considered as a proof of an anatomical substrate for left hemisphere dominance for language. Cytoarchitectonic studies have further refined our knowledge by showing that the asymmetric PT cortex corresponds to the Tpt area, which hosts the unimodal associative auditory cortex (Galaburda et al. 1978). PT area measurements in healthy subjects using modern neuroimaging techniques started in the 1980's (Steinmetz et al. 1989), confirming that right-handers have a large leftward PT asymmetry [for a review, see Shapleske et al. (1999)].

PT asymmetry is related to a global brain torsion, named the brain Yakovlevian torque (Barrick et al. 2005), which leads to a protrusion of the right inferior frontal gyrus and of the left occipital areas [review in Toga and Thompson (2003)]. Such a torsion is also observed in 25 % of great apes but its occurrence rises to more than 80 % in modern humans. This asymmetrical torsion is associated with a backward shift of the left hemisphere temporal sulci, leaving a larger space at the surface of the left Sylvian fissure that hosts the PT (Lyttelton et al. 2009).

Because of the reduced occurrence of left hemisphere dominance for language in left-handers (Hécaen et al. 1981), a way to test the relationship between PT asymmetry and HS for language has been to search for differences in asymmetry between right- and left-handers. While Steinmetz reported lower PT asymmetry in left-handers (Steinmetz et al. 1991), others did not find such a difference (Habib et al. 1991; Foundas et al. 1995). This discrepancy is likely due to the fact that PT is a highly variable structure, as shown by probabilistic mapping revealing that only one voxel is common to 60 % of individuals after brain normalization in the stereotaxic space (Westbury et al. 1999). This huge variability calls for large sample investigations, and we have recently reported in a sample of 273 healthy subjects that manual preference has no effect on left PT surface area or asymmetry (Tzourio-Mazoyer et al. 2010b).

Another anatomical marker of language lateralization is Heschl's gyrus, hosting the primary auditory cortex. In the left hemisphere, the size of this area is related to the volume of activated cortex during temporal processing of language sound, a

mandatory component of language understanding (Warrier et al. 2009). Such a relationship between Heschl's structural asymmetry, or more precisely its pattern of duplication, and its functional asymmetry during speech listening has been recently reported in a large sample of healthy volunteers (Tzourio-Mazoyer et al. 2015).

In the frontal lobe, results concerning an asymmetry of the inferior frontal gyrus, hosting Broca's area in the left hemisphere, have been inconsistent, but a recent report in a large sample of 200 healthy adults showed a leftward asymmetry of the insula that was related to word recognition lateralization (Chiarello et al. 2013). Moreover, this work revealed that the anatomo-functional relationship between these asymmetries was stronger than the one observed with the PT, demonstrating that the search for anatomical markers of HS is still lively.

However, one should keep in mind that, even if anatomical and functional asymmetries during language tasks can be found to be correlated, such a relationship must be quite weak, considering that some studies found evidence for it (Tzourio et al. 1998; Josse et al. 2006, 2009) whereas others did not (Eckert et al. 2006). As will be further developed, this discrepancy is likely due to a stronger correspondence existing in primary areas having an early anatomical and functional maturation than in high-order cortices that show a delayed anatomical and functional development (Hill et al. 2010b), leaving environmental factors to exert a stronger influence.

White Matter Connections Supporting HS

In terms of White Matter (WM) anatomy, HS is grounded both in intra-hemispheric connections supported by associative bundles and in inter-hemispheric connections between cortical areas located in mirrored positions (homotopic) connected by the corpus callosum [review in van der Knaap and van der Ham (2011)].

Corpus Callosum

The two hemispheres are connected by the CC, which is made up of 200 million fibers issuing from pyramidal cells of cortical layers II and III with homotopic projections on contralateral neurons of the same layer. Major advances in defining the functional role of the CC have come from investigations of split-brain patients with partial or total hemispheric disconnection after callosotomy. Cases of partial callosotomy have shown that CC is topographically organized, with transfer of visual, auditory and somatosensory information in its posterior parts and of attentional resources and higher cognitive information in more anterior regions. Investigations conducted by Sperry and Gazzaniga established the allocation of functions between the two hemispheres and the fundamental role of CC in the transfer of information between them [review in Gazzaniga (2000)]. They also described the alien-hand syndrome and conflicting hand-motor behavior in the acute phase after

CC surgery, demonstrating that the CC also has an inhibitory role that is crucial for human behavior. The CC has thus been at center stage in the investigation of HS anatomical support.

Considering that, in the course of evolution, there has been a decrease in CC size with increasing brain size and complexity, it is assumed that a smaller CC was associated with increased hemispheric lateralization of functions (Hopkins and Cantalupo 2008). In humans, it has also been shown that large brains have relatively smaller CC surface area (Jäncke and Steinmetz 1998); these authors considered that this finding supported the theory proposed by Ringo that increasing size, and thereby inter-hemispheric transfer, was a mechanical factor favoring the grouping of areas supporting a given function within one hemisphere (Ringo et al. 1994). However, there is also evidence of increased hemispheric lateralization associated with increased CC size, at least in some of its subparts. For example, in 74 healthy volunteers in whom language lateralization was measured during a semantic decision task on written words, a stronger lateralization was associated with increased mid-sagittal CC size (Josse et al. 2008). These apparent discrepancies in the literature are likely due to several difficulties in CC functional exploration. First, CC contains both small diameter fibers conveying inhibitory connections across high-order areas and large fast-conducting fibers connecting primary and unimodal associative areas; it is thus difficult to infer its role only from anatomical variables. Second, the topographical organization of CC is complex and fine-grained, and until now, most investigations have mainly relied on the total surface area or on a coarse parcellation scheme. A detailed mapping of the topographical organization of CC based on DTI data is ongoing in healthy volunteers, and its findings will be very useful for future research (Putnam et al. 2010; Chao et al. 2009).

Intra-hemispheric Structural Connectivity

The two hemispheres appear to have a very comparable anatomical organization in terms of WM fiber bundles. The coarse picture that one gets from long-distance fasciculus organization in the brain is that of a globally symmetrical pattern, in accordance with the fact that the right and left hemispheres have comparable organization in terms of cortical hierarchy and cognitive network organization (Mesulam 2000; Fuster 2009). Only a few investigations have reported WM asymmetries, and all focused on the arcuate fasciculus, which is known to support language on the left, and on the cortico-spinal tract that connects the motoneurons to the medulla. Using DTI, the initial observation of bilateral arcuate fasciculus, with subjects without a right arcuate fasciculus (Catani et al. 2007), has not been replicated, although a leftward asymmetry of the arcuate fasciculus and corticospinal tracts seems present in healthy adults (Thiebaut de Schotten et al. 2011). A leftward asymmetry in terms of fractional anisotropy has also been observed in the WM connecting frontal and occipital areas (Suchan et al. 2013).

The picture is clearer in newborns, where leftward asymmetry of the arcuate fasciculus has been observed at birth (Dubois et al. 2009; Leroy et al. 2011). Thus,

even if hemispheric dominance corresponds to differences in cognitive processes, the structure of the two hemispheres follows the same anatomo-functional organizational rules. Differences are thus likely to be subtle.

Even though investigating differences in WM intra-hemispheric organization may seem complex, Iturria-Medina et al. (2011) have developed a promising approach, applying graph analyses to WM images obtained with DTI. The originality of this approach is that WM hemisphere graphs are computed after a virtual cut of the inter-hemispheric callosal connections, making it possible to unravel potential differences that were probably masked by the strength of existing callosal connections. Although the results were obtained in a limited sample of individuals, they evidenced hemispheric differences: the left hemisphere was hosting more nodes, whereas the right had more connections. Comparison of this observation to functional or behavioral observations will allow us to progress in understanding these hemispheric differences in WM connectivity.

Functional Asymmetries and Hemispheric Dominance for Language Assessed with Meta-analysis

Language was one of the first cognitive functions scrutinized with functional imaging (Petersen et al. 1988). Since its advent, functional imaging has developed tools allowing for the averaging of different brains in a common reference system (Fox et al. 1985). This approach allowed for conducting a posteriori meta-analyses that permitted a precise description of the localization of brain areas activated during various tasks. Using the localization of activated regions as the starting point, it is possible to speculate about the role of these regions by analyzing their involvement in different tasks.

Using a meta-analysis approach, we evaluated the relative roles of the left and right hemispheres during linguistic tasks by analyzing 128 functional imaging studies dealing with language tasks in healthy, right-handed participants (Vigneau et al. 2006). We found 59 articles reporting right-hemisphere participation, with 105 language contrasts providing 218 peaks that were analyzed in a second step (Vigneau et al. 2011). Compared to the 728 peaks observed in the left hemisphere, the low proportion of right-hemisphere participation in the same studies was early evidence of the left-hemisphere language dominance. To better characterize hemispheric participation, we described inter-hemispheric interactions in each of the language contrasts involving both hemispheres. We classified peaks as unilateral or bilateral. During a given task of a given study, a unilateral peak should not exhibit any homotopic activation, homotopic activation being defined as the presence of an activation focus located in a mirror position in the other hemisphere. In contrast, a bilateral peak was defined when it was accompanied by homotopic activation in the opposite hemisphere during the same contrast.

We computed the proportion of unilateral and bilateral peaks in each hemisphere and observed that, while the majority of left hemisphere peaks were unilateral (79 %), a reverse pattern was observed on the right (67 % bilateral). These results demonstrated that the left hemisphere works in an intra-hemispheric manner in adults, in contrast to the right hemisphere, which is under the dominance of the left hemisphere (Vigneau et al. 2011). As developed below, this observation accords with recent investigations of intrinsic connectivity (Perani et al. 2011) and functional connectivity during sentence listening (Friederici 2011), which demonstrated with a seed approach the existence of strong intra-hemispheric temporal connectivity across frontal and temporal high-order language areas.

Developmental Course of the Setting Up of Anatomical and Functional Asymmetries

Anatomical asymmetries, in terms of depth of the Sylvian fissure, have been observed with MRI as early as the 26th week of gestation (Habas et al. 2012), and such an asymmetry is at birth identical to that of adults (Hill et al. 2010a). It is important to underline that later studies have shown that these asymmetries do not evolve much during childhood (Li et al. 2013). On the functional side, in utero, neuroimaging investigations have revealed that intrinsic connectivity remains local until birth, when inter-hemispheric connectivity appears (Smyser et al. 2011). Applying a seed approach, Perani et al. (2011) specifically investigated the intrinsic connectivity of the left inferior frontal gyrus and the left superior temporal gyrus, two areas where language develops. They showed that that, at birth, these regions were only connected to homotopic areas, with no intra-hemispheric intrinsic connectivity. This birth pattern was opposed to that of adults included in the same study, who exhibited a preeminent left intra-hemispheric synchronization of BOLD variation at rest in this fronto-temporal network (Perani et al. 2011). However, one should note that, in primary auditory cortices that exhibit a leftward anatomical asymmetry at birth (Li et al. 2013), a leftward functional asymmetry is present when infants listen to language, whereas a rightward one is revealed when they listen to music (Dehaene-Lambertz et al. 2010). This latter study demonstrates a consistency between anatomical and functional asymmetries of the Sylvian fissure cortex at birth and that the inter-hemispheric connectivity is a key element of the development of the lateralization of auditory cortices. However, the change in the organization of higher-order language areas from an initial inter- to the intra-hemispheric organization of adults is still not in place at 7 years of age (Friederici et al. 2011). In this study, 5–7-year-old children were presented with four conditions: two including correct sentences, one including semantically incorrect sentences, and one including syntactically incorrect sentences. The children's task was to judge the acceptability of the sentences. Applying a seed in areas that had been identified in functional MRI studies as supporting sentence processing

[namely, the left dorsal inferior frontal gyrus (IFG) and the left posterior superior temporal gyrus (STG) and sulcus (STS)], the authors showed that, when seeded in the left posterior STS, strong correlations with the left IFG were found in adults. For children, in contrast to adults, the analysis revealed strong correlations with the contralateral temporal region. The same observation was present when the seed was in the IFG. Within the same period in which homotopic connections prevail, a 5-year longitudinal study showed a linear increase with age of the left hemisphere involvement in the IFG during verb generation (Szaflarski et al. 2006), an additional demonstration that language left-hemisphere specialization develops first through callosal interactions.

As a whole, these recent functional imaging studies show that anatomical and functional asymmetries of auditory primary areas are in place at birth, whereas in high-order language areas (IFG, STS, STG) leftward asymmetries develop slowly along with verbal acquisition, before reaching the adult pattern of a dominant intra-hemispheric processing of language. To our knowledge, the exact time course and the physiological underpinnings of this developmental switch from inter- to intra-hemispheric functioning during language processing remain to be established. It is not known whether this type of developmental scenario is also at stake for other left-lateralized function, such as praxis (Vingerhoets et al. 2013), or for right-lateralized functions, such as spatial attention.

HS, Cognitive Abilities and Developmental/Psychiatric Diseases

Cognitive Skills and Asymmetries

How does this developmental change in brain organization relate to cognitive development and abilities? Everts et al. (2009) mapped 9–21-year-old healthy participants during rhyming and synonym language tasks and measured both their hemispheric asymmetry and their verbal abilities. They observed that the increase in leftward asymmetry was linearly correlated with age but also, independently of age, with verbal performances. Importantly, in the same individuals they measured hemispheric asymmetries during a visuospatial task and observed the reverse pattern for this right hemisphere-dominant function: a right asymmetry increase with age, and the larger the rightward asymmetry, the better the visuospatial performances of the participants (Everts et al. 2009).

As will be further developed, the case is not so clear in healthy adults, but there is a study pointing toward an association between leftward asymmetry and verbal performances in individuals who had suffered from pre- or perinatal stroke. Twenty-five of such subjects were mapped (7–23 years old) during a word generation task and a measure of asymmetry in their IFG activity during this task was computed. As opposed to a control group, they did not show a leftward asymmetry

because of the recruitment of the right IFG during the language task, which was considered as a compensatory or plastic participation. Importantly, the analysis of the relationship between verbal abilities of these patients and their laterality index evidenced that, the more leftward the asymmetry, the better the performances, showing that a good recovery was associated with the possibility of regaining a left-hemisphere dominance for language (Raja Beharelle et al. 2010).

As reviewed by Cathy Price (Price and Crinion 2005), the role of inter-hemispheric connections is essential and complex during the recovery of production aphasia after a stroke. The quality of recovery depends on slowly evolving activation changes in the left hemisphere. By contrast, right hemisphere activation observed after a left hemisphere lesion has been interpreted as the consequence of a transcallosal dis-inhibition that is not directly involved in recovery. Such activations occur early after stroke in areas homotopic to the lesion site, and their intensity does not correlate with the level of recovery, as opposed to that of peri-lesional activations (Rosen et al. 2000; Perani et al. 2003). Note that, unlike speech production, recovery of speech comprehension appears to depend on both left and right temporal lobe activation (Price and Crinion 2005).

Many investigations of the relationships between cognitive skills and brain asymmetries in healthy adults have been conducted through a comparison between right- and left-handers, whereas very few directly tested a relationship between hemispheric functional lateralization and cognitive performances. Based on the divided visual field paradigm, a series of behavioral studies in healthy participants have addressed the issue of the benefit of hemispheric lateralization (Boles et al. 2008; Chiarello et al. 2009; Hirnstein et al. 2010). In this paradigm, difference in performances following a presentation of the stimuli in either the left hemi-field (right hemisphere) or the right hemi-field (left hemisphere) is interpreted as an index reflecting the hemispheric dominance for the stimuli processing. These studies have reported divergent outcomes, some emphasizing a positive correlation between the index of lateralization for various linguistic tasks and reading skills (Chiarello et al. 2009) whereas other reported that high degrees of lateralization were detrimental to cognitive performance in word-matching and face-decision tasks (Hirnstein et al. 2010). A study that used functional transcranial Dopler sonography (fTCD) to directly assess the hemispheric dominance did not report any relationship between hemispheric asymmetry and the number of foreign languages spoken fluently, academic achievement and the practice of artistic activities or, in a sub-group of 21 participants, general IQ (Knecht et al. 2001). A recent study including 6–24-year-old right-handed participants revealed differences according to the language task used for measuring asymmetries. While there was a correlation between verbal IQ and the hemispheric functional lateralization index obtained by fMRI during language comprehension, the correlation was absent between verbal IQ and hemispheric asymmetries during language production. In addition, better performances were associated with larger right hemisphere participation (Lidzba et al. 2011).

In summary, there is an association between verbal abilities and a leftward hemispheric asymmetry during a language task in the developmental course.

Leftward asymmetry during language production is also associated with a good recovery of production aphasia. However, there is no such evidence of an association between language skills and leftward hemispheric lateralization in healthy adults, although the limited number of investigations leaves the question open. Moreover, one should tackle the issue of whether such an association is specific to language skills rather than to more general cognitive functioning abilities.

Language HS, Developmental and Psychiatric Diseases

Discovery of the PT leftward asymmetry triggered the search for an association between a decrease in this asymmetry and the occurrence of developmental language disorders such as dysphasia and dyslexia. Geschwind and Galaburda (1985a, b) have elaborated a model of the setting up of left hemisphere dominance based on the idea that asymmetries are due to a reduction of right-hemispheric structures through development. Their model linked developmental language pathologies to decreases in anatomical asymmetries. There have been numerous works showing an association between language developmental pathologies and language lateralization markers, in particular decreases in anatomical asymmetries [reviewed in Leonard and Eckert (2008)]. Such differences in language asymmetry in developmental pathologies are modest but have been associated with other severe pathologies encompassing language deficits such as schizophrenia and autism.

Failure to develop normal language comprehension is an early sign of autism and, in this developmental pathology, a deficit in the setting up of a language leftward functional asymmetry has also been reported by Eyler et al. (2012), who used fMRI to investigate hemispheric asymmetries in 12–48-month-old toddlers with autistic spectrum disorder who were later diagnosed with autism. Measuring their brain activity during story listening while toddlers were asleep, they observed not only a decreased leftward lateralization in the temporal cortex as compared to control children but also a trend to a rightward temporal increase in activation between 1 and 4 years of age, as opposed to the typical increase in leftward asymmetry in normally developing children. The authors interpreted their findings as attesting that a failure in the setting up of leftward asymmetry during language processing is a fundamental abnormality of autism (Eyler et al. 2012).

Decreases in the anatomical and functional asymmetry of language areas have also been reported in schizophrenia. Starting from the saliency of language defects in schizophrenic patients, Crow (1997) proposed that schizophrenia could be considered an anomaly of the function of language and that the pathophysiology of schizophrenia should be found in the mechanisms underlying the development of HS. Crow's hypothesis was based on the observation that pre-schizophrenic children were more likely to be rated as ambidextrous at the age of 7 years and were less strongly right-handed than their peers at the age of 11, suggesting a delay in the establishment of their HS (Crow et al. 1996). In addition, left hemisphere anatomical abnormalities centered on the temporal lobe were reported in schizophrenic

patients with a decreased asymmetry of the PT (DeLisi 1997; Sommer et al. 2001). In an fMRI investigation of right-handed schizophrenic patients during a language comprehension task, Dollfus et al. (2005) observed decreased left hemispheric activity in language regions in patients as compared to matched healthy controls. Such a finding was also reported in the first episode of schizophrenic patients during a language generation task, making the decrease in asymmetry independent of the type of language task and of the potential effects of the illness and its treatment (Bleich-Cohen et al. 2009). In addition, it was shown that the decreased leftward asymmetry during verbal production in schizophrenic patients was not related to auditory hallucinations (Diederen et al. 2010).

As a whole, a defect in the setting up of language leftward asymmetry is observed in severe mental pathologies that include language dysfunction among other symptoms. The deficit in leftward lateralization targets a dysfunction of HS as an early developmental mechanism fundamental to further harmonious development of functional brain architecture. Further research is needed to evaluate whether this developmental failure results in a pure language lateralization deficit or corresponds to a general dysfunction in the lateralization of cognitive functions.

Inter-individual Variability in HS: Factors at Play

Although encountered in pathological conditions, a decrease in language lateralization can also be found in healthy individuals, as revealed by neuroimaging studies describing between-individual variability of hemispheric or regional functional lateralization of language. As developed below, variability in language lateralization of healthy individuals is multifactorial and depends on both behavioral characteristics, such as handedness, and anatomical features, such as brain volume or size of the left PT. Variability in functional lateralization also depends on the type of language process targeted by the language task performed during imaging, language production being more strongly leftward lateralized than language comprehension. Finally, it must be underscored that language lateralization varies according to the hierarchical level of the regions studied: primary areas receiving bilateral sensory inputs have a lateralization that is weaker than that of high-order language areas, and factors explaining this regional variability may be different. For example, the pattern of gyrification of Heschl's gyrus explains the variability in asymmetry of this region during speech listening but not that of other areas activated during this task, such as the STS (Tzourio-Mazoyer et al. 2015).

Handedness was identified early on as a source of between-subject variability in language lateralization. The fact that more than 90 % of right-handers have a left dominance for language has nourished both evolutionary and genetic models of the origin of language [reviewed in Corballis et al. (2012)]. However, it must be stressed that around 80 % of left-handers exhibit the same typical left lateralization during language production and that the increased variability of language lateralization within left-handers is characterized by the existence of rare rightward

asymmetrical individuals, who in addition exhibit strong left-hand preference (Pujol et al. 1999; Knecht et al. 2000). Note, however, that apart from these rare individuals having reverse language lateralization, occurring with similar proportions in children and adults, handedness has no influence on the maturational increase of leftward asymmetries for language (Szaflarski et al. 2011).

The fact that dissociations have been observed between the lateralization of language areas involved during language production and those involved in language perception suggests that there are different factors related to specific aspects of speech processing. In favor of this hypothesis is the evidence that anatomical factors explain a part of the variability of anatomical or functional lateralization of speech processing areas. Among them, brain volume determines inter-hemispheric distance and transfer time. According to Ringo et al. (1994), brain volume constrains high-speed processes to intra-hemispheric clustering in bulky brains. This theory fits within the framework of perceptual theories of the origin of language lateralization postulating that it arises from speed constraints on speech perception. As a matter of fact, we found positive correlations between brain volume and both leftward functional asymmetry during speech perception (Josse et al. 2006; Tzourio-Mazoyer et al. 2010a) and leftward gray matter hemispheric asymmetry (Tzourio-Mazoyer et al. 2010b). These results support Ringo's theory of a 'mechanical' impact of brain volume on speech lateralization. Other arguments come from the fact that anatomical characteristics of the auditory cortices explain a part of the functional variability in language lateralization, as, for example, the positive correlation between the left PT surface area and lateralization of activations during story listening (Tzourio et al. 1998; Josse et al. 2003).

The picture is likely to be even more complex, given that factors can interact. For example, in right-handers, we showed that weaker manual lateralization decreases leftward lateralization for language only in individuals with familial sinistrality (Tzourio-Mazoyer et al. 2010a). Moreover, factors that influence variability in HS, such as gender and brain volume, may also be partially confounded (Leonard et al. 2008). Finally, it must be emphasized that, although much is known about HS for language, the factors that might influence right hemisphere specialization remain to be discovered.

BIL&GIN: A Multimodal Database for Investigating HS

To address some of the issues raised in this chapter and to make progress in our understanding of the role of HS in shaping the large-scale organization of the human brain, we acquired a multimodal (neuroimaging, cognitive/behavioral abilities, genetic) database designed for the investigation of HS. This database, named BIL&GIN (Brain Imaging of Lateralization by the Groupe d'Imagerie Neurofonctionnelle), included a sample of 453 healthy adults (aged 18–54 years), balanced for sex and handedness (Mazoyer et al. 2015). For each participant, we recorded manual skills, hand and eye preference, and familial sinistrality. Verbal, spatial,

and numerical abilities were assessed with a large battery of tests. Finally, multimodal MRI data were acquired in each participant, namely T1 and DTI for conducting morphometric analysis of gray matter and WM, and resting-state fMRI data for assessing intrinsic connectivity. Finally, in a subsample of 300 individuals, task-related fMRI was performed using a battery of 15 language, motor and visuospatial tasks designed to explore various aspects of HS. The first analyses of the BIL&GIN illustrate the power of combining a large sample with a multimodal approach. For example, we recently reported that the verbal and spatial abilities increase with right asymmetry in motor skills and that cognitive performance is reduced in participants having a familial sinistrality combined with non-maximal preference strength of the dominant hand (Mellet et al. 2014). Original findings regarding the Heschl's gyrus interhemispheric duplication pattern (Marie et al. 2015) and its relationship with the functional asymmetry of this area during speech listening (Tzourio-Mazoyer et al. 2015) were also previously mentioned in this chapter.

Conclusion

HS, which is grounded mainly by inter-hemispheric connectivity, is an essential feature of human anatomo-functional brain architecture. This very simple right-left connection is essential to the development of language and, likely, to optimal cognitive functioning. We believe that its investigation within the framework of the research on the connectomics of the brain will provide important knowledge regarding the large-scale architecture supporting human cognition.

References

Barrick TR, Mackay CE, Prima S, Maes F, Vandermeulen D, Crow TJ, Roberts N (2005) Automatic analysis of cerebral asymmetry: an exploratory study of the relationship between brain torque and planum temporale asymmetry. Neuroimage 24:678–691

Bertrand P-M (2001) Histoire des gauchers: des gens à l'envers. Imago, Paris

Bleich-Cohen M, Hendler T, Kotler M, Strous RD (2009) Reduced language lateralization in first-episode schizophrenia: an fMRI index of functional asymmetry. Psychiatry Res 171:82–93

Boles DB, Barth JM, Merrill EC (2008) Asymmetry and performance: toward a neurodevelopmental theory. Brain Cogn 66:124–139

Casasanto D, Henetz T (2012) Handedness shapes children's abstract concepts. Cogn Sci 36:359–372

Catani M, Allin MP, Husain M, Pugliese L, Mesulam MM, Murray RM, Jones DK (2007) Symmetries in human brain language pathways correlate with verbal recall. Proc Natl Acad Sci USA 104:17163–17168

Chao YP, Cho KH, Yeh CH, Chou KH, Chen JH, Lin CP (2009) Probabilistic topography of human corpus callosum using cytoarchitectural parcellation and high angular resolution diffusion imaging tractography. Hum Brain Mapp 30:3172–3187

Chiarello C, Welcome SE, Halderman LK, Towler S, Julagay J, Otto R, Leonard CM (2009) A large-scale investigation of lateralization in cortical anatomy and word reading: are there sex differences? Neuropsychology 23:210–222

Chiarello C, Vazquez D, Felton A, Leonard CM (2013) Structural asymmetry of anterior insula: behavioral correlates and individual differences. Brain Lang 126:109–122

Corballis MC, Badzakova-Trajkov G, Häberling IS (2012) Right hand, left brain: genetic and evolutionary bases of cerebral asymmetries for language and manual action. Wiley Interdiscip Rev Cogn Sci 3:1–17

Crow TJ (1997) Is schizophrenia the price that Homo sapiens pays for language? Schizophr Res 28:127–141

Crow TJ, Done DJ, Sacker A (1996) Cerebral lateralization is delayed in children who later develop schizophrenia. Schizophr Res 22:181–185

Dehaene-Lambertz G, Montavont A, Jobert A, Allirol L, Dubois J, Hertz-Pannier L, Dehaene S (2010) Language or music, mother or Mozart? Structural and environmental influences on infants' language networks. Brain Lang 114:53–65

DeLisi LE (1997) Anomalous cerebral asymmetry and language processing in schizophrenia. Schizophr Bull 23:536

Diederen KM, De Weijer AD, Daalman K, Blom JD, Neggers SF, Kahn RS, Sommer IE (2010) Decreased language lateralization is characteristic of psychosis, not auditory hallucinations. Brain 133:3734–3744

Dollfus S, Razafimandimby A, Delamillieure P, Brazo P, Joliot M, Mazoyer B, Tzourio-Mazoyer N (2005) Atypical hemispheric specialization for language in right-handed schizophrenia patients. Biol Psychiatry 57:1020–1028

Dubois J, Hertz-Pannier L, Cachia A, Mangin JF, Le Bihan D, Dehaene-Lambertz G (2009) Structural asymmetries in the infant language and sensori-motor networks. Cereb Cortex 19:414–423

Dym RJ, Burns J, Freeman K, Lipton ML (2011) Is functional MR imaging assessment of hemispheric language dominance as good as the Wada test?: a meta-analysis. Radiology 261:446–455

Eckert MA, Leonard CM, Possing ET, Binder JR (2006) Uncoupled leftward asymmetries for planum morphology and functional language processing. Brain Lang 98:102–111

Everts R, Lidzba K, Wilke M, Kiefer C, Mordasini M, Schroth G, Perrig W, Steinlin M (2009) Strengthening of laterality of verbal and visuospatial functions during childhood and adolescence. Hum Brain Mapp 30:473–483

Eyler LT, Pierce K, Courchesne E (2012) A failure of left temporal cortex to specialize for language is an early emerging and fundamental property of autism. Brain 135:949–960

Foundas AL, Leonard CM, Heilman KM (1995) Morphological asymmetries and handedness. The pars triangularis and planum temporale. Arch Neurol 52:501–508

Fox PT, Perlmutter JSA, Raichle ME (1985) A stereotactic method of anatomical localization for positron emission tomography. J Comput Assist Tomogr 9:141–153

Friederici AD (2011) The brain basis of language processing: from structure to function. Physiol Rev 91:1357–1392

Friederici AD, Brauer J, Lohmann G (2011) Maturation of the language network: from inter- to intrahemispheric connectivities. PLoS One 6:e20726

Fuster JM (2009) Cortex and memory: emergence of a new paradigm. J Cogn Neurosci 21:2047–2072

Galaburda AM, LeMay M, Kemper TL, Geschwind N (1978) Right-left asymmetries in the brain. Science 199:852–856

Gazzaniga MS (2000) Cerebral specialization and interhemispheric communication—does the corpus callosum enable the human condition? Brain 123:1293–1326

Geschwind N, Galaburda AM (1985a) Cerebral lateralization. Biological mechanisms, associations, and pathology:1. A hypothesis and a programm for research. Arch Neurol 42:428–459

Geschwind N, Galaburda AM (1985b) Cerebral lateralization. Biological mechanisms, associations, and pathology: 2. A hypothesis and a programm for research. Arch Neurol 42:521–552

Geschwind N, Levitsky W (1968) Human brain left-right asymmetries in temporal speech region. Science 161:186–187

Habas PA, Scott JA, Roosta A, Rajagopalan V, Kim K, Rousseau F, Barkovich AJ, Glenn OA, Studholme C (2012) Early folding patterns and asymmetries of the normal human brain detected from in utero MRI. Cereb Cortex 22:13–25

Habib M, Gayraud D, Oliva A, Regis J, Salamon G, Khalil R (1991) Effects of handedness and sex on the morphology of the corpus callosum: a study with brain magnetic resonance imaging. Brain Cogn 16:41–61

Hécaen H, De Agostini M, Monzon-Montes A (1981) Cerebral organization in left-handers. Brain Lang 12:261–284

Hill J, Dierker D, Neil J, Inder T, Knutsen A, Harwell J, Coalson T, Van Essen D (2010a) A surface-based analysis of hemispheric asymmetries and folding of cerebral cortex in term-born human infants. J Neurosci 30:2268–2276

Hill J, Inder T, Neil J, Dierker D, Harwell J, Van Essen D (2010b) Similar patterns of cortical expansion during human development and evolution. Proc Natl Acad Sci USA 107:13135–13140

Hirnstein M, Leask S, Rose J, Hausmann M (2010) Disentangling the relationship between hemispheric asymmetry and cognitive performance. Brain Cogn 73:119–127

Hopkins WD, Cantalupo C (2008) Theoretical speculations on the evolutionary origins of hemispheric specialization. Curr Dir Psychol Sci 17:233–237

Iturria-Medina Y, Pérez Fernández A, Morris DM, Canales-Rodríguez EJ, Haroon HA, García Pentón L, Augath M, Galán García L, Logothetis N, Parker GJ, Melie-García L (2011) Brain hemispheric structural efficiency and interconnectivity rightward asymmetry in human and nonhuman primates. Cereb Cortex 21:56–67

Jäncke L, Steinmetz H (1998) Brain size: a possible source of interindividual variability in corpus callosum morphology. In: Zaidel E, Iacoboni M, Pascual-Leone A (eds) Brain size: a possible source of interindividual variability in corpus callosum morphology. Plenum Press, New York, pp 1–15

Josse G, Mazoyer B, Crivello F, Tzourio-Mazoyer N (2003) Left planum temporale: an anatomical marker of left hemispheric specialization for language comprehension. Brain Res Cogn Brain Res 18:1–14

Josse G, Hervé PY, Crivello F, Mazoyer B, Tzourio-Mazoyer N (2006) Hemispheric specialization for language: brain volume matters. Brain Res 1068:184–193

Josse G, Seghier ML, Kherif F, Price CJ (2008) Explaining function with anatomy: language lateralization and corpus callosum size. J Neurosci 28:14132–14139

Josse G, Kherif F, Flandin G, Seghier ML, Price CJ (2009) Predicting language lateralization from gray matter. J Neurosci 29:13516–13523

Knecht S, Dräger B, Deppe M, Bobe L, Lohmann H, Flöel A, Ringelstein EB, Henningsen H (2000) Handedness and hemispheric language dominance in healthy humans. Brain 123:2512–2518

Knecht S, Drager B, Floel A, Lohmann H, Breitenstein C, Deppe M, Henningsen H, Ringelstein EB (2001) Behavioural relevance of atypical language lateralization in healthy subjects. Brain 124:1657–1665

Leonard CM, Eckert MA (2008) Asymmetry and dyslexia. Dev Neuropsychol 33:663–681

Leonard CM, Towler S, Welcome S, Halderman LK, Otto R, Eckert MA, Chiarello C (2008) Size matters: cerebral volume influences sex differences in neuroanatomy. Cereb Cortex 18:2920–2931

Leroy F, Glasel H, Dubois J, Hertz-Pannier L, Thirion B, Mangin JF, Dehaene-Lambertz G (2011) Early maturation of the linguistic dorsal pathway in human infants. J Neurosci 31:1500–1506

Li G, Nie J, Wang L, Shi F, Lyall AE, Lin W, Gilmore JH, Shen D (2013) Mapping longitudinal hemispheric structural asymmetries of the human cerebral cortex from birth to 2 years of age. Cereb Cortex 24:1289–1300

Lidzba K, Schwilling E, Grodd W, Krägeloh-Mann I, Wilke M (2011) Language comprehension vs. language production: age effects on fMRI activation. Brain Lang 119:6–15

Lyttelton OC, Karama S, Ad-Dab'bagh Y, Zatorre RJ, Carbonell F, Worsley K, Evans AC (2009) Positional and surface area asymmetry of the human cerebral cortex. Neuroimage 46:895–903

Manning L, Thomas-Antérion C (2011) Marc Dax and the discovery of the lateralisation of language in the left cerebral hemisphere. Rev Neurol (Paris) 167:868–872

Marie D, Jobard G, Crivello F, Perchey G, Petit L, Mellet E, Joliot M, Zago L, Mazoyer B, Tzourio-Mazoyer N (2015) Descriptive anatomy of Heschl's gyri in 430 healthy volunteers, including 198 left-handers. Brain Struct Funct 220:729–743

Mazoyer B, Mellet E, Perchey G, Zago L, Crivello F, Jobard G, Delcroix N, Vigneau M, Leroux G, Petit L, Joliot M, Tzourio-Mazoyer N (2015) BIL&GIN: a neuroimaging, cognitive, behavioral, and genetic database for the study of human brain lateralization. Neuroimage 124: 1225–1231

Mellet E, Jobard G, Zago L, Crivello F, Petit L, Joliot M, Mazoyer B, Tzourio-Mazoyer N (2014) Relationships between hand laterality and verbal and spatial skills in 436 healthy adults balanced for handedness. Laterality 2014(19):383–404

Mesulam MM (2000) In: Mesulam MM (ed) Principles of behavioral neurology. Oxford University Press, Oxford

Perani D, Cappa SF, Tettamanti M, Rosa M, Scifo P, Miozzo A, Basso A, Fazio F (2003) A fMRI study of word retrieval in aphasia. Brain Lang 85:357–368

Perani D, Saccuman MC, Scifo P, Anwander A, Awander A, Spada D, Baldoli C, Poloniato A, Lohmann G, Friederici AD (2011) Neural language networks at birth. Proc Natl Acad Sci USA 108:16056–16061

Petersen SE, Fox PT, Posner MI, Mintun MA, Raichle ME (1988) Positron emission tomographic studies of the cortical anatomy of single-word processing. Nature 331:585–589

Price CJ, Crinion J (2005) The latest on functional imaging studies of aphasic stroke. Curr Opin Neurol 18:429–434

Pujol J, Deus J, Losilla JM, Capdevela A (1999) Cerebral lateralization of language in normal left-handed people studied by functional MRI. Neurology 52:1038–1043

Putnam MC, Steven MS, Doron KW, Riggall AC, Gazzaniga MS (2010) Cortical projection topography of the human splenium: hemispheric asymmetry and individual differences. J Cogn Neurosci 22:1662–1669

Raja Beharelle A, Dick AS, Josse G, Solodkin A, Huttenlocher PR, Levine SC, Small SL (2010) Left hemisphere regions are critical for language in the face of early left focal brain injury. Brain 133:1707–1716

Ringo JL, Doty RW, Demeter S, Simard PY (1994) Time is of the essence: a conjecture that hemispheric specialization arises from interhemispheric conduction delay. Cereb Cortex 4:331–343

Rosen HJ, Petersen SE, Linenweber MR, Snyder AZ, White DA, Chapman L, Dromerick AW, Fiez JA, Corbetta M (2000) Neural correlates of recovery from aphasia after damage to left inferior frontal cortex. Neurology 55:1883–1894

Shapleske J, Rossell SL, Woodruff PW, David AS (1999) The planum temporale: a systematic, quantitative review of its structural, functional and clinical significance. Brain Res Rev 29:26–49

Smyser CD, Snyder AZ, Neil JJ (2011) Functional connectivity MRI in infants: exploration of the functional organization of the developing brain. Neuroimage 56:1437–1452

Sommer IEC, Ramsey NF, Kahn RS (2001) Language lateralization in schizophrenia, an fMRI study. Schizophr Res 52:57–67

Steinmetz H, Rademacher J, Huang Y, Hefter H, Zilles K, Thron A, Freund H (1989) Cerebral asymmetry: MR planimetry of the human planum temporale. J Comput Assist Tomogr 13:996–1005

Steinmetz H, Volkmann J, Jäncke L, Freund H (1991) Anatomical left-right asymmetry of language-related temporal cortex is different in left- and right-handers. Ann Neurol 29:315–319

Suchan J, Umarova R, Schnell S, Himmelbach M, Weiller C, Karnath HO, Saur D (2013) Fiber pathways connecting cortical areas relevant for spatial orienting and exploration. Hum Brain Mapp 35:1031–1043

Szaflarski JP, Holland SK, Schmithorst VJ, Byars AW (2006) fMRI study of language lateralization in children and adults. Hum Brain Mapp 27:202–212

Szaflarski JP, Rajagopal A, Altaye M, Byars AW, Jacola L, Schmithorst VJ, Schapiro MB, Plante E, Holland SK (2011) Left-handedness and language lateralization in children. Brain Res 1433:85–97

Thiebaut de Schotten M, Ffytche DH, Bizzi A, Dell'Acqua F, Allin M, Walshe M, Murray R, Williams SC, Murphy DG, Catani M (2011) Atlasing location, asymmetry and inter-subject variability of white matter tracts in the human brain with MR diffusion tractography. Neuroimage 54:49–59

Toga AW, Thompson PM (2003) Mapping brain asymmetry. Nat Rev Neurosci 4:37–48

Tzourio N, Nkanga-Ngila B, Mazoyer B (1998) Left planum temporale surface correlates with functional dominance during story listening. Neuroreport 9:829–833

Tzourio-Mazoyer N, Petit L, Razafimandimby A, Crivello F, Zago L, Jobard G, Joliot M, Mellet E, Mazoyer B (2010a) Left hemisphere lateralization for language in right-handers is controlled in part by familial sinistrality, manual preference strength, and head size. J Neurosci 30:13314–13318

Tzourio-Mazoyer N, Simon G, Crivello F, Jobard G, Zago L, Perchey G, Hervé PY, Joliot M, Petit L, Mellet E, Mazoyer B (2010b) Effect of familial sinistrality on planum temporale surface and brain tissue asymmetries. Cereb Cortex 20:1476–1485

Tzourio-Mazoyer N, Marie D, Zago L, Jobard G, Perchey G, Leroux G, Mellet E, Joliot M, Crivello F, Petit L, Mazoyer B (2015) Heschl's gyrification pattern is related to speech-listening hemispheric lateralization: FMRI investigation in 281 healthy volunteers. Brain Struct Funct 220:1585–1599

van der Knaap LJ, van der Ham IJ (2011) How does the corpus callosum mediate interhemispheric transfer? A review. Behav Brain Res 223:211–221

Vigneau M, Beaucousin V, Hervé PY, Duffau H, Crivello F, Houdé O, Mazoyer B, Tzourio-Mazoyer N (2006) Meta-analyzing left hemisphere language areas: phonology, semantics, and sentence processing. Neuroimage 30:1414–1432

Vigneau M, Beaucousin V, Hervé PY, Jobard G, Petit L, Crivello F, Mellet E, Zago L, Mazoyer B, Tzourio-Mazoyer N (2011) What is right-hemisphere contribution to phonological, lexico-semantic, and sentence processing? Insights from a meta-analysis. Neuroimage 54:577–593

Vingerhoets G, Alderweireldt AS, Vandemaele P, Cai Q, Van der Haegen L, Brysbaert M, Achten E (2013) Praxis and language are linked: evidence from co-lateralization in individuals with atypical language dominance. Cortex 49:172–183

Warrier C, Wong P, Penhune V, Zatorre R, Parrish T, Abrams D, Kraus N (2009) Relating structure to function: Heschl's gyrus and acoustic processing. J Neurosci 29:61–69

Westbury CF, Zatorre RJ, Evans AC (1999) Quantifying variability in the planum temporale: a probability map. Cereb Cortex 9:392–405

Genetics of the Connectome and the ENIGMA Project

Paul M. Thompson, Derrek P. Hibar, Jason L. Stein, Gautam Prasad, and Neda Jahanshad

Abstract Here we give an overview of a worldwide effort, called the ENIGMA Consortium (http://enigma.ini.usc.edu), which unites scientists worldwide to determine how variants in our genetic code influence the brain, and how 12 major diseases affect the brain worldwide. At the time of writing, ENIGMA involves over 500 scientists from 185 institutions worldwide, working together on around 30 projects to discover factors that may help or harm the brain. By pooling genome-wide genomic data and brain imaging from over 33,000 people, ENIGMA has been able to identify single-nucleotide differences in the genome that are associated with differences in human brain structure and function. Given the broad interest in brain connectivity and the factors that affect it, we outline some tactics adopted by ENIGMA to discover specific genes that affect the brain; then we describe how ENIGMA is extending these methods to discover genetic influences on brain connectivity.

Background to ENIGMA

ENIGMA (Enhancing Neuroimaging Genetics through Meta-Analysis) is a worldwide network of researchers who work together to investigate various questions about the brain. The consortium pools brain imaging and genetic data from over 200 institutions around the world. The main goals of ENIGMA are to discover factors that help and harm the brain; the sheer size of the dataset is unprecedented, making it possible to see which effects on the brain are robust and consistent by pooling data worldwide. The idea for ENIGMA originated in late 2009 and the consortium has since published some of the largest brain imaging studies in the world—both in terms of the total number of individuals genotyped and scanned (now over 33,000) and in terms of the number of scientists collaborating [several hundred co-authors, in Stein et al. (2012), Thompson et al. (2014), and Hibar et al. (2015)]. Also, by pooling brain imaging and genomic data from tens of thousands of people, we were able to overcome several technical and sociological barriers; here

P.M. Thompson (✉) • D.P. Hibar • J.L. Stein • G. Prasad • N. Jahanshad
Imaging Genetics Center, University of Southern California, Los Angeles, CA, USA
e-mail: pthomp@usc.edu

H. Kennedy et al. (eds.), *Micro-, Meso- and Macro-Connectomics of the Brain*,
Research and Perspectives in Neurosciences, DOI 10.1007/978-3-319-27777-6_10

we outline some of the strategies employed and the main findings and lessons learned. As befits a chapter in a book on brain connectivity, we also summarize the tactics that ENIGMA is beginning to employ to discover genetic influences on brain connectivity.

Genetic Influences on the Brain

By 2009, nearly 100 studies had been published showing that numerous measures of brain structure are *heritable* (Blokland et al. 2012). In other words, individual differences in our genetic code do affect specific features of the brain, such as the overall volume of the brain, the size of the hippocampus, and even measures of functional activity based on EEG or functional MRI. To establish this, researchers began by studying family-based cohorts or twins who were scanned with anatomical or functional MRI; when people with greater genetic similarity were compared, their brains were found to be more similar, on average, than were unrelated people of the same age and sex.

To formalize these ideas, the *classical twin design* has often been used to estimate the heritability of a behavioral trait by studying both identical and fraternal twins (siblings or other family members are often evaluated as well; Boomsma et al. 2002). Based on structural equation models, or even based on simpler approaches involving correlations, twin studies are able to estimate what fraction of the observed variability in a brain measure is due to genetics, that is, due to the genetic differences among individuals. Many measures of brain structure, such as the total amount of gray or white matter in the brain or the overall volume of the ventricles, were found to be heritable; that is to say, genetic factors are involved in determining their eventual values. Note that this type of genetic analysis does not require the direct examination of the DNA sequence, only the study of resemblances among family members with different degrees of familial relatedness (e.g., identical twins, siblings, etc.).

Soon afterwards, 3D "maps" of heritability began to be produced for a variety of brain measures, such as regional gray matter volumes in the cortex (Thompson et al. 2001), cortical thickness (Joshi et al. 2012), surface area (Chen et al. 2012), and fiber microstructure in diffusion-weighted MRI scans (Chiang et al. 2009). The proportion of variance due to genetic factors is not expected to be completely uniform across the brain. In general, genetic variation accounts for around half of the observed variance for many brain measures, in some cases more, making neuroimaging measures an attractive target for in-depth genetic analysis (Glahn et al. 2007).

The high heritability of brain structure is in line with many behavioral genetic studies showing substantial genetic effects on behavior and even risk for neurological and psychiatric illnesses, such as Alzheimer's disease and schizophrenia. Genetic studies have shown that numerous traits relating to personality, cognition, and even risk for neurological or psychiatric disease are influenced by genetics to some degree. The influence of genetic versus environmental factors on cognition

and intellectual performance was one of the most hotly debated scientific topics of the twentieth century (Jensen 1969; Lewontin et al. 1984). Of course, even if we concede that genes play some role in behavior, several caveats to heritability calculations apply: genetic variants do not influence the brain independently of other factors, and their effects may depend on a person's age, sex, level of nutrition, education, or many other contextual factors in the population (Visscher et al. 2008). Although they are not necessarily heritable, epigenetic factors, such as methylation and acetylation, act on the genome to switch off or promote the action of certain parts of our genetic code. Also, an individual's environment may be correlated to some degree with their genotype; for example, people with a natural aptitude for certain kinds of activity may seek out environments that promote those activities. This makes the effects of genes and environment difficult or impossible to disentangle. Gene x Environment interactions are also found, where a gene's effect on the brain or behavior is accentuated or suppressed under certain conditions. In fact, much work in the fields of pharmacogenomics and personalized medicine depends on the notion that people with certain genetic risk factors may be less or more responsive to medication or other kinds of therapy. As such, the quest to identify genetic variants that relate to brain measures is likely to accelerate our genetic understanding of brain disease and mental illness. With this in mind, ENIGMA has several projects that relate brain measures to genomic variation and to disease, a topic that we will return to later.

Finding the Genes Involved

Knowing that a brain measure is heritable—or influenced by genetic factors—is the first step on the long road towards identifying *specific* differences in the genome that influence it. By 2009, genetic "sequencing" had become relatively inexpensive, and it was possible to reliably identify a person's individual DNA sequence at each of over one million genetic locations, based on a person's blood or saliva sample. Although well over 99 % of the genetic code is identical across healthy individuals, people do differ substantially in specific areas of the genetic code: there are deletions, expansions, and even single-nucleotide or single "letter" spelling differences in the base pair sequence. Some of these genetic differences do not affect the protein product, if the gene is expressed at all. Other genetic differences render the protein product dysfunctional or modify its activity, and they may influence brain function and behavior and our risk for disease.

Genotyping companies began to offer genotyping services whereby over a million common genetic variants—or single nucleotide polymorphisms (SNPs)—could be assessed cheaply; in the United States, for example, some personalized genomics companies offered to send a person a million "letters," or nucleotides, of their genetic code for $99 (in U.S. dollars). This ability to genotype common variants in the genome led to a surge in the popularity of genome-wide association studies (GWAS), efforts to identify markers or common variants in the human

genome that are statistically associated with a certain trait, such as obesity, schizophrenia, depression, or Alzheimer's disease. Many of these genomic screens were very successful. For instance, certain "risk genes," such as *APOE, CLU,* and *TREM2*, have alternative sequences wherein one form is more commonly found in patients with Alzheimer's disease (Harold et al. 2009; Jonsson et al. 2013). The quest to find these risk-associated genetic variants is motivated by finding new drug targets or, in the short term, evaluating a person's risk for a specific disease, which can help in clinical trial design.

Again, several caveats apply. Common variants are not the only source of genetic variations that have an impact on the brain; in fact, rare variants—or even *private* variants found only within a single family or individual—have been found that associate with risk for autism or other disorders (Sanders et al. 2012; Purcell et al. 2014). When GWAS was first feasible on a large scale, studies of tens of thousands of individuals began to unearth common genetic differences associated with cholesterol levels in the blood and with bone density, obesity, or stroke, and a range of other common conditions. In each study, the genome was scanned for sequence variations associated with a single trait, such as a person's height, body mass index, or a psychiatric diagnosis such as schizophrenia or bipolar illness, for example. Because of the high risk of false positives—searching millions of letters of the genetic code would likely detect many false associations—geneticists began to enforce a very high statistical threshold to implicate a genetic variant in a disorder, often requiring tens of thousands of subjects to find an association and replicate it.

GWAS of the Brain

Around 2009, GWAS began to be performed on brain measures [see supplementary information in Medland et al. (2014)], such as temporal lobe volume (Stein et al. 2010). Although some of the top "hits" in these studies seemed convincing from a mechanistic point of view, many geneticists argued that the power to detect common genetic variants that affect the brain was very limited, even in samples of approximately 1000 subjects. As brain imaging data are expensive and time-consuming to collect, only the largest national initiatives could even achieve sample sizes of 1000 subjects; the Alzheimer's Disease Neuroimaging Initiative (ADNI; Jack et al. 2008), for example, was one of the largest studies ever attempted with neuroimaging. ADNI still took many years to recruit and scan a cohort of 800 people at 58 sites across North America. Power calculations suggest that cohorts of 10,000 or more subjects should be needed to zero in on genomic regions with reliable associations to brain measures, unless of course their effect sizes are extremely large. And so began a debate as to whether imaging would offer a more efficient way to detect influential genetic variants.

Counterarguments and Power

Two arguments were commonly advanced to suggest that large samples might not be required for successful genetic studies of brain images, but the evidence for each argument began to wane. The first was that some image-derived measures might be more highly reproducible than psychiatric diagnostic tests or cognitive scores; some measures from images (such as the density of connections between brain regions) might be closer to the biology of the gene action as well and therefore show a stronger effect. For example, a growth factor gene, such as *BDNF*, might influence the cell numbers or cell volumes in a specific structure of the brain, such as the hippocampus. If so, then the statistical association between common variants influencing the function of that gene and the size of the brain structure should be fairly easy to identify in a database of brain scans. As we shall see, this optimism had to be tempered; at least for the brain measures assessed so far, sample sizes needed for successful genetic association studies have been about the same as those needed to discover risk genes for clinical conditions such as Alzheimer's disease or schizophrenia, though less than those for major depression, and have been on the order of tens of thousands. Even so, one should bear in mind that the large samples required to detect effects does not mean effects are trivial or unimportant. Rare variants with large effect, for example *TREM2*, appear to double a person's risk for Alzheimer's disease (Guerreiro et al. 2013; Jonsson et al. 2013) and cause brain tissue loss at twice the normal rate (Rajagopalan et al. 2013). Despite the fact that only 1 % of people carry this risk allele, the aggregate effect on society is no doubt substantial, perhaps similar to other mental disorders with similar prevalence but with devastating impact.

A second argument was that we should focus on candidate genes when looking for factors that affect the brain, rather than performing a completely open-ended, genome-wide search. Because certain growth factors in the brain—BDNF, and NGF, for example—have polymorphic variants within their genes, they could be natural candidates for affecting volumes of the brain and perhaps other more subtle features of brain function, such as functional activation or metabolism. Except for major risk genes such as *APOE*, a risk factor for late-onset Alzheimer's disease, ENIGMA's data would ultimately show that many of these candidate genes, long thought to affect brain measures, did not appear to do so in much larger sample sizes. This finding was confirmed in samples of 10,000 brain scans or more, samples large enough to detect effects accounting for as little as 1 % of the variance in a brain measure.

Between 2009 and 2012, over 20 cohorts worldwide came together to form ENIGMA. The initial study (called "ENIGMA1"; Stein et al. 2012) found common variants near the *TESC* gene that were associated with hippocampal volume measured in MRI scans of the brain. The SNPs involved also affected gene expression in living brain tissue, as confirmed by analysis of post-mortem brain tissue. Carrying one form of the gene was associated with a hippocampal volume that was smaller by an amount equivalent to about 3 years of brain aging, a small

but substantial effect on a brain scan; the possible cognitive effects of this genetic change, and their effects on disease risk, are now the target of study. Other findings of ENIGMA1 included an association between intracranial volume in healthy subjects and a genetic variant in *HMGA2*, a gene that had formerly been associated with height and whose role in cell proliferation was beginning to be understood. ENIGMA would not have been able to demonstrate that these associations were robust without the help of another large consortium, CHARGE (Cohorts for Heart and Aging Research in Genomic Epidemiology), whose GWAS studies of the aging brain in five large elderly cohorts were crucial in establishing the generality of the findings. In fact, when the two consortia exchanged their top findings for genetic variants associated with hippocampal and intracranial volumes, their top five hits were the same. The most associated SNPs in each consortium were the same ones, even though the studies assessed different individuals and were designed independently (Bis et al. 2012).

Non-biological Information Arising from ENIGMA

After ENIGMA's first study, some hypotheses had to be revised about which genes might affect brain measures and how easy it would be to detect their effects. Some of the "hallowed" candidate genes in psychiatric genetics—*COMT,* for example—were initially hailed as explaining a fair proportion of the risk for psychiatric illness, only to be found less relevant or not well supported in follow-up studies [see Button et al. (2013) for an analysis of this "winner's curse" effect]. Perhaps for the same reasons, many genes expected to influence brain structure were not found to do so, even in ENIGMA's highly powered study. Only *APOE* had a convincing effect on hippocampal volume, with many growth factors and common psychiatric risk genes not showing demonstrable effects in much larger sample sizes than previously studied. Although it is not possible to rule out an effect that is undetected, the effects of these genes would likely be less than 1 % of the measured variance, much smaller than some originally thought.

On the bright side, the power to replicate findings across the whole diverse range of cohorts and populations in ENIGMA was surprising and encouraging. Most studies contributing to ENIGMA were designed with other goals in mind, on different scanners and some on different continents. As the data were pooled after the fact, substantial work went into showing that reproducible and accurate measures could be made of the same brain regions across sites and scanners [see Supplemental Materials in Stein et al. (2012)]. On the genomic side, ENIGMA's use of reference panels such as HapMap3 and the 1000 Genomes datasets to "impute" genetic data collected from different genotyping chips also made it possible to pool data across sites, attaining a power not previously imagined for a brain imaging study.

But Do the ENIGMA Genes Affect Disease Risk?

Shortly after the initial study was published, a second initiative was started to screen the genome for common variants associated with volumes of seven other subcortical structures (the project was called "ENIGMA2"; Hibar et al. 2015) and 34 other cortical structures (ENIGMA3; in progress). In the course of these studies, a collaborative partnership began with the Psychiatric Genomics Consortium (PGC) to see if any of the brain-relevant genes were "enriched" in the PGC's own screens for genes associated with psychiatric illnesses such as schizophrenia. ENIGMA studies of schizophrenia, epilepsy, obsessive compulsive disorder, and Alzheimer's disease are currently underway. There is some optimism that these enrichment analyses may show that some of the same genes that affect the structure of the brain also create risk for disease. Several disease risk genes are known to be convincingly associated with brain differences: many of the top 20 or so Alzheimer's risk genes (according to alzgene.org) are associated with differences in brain structure, metabolism, or pathology identifiable with brain imaging. Some of the logistics involved in looking up ENIGMA's genes in other psychiatric GWAS involves performing "checksum" tests to exclude people who have taken part in both GWAS studies; such participants could cause spurious associations, making it important to screen out non-independent data.

In parallel, ENIGMA launched several working groups to identify brain measures that showed the greatest patient vs. control differences in cohorts of patients with schizophrenia (Turner et al. 2014; van Erp et al. 2015), bipolar illness (Hibar et al. 2014), depression (Schmaal et al. 2014, 2015), and ADHD (Hoogman et al. 2014). Some of these studies now number 4000–8000 subjects, making them the largest studies ever of their respective disorders. Clearly, the power to identify correlates of behavioral and cognitive dysfunction, and relevant modulators of illness such as medication effects, makes these efforts highly informative. All these studies are in their earlier phases now, but ultimately they may yield new sources of information to distinguish psychiatric profiles based on brain imaging and genetics and for differential diagnosis and even perhaps prognosis.

Searching Brain Images for Statistical Effects

In brain imaging studies more generally, it is common to align a group of subjects' images to a standardized coordinate space and try to find parts of the brain with consistent activations or brain regions whose activity relates to modifiable parameters of the experimental design. One such approach, called *statistical parametric mapping*, or SPM, can identify brain regions where brain signals relate to some external predictor, such as a task performed in the scanner, or psychiatric diagnosis. To do this, often a regression model is fitted at thousands to millions of different

locations in a 3D brain image and the significant regions are shown, after some suitable correction for the multiple statistical tests made in the image.

Brain-Wide Genome-Wide Scanning

Although it may seem a daunting task, Stein et al. (2010) proposed a method to screen every voxel (location) in the brain and every genotyped variant in a genomic screen to search both images and genomes at once for promising associations. The sheer number of computations can exceed one billion statistical tests. The first such efforts found no genuinely replicated associations and were computationally feasible only on a massively parallel computer cluster.

Due to the massive number of statistical tests, the significance threshold that needs to be achieved to control for false positives is around a billion to one (see Medland et al. 2014). Even so, this threshold was achievable and far exceeded by several "hits" (i.e., genetic associations) in ENIGMA2, making the approach feasible statistically as well. Although voxel-wise GWAS is a tour de force computationally, it can be combined with other techniques for dimension reduction to focus the search on promising signals. These methods can be statistical, based on genetic clustering or prioritizing brain measures with highest heritability, or they can be based on biology and known genetic pathways. Such efforts are reviewed in Thompson et al. (2013, 2014, 2015).

Genetic Screening of the Connectome

Based on the power that has been achieved so far through ENIGMA to discover common genetic influences on brain structure, it should now be clear that genome-wide analysis can also be extended to measures beyond that of individual neuroanatomical structures to discover factors that influence how regions of the brain are connected or work together, i.e., measures of brain connectivity. Brain connectivity can be modeled in terms of networks describing how different regions of the brain function together (functional connectivity) or how they are physically connected in terms of the strength, integrity, or pattern of the white matter fibers (structural connectivity) (Fig. 1).

Family and twin studies found that specific connections and global organizational measures are heritable in both functional and structural networks. Glahn et al. (2010) found that the resting state functional network, derived from blood oxygen level-dependent functional MRI imaging, is remarkably heritable; Smit et al. (2010) used EEG-based measures of connectivity to study the heritability of measures of network "clustering" and path length. Fornito et al. (2011) examined local and global measures of efficiency and connection distance, along with overall density for resting state networks. In a similar investigation of functional

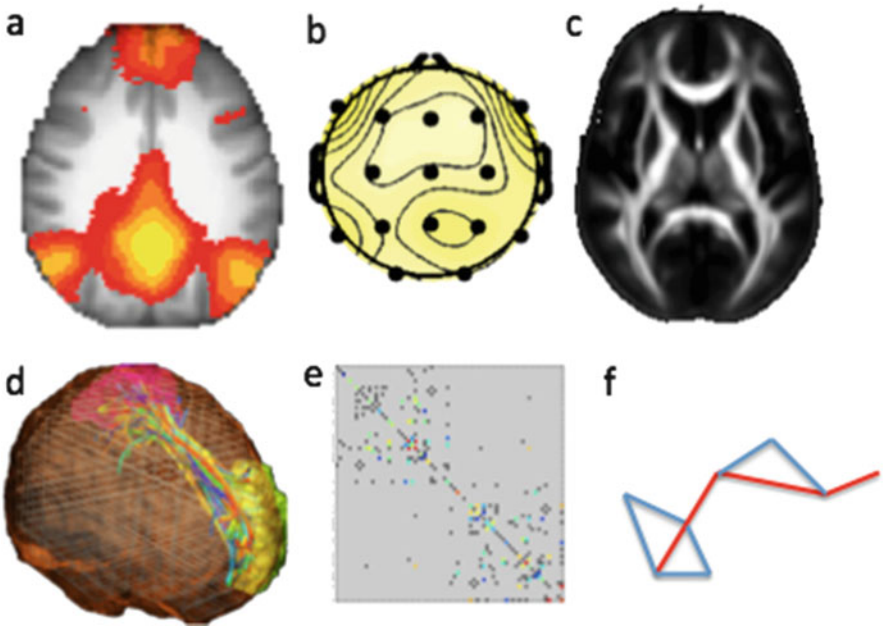

Fig. 1 Various forms of connectivity measures extracted from brain images; all these methods allow us to study the brain from a higher dimensional perspective and observe correlations and connections between regions. In the more classical approaches, voxelwise maps of activity or DTI-based integrity measures can be mapped out. In addition to MRI-based imaging, electrodes can be placed around the brain to obtain functional activation or electrophysiological signals. Structural or functional connections between different regions can be estimated. A broad search over all possible connections can lead to mapping the information in a matrix to form a mathematical graph representation. Global properties of this matrix can then be thought of as measures that describe the network as a whole. For example, one measure of interest examines the shortest path lengths in the network or the paths with the lowest numbers of connections between one region, or node, and all the others

connectivity in children, however, van den Heuvel et al. (2013) did not detect significant heritability for certain local measures while robustly finding that more global measures of network organization were heritable. Structural connectivity and patterns of organization are also influenced by genetic factors. Jahanshad et al. (2013b) showed that a fraction of the total number of detected connections are indeed highly heritable, while Bohlken et al. (2014) studied the network's topology to establish heritability for other global measures of fiber connections.

The genetic influences on these brain measures have also been established by exploring the effect of known disease risk genes on the connectome. Candidate gene analyses have even suggested that connectome properties may be associated with genetic risk factors for diseases and disorders such as autism (Scott-Van Zeeland et al. 2010; Dennis et al. 2011), schizophrenia (Braskie et al. 2012), and dementia (Brown et al. 2011; Jahanshad et al. 2012); given the history of candidate gene associations in psychiatric genetics, these findings will need to be replicated

and assessed in larger samples. There is clear potential for using connectivity measures as targets for genetic analysis or perhaps even for successfully discovering disease risk genes through a genome-wide search.

While functional connectivity measures also appear to be promising targets for genetic study, here we focus our discussion on expanding structural connectivity analyses for large-scale genetic analyses in ENIGMA. Figure 2 shows the structural connectivity matrix from an individual: it stores information on the proportion of detected fibers connecting each pair of brain regions. Jahanshad et al. (2013a, b) proposed a method to map structural connectivity based on diffusion-weighted MRI and prioritize the resulting connections for a genome-wide screen to identify common variants that affect brain connectivity. Not all possible connections are found in all individuals and not all parts of the brain are directly connected to all the others, so the connectivity matrices are relatively sparse (see Fig. 2). As such, a matrix that represents some measure of the quality or density of connections between all pairs of regions on the cortex may represent a number of possible connections that is equal to the square of the number of regions, in theory. For example, breaking up the cortex into 70 regions (Desikan et al. 2006) would lead to a connectivity matrix of almost 5000 elements, but only around 1 % of these might show high reproducibility and heritability in a population.

Using a classical twin model based on identical and fraternal twins, Jahanshad et al. (2013a, b) identified the heritable connections within structural connectivity

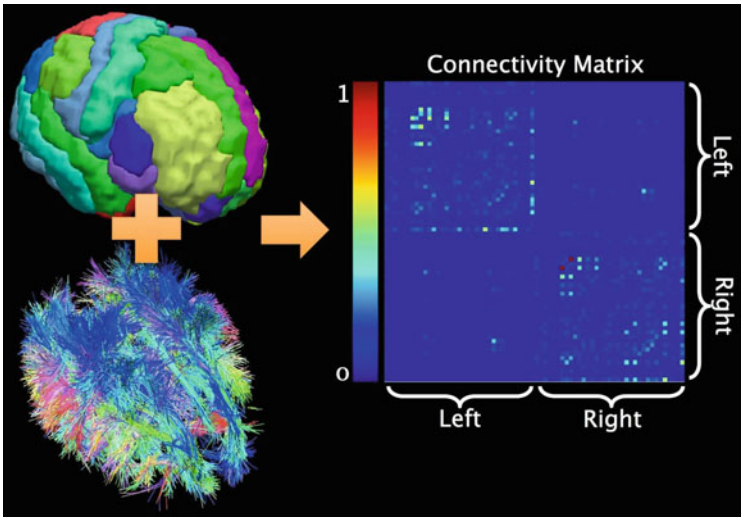

Fig. 2 The structural connectivity matrix. Using standard anatomical MRI and a variant called diffusion-weighted MRI for fiber tracking, we can map out the structural connectivity network of the brain. To do this, we combine a cortical parcellation (*top left*) with a set of fiber pathways computed using tractography algorithms (*bottom left*). The resulting connections between all pairs of cortical regions are organized into a connectivity matrix (*right*). Its rows and columns correspond to the cortical regions and the magnitudes of the elements represent properties of the connections detected between them, such as fiber integrity or density

matrices of several thousand elements and carried forward only the approximately 50 heritable connections into a genome-wide screen. The gene showing a genome-wide and connectome-wide level association with a particular connection within the connectome, *SPON1*, was subsequently also associated with cognitive decline in an independent study, albeit at a different locus (Sherva et al. 2014). This gene is also implicated in amyloid processing (Hafez et al. 2012), a key component of Alzheimer's disease pathology.

Clearly, the ability to pursue such an approach on a large scale, within ENIGMA, depends on several factors: a working group, ENIGMA-DTI, was set up to assess its feasibility. First, unless diffusion-weighted MRI measures show greater genetic effect sizes than other traits assessed so far, there must be tens of thousands of DTI scans available from people with GWAS for such a study to be well powered. Second, the format of the connectivity matrix must be sufficiently standardized and agreed on in advance, to allow the exchange and pooling of brain connectivity data across sites.

Encouragingly, by mid-2014, the ENIGMA-DTI working group had amassed around 10,000 DTI scans. Pilot studies showed that the data could be analyzed in a consistent way (Jahanshad et al. 2013a; Kochunov et al. 2014). As the ENIGMA3 project involves a cortical volumetric analysis, the current plan is for ENIGMA to use those cortical regions as the basis for a structural connectivity analysis, using the same voxel-wise analysis of the connections as advocated in Stein et al. (2010) and Jahanshad et al. (2013b). It will be interesting to see if similar sample sizes, tens of thousands, are needed to find and replicate genetic associations with measures of structural brain connectivity. It could be that mathematical tactics for dimension reduction, or network-based measures, are also attractive targets for genetic analysis; so far the relative merits of each of these measures remains to be seen.

Caveats for Multi-site Genomic Analysis of the Connectome

In addition to the caveats noted for pooling multi-site structural MRI data, several additional caveats make the analysis of connectivity challenging. First, the choice of tractography methods can result in different matrices; the method only detects fibers that the algorithm can identify, so many true connections may be missed and some "false positive" connections will also be detected. As with standard MRI, these factors are largely influenced by the signal to noise ratio and resolutions of the images. Often, an arbitrary threshold is implemented to remove the false positive connections, but short fibers can be filtered out. If a connection appears to be weak or inconsistent across subjects, this connection may also be removed. Interestingly, Fornito et al. (2011) found that, for resting state networks at different thresholds, the degree of heritability varied for different global measures, and heritability was not uniform across all nodes; there were various levels of genetic influence for each measure. Lastly, while seemingly intuitive, the results do depend on the parcellation of the cortex, the way the cortical surface is split up into regions of

interest. Depending on the goals of the study, parcellation schemes can be improved to maximize power.

Before embarking on large-scale collaborative efforts combining connectivity matrices and network metrics, confounding factors such as these should be properly investigated as is currently being done in ENIGMA's working groups, such as the ENIGMA-DTI and EEG working groups, among others. For example, in single site studies, Buchanan et al. (2014) performed test-retest reliability analyses to explore the reliability of measures after exploring a variety of commonly used approaches. Dennis et al. (2012) and Zhan et al. (2013) explored the consequences of altering the thresholds used to define networks as well as different methods of tractography, respectively.

Future Directions: Adaptive Connectomics and EPIC

In Prasad et al. (2014), we introduced a method called "EPIC" (Evolving Partitions in Connectomics) to compute brain connectivity in such a way as to be optimally sensitive to statistical effects in a population, such as the effect of Alzheimer's disease or depression. Clearly, the brain can be divided into regions in many different ways, such as spectral clustering (Craddock et al. 2012), hierarchical clustering (Blumensath et al. 2013), or even genetic clustering (Chen et al. 2012). Each one leads to a different definition of brain connectivity between the resulting regions. Although the set of possible partitions is truly astronomical in number, EPIC offers a principled approach to identify the optimal set of brain regions to find specific statistical effects on the connectivity of the resulting regions. Put another way, if we are seeking brain regions whose connectivity is disrupted in Alzheimer's disease, the algorithm will merge and split parts of the brain until it reaches a set of connections that best differentiates Alzheimer's disease patients from controls.

With this adaptive method in mind, it is easy to see how the brain could be partitioned in such a way to maximize the heritability of the connections, automatically de-selecting unfavorable measures before performing a genome-wide screen. If that were done, genomic screens of the connectome might be more efficient, allowing a two-way interplay between discovered genes and the search for connections they might affect.

Still further potential is available once a genome-wide hit is detected; in that case, it should be possible to merge and split cortical sectors so that the genetic effect of a SNP or set of SNPs is more powerfully detected. In other words, one could adjust the cortical partition to maximize the proportion of variance that can be attributed to SNPs or common genetic variants. These high-dimensional searches of the connectome and genome at once will draw upon the full breadth of ingenuity of mathematicians and geneticists alike.

With the scale of ENIGMA and other consortia now planned, it seems likely that we may crack the "Enigma code" of the brain's connectivity network, using intelligent algorithms and the concerted efforts of the worldwide scientific

community. Identifying the genetic influences on the structure and function of the human brain can allow us to understand what makes us human and help uncover the mechanisms causing psychiatric illness.

Acknowledgments All authors are funded by the National Institutes of Health, including support from the NIH "Big Data to Knowledge" (BD2K) program.

References

Bis JC, DeCarli C, Smith AV, van der Lijn F, Crivello F, Fornage M, Debette S, Shulman JM, Schmidt H, Srikanth V, Schuur M, Yu L, Choi SH, Sigurdsson S, Verhaaren BF, DeStefano AL, Lambert JC, Jack CR Jr, Struchalin M, Stankovich J, Ibrahim-Verbaas CA, Fleischman D, Zijdenbos A, den Heijer T, Mazoyer B, Coker LH, Enzinger C, Danoy P, Amin N, Arfanakis K, van Buchem MA, de Bruijn RF, Beiser A, Dufouil C, Huang J, Cavalieri M, Thomson R, Niessen WJ, Chibnik LB, Gislason GK, Hofman A, Pikula A, Amouyel P, Freeman KB, Phan TG, Oostra BA, Stein JL, Medland SE, Vasquez AA, Hibar DP, Wright MJ, Franke B, Martin NG, Thompson PM, Enhancing Neuro Imaging Genetics through Meta-Analysis Consortium, Nalls MA, Uitterlinden AG, Au R, Elbaz A, Beare RJ, van Swieten JC, Lopez OL, Harris TB, Chouraki V, Breteler MM, De Jager PL, Becker JT, Vernooij MW, Knopman D, Fazekas F, Wolf PA, van der Lugt A, Gudnason V, Longstreth WT Jr, Brown MA, Bennett DA, van Duijn CM, Mosley TH, Schmidt R, Tzourio C, Launer LJ, Ikram MA, Seshadri S (2012) Cohorts for heart and aging research in genomic epidemiology consortium. Common variants at 12q14 and 12q24 are associated with hippocampal volume. Nat Genet 44:545–551

Blokland GA, de Zubicaray GI, McMahon KL, Wright MJ (2012) Genetic and environmental influences on neuroimaging phenotypes: a meta-analytical perspective on twin imaging studies. Twin Res Hum Genet 15:351–371

Blumensath T, Jbabdi S, Glasser MF, Van Essen DC, Ugurbil K, Behrens TE, Smith SM (2013) Spatially constrained hierarchical parcellation of the brain with resting-state fMRI. Neuroimage 76:313–324

Bohlken MM, Mandl RC, Brouwer RM, van den Heuvel MP, Hedman AM, Kahn RS, Hulshoff Pol HE (2014) Heritability of structural brain network topology: a DTI study of 156 twins. Hum Brain Mapp 35:5295–5305

Boomsma D, Busjahn A, Peltonen L (2002) Classical twin studies and beyond. Nat Rev Genet 3:872–882

Braskie MN, Jahanshad N, Stein JL, Barysheva M, Johnson K, McMahon KL, de Zubicaray GI, Martin NG, Wright MJ, Ringman JM, Toga AW, Thompson PM (2012) Relationship of a variant in the NTRK1 gene to white matter microstructure in young adults. J Neurosci 32 (17):5964–72. doi:10.1523/JNEUROSCI.5561-11.2012

Brown JA, Terashima KH, Burggren AC, Ercoli LM, Miller KJ, Small GW, Bookheimer SY (2011) Brain network local interconnectivity loss in aging APOE-4 allele carriers. Proc Natl Acad Sci USA 108(51):20760–20765

Buchanan CR, Pernet CR, Gorgolewski KJ, Storkey AJ, Bastin ME (2014) Test-retest reliability of structural brain networks from diffusion MRI. Neuroimage 86:231–243

Button KS, Ioannidis JPA, Mokrysz C, Nosek BA, Flint J, Robinson ESJ, Munafò MR (2013) Power failure: why small sample size undermines the reliability of neuroscience. Nat Rev Neurosci 14:365–376

Chen CH, Gutierrez ED, Thompson W, Panizzon MS, Jernigan TL, Eyler LT, Fennema-Notestine-C, Jak AJ, Neale MC, Franz CE, Lyons MJ, Grant MD, Fischl B, Seidman LJ, Tsuang MT, Kremen WS, Dale AM (2012) Hierarchical genetic organization of human cortical surface area. Science 335(6076):1634–1636

Chiang MC, Barysheva M, Shattuck DW, Lee AD, Madsen SK, Avedissian C, Klunder AD, Toga AW, McMahon KL, de Zubicaray GI, Wright MJ, Srivastava A, Balov N, Thompson PM (2009) Genetics of brain fiber architecture and intellectual performance. J Neurosci 29:2212–2224

Craddock RC, James GA, Holtzheimer PE 3rd, Hu XP, Mayberg HS (2012) A whole brain fMRI atlas generated via spatially constrained spectral clustering. Hum Brain Mapp 33:1914–1928

Dennis EL, Jahanshad N, Rudie JD, Brown JA, Johnson K, McMahon KL, de Zubicaray GI, Montgomery G, Martin NG, Wright MJ (2011) Altered structural brain connectivity in healthy carriers of the autism risk gene, CNTNAP2. Brain Connect 1(6):447–459

Dennis EL, Jahanshad N, Toga AW, McMahon KL, de Zubicaray GI, Martin NG, Wright MJ, Thompson PM (2012) Test-retest reliability of graph theory measures of structural brain connectivity. In: Ayache N, Delingette H, Golland P, Mori S (eds) Medical image computing and computer-assisted intervention, MICCAI 2012. Springer, Heidelberg, pp 305–312

Desikan RS, Segonne F, Fischl B, Quinn BT, Dickerson BC, Blacker D, Buckner RL, Dale AM, Maguire RP, Hyman BT, Albert MS, Killiany RJ (2006) An automated labeling system for subdividing the human cerebral cortex on MRI scans into gyral based regions of interest. Neuroimage 31(3):968–980

Fornito A, Zalesky A, Bassett DS, Meunier D, Ellison-Wright I, Yucel M, Wood SJ, Shaw K, O'Connor J, Nertney D, Mowry BJ, Pantelis C, Bullmore ET (2011) Genetic influences on cost-efficient organization of human cortical functional networks. J Neurosci 31(9):3261–3270

Glahn DC, Thompson PM, Blangero J (2007) Neuroimaging endophenotypes: strategies for finding genes influencing brain structure and function. Hum Brain Mapp 28(6):488–501

Glahn DC, Winkler AM, Kochunov P, Almasy L, Duggirala R, Carless MA, Curran JC, Olvera RL, Laird AR, Smith SM, Beckmann CF, Fox PT, Blangero J (2010) Genetic control over the resting brain. Proc Natl Acad Sci USA 107(3):1223–1228

Guerreiro R, Wojtas A, Bras J, Carrasquillo M, Rogaeva E, Majounie E, Cruchaga C, Sassi C, Kauwe JS, Younkin S, Hazrati L, Collinge J, Pocock J, Lashley T, Williams J, Lambert JC, Amouyel P, Goate A, Rademakers R, Morgan K, Powell J, St George-Hyslop P, Singleton A, Hardy J, Alzheimer Genetic Analysis Group (2013) TREM2 variants in Alzheimer's disease. N Engl J Med 368:117–127

Hafez DM, Huang JY, Richardson JC, Masliah E, Peterson DA, Marr RA (2012) F-spondin gene transfer improves memory performance and reduces amyloid-beta levels in mice. Neuroscience 223:465–472

Harold D, Abraham R, Hollingworth P, Sims R, Gerrish A, Hamshere ML, Pahwa JS, Moskvina V, Dowzell K, Williams A, Jones N, Thomas C, Stretton A, Morgan AR, Lovestone S, Powell J, Proitsi P, Lupton MK, Brayne C, Rubinsztein DC, Gill M, Lawlor B, Lynch A, Morgan K, Brown KS, Passmore PA, Craig D, McGuinness B, Todd S, Holmes C, Mann D, Smith AD, Love S, Kehoe PG, Hardy J, Mead S, Fox N, Rossor M, Collinge J, Maier W, Jessen F, Schürmann B, Heun R, van den Bussche H, Heuser I, Kornhuber J, Wiltfang J, Dichgans M, Frölich L, Hampel H, Hüll M, Rujescu D, Goate AM, Kauwe JS, Cruchaga C, Nowotny P, Morris JC, Mayo K, Sleegers K, Bettens K, Engelborghs S, De Deyn PP, Van Broeckhoven C, Livingston G, Bass NJ, Gurling H, McQuillin A, Gwilliam R, Deloukas P, Al-Chalabi A, Shaw CE, Tsolaki M, Singleton AB, Guerreiro R, Mühleisen TW, Nöthen MM, Moebus S, Jöckel KH, Klopp N, Wichmann HE, Carrasquillo MM, Pankratz VS, Younkin SG, Holmans PA, O'Donovan M, Owen MJ, Williams J (2009) Genome-wide association study identifies variants at CLU and PICALM associated with Alzheimer's disease. Nat Genet 41:1088–1093

Hibar DP, Westlye L, Thompson PM, Andreassen O, ENIGMA Bipolar Disorder Working Group (2014) ENIGMA bipolar disorder working group findings from 1,747 cases and 2,615 controls. Organization for Human Brain Mapping Conference, Hamburg, Germany

Hibar DP et al (2015) Common genetic variants influence human subcortical brain structures. Nature 520(7546):224–229

Hoogman M, Zwiers M, Mennes M, Franke B, ENIGMA ADHD Working Group (2014) Brain structure and ADHD across the life span: an ENIGMA collaboration. Organization for Human Brain Mapping Conference, Hamburg, Germany

Jack CR, Bernstein MA, Fox NC, Thompson P, Alexander G, Harvey D, Borowski B, Britson PJ, L Whitwell J, Ward C, Dale AM, Felmlee JP, Gunter JL, Hill DL, Killiany R, Schuff N, Fox-Bosetti S, Lin C, Studholme C, DeCarli CS, Krueger G, Ward HA, Metzger GJ, Scott KT, Mallozzi R, Blezek D, Levy J, Debbins JP, Fleisher AS, Albert M, Green R, Bartzokis G, Glover G, Mugler J, Weiner MW (2008) The Alzheimer's disease neuroimaging initiative (ADNI): MRI methods. J Magn Reson Imaging 27(4):685–691

Jahanshad N, Valcour VG, Nir TM, Kohannim O, Busovaca E, Nicolas K, Thompson PM (2012) Disrupted brain networks in the aging HIV+ population. Brain Connect 2(6):335–344

Jahanshad N, Kochunov PV, Sprooten E, Mandl RC, Nichols TE, Almasy L, Blangero J, Brouwer RM, Curran JE, de Zubicaray GI, Duggirala R, Fox PT, Hong LE, Landman BA, Martin NG, McMahon KL, Medland SE, Mitchell BD, Olvera RL, Peterson CP, Starr JM, Sussmann JE, Toga AW, Wardlaw JM, Wright MJ, Hulshoff Pol HE, Bastin ME, McIntosh AM, Deary IJ, Thompson PM, Glahn DC (2013a) Multi-site genetic analysis of diffusion images and voxelwise heritability analysis: a pilot project of the ENIGMA-DTI working group. Neuroimage 81:455–469

Jahanshad N, Rajagopalan P, Hua X, Hibar DP, Nir TM, Toga AW, Jack CR Jr, Saykin AJ, Green RC, Weiner MW, Medland SE, Montgomery GW, Hansell NK, McMahon KL, de Zubicaray GI, Martin NG, Wright MJ, Thompson PM (2013b) Genome-wide scan of healthy human connectome discovers SPON1 gene variant influencing dementia severity. Proc Natl Acad Sci USA 110:4768–4773

Jensen AR (1969) How much can we boost IQ and scholastic achievement? Harvard Educ Rev 39:1–123

Jonsson T, Stefansson H, Steinberg S, Jonsdottir I, Jonsson PV, Snaedal J, Bjornsson S, Huttenlocher J, Levey AI, Lah JJ, Rujescu D, Hampel H, Giegling I, Andreassen OA, Engedal K, Ulstein I, Djurovic S, Ibrahim-Verbaas C, Hofman A, Ikram MA, van Duijn CM, Thorsteinsdottir U, Kong A, Stefansson K (2013) Variant of TREM2 associated with the risk of Alzheimer's disease. N Engl J Med 368:107–116

Joshi AA, Leporé N, Joshi SH, Lee AD, Barysheva M, Stein JL, McMahon KL, Johnson K, de Zubicaray GI, Martin NG, Wright MJ, Toga AW, Thompson PM (2012) The contribution of genes to cortical thickness and volume. Neuroreport 22:101–105

Kochunov P, Jahanshad N, Sprooten E, Nichols TE, Mandl RC, Almasy L, Booth T, Brouwer RM, Curran JE, de Zubicaray GI, Dimitrova R, Duggirala R, Fox PT, Hong LE, Landman BA, Lemaitre H, Lopez L, Martin NG, McMahon KL, Mitchell BD, Olvera RL, Peterson CP, Starr JM, Sussmann JE, Toga AW, Wardlaw JM, Wright MJ, Wright SN, Bastin ME, McIntosh AM, Boomsma DI, Kahn RS, den Braber A, de Geus EJ, Deary IJ, Pol HEH, Williamson D, Blangero J, van 't Ent D, Thompson PM, Glahn DC (2014) Multi-site study of additive genetic effects on fractional anisotropy of cerebral white matter: comparing meta and mega analytical approaches for data pooling. Neuroimage 95:136–150

Lewontin RC, Rose SPR, Kamin LJ (1984) Not in our genes: biology, ideology, and human nature. Pantheon Books, New York

Medland SE, Jahanshad N, Neale BM, Thompson PM (2014) Whole-genome analyses of whole-brain data: working within an expanded search space. Nat Neurosci 17:791–800

Prasad G, Joshi SH, Thompson PM (2014) Optimizing brain connectivity networks for disease classification using EPIC. IEEE 11th International Symposium on Biomedical Imaging, Beijing, China

Purcell SM, Moran JL, Fromer M, Ruderfer D, Solovieff N, Roussos P, O'Dushlaine C, Chambert K, Bergen SE, Kähler A, Duncan L, Stahl E, Genovese G, Fernández E, Collins MO, Komiyama NH, Choudhary JS, Magnusson PK, Banks E, Shakir K, Garimella K, Fennell T, DePristo M, Grant SG, Haggarty SJ, Gabriel S, Scolnick EM, Lander ES, Hultman CM, Sullivan PF, McCarroll SA, Sklar P (2014) A polygenic burden of rare disruptive mutations in schizophrenia. Nature 506:185–190

Rajagopalan P, Hibar DP, Thompson PM (2013) TREM2 Alzheimer risk gene carriers lose brain tissue faster. N Engl J Med 369:1565–1567

Sanders SJ, Murtha MT, Gupta AR, Murdoch JD, Raubeson MJ, Willsey AJ, Ercan-Sencicek AG, DiLullo NM, Parikshak NN, Stein JL, Walker MF, Ober GT, Teran NA, Song Y, El-Fishawy P, Murtha RC, Choi M, Overton JD, Bjornson RD, Carriero NJ, Meyer KA, Bilguvar K, Mane SM, Sestan N, Lifton RP, Günel M, Roeder K, Geschwind DH, Devlin B, State MW (2012) De novo mutations revealed by whole-exome sequencing are strongly associated with autism. Nature 485:237–241

Schmaal L, Veltman DJ, Hibar DP (2014) Subcortical brain volume abnormalities in major depressive disorder: prospective meta-analytic findings from the Enigma Major Depressive Disorder Working Group. Society for Neuroscience Conference in Washington DC, USA, abstract 614.05

Schmaal L (2015) Subcortical brain alterations in major depressive disorder: findings from the ENIGMA Major Depressive Disorder working group. Mol Psychiatry. doi:10.1038/mp.2015.69

Scott-Van Zeeland AA, Abrahams BS, Alvarez-Retuerto AI, Sonnenblick LI, Rudie JD, Ghahremani D, Mumford JA, Poldrack RA, Dapretto M, Geschwind DH, Bookheimer SY (2010) Altered functional connectivity in frontal lobe circuits is associated with variation in the autism risk gene CNTNAP2. Sci Transl Med 2(56):56–80

Sherva R, Tripodis Y, Bennett DA, Chibnik LB, Crane PK, de Jager PL, Farrer LA, Saykin AJ, Shulman JM, Naj A, Green RC, GENAROAD Consortium, Alzheimer's Disease Neuroimaging Initiative, Alzheimer's Disease Genetics Consortium (2014) Genome-wide association study of the rate of cognitive decline in Alzheimer's disease. Alzheimers Dement 10:45–52

Smit DJ, Boersma M, van Beijsterveldt CE, Posthuma D, Boomsma DI, Stam CJ, de Geus EJ (2010) Endophenotypes in a dynamically connected brain. Behav Genet 40(2):167–177

Stein JL, Hua X, Lee S, Ho AJ, Leow AD, Toga AW, Saykin AJ, Shen L, Foroud T, Pankratz N, Huentelman MJ, Craig DW, Gerber JD, Allen AN, Corneveaux JJ, Dechairo BM, Potkin SG, Weiner MW, Thompson P (2010) Voxelwise genome-wide association study (vGWAS). Neuroimage 53:1160–1174

Stein JL, Medland SE, Vasquez AA, Hibar DP, Senstad RE, Winkler AM, Toro R, Appel K, Bartecek R, Bergmann O, Bernard M, Brown AA, Cannon DM, Chakravarty MM, Christoforou A, Domin M, Grimm O, Hollinshead M, Holmes AJ, Homuth G, Hottenga JJ, Langan C, Lopez LM, Hansell NK, Hwang KS, Kim S, Laje G, Lee PH, Liu X, Loth E, Lourdusamy A, Mattingsdal M, Mohnke S, Maniega SM, Nho K, Nugent AC, O'Brien C, Papmeyer M, Putz B, Ramasamy A, Rasmussen J, Rijpkema M, Risacher SL, Roddey JC, Rose EJ, Ryten M, Shen L, Sprooten E, Strengman E, Teumer A, Trabzuni D, Turner J, van Eijk K, van Erp TG, van Tol MJ, Wittfeld K, Wolf C, Woudstra S, Aleman A, Alhusaini S, Almasy L, Binder EB, Brohawn DG, Cantor RM, Carless MA, Corvin A, Czisch M, Curran JE, Davies G, de Almeida MA, Delanty N, Depondt C, Duggirala R, Dyer TD, Erk S, Fagerness J, Fox PT, Freimer NB, Gill M, Goring HH, Hagler DJ, Hoehn D, Holsboer F, Hoogman M, Hosten N, Jahanshad N, Johnson MP, Kasperaviciute D, Kent JW Jr, Kochunov P, Lancaster JL, Lawrie SM, Liewald DC, Mandl R, Matarin M, Mattheisen M, Meisenzahl E, Melle I, Moses EK, Muhleisen TW, Nauck M, Nothen MM, Olvera RL, Pandolfo M, Pike GB, Puls R, Reinvang I, Renteria ME, Rietschel M, Roffman JL, Royle NA, Rujescu D, Savitz J, Schnack HG, Schnell K, Seiferth N, Smith C, Steen VM, Valdes Hernandez MC, Van den Heuvel M, van der Wee NJ, Van Haren NE, Veltman JA, Volzke H, Walker R, Westlye LT, Whelan CD, Agartz I, Boomsma DI, Cavalleri GL, Dale AM, Djurovic S, Drevets WC, Hagoort P, Hall J,

Heinz A, Jack CR Jr, Foroud TM, Le Hellard S, Macciardi F, Montgomery GW, Poline JB, Porteous DJ, Sisodiya SM, Starr JM, Sussmann J, Toga AW, Veltman DJ, Walter H, Weiner MW, Alzheimer's Disease Neuroimaging Initiative, EPIGEN Consortium, IMAGEN Consortium, Saguenay Youth Study Group, Bis JC, Ikram MA, Smith AV, Gudnason V, Tzourio C, Vernooij MW, Launer LJ, DeCarli C, Seshadri S, Cohorts for Heart and Aging Research in Genomic Epidemiology Consortium, Andreassen OA, Apostolova LG, Bastin ME, Blangero J, Brunner HG, Buckner RL, Cichon S, Coppola G, de Zubicaray GI, Deary IJ, Donohoe G, de Geus EJ, Espeseth T, Fernández G, Glahn DC, Grabe HJ, Hardy J, Hulshoff Pol HE, Jenkinson M, Kahn RS, McDonald C, McIntosh AM, McMahon FJ, McMahon KL, Meyer-Lindenberg A, Morris DW, Müller-Myhsok B, Nichols TE, Ophoff RA, Paus T, Pausova Z, Penninx BW, Potkin SG, Sämann PG, Saykin AJ, Schumann G, Smoller JW, Wardlaw JM, Weale ME, Martin NG, Franke B, Wright MJ, Thompson PM, Enhancing Neuro Imaging Genetics through Meta-Analysis Consortium (2012) Identification of common variants associated with human hippocampal and intracranial volumes. Nat Genet 44:552–561

Thompson PM, Cannon TD, Narr KL, van Erp T, Poutanen VP, Huttunen M, Lönnqvist J, Standertskjöld-Nordenstam CG, Kaprio J, Khaledy M, Dail R, Zoumalan CI, Toga AW (2001) Genetic influences on brain structure. Nat Neurosci 4(12):1253–1258

Thompson PM, Ge T, Glahn DC, Jahanshad N, Nichols TE (2013) Genetics of the connectome. Neuroimage 80:475–488

Thompson PM, Stein JL, Medland SE, Hibar DP, Vasquez AA, Renteria ME, Toro R, Jahanshad N, Schumann G, Franke B, Wright MJ, Martin NG, Agartz I, Alda M, Alhusaini S, Almasy L, Almeida J, Alpert K, Andreasen NC, Andreassen OA, Apostolova LG, Appel K, Armstrong NJ, Aribisala B, Bastin ME, Bauer M, Bearden CE, Bergmann O, Binder EB, Blangero J, Bockholt HJ, Boen E, Bois C, Boomsma DI, Booth T, Bowman IJ, Bralten J, Brouwer RM, Brunner HG, Brohawn DG, Buckner RL, Buitelaar J, Bulayeva K, Bustillo JR, Calhoun VD, Cannon DM, Cantor RM, Carless MA, Caseras X, Cavalleri GL, Chakravarty MM, Chang KD, Ching CR, Christoforou A, Cichon S, Clark VP, Conrod P, Coppola G, Crespo-Facorro B, Curran JE, Czisch M, Deary IJ, de Geus EJ, den Braber A, Delvecchio G, Depondt C, de Haan L, de Zubicaray GI, Dima D, Dimitrova R, Djurovic S, Dong H, Donohoe G, Duggirala R, Dyer TD, Ehrlich S, Ekman CJ, Elvsashagen T, Emsell L, Erk S, Espeseth T, Fagerness J, Fears S, Fedko I, Fernandez G, Fisher SE, Foroud T, Fox PT, Francks C, Frangou S, Frey EM, Frodl T, Frouin V, Garavan H, Giddaluru S, Glahn DC, Godlewska B, Goldstein RZ, Gollub RL, Grabe HJ, Grimm O, Gruber O, Guadalupe T, Gur RE, Gur RC, Goring HH, Hagenaars S, Hajek T, Hall GB, Hall J, Hardy J, Hartman CA, Hass J, Hatton SN, Haukvik UK, Hegenscheid K, Heinz A, Hickie IB, Ho BC, Hoehn D, Hoekstra PJ, Hollinshead M, Holmes AJ, Homuth G, Hoogman M, Hong LE, Hosten N, Hottenga JJ, Hulshoff Pol HE, Hwang KS, Jack CR Jr, Jenkinson M, Johnston C, Jonsson EG, Kahn RS, Kasperaviciute D, Kelly S, Kim S, Kochunov P, Koenders L, Kramer B, Kwok JB, Lagopoulos J, Laje G, Landen M, Landman BA, Lauriello J, Lawrie SM, Lee PH, Le Hellard S, Lemaitre H, Leonardo CD, Li CS, Liberg B, Liewald DC, Liu X, Lopez LM, Loth E, Lourdusamy A, Luciano M, Macciardi F, Machielsen MW, Macqueen GM, Malt UF, Mandl R, Manoach DS, Martinot JL, Matarin M, Mather KA, Mattheisen M, Mattingsdal M, Meyer-Lindenberg A, McDonald C, McIntosh AM, McMahon FJ, McMahon KL, Meisenzahl E, Melle I, Milaneschi Y, Mohnke S, Montgomery GW, Morris DW, Moses EK, Mueller BA, Munoz Maniega S, Muhleisen TW, Muller-Myhsok B, Mwangi B, Nauck M, Nho K, Nichols TE, Nilsson LG, Nugent AC, Nyberg L, Olvera RL, Oosterlaan J, Ophoff RA, Pandolfo M, Papalampropoulou-Tsiridou M, Papmeyer M, Paus T, Pausova Z, Pearlson GD, Penninx BW, Peterson CP, Pfennig A, Phillips M, Pike GB, Poline JB, Potkin SG, Putz B, Ramasamy A, Rasmussen J, Rietschel M, Rijpkema M, Risacher SL, Roffman JL, Roiz-Santianez R, Romanczuk-Seiferth N, Rose EJ, Royle NA, Rujescu D, Ryten M, Sachdev PS, Salami A, Satterthwaite TD, Savitz J, Saykin AJ, Scanlon C, Schmaal L, Schnack HG, Schork AJ, Schulz SC, Schur R, Seidman L, Shen L, Shoemaker JM, Simmons A, Sisodiya SM, Smith C, Smoller JW, Soares JC, Sponheim SR, Sprooten E, Starr JM, Steen VM,

Strakowski S, Strike L, Sussmann J, Samann PG, Teumer A, Toga AW, Tordesillas-Gutierrez-D, Trabzuni D, Trost S, Turner J, Van den Heuvel M, van der Wee NJ, van Eijk K, van Erp TG, van Haren NE, van 't Ent D, van Tol MJ, Valdes Hernandez MC, Veltman DJ, Versace A, Volzke H, Walker R, Walter H, Wang L, Wardlaw JM, Weale ME, Weiner MW, Wen W, Westlye LT, Whalley HC, Whelan CD, White T, Winkler AM, Wittfeld K, Woldehawariat G, Wolf C, Zilles D, Zwiers MP, Thalamuthu A, Schofield PR, Freimer NB, Lawrence NS, Drevets W, The Alzheimer's Disease Neuroimaging Initiative (2014) The ENIGMA Consortium: large-scale collaborative analyses of neuroimaging and genetic data. Brain Imaging Behav 8:153–182

Thompson PM et al (2015) ENIGMA and the individual: predicting factors that affect the brain in 35 countries worldwide. NeuroImage. doi:10.1016/j.neuroimage.2015.11.057

Turner J, van Erp T, Hibar D, Thompson PM, and the ENIGMA Schizophrenia Working Group (2014) Subcortical and cortical variations in schizophrenia: the ENIGMA SZ Working Group. Organization for Human Brain Mapping Conference, Hamburg, Germany

van den Heuvel MP, van Soelen IL, Stam CJ, Kahn RS, Boomsma DI, Hulshoff Pol HE (2013) Genetic control of functional brain network efficiency in children. Eur Neuropsychopharmacol 23:19–23

van Erp TG et al (2015) Subcortical brain volume abnormalities in 2028 individuals with schizophrenia and 2540 healthy controls via the ENIGMA consortium. Mol Psychiatry. doi:10.1038/mp.2015.118

Visscher PM, Hill WG, Wray NR (2008) Heritability in the genomics era--concepts and misconceptions. Nat Rev Genet 9:255–266

Zhan L, Mueller BA, Jahanshad N, Jin Y, Lenglet C, Yacoub E, Sapiro G, Ugurbil K, Harel N, Toga AW (2013) Magnetic resonance field strength effects on diffusion measures and brain connectivity networks. Brain Connect 3(1):72–86

Index

H. Kennedy et al. (eds.), *Micro-, Meso- and Macro-Connectomics of the Brain*,
Research and Perspectives in Neurosciences, DOI 10.1007/978-3-319-27777-6